NASA Technical Paper 2991

1990

Internal Performance of Two Nozzles Utilizing Gimbal Concepts for Thrust Vectoring

Bobby L. Berrier
and John G. Taylor
Langley Research Center
Hampton, Virginia

National Aeronautics and Space Administration
Office of Management
Scientific and Technical Information Division

Summary

An investigation was conducted in the static test facility of the Langley 16-Foot Transonic Tunnel to evaluate the internal performance of an axisymmetric convergent-divergent nozzle and a nonaxisymmetric convergent-divergent nozzle, both of which utilized a gimbal-type mechanism for thrust vectoring in at least one plane. The nonaxisymmetric nozzle used the gimbal concept for yaw thrust vectoring only, and pitch thrust vectoring was accomplished by simultaneous deflection of the upper and lower divergent flaps. The model geometric parameters investigated were pitch vector angle for the axisymmetric nozzle and pitch vector angle, yaw vector angle, nozzle throat aspect ratio, and nozzle expansion ratio for the nonaxisymmetric nozzle. All tests were conducted with no external flow, and nozzle pressure ratio was varied from 2.0 to approximately 12.0.

Results of this study indicate that a gimbal mechanism upstream of the nozzle throat is a highly effective and efficient thrust-vectoring device. The gimbal concepts of this investigation produced resultant thrust vector angles equal to the geometric thrust vector angles with little or no loss in resultant gross thrust. For the nonaxisymmetric nozzle, rotation of the divergent flaps produced resultant pitch vector angles which, although dependent on nozzle pressure ratio, were nearly equal to the geometric pitch vector angle. The losses in resultant gross thrust due to pitch vectoring were small or negligible.

Introduction

Many studies have shown the benefits of thrust vectoring (and, in particular, multiaxis thrust vectoring) on fighter aircraft performance (refs. 1 to 22). Some of these potential benefits are aircraft control augmentation (refs. 8, 9, and 12 to 21), reduced aircraft weight (refs. 3 and 20), and improved aircraft survivability (refs. 3, 9, 10, and 20). Thrust vectoring will also allow aircraft to operate in flight regimes where conventional aircraft cannot operate, namely, at the very low speeds occurring during vertical or short takeoff and landing operation (refs. 4 and 8 to 10) and at the very high angles of attack occurring during "supermaneuverability" or poststall maneuvers (refs. 12, 16, and 19 to 21).

In an attempt to provide thrust-vectoring capability with minimum adverse impact on aircraft performance, many thrust-vectoring concepts have been considered (refs. 4, 6, 13, and 22 to 29). Early thrust-vectoring concepts were for pitch thrust vectoring only, but more recent studies have concentrated on multiaxis (pitch and yaw) thrust-vectoring capability. One of the earliest thrust-vectoring concepts considered by engine manufacturers was a gimbal or swivel mechanism inserted in the nozzle tail pipe. Examples of these designs and associated performance can be found in references 4, 6, 23, and 24. In general, this concept was directed toward vertical or short takeoff and landing applications and, as such, had vectoring capabilities equal to or greater than 90°. Since the gimbal or swivel mechanism is located upstream of the exhaust nozzle, this concept can be utilized with any nozzle design including axisymmetric and nonaxisymmetric types. Another advantage of this concept is that flow turning is accomplished in the low-speed, subsonic exhaust flow ahead of the nozzle throat, and thus flow-turning losses on nozzle thrust are expected to be small. However, because of high gimbal system weight and difficulties with propulsion airframe integration (airframe doors were often required to allow high nozzle thrust vector angles), the gimbal concept was essentially abandoned in favor of more integral nozzle/thrust-vectoring systems. (See ref. 4.)

Recently, interest in the gimbal thrust-vectoring concept has been revived for the following three reasons: (1) the lower angle thrust-vectoring requirements for control augmentation may allow gimbal-system weight penalties to be reduced and also minimize problems associated with airframe integration; (2) for axisymmetric exhaust nozzles, the gimbal concept is one of the few options available; and (3) for nonaxisymmetric nozzles, integration of the round gimbal mechanism with the convergent section of the nozzle (changing nozzle high-pressure sections upstream of nozzle throat from rectangular to round) may help to reduce the inherent weight penalty for nonaxisymmetric nozzles.

The purpose of the present paper is to present the results of a static investigation to evaluate the internal performance of an axisymmetric convergent-divergent nozzle and a nonaxisymmetric convergent-divergent nozzle, both of which utilized a gimbal-type mechanism for thrust vectoring. The nonaxisymmetric nozzle used the gimbal concept for yaw thrust vectoring only, and pitch thrust vectoring was accomplished by simultaneous deflection of the upper and lower divergent flaps. Previous studies of nonaxisymmetric nozzles have indicated that divergent-flap deflection is an effective and efficient method to obtain pitch thrust vector angles. (See refs. 6, 11, 22, 25, and 26.) The experimental investigation was conducted in the static test facility of the Langley 16-Foot Transonic Tunnel at static (no external flow) conditions. The model geometric parameters investigated were pitch vector angle for the axisymmetric nozzle and pitch vector angle, yaw vector angle, nozzle aspect ratio (throat width divided by throat height), and nozzle expansion ratio for the nonaxisymmetric nozzle. High-pressure air was used to simulate the jet exhaust flow at nozzle pressure ratios from 2.0 to approximately 12.0.

Symbols

All forces (with the exception of resultant gross thrust) and angles are referred to the model body axis.

AR	nozzle throat aspect ratio, w_t/h_t
A_e	nozzle exit area, in^2
A_e/A_t	nozzle expansion ratio
A_t	nozzle throat area, in^2
C_d	nozzle discharge coefficient, w_p/w_i
F	measured thrust along body axis, positive in forward direction, lbf
F_i	ideal isentropic gross thrust, $w_p\sqrt{\frac{R_jT_{t,j}}{g^2}\frac{2\gamma}{\gamma-1}\left[1-\left(\frac{p_a}{p_{t,j}}\right)^{(\gamma-1)/\gamma}\right]}$, lbf
F_N	measured normal force, lbf
F_r	resultant gross thrust, $\sqrt{F^2+F_N^2+F_S^2}$, lbf
F_S	measured side force, lbf
g	acceleration due to gravity ($1g \approx$ 32.174 ft/sec^2)
h_t	nozzle duct height at throat, in.
L	length of divergent flaps along nozzle centerline, in.
NPR	nozzle pressure ratio, $p_{t,j}/p_a$
$(\mathrm{NPR})_d$	design nozzle pressure ratio (NPR for fully expanded flow at nozzle exit)
p	local static pressure, psi
p_a	ambient pressure, psi
$p_{t,j}$	average jet total pressure, psi
R_j	gas constant, 1716 ft^2/sec^2 - °R for air
$T_{t,j}$	jet total temperature, °R
w_i	ideal weight-flow rate (for NPR > 1.89), lbf/sec, $A_tp_{t,j}\left(\frac{2}{\gamma+1}\right)^{(\gamma+1)/2(\gamma-1)}\sqrt{\frac{\gamma g^2}{T_{t,j}R_j}}$
w_p	measured weight-flow rate, lbf/sec
w_t	nozzle duct width at throat, in.
x	axial distance downstream of nozzle throat, in.
x'	rotated model coordinate axis (see figs. 8 and 9), in.
y	lateral distance measured from model centerline, positive to right side when looking upstream, in.
α	nozzle divergence half-angle, deg
γ	ratio of specific heats
δ_p	resultant pitch thrust vector angle, $\tan^{-1}(F_N/F)$, deg
$\delta_{v,p}$	geometric pitch vector angle measured from model centerline, (positive angle produces positive normal force), deg
$\delta_{v,y}$	geometric yaw vector angle measured from model centerline, (positive angle produces positive side force), deg
δ_y	resultant yaw thrust vector angle, $\tan^{-1}(F_S/F)$, deg
ϕ	roll angle about model centerline, positive in clockwise direction when looking upstream, deg

Abbreviations:

Axi.	axisymmetric
C-D	convergent-divergent
SCF	spherical convergent flap
Sta	model station, in.
T.E.	trailing edge
WL	waterline
2-D	two-dimensional or nonaxisymmetric

Apparatus and Methods

Static Test Facility

This investigation was conducted in the static test facility of the Langley 16-Foot Transonic Tunnel. Testing is conducted in a large room where the jet from a simulated single-engine propulsion system exhausts to the atmosphere through an acoustically treated exhaust passage. A control room is remotely located from the test area, and a closed-circuit television is used to observe the model when the jet is operating. The static test facility has an air control system that is similar to that of the 16-Foot Transonic Tunnel and includes valving, filters, and a heat exchanger to maintain the jet flow at constant stagnation temperature. The air system utilizes the same clean, dry air supply as that used by the 16-Foot Transonic Tunnel (ref. 30).

Single-Engine Propulsion Simulation System

A sketch of the single-engine, air-powered nacelle model on which various nozzle configurations were tested is presented in figure 1. The propulsion simulation system is shown with an unvectored, gimballed axisymmetric nozzle installed.

An external high-pressure air system provided a continuous flow of clean, dry air at a controlled temperature of about 540°R. This high-pressure air was varied during jet simulation up to about 175 psi in the nozzle. The pressurized air was brought by six air lines through a dolly-mounted support strut and into a high-pressure plenum chamber. The air was then discharged perpendicularly into the model low-pressure plenum through eight multiholed sonic nozzles equally spaced around the high-pressure plenum. (See fig. 1.) This airflow system was designed to minimize any forces imposed by the transfer of axial momentum as the air is passed from the nonmetric high-pressure plenum to the metric (attached to the balance) low-pressure plenum. Two flexible metal bellows sealed the air system (between metric and nonmetric model parts) and compensated for axial forces caused by pressurization. The air then passed from the low-pressure plenum through a circular choke plate and instrumentation section, which were common for all nozzle configurations tested. All test configurations attached to the instrumentation section at model station 39.00.

Nozzle Designs

Two different nozzle types were tested: an axisymmetric convergent-divergent (Axi. C-D) nozzle and a nonaxisymmetric (two-dimensional) convergent-divergent (2-D C-D) nozzle. Both nozzle types utilized a gimbal mechanism to provide part or all their thrust-vectoring capability. Table 1 provides a list of all nozzle configurations tested.

Gimballed axisymmetric nozzle. The Axi. C-D nozzle tested is shown in the three-view sketch of figure 2 and photographs of figure 3. This nozzle utilized a gimbal-type mechanism (simulated by fixed-geometry model hardware) in the tail pipe ahead of the nozzle to provide both pitch and yaw thrust-vectoring capability. Geometric details of the gimbal section and nozzle are provided in figure 4.

Since the Axi. C-D nozzle configuration was symmetric about the model centerline and the gimbal section geometry for yaw thrust vectoring would be identical to that for pitch thrust vectoring (the nozzle deflection would be in the lateral rather than vertical plane), only the pitch thrust vector angle was varied during the test. Geometric pitch thrust vector angles $\delta_{v,p}$ of 0°, 10°, 20°, and 25° were tested. (See table 1.) Pitch thrust-vectoring results can be rotated directly to the yaw thrust-vectoring plane. The Axi. C-D nozzle was designed with an expansion ratio A_e/A_t of 1.80 which corresponds to a design nozzle pressure ratio $(\mathrm{NPR})_d$ of 8.81.

Spherical-convergent-flap nonaxisymmetric nozzle. The 2-D C-D nozzle of the current test is shown in the three-view sketch of figure 5 and in the photograph of figure 6. A gimbal mechanism is integrated with the nozzle just upstream of the throat such that the nozzle convergent duct is spherical in shape and the duct retains the structurally efficient circular cross section. The throat and divergent section of the nozzle are rectangular in cross-sectional shape. The nozzle sidewall trailing edges were located at approximately 72 percent of the divergent-flap length. Geometric details of the SCF 2-D C-D nozzle are shown in the sketches of figure 7.

As indicated in table 1 and figures 7(b) and 7(c), the SCF 2-D C-D nozzle configuration was tested with throat aspect ratios of 1.265, 2.083, and 2.508. Each of these throat aspect ratios represents a different nozzle design. All other model parameters investigated (A_e/A_t, $\delta_{v,y}$, and $\delta_{v,p}$) represent geometric variations that would be obtained on actual full-scale hardware through variable geometry. The gimbal mechanism of the SCF 2-D C-D nozzle was utilized to provide a yaw thrust-vectoring capability only. Geometric yaw vector angles $\delta_{v,y}$ up to 25° (depending on AR) were tested. As shown in figure 7(b), the width of the throat cutout in the SCF section increased as nozzle throat aspect ratio AR increased. The larger width cutout of the AR = 2.083 and 2.508 nozzles limited the geometric yaw vector angles for these configurations to 20° and 15°, respectively. (See table 1.)

The pitch thrust-vectoring capability is provided by deflection of the 2-D divergent flaps of the SCF 2-D C-D nozzle. This method for providing a pitch thrust-vectoring capability has been shown to be very effective and efficient for 2-D C-D nozzle types. (See refs. 6, 11, 22, and 27.) Geometric pitch vector angles $\delta_{v,p}$ up to 25° were tested without and with simultaneous yaw thrust vectoring.

Lastly, each combination of throat aspect ratio, geometric yaw vector angle, and geometric pitch vector angle for the SCF 2-D C-D nozzle was tested at nozzle expansion ratios of 1.46 and 1.63 which have associated values of $(\mathrm{NPR})_d$ of 5.92 and 7.33, respectively. The expansion ratio was varied by varying the trailing-edge waterline location of the nozzle divergent flap (see fig. 7(c)) which results in a variation of nozzle exit area.

Instrumentation

A six-component strain-gauge balance was used to measure forces and moments on the model downstream of model station 20.50. Jet total pressure was measured at a fixed station in the instrumentation section by a five-probe rake (see fig. 1) and a single-probe rake (not shown). A thermocouple was also positioned in the instrumentation section to measure jet total temperature. The weight flow of the high-pressure air supplied to the nozzle was determined from two calibrated, choked venturi located in the air system upstream of the model.

Internal (jet flow) static pressure distributions were measured on each configuration tested. Static pressure orifice locations on the gimballed axisymmetric nozzle are shown in the sketches of figure 4. Two rows, one on top and one on bottom, of static pressure orifices were located along the internal flow path. For the $\delta_{v,p} = 20^\circ$ and 25° configurations, one of the bottom-row orifice locations in the gimbal section was moved to the top row. (See fig. 4(a).)

Static pressure orifice locations on the SCF 2-D C-D configurations are shown in figure 7. A row of internal static pressure orifices was located on each side of the transition section (see fig. 7(a)) and spherical convergent-flap section (see fig. 7(b)). It should be noted that as geometric yaw vector angle was increased, some of the orifices on the rotating spherical convergent-flap section were covered on one side by the stationary transition section. As shown in figure 7(c), static pressure orifices downstream of the throat were located on the model centerline of the left and right sidewalls and also on the upper and lower divergent flaps. Orifice locations on the divergent flaps are given in table 2, and orifice locations on the sidewalls are given in table 3.

For presentation purposes, an alternate x-axis coordinate system (x') was defined. The x'-axis for both nozzle types rotates about the gimbal pivot point on the model centerline. The alternate coordinate system for the gimballed axisymmetric nozzle is shown in figure 8. The x'-axis rotates equally with $\delta_{v,p}$. The value of $x' = 0$ is defined as the throat station. For $\delta_{v,p} = 0^\circ$, the x- and x'-axes are coincident. Static pressure orifice locations on the x'-axis for the gimballed Axi. nozzle are given in table 4. The alternate coordinate system for the SCF 2-D C-D nozzles is shown in figure 9. This coordinate system is similar to that defined for the gimballed Axi. nozzle except that the x'-axis rotates equally with $\delta_{v,y}$ since the gimbal mechanism operates in the yaw plane for the SCF 2-D C-D nozzles. Static pressure orifice locations on the x'-axis for the SCF 2-D C-D nozzles are given in table 5 for the divergent flaps and in table 6 for the sidewalls.

Data Reduction

Approximately 50 frames of data, taken at a rate of 10 frames per second, were used for each data point; average values were used in the computations. With the exception of resultant gross thrust F_r, all data in this report are referenced to the model centerline (x-axis). Five basic performance parameters are used in the presentation of results; they are internal thrust ratio F/F_i, resultant gross-thrust ratio F_r/F_i, discharge coefficient C_d, and two resultant thrust vector angles—δ_p for pitch and δ_y for yaw. Reference 31 presents a detailed description of the data reduction procedures used for the current investigation.

The internal thrust ratio F/F_i is the ratio of the measured nozzle thrust along the body axis to the ideal nozzle thrust. Ideal thrust F_i is based on measured weight flow w_p, jet total pressure $p_{t,j}$, and jet total temperature $T_{t,j}$. (See the symbols section.) The balance axial-force measurement, from which the measured nozzle thrust F is subsequently obtained, is initially corrected for model weight tares and balance interactions. Although the bellows arrangement in the air pressurization system was designed to eliminate pressure and momentum interactions with the balance, small bellows tares on the six balance components still exist. These tares result from a small pressure difference between the ends of the bellows when air system internal velocities are high and from small differences in the spring constant of the forward and aft bellows when the bellows are pressurized. These bellows tares were determined by running Stratford choke calibration nozzles with known performance over a range of expected internal pressures and external forces and moments. The resulting tares were then applied to the six-component balance data obtained during the current investigation. Balance axial force obtained in this manner is a direct measurement of the thrust along the body axis. The procedure for computing the bellows tares is discussed in detail in reference 30.

The resultant thrust ratio F_r/F_i is the resultant gross thrust divided by the ideal thrust. Resultant gross thrust is obtained from the measured axial, normal, and side components of the jet resultant force. From the definitions of F and F_r, it is obvious that the thrust along the body axis F includes losses that result from turning the exhaust vector away from the axial direction, whereas the resultant gross thrust F_r does not.

The nozzle discharge coefficient C_d is the ratio of measured weight flow to ideal weight flow and reflects the ability of a nozzle to pass exhaust flow. The discharge coefficient is reduced by any momentum and vena contracta losses (effective throat area less than A_t). Nozzle throat area A_t is the measured geometric minimum area in the nozzle.

The resultant vector angles δ_p and δ_y are effective angles at which the thrust-vectoring mechanism turns the exhaust flow from the axial direction. As indicated in the symbols section, determination of these angles requires the measurement of axial, normal, and side forces on the model.

Results and Discussion

Gimballed Axisymmetric Nozzle

Internal static pressure distributions are presented in figures 10 and 11, and nozzle internal performance parameters are presented in figure 12 for the gimballed axisymmetric nozzle. Nozzle internal static pressure ratios $p/p_{t,j}$ are given in table 7 for each gimballed axisymmetric nozzle configuration and nozzle pressure ratio NPR tested.

The effect of nozzle pressure ratio on internal static pressure distributions is shown in figure 10. Ratios of static pressure to total pressure ahead of the nozzle ($x'/L < -0.266$) indicate exhaust Mach numbers less than 0.30 in the gimbal section. Internal static pressure distributions in the nozzle ($x'/L > -0.266$) exhibit trends typical of C-D nozzles (ref. 32). Typical of an overexpanded nozzle, a sudden pressure rise across an exhaust-flow shock occurs at about 35 percent of the divergent-flap length for NPR = 2.012. Exhaust-flow separation from the divergent flap probably occurs downstream of the shock. Since $(\text{NPR})_d = 8.81$ for the gimballed axisymmetric nozzle, the nozzle is overexpanded for all NPR's less than 8.81. For $4.011 \leq \text{NPR} < 8.81$, the shock has apparently moved downstream of the last static pressure orifice ($x'/L = 0.789$), and any associated pressure rise over the last 20 percent of the divergent-flap length is not measured.

The effect of geometric pitch thrust vector angle on the internal static pressure distributions of the gimballed Axi. nozzle is shown in figure 11. In general, except for a very slight increase in exhaust-flow expansion in the gimbal section, geometric pitch vector angle had no effect on nozzle static pressures. This might be expected since exhaust-flow turning occurs upstream of the nozzle in the gimbal section where exhaust-flow velocities are very low.

Since past studies have indicated that concepts with subsonic flow-turning mechanisms generally produce the highest thrust-vectoring performance (ref. 6), it might be expected that the gimballed Axi. nozzle will provide substantial levels of resultant thrust vector angle with only small thrust losses. The static pressure distributions shown in figure 11 also indicate that thrust-vectoring operation will have little effect on the gimballed Axi. nozzle performance.

The nozzle internal performance data shown in figure 12 indicate that the above hypotheses are valid. The effects of geometric pitch thrust vector angle on resultant thrust ratio F_r/F_i are negligible. The variation of F_r/F_i at high NPR (slightly outside an error band of 1/2 percent) was probably caused by a summation of measurement errors in F, F_N, and F_S (see the definition of F_r in the symbols section) for high pitch vector angles. The body-axis thrust ratio F/F_i, as expected, decreases with increasing $\delta_{v,p}$ since the thrust vector is being turned away from the body axis. Since the exhaust-flow-turning mechanism does not affect nozzle geometry, the nozzle discharge coefficient C_d is independent of both NPR and $\delta_{v,p}$. The magnitude of C_d is somewhat low when compared with that of other axisymmetric nozzles (refs. 11 and 28); the low discharge coefficient for the axisymmetric nozzle of the current investigation is probably caused by the sharp corner at the nozzle throat (ref. 33). The measured resultant thrust vector angles δ_p and δ_y were generally within 1° of the design geometric values.

Overall, the data presented in figure 12 indicate that a gimbal mechanism located in the tail pipe ahead of the nozzle is a highly effective thrust-vectoring device that results in little or no gross thrust F_r losses. Although the data were acquired for an axisymmetric nozzle, it is believed that similar results would also apply to a nonaxisymmetric nozzle.

SCF Two-Dimensional Convergent-Divergent Nozzle

Internal static pressure distributions are presented in figures 13 to 15, and nozzle internal performance parameters are presented in figures 16 to 21 for the SCF 2-D C-D nozzle configurations tested. Nozzle internal static pressure ratios $p/p_{t,j}$ are given in tables 8 to 47 for each nozzle configuration and nozzle pressure ratio tested.

The effects of nozzle pressure ratio on the internal static pressure distributions of the SCF 2-D C-D configurations are shown in figures 13 to 15. Static pressure distributions on the nozzle upper and lower flaps and on the nozzle sidewalls are similar to those reported from previous investigations of 2-D C-D nozzle types. (See ref. 34.) Ratios of static pressure to total pressure on the sides ($\phi = 90°$ and $270°$) of the transition section (fig. 7(a)) indicate an acceleration of the exhaust flow from Mach numbers of about 0.15 to 0.40 in the AR = 2.508 configurations (fig. 13) and from Mach numbers of about 0.15 to 0.50 in the AR = 2.083 and 1.265 configurations (figs. 14 and 15). Before accelerating to sonic conditions ($p/p_{t,j} = 0.528$) at the actual nozzle throat (the geometric nozzle throat is at $x'/L = 0$), the flow first decelerates in the aft portion of the transition section and in the forward portion of the spherical convergent-flap section. (See fig. 7(b).) The sidewall static pressure distributions near the nozzle throat indicate that exhaust-flow overexpansion may occur in the AR = 2.083 and 1.265 configurations and cause a pressure correction (compression) just upstream or at the geometric throat ($x'/L = 0$). This behavior could indicate a flow-separation bubble in the spherical convergent-flap section near the intersection of the spherical contour with the flat sidewalls of the rectangular opening. (See fig. 7(b).)

The actual nozzle throat (sonic line) appears to occur upstream of the geometric throat for the AR = 2.508 and 2.083 configurations and downstream of the geometric throat for the AR = 1.265 configurations. Downstream of the throat, the exhaust flow tends to expand smoothly down the nozzle sidewalls and divergent flaps until an exhaust-flow shock or other compression is encountered. The only significant effect of nozzle pressure ratio was on the existence and location of an exhaust-flow shock at NPR $\approx$ 2.0. For the $A_e/A_t = 1.46$ configurations, the nozzle is overexpanded for NPR < 5.92 and a strong shock occurs at about $x'/L = 0.40$ on the nozzle flaps and sidewalls for NPR $\approx$ 2.0. Similar to the axisymmetric nozzle discussed previously, exhaust-flow shocks at other NPR's below 5.92 occur downstream of the last static pressure orifice and thus are not measured. For the $A_e/A_t = 1.63$ configurations ($(\text{NPR})_d = 7.33$), the exhaust-flow shock at NPR $\approx$ 2.0 tends to move upstream in the nozzle (the nozzle is more highly overexpanded) to $x'/L \approx 0.32$. In addition to the exhaust-flow shock discussed above, a compression can be noted on the divergent flaps of all configurations aft of $x'/L = 0.60$. This compression may be associated with the cutback nozzle sidewalls that ended at $x'/L = 0.722$.

Except near the throat station ($-0.3 < x'/L < 0.3$) for AR = 2.508 configurations (fig. 13), the exhaust flow was generally symmetric in the nozzle from top to bottom and from side to side. Asymmetric pressure distributions were probably caused by slight fabrication differences in the spherical convergent-flap section near the nozzle throat.

The effects of nozzle pressure ratio on the various internal performance parameters shown in figures 16 to 21 are typical of those reported from previous studies of 2-D C-D nozzle types. (See refs. 11, 22, 25, 26, 33, and 34.) For cruise (unvectored) configurations, peak internal thrust ratio F/F_i and resultant thrust ratio F_r/F_i tend to occur near the design nozzle pressure ratio for each nozzle expansion ratio tested. (That is, $(\text{NPR})_d = 5.92$ for $A_e/A_t = 1.46$ and $(\text{NPR})_d = 7.33$ for $A_e/A_t = 1.63$.) Nozzle overexpansion losses occur at NPR below design, and nozzle underexpansion losses occur at NPR above design. As expected for NPR above choke (NPR > 1.89), the nozzle discharge coefficient was independent of NPR. The measured resultant yaw vector angle δ_y was nearly independent of NPR, but the resultant pitch vector angle δ_p varied up to 8° with varying NPR. The independence of δ_y with NPR suggests that yaw flow turning is being accomplished in the subsonic exhaust flow upstream of the nozzle throat (spherical convergent-flap gimbal section) rather than on the nozzle sidewalls downstream of the throat where an impact on thrust performance might occur. This effect will be discussed in more detail in a later section of this paper. The dependence of δ_p with NPR is common in nonaxisymmetric nozzles whenever one flap is longer than the other relative to the exhaust-flow centerline. (See ref. 33.) This is the case for the SCF 2-D C-D nozzle of the current investigation when geometric pitch vector angle is not equal to zero. (See fig. 7(c).) This type of nozzle geometry presents expansion surfaces of unequal length for the exhaust flow to work against, with the result that one side of the flow is contained longer by a solid surface (the lower divergent flap in this investigation) while the other side of the exhaust flow is unbounded.

The separate effects of geometric thrust vector angles, expansion ratio, and nozzle throat aspect ratio on nozzle performance will be discussed in more detail in later sections of this paper. However, even a cursory examination of figures 16 to 21 indicates that the SCF 2-D C-D multiaxis vectoring-nozzle concept provides excellent internal performance. Measured resultant thrust vector angles were nearly equal to the geometric thrust vector angles for both pitch and yaw, thus indicating highly effective flow-turning mechanisms. Resultant thrust losses due to thrust vectoring were small or negligible, thus indicating very efficient flow-turning mechanisms. Peak cruise (unvectored) nozzle performance was equal to levels reported from other investigations on standard

2-D C-D nozzles that had two-dimensional (rectangular) convergent-flap sections and no yaw gimbal mechanism. (See refs. 22, 25, 27, 33, and 34.) In short, the SCF 2-D C-D nozzle appears to be highly competitive with other multiaxis thrust-vectoring nozzle concepts.

Effect of geometric thrust vector angles. The effects of geometric pitch and yaw thrust vector angles on nozzle performance are presented in figure 22. The data in figure 22 were obtained by cross plots of the data presented in figures 16 to 21 at the design nozzle pressure ratio for each nozzle expansion ratio. Thus, the plots of F_r/F_i represent near-peak values. (The nozzle over- and under-expansion losses equal zero.)

Increasing the geometric yaw vector angle produced a nearly linear and directly proportional increase in resultant yaw vector angle with little or no effect on resultant thrust ratio. This result indicates that a gimbal mechanism upstream of the nozzle throat is a very effective and efficient flow-turning device. Increasing $\delta_{v,y}$ had little or no effect on nozzle discharge coefficient C_d except for the highest geometric yaw vector angle tested on the AR = 2.083 and 1.265 nozzle configurations. For the AR = 2.083 and 1.265 configurations, the fixed-transition section (see fig. 7(a)) started to intrude into the nozzle throat on the left side of the nozzle flow path (see fig. 9) at the highest value of $\delta_{v,y}$ tested. This intrusion caused a reduction in actual nozzle throat area (the geometric nozzle throat defined at $x' = 0$) and a corresponding decrease in C_d (defined as w_p/w_i, where w_i is based on the geometric throat area, as seen in the symbols section).

Increasing $\delta_{v,y}$ caused a slight increase in measured resultant pitch vector angle δ_p. This increase is an apparent increase rather than a real increase in pitch flow-turning capability. As $\delta_{v,y}$ is increased, the axial thrust component F is decreased because part of the jet momentum is converted to a side-force component F_S. Although not shown, the normal-force component F_N remains nearly constant during this process. Therefore, resultant pitch vector angle δ_p (a function of F_N/F) increases as the axial component F decreases. (See the symbols section.)

Increasing geometric pitch thrust vector angle $\delta_{v,p}$ produces large values of resultant pitch vector angle δ_p that are somewhat dependent on nozzle expansion ratio. Geometric pitch thrust vector angle had little or no effect on peak resultant thrust ratio. These results were expected since previous investigations have shown that divergent-flap rotation is an effective and efficient method of providing a pitch thrust-vectoring capability for 2-D C-D nozzles. (See ref. 22.) Increasing $\delta_{v,p}$ decreased nozzle discharge coefficient C_d, probably because of a sharper throat corner on the lower divergent flap and a shifting of the actual throat location on the upper divergent flap. Geometric pitch vector angle had little or no effect on measured resultant yaw vector angle. However, because of the decrease in F (the axial component of thrust) that occurs as $\delta_{v,p}$ increases, the actual side-force thrust component F_S decreases with increasing $\delta_{v,p}$. Even though the resultant thrust vector angles δ_p and δ_y have apparent values that are too high (results from definition of terms) when simultaneous pitch and yaw thrust vectoring occur, it is still obvious that large amounts of control power (in the form of F_N and F_S) are generated by the multiaxis thrust-vectoring SCF 2-D C-D nozzle concept.

The effects of geometric pitch and yaw vector angles on the nozzle internal static pressure distributions are presented in figure 23. Geometric yaw vector angle $\delta_{v,y}$ had little effect on the internal static pressure distributions except on the left sidewall near and upstream of the throat. The left side of the nozzle throat plane moves into closer proximity with the fixed transition section (see fig. 9) as $\delta_{v,y}$ increases. The absence of any effects on the static pressure distributions downstream of the throat indicates that flow turning in the yaw plane is being accomplished by the gimbal mechanism in the subsonic flow region ahead of the nozzle throat. Previous studies have shown that very low thrust losses are associated with subsonic flow turning (refs. 6 and 22).

Increasing the geometric pitch vector angle $\delta_{v,p}$ (rotating the divergent flaps down) increased the static pressures on the upper divergent flap (see fig. 23(a)) up to $x'/L = 0.6$ and decreased the static pressures on the lower divergent flap up to $x'/L = 0.3$. The net result is a positive pressure increment (produces positive F_N) between the upper and lower flaps up to $x'/L = 0.5$. This static pressure increment is very large near the geometric throat. The actual throat (sonic line) rotates about the lower divergent-flap wall, thus becoming inclined in the pitch plane relative to the nozzle centerline. For the configuration shown in figure 23, the throat ($p/p_{t,j} = 0.528$) has moved from $x'/L = 0$ to $x'/L = 0.24$ on the upper divergent flap. Although not defined by the limited static pressure instrumentation, the throat probably remains at $x'/L = 0$ on the lower divergent flap. This inclination of the throat plane when $\delta_{v,p} \neq 0°$ indicates that part of the pitch flow-turning process occurs in the subsonic flow region ahead of the nozzle throat. As stated previously, low thrust losses are generally associated with subsonic flow turning.

Increasing $\delta_{v,p}$ also increased static pressures on the nozzle sidewalls (fig. 23(b)). However, as shown in figure 9, the sidewall does not rotate with the divergent flaps as $\delta_{v,p}$ is increased, and thus the sidewall static pressure orifices are physically closer to the high pressures on the upper divergent flap when $\delta_{v,p} > 0°$. (See fig. 23(a) which shows the upper-flap data for $x'/L < 0.6$.) For the data shown in figure 23(b), the sides of the divergent flap actually cover the last two sidewall static pressure orifices (both sidewalls) when $\delta_{v,p} = 25°$, and thus these data are not shown.

Effect of nozzle expansion ratio. Figure 24 presents the effect of nozzle expansion ratio on the flow-turning (thrust-vectoring) capabilities of the SCF 2-D C-D nozzle concept. Data are shown at the design nozzle pressure ratio for each expansion ratio A_e/A_t tested. Except for resultant pitch vector angle when the nozzle was pitch vectored, nozzle expansion ratio had no effect on the flow-turning capabilities of the nozzle. During the pitch-vectoring operation, increasing the nozzle expansion ratio increased the resultant pitch vector angle. During positive pitch thrust-vectoring operation, the lower divergent flap generally has lower static pressures than the upper divergent flap. (See fig. 23.) For this reason, the exhaust flow tends to be forced toward the wall of the lower divergent flap. For equal values of geometric pitch vector angle, the divergence half-angle α of the lower divergent flap is larger for higher nozzle expansion ratios. (See fig. 7(c).) Thus, the exhaust flow tends to turn through a larger turning angle for the $A_e/A_t = 1.63$ configurations than for the $A_e/A_t = 1.46$ configurations and results in larger values of δ_p.

Effect of nozzle throat aspect ratio. The effects of nozzle throat aspect ratio AR on nozzle performance and internal static pressure distributions are presented in figures 25 and 26, respectively. Results reported in reference 27 indicate that the effect of nozzle throat aspect ratio (which varied from 1.65 to 4.40) on F_r/F_i and C_d was small (less than 1.5 percent). Results from the current investigation (see fig. 25) indicate a similar conclusion. Resultant thrust ratio and discharge coefficient generally varied less than 1 percent over the throat aspect-ratio range of the current investigation. The slight decrease in F_r/F_i as AR was decreased was probably caused by two factors. First, the wetted area of the divergent-flap section increased with decreasing AR (i.e., the divergent flaps became longer as shown in fig. 7(c)). Thus, friction losses were higher for the lower AR nozzles. Second, as shown in figure 26, static pressures (especially on the nozzle sidewall) tended to expand to lower values (higher exhaust velocities and thus viscous losses) with decreasing AR, and a pressure adjustment shock (with attendant losses) appears to occur on the AR = 1.265 nozzle near the sidewall trailing edge (which does not occur on the higher AR nozzle configurations).

Variations in C_d appear to be associated with changes in geometry upstream of and near the nozzle throat. Figure 26 indicates large static pressure variations with varying AR in the region of x'/L from -0.3 to 0.2. In fact, separation bubbles (indicated by sharp compression regions near the throat) may exist for the AR = 1.265 and 2.083 configurations. The movement of the actual throat (the actual throat or sonic line is located at the x'/L station where $p/p_{t,j} = 0.528$) and the existence of separation bubbles could result in a reduction in actual throat area (as opposed to geometric A_t) and nozzle discharge coefficient.

In general, the effect of nozzle throat aspect ratio on resultant thrust vector angles (δ_p and δ_y) was small. The only significant variation measured was at $\delta_{v,p} = 25°$ for the $A_e/A_t = 1.46$ nozzle (fig. 25(b)); for this configuration, δ_p decreased about 1.5° as AR was increased from 1.265 to 2.508. Although this amount of variation is still considered to be small, it was an unexpected result since it was believed that the wider divergent flaps of the higher AR configurations would provide higher values of δ_p rather than lower values. The cause of this slight anomaly is not currently known; however, it may be related to the fact that divergent-flap length decreases as nozzle aspect ratio increases. (See fig. 7.) Thus, the higher aspect-ratio nozzles did not have as much length in which to turn the flow through a geometric pitch vector angle. It should be noted that divergent-flap surface areas were approximately the same for all three throat aspect ratios tested.

Conclusions

A static (no external flow) test has been conducted in the static test facility of the Langley 16-Foot Transonic Tunnel to evaluate the internal performance of an axisymmetric convergent-divergent nozzle and a nonaxisymmetric convergent-divergent nozzle, both of which utilized a gimbal-type mechanism to provide a thrust-vectoring capability in at least one plane. The test was conducted at nozzle pressure ratios from 2.0 to approximately 12.0. The results of this investigation indicate the following conclusions:

1. A gimbal-type mechanism located upstream of the throat of an axisymmetric or nonaxisymmetric nozzle is a highly effective and efficient thrust-vectoring device. The gimbal concepts of this investigation produced measured resultant thrust vector angles equal to the geometric thrust vector angles (up to 25°) with little or no loss in resultant gross thrust.

2. Varying gimbal thrust vector angle had little effect on the internal static pressure distributions in the divergent section of the nozzles. This result indicates that the gimbal concept provides a thrust-vectoring capability by highly efficient subsonic flow turning upstream of the nozzle throat.

3. For the nonaxisymmetric nozzle, use of divergent-flap rotation for pitch thrust vectoring provided resultant vector angles which, although dependent on nozzle pressure ratio, were nearly equal to the geometric pitch vector angle. Also, the losses in resultant gross thrust due to pitch vectoring were small or negligible.

4. For the nonaxisymmetric nozzle operating at design pressure ratio, increasing the expansion ratio increased the resultant pitch vector angle during the pitch thrust-vectoring operation. The effect of nozzle expansion ratio on all other performance parameters was small.

5. Varying the throat aspect ratio of the nonaxisymmetric nozzle had only small effects on nozzle performance.

NASA Langley Research Center
Hampton, VA 23665-5225
February 26, 1990

References

1. Capone, Francis J.: Summary of Propulsive-Lift Research in the Langley 16-Ft. Transonic Tunnel. *J. Aircr.*, vol. 13, no. 10, Oct. 1976, pp. 803–808.
2. Berrier, Bobby L.; Palcza, J. Lawrence; and Richey, G. Keith: Nonaxisymmetric Nozzle Technology Program—An Overview. AIAA Paper 77-1225, Aug. 1977.
3. Hiley, P. E.; Wallace, H. W.; and Booz, D. E.: Study of Non-Axisymmetric Nozzles Installed in Advanced Fighter Aircraft. AIAA Paper No. 75-1316, Sept.–Oct. 1975.
4. Lander, J. A.; and Palcza, J. Lawrence: Exhaust Nozzle Deflector Systems for V/STOL Fighter Aircraft. AIAA Paper No. 74-1169, Oct. 1974.
5. Wasson, H. R.; Hall, G. R.; and Palcza, J. L.: Results of a Feasibility Study To Add Canards and ADEN Nozzle to the YF-17. AIAA Paper 77-1227, Aug. 1977.
6. Berrier, B. L.; and Re, R. J.: A Review of Thrust-Vectoring Schemes for Fighter Aircraft. AIAA Paper No. 78-1023, July 1978.
7. Capone, Francis J.: The Nonaxisymmetric Nozzle—It Is for Real. AIAA Paper 79-1810, Aug. 1979.
8. Richey, G. K.; Surber, L. E.; and Berrier, B. L.: Airframe-Propulsion Integration for Fighter Aircraft. AIAA-83-0084, Jan. 1983.
9. Nelson, B. D.; and Nicolai, L. M.: Application of Multi-Function Nozzles to Advanced Fighters. AIAA-81-2618, Dec. 1981.
10. *F-15 2-D Nozzle System Integration Study. Volume I—Technical Report.* NASA CR-145295, 1978.
11. Capone, Francis J.; and Berrier, Bobby L.: *Investigation of Axisymmetric and Nonaxisymmetric Nozzles Installed on a 0.10-Scale F-18 Prototype Airplane Model.* NASA TP-1638, 1980.
12. Herbst, W. B.: Future Fighter Technologies. *J. Aircr.*, vol. 17, no. 8, Aug. 1980, pp. 561–566.
13. Lacey, David W.: *Air Combat Advantages From Reaction Control Systems.* SAE Tech. Paper Ser. 801177, Oct. 1980.
14. White, S. N.: *Feasibility Study for Integrating Thrust Vectoring as Primary Flight Control System.* NASA CR-165758, 1981.
15. Kraus, W.; Przibilla, H.; and Haux, U.: Stability and Control for High Angle of Attack Maneuvering. *Criteria for Handling Qualities of Military Aircraft*, AGARD-CP-333, June 1982, pp. 15-1–15-11.
16. Herbst, W. B.: Supermaneuverability. *Workshop on Unsteady Separated Flow, Michael S. Francis and Marvin W. Luttges, eds.*, AFOSR-TR-84-0911, U.S. Air Force, May 1984, pp. 1–9. (Available from DTIC as AD P004 153.)
17. Joshi, Dinesh S.; Shaw, Peter D.; Hodgkinson, John; Rock, Steven M.; Vincent, James H.; and Fisk, William S.: *A Design Approach to Integrated Flight and Propulsion Control.* SAE Tech. Paper Ser. 831482, Oct. 1983.
18. Hienz, Egon; and Vedova, Ralph: Requirements, Definition and Preliminary Design for an Axisymmetric Vectoring Nozzle, To Enhance Aircraft Maneuverability. AIAA-84-1212, June 1984.
19. Miller, L. Earl: *Post Stall Maneuvers and Thrust Vectoring Performance Analysis.* AFWAL-TR-84-3109, U.S. Air Force, July 1984. (Available from DTIC as AD A158 100.)
20. Herrick, Paul W.: Propulsion Influences on Air Combat. AIAA-85-1457, July 1985.
21. Gallaway, C. R.; and Osborn, R. F.: Aerodynamics Perspective of Supermaneuverability. AIAA-85-4068, Oct. 1985.
22. Berrier, Bobby L.: Results From NASA Langley Experimental Studies of Multiaxis Thrust Vectoring Nozzles. *SAE 1988 Transactions—Journal of Aerospace*, Section 1—Volume 97, c.1989, pp. 1.1289–1.1304. (Available as SAE Paper 881481.)
23. Rolls, L. Stewart; and Aoyagi, Kiyoshi: Experimental Investigations of Thrust Vectoring Systems for VTOL Aircraft. AIAA Paper 77-805, July 1977.
24. Hiley, P. E.; Wallace, H. W.; and Booz, D. E.: Nonaxisymmetric Nozzles Installed in Advanced Fighter Aircraft. *J. Aircr.*, vol. 13, no. 12, Dec. 1976, pp. 1000–1006.
25. Mason, Mary L.; and Berrier, Bobby L.: *Static Investigation of Several Yaw Vectoring Concepts on Nonaxisymmetric Nozzles.* NASA TP-2432, 1985.

26. Capone, Francis J.; and Mason, Mary L.; *Multiaxis Aircraft Control Power From Thrust Vectoring at High Angles of Attack.* NASA TM-87741, 1986.
27. Mason, Mary L.; and Berrier, Bobby L.: *Static Performance of Nonaxisymmetric Nozzles With Yaw Thrust-Vectoring Vanes.* NASA TP-2813, 1988.
28. Berrier, Bobby L.; and Mason, Mary L.: *Static Performance of an Axisymmetric Nozzle With Post-Exit Vanes for Multiaxis Thrust Vectoring.* NASA TP-2800, 1988.
29. Capone, Francis J.: *Effects of Nozzle Exit Location and Shape on Propulsion-Induced Aerodynamic Characteristics Due to Vectoring Twin Nozzles at Mach Numbers From 0.40 to 1.2.* NASA TM X-3313, 1976.
30. Peddrew, Kathryn H., compiler: *A User's Guide to the Langley 16-Foot Transonic Tunnel.* NASA TM-83186, 1981.
31. Mercer, Charles E.; Berrier, Bobby L.; Capone, Francis J.; Grayston, Alan M.; and Sherman, C. D.: *Computations for the 16-Foot Transonic Tunnel—NASA, Langley Research Center, Revision 1.* NASA TM-86319, 1987. (Supersedes NASA TM-86319, 1984.)
32. Shapiro, Ascher H.: *The Dynamics and Thermodynamics of Compressible Fluid Flow,* Volume I. Ronald Press Co., c.1953.
33. Re, Richard J.; and Leavitt, Laurence D.: *Static Internal Performance Including Thrust Vectoring and Reversing of Two-Dimensional Convergent-Divergent Nozzles.* NASA TP-2253, 1984.
34. Berrier, Bobby L.; and Re, Richard J.; *Effect of Several Geometric Parameters on the Static Internal Performance of Three Nonaxisymmetric Nozzle Concepts.* NASA TP-1468, 1979.

Table 1. List of Nozzle Configurations Tested

Nozzle type	AR	A_e/A_t	$\delta_{v,y}$, deg	$\delta_{v,p}$ 0°	10°	20°	25°
Nonaxisymmetric	2.508	1.46	0	X			X
	↓	1.46	7	X			X
		1.46	15	X			X
		1.63	0	X			X
		1.63	7	X			X
		1.63	15	X			X
	2.083	1.46	0	X			X
	↓	↓	7	X			X
			15	X			X
			20	X			X
		1.63	0	X		X	
		↓	7	X		X	
			15	X		X	
			20	X		X	
	1.265	1.46	0	X			X
	↓	1.46	15	X			X
		1.46	25	X			X
		1.63	0	X			X
		1.63	15	X			X
		1.63	25	X			X
Axisymmetric		1.80	0	X	X	X	X

Table 2. Static Pressure Orifice Locations on Divergent Flaps of SCF Nonaxisymmetric Nozzle Concept

(a) AR = 2.508

$A_e/A_t = 1.46$

	Upper flap					Lower flap			
	$\delta_{v,p} = 0^o$		$\delta_{v,p} = 25^o$			$\delta_{v,p} = 0^o$		$\delta_{v,p} = 25^o$	
y, in.	x, in.	Sta, in.	x, in.	Sta, in.	y, in.	x, in.	Sta, in.	x, in.	Sta, in.
0.740	1.017	44.347	0.960	44.290	0.740	1.017	44.347	0.883	44.213
0.740	2.033	45.363	1.919	45.249	0.740	2.033	45.363	1.766	45.096
0.000	0.610	43.940	0.575	43.905	0.000	0.610	43.940	0.530	43.860
	1.220	44.550	1.152	44.482		1.220	44.550	1.060	44.390
	1.830	45.160	1.727	45.057		1.830	45.160	1.590	44.920
	2.440	45.770	2.303	45.633		2.440	45.770	2.120	45.450
-0.740	1.017	44.347	0.960	44.290	-0.740	1.017	44.347	0.883	44.213
-0.740	2.033	45.363	1.919	45.249	-0.740	2.033	45.363	1.766	45.096

$A_e/A_t = 1.63$

	Upper flap					Lower flap			
	$\delta_{v,p} = 0^o$		$\delta_{v,p} = 25^o$			$\delta_{v,p} = 0^o$		$\delta_{v,p} = 25^o$	
y, in.	x, in.	Sta, in.	x, in.	Sta, in.	y, in.	x, in.	Sta, in.	x, in.	Sta, in.
0.740	1.013	44.343	0.971	44.301	0.740	1.013	44.343	0.866	44.196
0.740	2.026	45.356	1.941	45.271	0.740	2.026	45.356	1.731	45.061
0.000	0.607	43.937	0.582	43.912	0.000	0.607	43.937	-0.519	43.849
	1.216	44.546	1.165	44.495		1.216	44.546	1.039	44.369
	1.823	45.153	1.747	45.077		1.823	45.153	1.558	44.888
	2.432	45.762	2.330	45.660		2.432	45.762	2.078	45.408
-0.740	1.013	44.343	0.971	44.301	-0.740	1.013	44.343	0.866	44.196
-0.740	2.026	45.356	1.941	45.271	-0.740	2.026	45.356	1.731	45.061

Table 2. Continued

(b) AR = 2.083

$A_e/A_t = 1.46$									
Upper flap					Lower flap				
	$\delta_{v,p} = 0^o$		$\delta_{v,p} = 25^o$			$\delta_{v,p} = 0^o$		$\delta_{vp} = 25^o$	
y, in.	x, in.	Sta, in.	x, in.	Sta, in.	y, in.	x, in.	Sta, in.	x, in.	Sta, in.
0.675	1.117	44.417	1.054	44.354	0.675	1.117	44.417	0.970	44.270
0.675	2.233	45.533	2.108	45.408	0.675	2.233	45.533	1.940	45.240
0.000	0.670	43.970	0.633	43.933	0.000	0.670	43.970	0.582	43.882
	1.340	44.640	1.265	44.565		1.340	44.640	1.164	44.464
	2.010	45.310	1.897	45.197		2.010	45.310	1.746	45.046
	2.679	45.979	2.529	45.829		2.679	45.979	2.328	45.628
-0.675	1.117	44.417	1.054	44.354	-0.675	1.117	44.417	0.970	44.270
-0.675	2.233	45.533	2.108	45.408	-0.675	2.233	45.533	1.940	45.240
$A_e/A_t = 1.63$									
Upper flap					Lower flap				
	$\delta_{v,p} = 0^o$		$\delta_{v,p} = 20^o$			$\delta_{v,p} = 0^o$		$\delta_{v,p} = 20^o$	
y, in.	x, in.	Sta, in.	x, in.	Sta, in.	y, in.	x, in.	Sta, in.	x, in.	Sta, in.
0.675	1.113	44.413	1.092	44.392	0.675	1.113	44.413	0.999	44.299
0.675	2.225	45.525	2.184	45.484	0.675	2.225	45.525	1.998	45.298
0.000	0.668	43.968	0.656	43.956	0.000	0.668	43.968	0.600	43.900
	1.335	44.635	1.310	44.610		1.335	44.635	1.199	44.499
	2.003	45.303	1.966	45.266		2.003	45.303	1.798	45.098
	2.670	45.970	2.621	45.921		2.670	45.970	2.397	45.697
-0.675	1.113	44.413	1.092	44.392	-0.675	1.113	44.413	0.999	44.299
-0.675	2.225	45.525	2.184	45.484	-0.675	2.225	45.525	1.998	45.298

Table 2. Concluded

(c) AR = 1.265

$A_e/A_t = 1.46$									
Upper flap					Lower flap				
	$\delta_{v,p} = 0^{\circ}$		$\delta_{v,p} = 25^{\circ}$			$\delta_{v,p} = 0^{\circ}$		$\delta_{v,p} = 25^{\circ}$	
y, in.	x, in.	Sta, in.	x, in.	Sta, in.	y, in.	x, in.	Sta, in.	x, in.	Sta, in.
0.525	1.416	44.634	1.337	44.555	0.525	1.416	44.634	1.230	44.448
0.525	2.834	45.052	2.676	45.894	0.525	2.834	45.052	2.461	45.679
0.000	0.850	44.068	0.802	44.020	0.000	0.850	43.068	0.738	43.956
	1.700	44.918	1.605	44.823		1.700	44.918	1.476	44.694
	2.550	45.768	2.408	45.626		2.550	45.768	2.214	45.432
	3.400	46.618	3.211	46.429		3.400	46.618	2.953	46.171
-0.525	1.416	44.634	1.337	44.555	-0.525	1.416	44.634	1.230	44.448
-0.525	2.834	46.052	2.676	45.894	-0.525	2.834	46.052	2.461	45.679

$A_e/A_t = 1.63$									
Upper flap					Lower flap				
	$\delta_{v,p} = 0^{\circ}$		$\delta_{v,p} = 25^{\circ}$			$\delta_{v,p} = 0^{\circ}$		$\delta_{v,p} = 25^{\circ}$	
y, in.	x, in.	Sta, in.	x, in.	Sta, in.	y, in.	x, in.	Sta, in.	x, in.	Sta, in.
0.525	1.411	44.629	1.353	44.571	0.525	1.411	44.629	1.205	44.423
0.525	2.824	46.042	2.706	45.924	0.525	2.824	46.042	2.412	45.630
0.000	0.847	44.065	0.811	44.029	0.000	0.847	44.065	0.723	43.941
	1.694	44.912	1.624	44.842		1.694	44.912	1.447	44.665
	2.541	45.759	2.435	45.653		2.541	45.759	2.170	45.388
	3.388	46.606	3.248	46.466		3.388	46.606	2.894	46.112
-0.525	1.411	44.629	1.353	44.571	-0.525	1.411	44.629	1.205	44.423
-0.525	2.824	46.042	2.706	45.924	-0.525	2.824	46.042	2.412	45.630

Table 3. Static Pressure Orifice Locations on Sidewalls of SCF Nonaxisymmetric Nozzle Concept

WL, in.	AR = 2.508		AR = 2.083		AR = 1.265	
	Both sidewalls					
	x, in.	Sta, in.	x, in.	Sta, in.	x, in.	Sta, in.
0	0.244	43.574	0.269	43.569	0.341	43.559
↓	.488	43.818	.538	43.838	0.682	43.900
↓	.733	44.063	.807	44.107	1.023	44.241
↓	.977	44.307	1.076	44.376	1.364	44.582
↓	1.222	44.552	1.344	44.644	1.706	44.924
↓	1.466	44.796	1.613	44.913	2.047	45.265
↓	1.711	45.041	1.882	45.182	2.388	45.606
↓	1.955	45.285	2.151	45.451	2.729	45.947

Table 4. Static Pressure Orifice Locations on Gimballed Axisymmetric Nozzle Concept

$\delta_{v,p} = 0°$	$\delta_{v,p} = 10°$	$\delta_{v,p} = 20°$	$\delta_{v,p} = 25°$
Stations for bottom row, x'/L, at—			
−0.617	−0.562	−0.581	−0.547
−.493	−.448	−.455	−.429
−.369	−.342	−.328	−.310
−.055	−.055	−.055	−.055
.156	.156	.156	.156
.367	.367	.367	.367
.578	.578	.578	.578
.789	.789	.789	.789
Stations for top row, x'/L, at—			
−0.493	−0.569	−0.540	−0.585
−.369	−.433	−.390	−.432
−.316	−.354	−.286	−.322
−.055	−.055	−.055	−.055
.156	.156	.156	.156
.367	.367	.367	.367
.578	.578	.578	.578
.789	.789	.789	.789

Table 5. Static Pressure Orifice Locations on Divergent Flaps of SCF Concept

(a) AR = 2.508

$A_e/A_t = 1.46$					
Upper flap			Lower flap		
y/L	x'/L at $\delta_{v,p} = 0°$	x'/L at $\delta_{v,p} = 25°$	y/L	x'/L at $\delta_{v,p} = 0°$	x'/L at $\delta_{v,p} = 25°$
0.50	0.333	0.315	0.50	0.333	0.290
.50	.667	.629	.50	.667	.579
0	.200	.189	0	.200	.174
$\vert$	.400	.378	$\vert$	.400	.348
$\vert$	.600	.566	$\vert$	.600	.521
$\downarrow$	.800	.755	$\downarrow$	.800	.695
−.50	.333	.315	−.50	.333	.290
−.50	.667	.629	−.50	.667	.579

$A_e/A_t = 1.63$					
Upper flap			Lower flap		
y/L	x'/L at $\delta_{v,p} = 0°$	x'/L at $\delta_{v,p} = 25°$	y/L	x'/L at $\delta_{v,p} = 0°$	x'/L at $\delta_{v,p} = 25°$
0.50	0.333	0.320	0.50	0.333	0.285
.50	.667	.639	.50	.667	.570
0	.200	.192	0	.200	.171
$\vert$	.400	.383	$\vert$	.400	.342
$\vert$	.600	.575	$\vert$	.600	.513
$\downarrow$	.800	.767	$\downarrow$	.800	.684
−.50	.333	.320	−.50	.333	.285
−.50	.667	.639	−.50	.667	.570

Table 5. Continued

(b) AR = 2.083

$A_e/A_t = 1.46$					
Upper flap			Lower flap		
y/L	x'/L at $\delta_{v,p} = 0°$	x'/L at $\delta_{v,p} = 25°$	y/L	x'/L at $\delta_{v,p} = 0°$	x'/L at $\delta_{v,p} = 25°$
0.50	0.333	0.315	0.50	0.333	0.290
.50	.667	.629	.50	.667	.579
0	.200	.189	0	.200	.174
↓	.400	.378	↓	.400	.348
	.600	.566		.600	.521
	.800	.755		.800	.695
−.50	.333	.315	−.50	.333	.290
−.50	.667	.629	−.50	.667	.579

$A_e/A_t = 1.63$					
Upper flap			Lower flap		
y/L	x'/L at $\delta_{v,p} = 0°$	x'/L at $\delta_{v,p} = 20°$	y/L	x'/L at $\delta_{v,p} = 0°$	x'/L at $\delta_{v,p} = 20°$
0.50	0.333	0.327	0.50	0.333	0.299
.50	.667	.654	.50	.667	.599
0	.200	.197	0	.200	.180
↓	.400	.392	↓	.400	.359
	.600	.589		.600	.539
	.800	.785		.800	.718
−.50	.333	.327	−.50	.333	.299
−.50	.667	.654	−.50	.667	.599

Table 5. Concluded

(c) AR = 1.265

$A_e/A_t = 1.46$					
Upper flap			Lower flap		
y/L	x'/L at $\delta_{v,p} = 0°$	x'/L at $\delta_{v,p} = 25°$	y/L	x'/L at $\delta_{v,p} = 0°$	x'/L at $\delta_{v,p} = 25°$
0.50	0.333	0.315	0.50	0.333	0.289
.50	.667	.629	.50	.667	.579
0	.200	.189	0	.200	.174
↓	.400	.378	↓	.400	.347
↓	.600	.567	↓	.600	.521
↓	.800	.756	↓	.800	.695
−.50	.333	.315	−.50	.333	.289
−.50	.667	.630	−.50	.667	.579

$A_e/A_t = 1.63$					
Upper flap			Lower flap		
y/L	x'/L at $\delta_{v,p} = 0°$	x'/L at $\delta_{v,p} = 25°$	y/L	x'/L at $\delta_{v,p} = 0°$	x'/L at $\delta_{v,p} = 25°$
0.50	0.333	0.319	0.50	0.333	0.285
.50	.667	.639	.50	.667	.570
0	.200	.191	0	.200	.171
↓	.400	.383	↓	.400	.342
↓	.600	.575	↓	.600	.512
↓	.800	.767	↓	.800	.683
−.50	.333	.319	−.50	.333	.285
−.50	.667	.639	−.50	.667	.570

Table 6. Static Pressure Orifice Locations on Sides of SCF Concept

AR = 2.508		AR = 2.083		AR = 1.265	
Values of x'/L at—		Values of x'/L at—		Values of x'/L at—	
$A_e/A_t = 1.46$	$A_e/A_t = 1.63$	$A_e/A_t = 1.46$	$A_e/A_t = 1.63$	$A_e/A_t = 1.46$	$A_e/A_t = 1.63$
−0.430	−0.431	−0.382	−0.383	−0.282	−0.283
−.318	−.319	−.281	−.282	−.194	−.195
−.207	−.207	−.179	−.180	−.106	−.106
−.095	−.095	−.078	−.078	−.018	−.018
.080	.080	.080	.081	.080	.081
.160	.161	.161	.161	.160	.161
.240	.241	.241	.242	.241	.242
.320	.321	.321	.322	.321	.322
.401	.402	.401	.403	.401	.403
.481	.482	.481	.483	.482	.483
.561	.563	.562	.564	.562	.564
.641	.643	.642	.644	.642	.644

Table 7. Nozzle Internal Static Pressure Ratios $p/p_{t,j}$ for Gimballed Axi. Nozzle

(a) $\delta_{v,p} = 0°$

x'/L, top row

NPR	-0.493	-0.369	-0.316	-0.055	0.156	0.367	0.578	0.789
2.012	0.980	0.983	0.980	0.906	0.337	0.212	0.358	0.432
4.011	0.988	0.951	0.972	0.902	0.334	0.196	0.188	0.139
5.997	0.990	0.962	0.978	0.902	0.333	0.195	0.182	0.137
6.999	0.989	0.973	0.980	0.902	0.333	0.195	0.178	0.136
8.010	0.991	0.979	0.985	0.902	0.333	0.194	0.180	0.136
8.996	0.992	0.985	0.987	0.901	0.332	0.194	0.184	0.135
9.901	0.992	0.983	0.986	0.901	0.332	0.194	0.184	0.135
11.007	0.992	0.981	0.987	0.901	0.332	0.194	0.182	0.135
11.495	0.992	0.977	0.987	0.901	0.332	0.194	0.174	0.135

x'/L, bottom row

NPR	-0.617	-0.493	-0.369	-0.055	0.156	0.367	0.789
2.012	0.997	0.994	0.995	0.908	0.343	0.221	0.425
4.011	0.995	0.994	0.994	0.908	0.338	0.195	0.137
5.997	0.994	0.994	0.994	0.907	0.337	0.193	0.136
6.999	0.994	0.994	0.994	0.906	0.337	0.192	0.135
8.010	0.994	0.994	0.994	0.906	0.337	0.192	0.135
8.996	0.994	0.994	0.994	0.906	0.338	0.191	0.135
9.901	0.994	0.994	0.994	0.906	0.338	0.191	0.135
11.007	0.994	0.994	0.994	0.906	0.338	0.190	0.134
11.495	0.993	0.993	0.994	0.906	0.337	0.190	0.134

(b) $\delta_{v,p} = 10°$

x'/L, top row

NPR	-0.569	-0.433	-0.354	-0.055	0.156	0.367	0.578	0.789
1.990	1.000	0.955	0.973	0.906	0.326	0.216	0.360	0.431
4.009	0.985	0.952	0.966	0.905	0.324	0.196	0.182	0.137
6.009	0.990	0.972	0.980	0.904	0.324	0.195	0.179	0.135
7.095	0.990	0.963	0.978	0.903	0.324	0.195	0.174	0.135
8.010	0.992	0.976	0.982	0.903	0.324	0.195	0.170	0.135
9.005	0.991	0.976	0.982	0.903	0.325	0.194	0.175	0.134
9.943	0.992	0.974	0.982	0.903	0.324	0.195	0.162	0.135
11.031	0.993	0.976	0.985	0.902	0.324	0.195	0.159	0.135
11.487	0.993	0.980	0.988	0.903	0.325	0.194	0.167	0.134
11.544	0.993	0.978	0.986	0.902	0.324	0.195	0.158	0.134

x'/L, bottom row

NPR	-0.562	-0.448	-0.342	-0.055	0.156	0.367	0.789
1.990	0.992	0.992	0.992	0.905	0.338	0.227	0.433
4.009	0.992	0.994	0.994	0.906	0.334	0.194	0.137
6.009	0.991	0.993	0.994	0.905	0.334	0.193	0.136
7.095	0.991	0.993	0.995	0.906	0.334	0.192	0.136
8.010	0.992	0.993	0.994	0.905	0.333	0.191	0.135
9.005	0.991	0.993	0.994	0.905	0.335	0.191	0.135
9.943	0.991	0.993	0.994	0.905	0.333	0.191	0.135
11.031	0.991	0.993	0.995	0.905	0.333	0.190	0.135
11.487	0.991	0.992	0.995	0.905	0.334	0.190	0.135
11.544	0.991	0.992	0.995	0.905	0.333	0.189	0.135

Table 7. Concluded

(c) $\delta_{v,p} = 20°$

x′/L, top row

NPR	−0.540	−0.390	−0.286	−0.055	0.156	0.367	0.578	0.789
1.998	0.943	0.945	0.995	0.910	0.324	0.207	0.354	0.427
3.998	0.977	0.987	0.995	0.906	0.322	0.196	0.187	0.137
6.005	0.978	0.984	0.995	0.906	0.322	0.195	0.180	0.136
6.999	0.975	0.981	0.995	0.905	0.321	0.195	0.182	0.135
7.996	0.985	0.990	0.994	0.905	0.321	0.195	0.181	0.135
9.009	0.975	0.984	0.994	0.905	0.321	0.195	0.175	0.135
9.923	0.978	0.987	0.993	0.905	0.321	0.195	0.174	0.134
11.008	0.982	0.988	0.993	0.905	0.322	0.194	0.172	0.134
11.599	0.984	0.989	0.992	0.904	0.321	0.194	0.172	0.134

x′/L, bottom row

NPR	−0.581	−0.455	−0.328	−0.055	0.156	0.367	0.789
1.998	0.991	0.991	0.992	0.905	0.336	0.218	0.433
3.998	0.989	0.990	0.992	0.905	0.332	0.195	0.136
6.005	0.989	0.990	0.992	0.904	0.331	0.192	0.136
6.999	0.989	0.991	0.993	0.904	0.331	0.192	0.135
7.996	0.989	0.990	0.993	0.904	0.332	0.191	0.135
9.009	0.989	0.990	0.993	0.904	0.331	0.190	0.135
9.923	0.989	0.990	0.993	0.904	0.331	0.190	0.135
11.008	0.989	0.990	0.993	0.904	0.332	0.189	0.134
11.599	0.988	0.990	0.993	0.903	0.332	0.188	0.134

(d) $\delta_{v,p} = 25°$

x′/L, top row

NPR	−0.585	−0.432	−0.322	−0.055	0.156	0.367	0.578	0.789
2.022	0.935	0.950	0.995	0.912	0.325	0.202	0.347	0.417
4.005	0.961	0.967	0.996	0.907	0.321	0.196	0.191	0.136
6.007	0.972	0.980	0.996	0.907	0.321	0.195	0.187	0.135
7.003	0.984	0.986	0.996	0.906	0.321	0.195	0.181	0.135
8.006	0.978	0.983	0.995	0.906	0.321	0.195	0.182	0.135
9.001	0.981	0.986	0.995	0.905	0.321	0.195	0.180	0.134
9.895	0.978	0.985	0.995	0.905	0.322	0.195	0.179	0.134
11.001	0.981	0.987	0.994	0.905	0.322	0.195	0.175	0.134

x′/L, bottom row

NPR	−0.547	−0.429	−0.310	−0.055	0.156	0.367	0.578	0.789
2.022	0.988	0.989	0.991	0.906	0.335	0.210	0.359	0.426
4.005	0.987	0.988	0.991	0.903	0.331	0.196	0.166	0.136
6.007	0.988	0.988	0.991	0.903	0.330	0.193	0.163	0.135
7.003	0.987	0.988	0.991	0.903	0.329	0.192	0.163	0.135
8.006	0.988	0.988	0.991	0.903	0.330	0.192	0.160	0.135
9.001	0.987	0.988	0.991	0.903	0.330	0.191	0.159	0.135
9.895	0.987	0.988	0.992	0.903	0.331	0.191	0.158	0.134
11.001	0.987	0.988	0.992	0.903	0.330	0.190	0.158	0.134

Table 8. Nozzle Internal Static Pressure Ratios $p/p_{t,j}$ for SCF 2-D C-D Nozzle at AR = 2.508, $A_e/A_t = 1.46$, $\delta_{v,p} = 0°$, and $\delta_{v,y} = 0°$

(a) Sidewall internal static pressure ratios

x′/L, left side

NPR	-0.318	-0.207	-0.095	0.080	0.160	0.240	0.320	0.401	0.481	0.561	0.641
2.002	0.935	0.823	0.779	0.513	0.392	0.374	0.330	0.286	0.440	0.461	0.471
4.004	0.937	0.822	0.780	0.513	0.388	0.371	0.330	0.284	0.246	0.213	0.187
5.007	0.937	0.823	0.781	0.513	0.387	0.371	0.330	0.284	0.245	0.212	0.186
5.894	0.937	0.824	0.780	0.513	0.387	0.371	0.329	0.284	0.244	0.211	0.185
7.015	0.937	0.824	0.780	0.513	0.387	0.371	0.330	0.283	0.243	0.210	0.184
9.018	0.936	0.824	0.780	0.513	0.387	0.371	0.327	0.283	0.241	0.210	0.183
11.130	0.935	0.824	0.781	0.513	0.387	0.373	0.326	0.282	0.242	0.211	0.183

x′/L, right side

NPR	-0.318	-0.207	-0.095	0.080	0.160	0.240	0.320	0.401	0.481	0.561	0.641
2.002	0.918	0.808	0.696	0.507	0.425	0.378	0.330	0.291	0.454	0.466	0.474
4.004	0.920	0.804	0.690	0.506	0.420	0.372	0.328	0.282	0.247	0.216	0.192
5.007	0.921	0.804	0.689	0.506	0.420	0.370	0.327	0.281	0.246	0.215	0.191
5.894	0.920	0.803	0.687	0.506	0.420	0.369	0.327	0.280	0.246	0.215	0.190
7.015	0.920	0.802	0.686	0.506	0.420	0.368	0.327	0.280	0.245	0.214	0.189
9.018	0.920	0.802	0.685	0.506	0.420	0.368	0.327	0.279	0.243	0.212	0.188
11.130	0.919	0.802	0.684	0.506	0.419	0.370	0.329	0.279	0.244	0.212	0.188

(b) Divergent-flap internal static pressure ratios

Upper flap

	y/wt/2 = -0.50		y/wt/2 = 0.00				y/wt/2 = 0.50	
	x′/L		x′/L				x′/L	
NPR	0.333	0.667	0.200	0.400	0.600	0.800	0.333	0.667
2.002	0.281	0.477	0.266	0.267	0.452	0.516	0.282	0.499
4.004	0.276	0.185	0.258	0.263	0.173	0.232	0.278	0.186
5.007	0.275	0.185	0.258	0.262	0.172	0.231	0.277	0.185
5.894	0.274	0.184	0.259	0.262	0.171	0.231	0.275	0.185
7.015	0.273	0.184	0.263	0.261	0.170	0.230	0.274	0.185
9.018	0.272	0.184	0.273	0.261	0.169	0.229	0.274	0.184
11.130	0.274	0.184	0.266	0.262	0.169	0.230	0.273	0.184

Lower flap

	y/wt/2 = -0.50		y/wt/2 = 0.00				y/wt/2 = 0.50	
	x′/L		x′/L				x′/L	
NPR	0.333	0.667	0.200	0.400	0.600	0.800	0.333	0.667
2.002	0.280	0.485	0.367	0.265	0.425	0.510	0.284	0.497
4.004	0.276	0.194	0.349	0.254	0.205	0.234	0.279	0.195
5.007	0.275	0.193	0.349	0.254	0.205	0.233	0.278	0.195
5.894	0.275	0.193	0.349	0.253	0.205	0.233	0.278	0.194
7.015	0.274	0.192	0.349	0.252	0.205	0.233	0.278	0.194
9.018	0.274	0.192	0.350	0.250	0.203	0.233	0.279	0.192
11.130	0.275	0.192	0.342	0.251	0.202	0.233	0.281	0.191

Table 9. Nozzle Internal Static Pressure Ratios $p/p_{t,j}$ for SCF 2-D C-D Nozzle at AR = 2.508, $A_e/A_t = 1.46$, $\delta_{v,p} = 0°$, and $\delta_{v,y} = 7°$

(a) Sidewall internal static pressure ratios

	x′/L, left side										
NPR	−0.318	−0.207	−0.095	0.080	0.160	0.240	0.320	0.401	0.481	0.561	0.641
2.009	0.940	0.815	0.778	0.512	0.391	0.371	0.328	0.286	0.440	0.460	0.469
4.008	0.941	0.821	0.779	0.512	0.386	0.367	0.328	0.283	0.245	0.212	0.185
5.024	0.941	0.820	0.779	0.512	0.386	0.368	0.328	0.283	0.244	0.211	0.184
5.904	0.940	0.820	0.778	0.512	0.386	0.368	0.327	0.283	0.243	0.210	0.184
6.989	0.941	0.821	0.779	0.512	0.385	0.368	0.328	0.282	0.241	0.210	0.183
8.995	0.940	0.821	0.779	0.512	0.385	0.368	0.325	0.282	0.240	0.210	0.182
11.106	0.939	0.822	0.779	0.512	0.385	0.369	0.323	0.281	0.241	0.210	0.182

	x′/L, right side											
NPR	−0.430	−0.318	−0.207	−0.095	0.080	0.160	0.240	0.320	0.401	0.481	0.561	0.641
2.009	0.967	0.923	0.812	0.700	0.509	0.427	0.382	0.332	0.288	0.452	0.465	0.472
4.008	0.969	0.922	0.806	0.692	0.508	0.422	0.373	0.329	0.282	0.247	0.217	0.193
5.024	0.969	0.921	0.805	0.690	0.507	0.421	0.372	0.328	0.282	0.247	0.215	0.191
5.904	0.969	0.921	0.805	0.689	0.508	0.421	0.372	0.328	0.281	0.246	0.214	0.191
6.989	0.970	0.921	0.804	0.688	0.507	0.421	0.370	0.328	0.280	0.246	0.214	0.190
8.995	0.970	0.921	0.804	0.687	0.507	0.421	0.370	0.328	0.280	0.244	0.213	0.189
11.106	0.971	0.920	0.804	0.686	0.507	0.421	0.372	0.330	0.280	0.245	0.212	0.188

(b) Divergent-flap internal static pressure ratios

Upper flap

	y/wt/2 = −0.50		y/wt/2 = 0.00				y/wt/2 = 0.50	
	x′/L		x′/L				x′/L	
NPR	0.333	0.667	0.200	0.400	0.600	0.800	0.333	0.667
2.009	0.281	0.472	0.267	0.266	0.447	0.514	0.283	0.493
4.008	0.275	0.184	0.259	0.263	0.173	0.232	0.278	0.186
5.024	0.274	0.183	0.259	0.262	0.172	0.231	0.277	0.185
5.904	0.273	0.183	0.260	0.262	0.171	0.231	0.275	0.185
6.989	0.272	0.183	0.263	0.261	0.170	0.231	0.275	0.185
8.995	0.271	0.183	0.273	0.261	0.169	0.230	0.274	0.185
11.106	0.273	0.183	0.267	0.262	0.169	0.230	0.273	0.185

Lower flap

	y/wt/2 = −0.50		y/wt/2 = 0.00				y/wt/2 = 0.50	
	x′/L		x′/L				x′/L	
NPR	0.333	0.667	0.200	0.400	0.600	0.800	0.333	0.667
2.009	0.279	0.485	0.368	0.261	0.423	0.508	0.285	0.490
4.008	0.275	0.193	0.348	0.254	0.205	0.234	0.281	0.195
5.024	0.274	0.193	0.347	0.253	0.205	0.233	0.280	0.195
5.904	0.274	0.192	0.347	0.252	0.206	0.233	0.280	0.194
6.989	0.273	0.192	0.347	0.252	0.205	0.233	0.279	0.194
8.995	0.273	0.191	0.348	0.250	0.203	0.233	0.281	0.192
11.106	0.273	0.191	0.341	0.250	0.202	0.233	0.282	0.191

Table 10. Nozzle Internal Static Pressure Ratios $p/p_{t,j}$ for SCF 2-D C-D Nozzle at AR = 2.508, $A_e/A_t = 1.46$, $\delta_{v,p} = 0°$, and $\delta_{v,y} = 15°$

(a) Sidewall internal static pressure ratios

x'/L, left side

NPR	-0.207	-0.095	0.080	0.160	0.240	0.320	0.401	0.481	0.561	0.641
2.016	0.797	0.770	0.509	0.403	0.370	0.326	0.284	0.436	0.456	0.468
4.004	0.804	0.770	0.507	0.398	0.368	0.325	0.281	0.243	0.211	0.187
4.997	0.803	0.770	0.507	0.396	0.368	0.325	0.281	0.242	0.211	0.185
5.906	0.804	0.770	0.507	0.395	0.368	0.324	0.280	0.241	0.210	0.184
7.029	0.804	0.769	0.506	0.395	0.368	0.325	0.280	0.240	0.209	0.183
9.017	0.806	0.769	0.506	0.396	0.368	0.322	0.279	0.239	0.209	0.182
11.155	0.805	0.768	0.506	0.395	0.369	0.321	0.279	0.240	0.209	0.182

x'/L, right side

NPR	-0.430	-0.318	-0.207	-0.095	0.080	0.160	0.240	0.320	0.401	0.481	0.561	0.641
2.016	0.968	0.926	0.816	0.701	0.512	0.429	0.383	0.334	0.288	0.449	0.463	0.470
4.004	0.971	0.925	0.811	0.693	0.509	0.425	0.374	0.331	0.284	0.248	0.217	0.193
4.997	0.971	0.924	0.809	0.693	0.509	0.425	0.373	0.330	0.283	0.247	0.216	0.192
5.906	0.971	0.924	0.809	0.691	0.510	0.425	0.372	0.330	0.282	0.247	0.215	0.191
7.029	0.971	0.923	0.809	0.690	0.509	0.425	0.371	0.329	0.281	0.246	0.214	0.190
9.017	0.972	0.923	0.808	0.689	0.509	0.424	0.372	0.330	0.280	0.244	0.213	0.188
11.155	0.972	0.923	0.809	0.688	0.509	0.424	0.373	0.331	0.281	0.245	0.213	0.188

(b) Divergent-flap internal static pressure ratios

Upper flap

	y/wt/2 = -0.50		y/wt/2 = 0.00				y/wt/2 = 0.50	
	x'/L		x'/L				x'/L	
NPR	0.333	0.667	0.200	0.400	0.600	0.800	0.333	0.667
2.016	0.280	0.468	0.265	0.265	0.443	0.512	0.284	0.488
4.004	0.274	0.183	0.257	0.262	0.172	0.231	0.279	0.186
4.997	0.273	0.182	0.256	0.262	0.171	0.231	0.277	0.185
5.906	0.272	0.182	0.257	0.261	0.170	0.230	0.276	0.185
7.029	0.272	0.182	0.260	0.261	0.169	0.230	0.275	0.185
9.017	0.271	0.182	0.270	0.261	0.168	0.229	0.274	0.185
11.155	0.272	0.181	0.263	0.262	0.169	0.229	0.274	0.185

Lower flap

	y/wt/2 = -0.50		y/wt/2 = 0.00				y/wt/2 = 0.50	
	x'/L		x'/L				x'/L	
NPR	0.333	0.667	0.200	0.400	0.600	0.800	0.333	0.667
2.016	0.280	0.478	0.366	0.259	0.422	0.505	0.284	0.487
4.004	0.276	0.192	0.345	0.255	0.208	0.232	0.280	0.195
4.997	0.274	0.192	0.343	0.254	0.207	0.232	0.279	0.195
5.906	0.274	0.191	0.343	0.254	0.207	0.232	0.279	0.194
7.029	0.273	0.191	0.342	0.253	0.207	0.231	0.279	0.194
9.017	0.273	0.190	0.344	0.251	0.204	0.231	0.280	0.192
11.155	0.273	0.191	0.338	0.251	0.204	0.231	0.281	0.191

Table 11. Nozzle Internal Static Pressure Ratios $p/p_{t,j}$ for SCF 2-D C-D Nozzle at AR = 2.508, $A_e/A_t = 1.46$, $\delta_{v,p} = 25°$, and $\delta_{v,y} = 0°$

(a) Sidewall internal static pressure ratios

x'/L, left side

NPR	-0.318	-0.207	-0.095	0.080	0.160	0.240	0.320	0.401	0.481
2.011	0.943	0.860	0.844	0.685	0.598	0.523	0.463	0.418	0.377
3.998	0.943	0.865	0.840	0.676	0.579	0.492	0.412	0.342	0.280
5.001	0.942	0.866	0.839	0.675	0.579	0.492	0.412	0.342	0.280
5.911	0.943	0.867	0.839	0.676	0.579	0.492	0.413	0.342	0.279
7.003	0.942	0.868	0.839	0.676	0.579	0.492	0.413	0.341	0.279
9.003	0.942	0.868	0.839	0.676	0.579	0.493	0.413	0.341	0.278
11.705	0.940	0.868	0.839	0.677	0.579	0.493	0.414	0.342	0.278

x'/L, right side

NPR	-0.318	-0.207	-0.095	0.080	0.160	0.240	0.320	0.401	0.481
2.011	0.938	0.866	0.802	0.687	0.607	0.526	0.471	0.413	0.383
3.998	0.938	0.859	0.791	0.675	0.584	0.481	0.414	0.339	0.291
5.001	0.937	0.858	0.789	0.675	0.584	0.480	0.413	0.339	0.289
5.911	0.938	0.858	0.789	0.674	0.584	0.479	0.414	0.338	0.289
7.003	0.937	0.857	0.788	0.675	0.583	0.479	0.414	0.337	0.287
9.003	0.937	0.857	0.787	0.674	0.583	0.479	0.414	0.337	0.286
11.705	0.937	0.857	0.787	0.674	0.583	0.479	0.415	0.338	0.285

(b) Divergent-flap internal static pressure ratios

Upper flap

	y/wt/2 = -0.50		y/wt/2 = 0.00				y/wt/2 = 0.50	
	x'/L		x'/L				x'/L	
NPR	0.315	0.629	0.189	0.378	0.566	0.755	0.315	0.629
2.011	0.504	0.304	0.639	0.443	0.315	0.407	0.507	0.297
3.998	0.457	0.187	0.607	0.368	0.217	0.137	0.457	0.185
5.001	0.458	0.186	0.605	0.367	0.216	0.136	0.455	0.184
5.911	0.458	0.186	0.605	0.366	0.215	0.136	0.454	0.184
7.003	0.459	0.185	0.605	0.366	0.215	0.135	0.454	0.184
9.003	0.459	0.185	0.605	0.367	0.215	0.135	0.454	0.184
11.705	0.459	0.185	0.604	0.368	0.215	0.135	0.454	0.184

Lower flap

	y/wt/2 = -0.50		y/wt/2 = 0.00				y/wt/2 = 0.50	
	x'/L		x'/L				x'/L	
NPR	0.290	0.579	0.174	0.348	0.521	0.695	0.290	0.579
2.011	0.356	0.412	0.359	0.353	0.385	0.418	0.357	0.411
3.998	0.282	0.244	0.130	0.295	0.284	0.220	0.289	0.245
5.001	0.281	0.244	0.128	0.296	0.283	0.219	0.288	0.245
5.911	0.280	0.244	0.127	0.297	0.283	0.219	0.287	0.244
7.003	0.279	0.244	0.125	0.297	0.283	0.219	0.286	0.244
9.003	0.278	0.243	0.126	0.295	0.282	0.219	0.286	0.244
11.705	0.277	0.243	0.127	0.292	0.282	0.219	0.286	0.244

Table 12. Nozzle Internal Static Pressure Ratios $p/p_{t,j}$ for SCF 2-D C-D Nozzle at AR = 2.508, $A_e/A_t = 1.46$, $\delta_{v,p} = 25°$, and $\delta_{v,y} = 7°$

(a) Sidewall internal static pressure ratios

x′/L, left side

NPR	−0.318	−0.207	−0.095	0.080	0.160	0.240	0.320	0.401	0.481
2.017	0.951	0.862	0.843	0.685	0.595	0.520	0.460	0.417	0.378
3.998	0.952	0.863	0.838	0.675	0.578	0.491	0.411	0.342	0.280
5.012	0.951	0.863	0.838	0.675	0.578	0.491	0.411	0.342	0.279
5.910	0.951	0.865	0.838	0.675	0.578	0.491	0.411	0.342	0.279
7.017	0.951	0.866	0.838	0.675	0.578	0.491	0.411	0.341	0.279
9.006	0.950	0.867	0.837	0.675	0.578	0.492	0.412	0.341	0.278
11.635	0.949	0.867	0.837	0.676	0.578	0.492	0.413	0.342	0.278

x′/L, right side

NPR	−0.430	−0.318	−0.207	−0.095	0.080	0.160	0.240	0.320	0.401	0.481
2.017	0.974	0.939	0.867	0.804	0.689	0.608	0.527	0.471	0.412	0.381
3.998	0.975	0.938	0.860	0.793	0.676	0.585	0.482	0.415	0.340	0.290
5.012	0.975	0.938	0.860	0.791	0.676	0.585	0.481	0.414	0.339	0.289
5.910	0.976	0.938	0.859	0.790	0.676	0.585	0.480	0.415	0.338	0.288
7.017	0.976	0.938	0.859	0.790	0.676	0.584	0.479	0.415	0.338	0.287
9.006	0.977	0.938	0.859	0.789	0.676	0.585	0.479	0.415	0.338	0.286
11.635	0.977	0.937	0.859	0.789	0.675	0.584	0.480	0.416	0.338	0.285

(b) Divergent-flap internal static pressure ratios

Upper flap

	y/wt/2 = −0.50		y/wt/2 = 0.00				y/wt/2 = 0.50	
	x′/L		x′/L				x′/L	
NPR	0.315	0.629	0.189	0.378	0.566	0.755	0.315	0.629
2.017	0.503	0.302	0.638	0.442	0.314	0.405	0.506	0.295
3.998	0.457	0.186	0.606	0.367	0.217	0.137	0.455	0.185
5.012	0.458	0.185	0.605	0.367	0.216	0.136	0.455	0.185
5.910	0.458	0.185	0.605	0.366	0.216	0.136	0.454	0.184
7.017	0.458	0.185	0.604	0.366	0.215	0.135	0.454	0.184
9.006	0.459	0.185	0.604	0.367	0.215	0.135	0.454	0.184
11.635	0.459	0.185	0.604	0.368	0.215	0.135	0.454	0.184

Lower flap

	y/wt/2 = −0.50		y/wt/2 = 0.00				y/wt/2 = 0.50	
	x′/L		x′/L				x′/L	
NPR	0.290	0.579	0.174	0.348	0.521	0.695	0.290	0.579
2.017	0.354	0.411	0.357	0.352	0.384	0.417	0.357	0.410
3.998	0.281	0.244	0.129	0.295	0.284	0.220	0.289	0.245
5.012	0.280	0.244	0.127	0.297	0.284	0.220	0.288	0.245
5.910	0.279	0.244	0.127	0.297	0.284	0.219	0.287	0.245
7.017	0.278	0.244	0.126	0.297	0.283	0.219	0.287	0.245
9.006	0.277	0.243	0.126	0.294	0.282	0.219	0.287	0.244
11.635	0.278	0.243	0.128	0.291	0.282	0.219	0.286	0.244

Table 13. Nozzle Internal Static Pressure Ratios $p/p_{t,j}$ for SCF 2-D C-D Nozzle at AR = 2.508, $A_e/A_t = 1.46$, $\delta_{v,p} = 25°$, and $\delta_{v,y} = 15°$

(a) Sidewall internal static pressure ratios

x′/L, left side

NPR	-0.207	-0.095	0.080	0.160	0.240	0.320	0.401	0.481
1.997	0.864	0.839	0.684	0.596	0.524	0.466	0.422	0.381
4.019	0.850	0.834	0.675	0.579	0.491	0.411	0.343	0.280
4.998	0.852	0.834	0.675	0.579	0.491	0.411	0.342	0.279
5.924	0.851	0.834	0.676	0.579	0.492	0.412	0.342	0.280
7.014	0.852	0.834	0.676	0.579	0.491	0.412	0.342	0.279
9.014	0.852	0.833	0.676	0.579	0.492	0.412	0.342	0.279
11.664	0.852	0.833	0.676	0.579	0.493	0.413	0.342	0.278

x′/L, right side

NPR	-0.430	-0.318	-0.207	-0.095	0.080	0.160	0.240	0.320	0.401	0.481
1.997	0.979	0.942	0.871	0.806	0.689	0.608	0.527	0.472	0.414	0.385
4.019	0.977	0.941	0.863	0.794	0.678	0.586	0.482	0.415	0.340	0.290
4.998	0.977	0.940	0.862	0.793	0.678	0.586	0.481	0.415	0.339	0.289
5.924	0.977	0.940	0.862	0.792	0.677	0.586	0.480	0.415	0.338	0.289
7.014	0.978	0.940	0.861	0.791	0.677	0.586	0.480	0.415	0.338	0.287
9.014	0.978	0.940	0.861	0.790	0.677	0.585	0.480	0.416	0.337	0.286
11.664	0.978	0.939	0.861	0.790	0.676	0.585	0.480	0.416	0.338	0.285

(b) Divergent-flap internal static pressure ratios

Upper flap

	y/wt/2 = -0.50		y/wt/2 = 0.00				y/wt/2 = 0.50	
	x′/L		x′/L				x′/L	
NPR	0.315	0.629	0.189	0.378	0.566	0.755	0.315	0.629
1.997	0.504	0.307	0.640	0.444	0.318	0.417	0.508	0.301
4.019	0.457	0.186	0.606	0.368	0.216	0.137	0.457	0.186
4.998	0.457	0.186	0.605	0.366	0.215	0.136	0.456	0.185
5.924	0.457	0.185	0.604	0.366	0.214	0.136	0.455	0.185
7.014	0.458	0.185	0.604	0.366	0.214	0.135	0.455	0.185
9.014	0.458	0.184	0.603	0.367	0.214	0.135	0.455	0.185
11.664	0.458	0.184	0.603	0.367	0.215	0.134	0.455	0.184

Lower flap

	y/wt/2 = -0.50		y/wt/2 = 0.00				y/wt/2 = 0.50	
	x′/L		x′/L				x′/L	
NPR	0.290	0.579	0.174	0.348	0.521	0.695	0.290	0.579
1.997	0.358	0.414	0.362	0.356	0.387	0.421	0.363	0.415
4.019	0.282	0.244	0.129	0.292	0.285	0.220	0.289	0.245
4.998	0.281	0.243	0.127	0.294	0.284	0.219	0.287	0.245
5.924	0.280	0.243	0.126	0.295	0.284	0.219	0.286	0.245
7.014	0.279	0.243	0.124	0.296	0.284	0.219	0.286	0.245
9.014	0.277	0.243	0.124	0.294	0.283	0.219	0.286	0.244
11.664	0.277	0.243	0.125	0.291	0.282	0.219	0.285	0.244

Table 14. Nozzle Internal Static Pressure Ratios $p/p_{t,j}$ for SCF 2-D C-D Nozzle at AR = 2.508, $A_e/A_t = 1.63$, $\delta_{v,p} = 0°$, and $\delta_{v,y} = 0°$

(a) Sidewall internal static pressure ratios

x′/L, left side

NPR	-0.319	-0.207	-0.095	0.080	0.161	0.241	0.321	0.402	0.482	0.563	0.643
2.007	0.935	0.819	0.779	0.505	0.359	0.324	0.303	0.317	0.446	0.458	0.470
4.009	0.937	0.820	0.779	0.507	0.358	0.317	0.302	0.263	0.226	0.194	0.169
6.006	0.937	0.822	0.779	0.508	0.360	0.316	0.302	0.262	0.225	0.192	0.167
7.307	0.937	0.822	0.780	0.508	0.359	0.315	0.302	0.262	0.225	0.191	0.166
8.020	0.936	0.821	0.779	0.507	0.359	0.316	0.301	0.262	0.224	0.190	0.165
10.000	0.935	0.823	0.780	0.508	0.360	0.314	0.302	0.261	0.224	0.190	0.166
11.291	0.935	0.823	0.780	0.507	0.360	0.314	0.301	0.261	0.224	0.190	0.166

x′/L, right side

NPR	-0.319	-0.207	-0.095	0.080	0.161	0.241	0.321	0.402	0.482	0.563	0.643
2.007	0.919	0.810	0.693	0.499	0.389	0.348	0.306	0.426	0.463	0.469	0.475
4.009	0.920	0.805	0.685	0.497	0.387	0.339	0.303	0.260	0.224	0.196	0.170
6.006	0.920	0.803	0.683	0.498	0.386	0.336	0.301	0.258	0.223	0.194	0.169
7.307	0.920	0.803	0.682	0.497	0.385	0.336	0.300	0.258	0.222	0.192	0.167
8.020	0.919	0.802	0.681	0.497	0.385	0.337	0.300	0.257	0.222	0.191	0.167
10.000	0.919	0.802	0.681	0.497	0.385	0.337	0.301	0.258	0.222	0.191	0.166
11.291	0.919	0.802	0.681	0.497	0.384	0.337	0.301	0.258	0.222	0.191	0.166

(b) Divergent-flap internal static pressure ratios

Upper flap

	y/wt/2 = -0.50		y/wt/2 = 0.00				y/wt/2 = 0.50	
	x′/L		x′/L				x′/L	
NPR	0.333	0.667	0.200	0.400	0.600	0.800	0.333	0.667
2.007	0.269	0.499	0.239	0.301	0.463	0.515	0.271	0.516
4.009	0.264	0.157	0.229	0.250	0.169	0.217	0.268	0.159
6.006	0.262	0.156	0.228	0.249	0.168	0.215	0.267	0.159
7.307	0.261	0.157	0.231	0.249	0.167	0.214	0.266	0.159
8.020	0.261	0.156	0.232	0.249	0.167	0.214	0.265	0.159
10.000	0.262	0.156	0.230	0.248	0.167	0.213	0.266	0.159
11.291	0.263	0.155	0.228	0.248	0.167	0.213	0.266	0.158

Lower flap

	y/wt/2 = -0.50		y/wt/2 = 0.00				y/wt/2 = 0.50	
	x′/L		x′/L				x′/L	
NPR	0.333	0.667	0.200	0.400	0.600	0.800	0.333	0.667
2.007	0.260	0.473	0.318	0.340	0.435	0.501	0.258	0.517
4.009	0.257	0.172	0.310	0.238	0.162	0.225	0.256	0.171
6.006	0.256	0.170	0.308	0.237	0.162	0.225	0.255	0.169
7.307	0.256	0.171	0.308	0.236	0.161	0.225	0.255	0.168
8.020	0.255	0.170	0.309	0.236	0.161	0.225	0.255	0.167
10.000	0.255	0.170	0.305	0.236	0.161	0.224	0.255	0.167
11.291	0.256	0.170	0.304	0.236	0.161	0.223	0.255	0.168

Table 15. Nozzle Internal Static Pressure Ratios $p/p_{t,j}$ for SCF 2-D C-D Nozzle at AR = 2.508, $A_e/A_t = 1.63$, $\delta_{v,p} = 0^\circ$, and $\delta_{v,y} = 7^\circ$

(a) Sidewall internal static pressure ratios

	x′/L, left side										
NPR	−0.319	−0.207	−0.095	0.080	0.161	0.241	0.321	0.402	0.482	0.563	0.643
2.018	0.942	0.811	0.778	0.504	0.357	0.321	0.301	0.319	0.442	0.452	0.462
4.010	0.942	0.818	0.778	0.505	0.357	0.316	0.300	0.261	0.225	0.192	0.167
6.002	0.943	0.820	0.778	0.506	0.358	0.314	0.300	0.260	0.224	0.190	0.166
7.334	0.942	0.820	0.778	0.506	0.358	0.313	0.300	0.260	0.223	0.189	0.166
8.006	0.944	0.821	0.778	0.506	0.358	0.312	0.300	0.261	0.223	0.189	0.165
10.012	0.943	0.821	0.779	0.506	0.358	0.313	0.300	0.260	0.223	0.189	0.165
11.562	0.942	0.821	0.778	0.506	0.358	0.312	0.300	0.259	0.223	0.189	0.165

	x′/L, right side											
NPR	−0.431	−0.319	−0.207	−0.095	0.080	0.161	0.241	0.321	0.402	0.482	0.563	0.643
2.018	0.966	0.920	0.812	0.693	0.501	0.392	0.349	0.308	0.404	0.458	0.465	0.472
4.010	0.969	0.921	0.807	0.687	0.499	0.389	0.340	0.304	0.261	0.225	0.196	0.171
6.002	0.970	0.920	0.806	0.685	0.499	0.387	0.338	0.302	0.259	0.223	0.193	0.169
7.334	0.970	0.920	0.806	0.684	0.499	0.386	0.338	0.303	0.259	0.223	0.192	0.167
8.006	0.970	0.920	0.805	0.684	0.499	0.386	0.338	0.303	0.259	0.223	0.191	0.167
10.012	0.970	0.920	0.805	0.683	0.499	0.385	0.338	0.303	0.259	0.222	0.191	0.167
11.562	0.970	0.920	0.805	0.683	0.499	0.385	0.338	0.303	0.259	0.223	0.192	0.167

(b) Divergent-flap internal static pressure ratios

Upper flap

	y/wt/2 = −0.50		y/wt/2 = 0.00				y/wt/2 = 0.50	
	x′/L		x′/L				x′/L	
NPR	0.333	0.667	0.200	0.400	0.600	0.800	0.333	0.667
2.018	0.268	0.484	0.240	0.281	0.457	0.512	0.272	0.511
4.010	0.264	0.155	0.230	0.249	0.169	0.216	0.269	0.160
6.002	0.262	0.155	0.229	0.249	0.168	0.214	0.267	0.160
7.334	0.261	0.155	0.235	0.249	0.167	0.213	0.267	0.160
8.006	0.261	0.155	0.235	0.249	0.167	0.213	0.266	0.160
10.012	0.262	0.154	0.230	0.248	0.167	0.212	0.266	0.159
11.562	0.263	0.154	0.228	0.248	0.167	0.212	0.267	0.159

Lower flap

	y/wt/2 = −0.50		y/wt/2 = 0.00				y/wt/2 = 0.50	
	x′/L		x′/L				x′/L	
NPR	0.333	0.667	0.200	0.400	0.600	0.800	0.333	0.667
2.018	0.259	0.462	0.316	0.330	0.428	0.492	0.258	0.509
4.010	0.256	0.171	0.309	0.238	0.162	0.226	0.256	0.171
6.002	0.255	0.169	0.309	0.237	0.162	0.225	0.256	0.169
7.334	0.255	0.169	0.309	0.236	0.161	0.226	0.255	0.168
8.006	0.255	0.169	0.309	0.236	0.161	0.226	0.256	0.168
10.012	0.255	0.169	0.306	0.236	0.161	0.224	0.256	0.168
11.562	0.255	0.169	0.304	0.236	0.161	0.223	0.256	0.168

Table 16. Nozzle Internal Static Pressure Ratios $p/p_{t,j}$ for SCF 2-D C-D Nozzle at AR = 2.508, A_e/A_t = 1.63, $\delta_{v,p} = 0°$, and $\delta_{v,y} = 15°$

(a) Sidewall internal static pressure ratios

x′/L, left side

NPR	-0.207	-0.095	0.080	0.161	0.241	0.321	0.402	0.482	0.563	0.643
2.003	0.809	0.769	0.498	0.357	0.330	0.299	0.356	0.443	0.458	0.469
4.009	0.802	0.768	0.499	0.356	0.325	0.298	0.259	0.223	0.191	0.167
6.008	0.803	0.768	0.499	0.356	0.323	0.299	0.258	0.222	0.189	0.165
7.313	0.803	0.767	0.499	0.356	0.324	0.299	0.257	0.221	0.188	0.164
8.002	0.804	0.767	0.498	0.356	0.324	0.298	0.257	0.221	0.187	0.164
9.996	0.804	0.767	0.499	0.357	0.325	0.298	0.257	0.221	0.187	0.163
11.500	0.804	0.766	0.498	0.357	0.325	0.297	0.257	0.220	0.187	0.163

x′/L, right side

NPR	-0.431	-0.319	-0.207	-0.095	0.080	0.161	0.241	0.321	0.402	0.482	0.563	0.643
2.003	0.971	0.923	0.817	0.696	0.502	0.390	0.348	0.310	0.411	0.461	0.468	0.474
4.009	0.971	0.923	0.812	0.690	0.501	0.387	0.339	0.306	0.262	0.225	0.196	0.170
6.008	0.971	0.924	0.811	0.687	0.501	0.387	0.338	0.305	0.261	0.224	0.194	0.168
7.313	0.971	0.923	0.810	0.687	0.501	0.385	0.337	0.305	0.260	0.223	0.193	0.167
8.002	0.971	0.923	0.810	0.686	0.501	0.386	0.338	0.305	0.260	0.223	0.192	0.167
9.996	0.972	0.923	0.809	0.685	0.501	0.384	0.338	0.305	0.259	0.223	0.192	0.167
11.500	0.972	0.923	0.809	0.685	0.501	0.384	0.338	0.306	0.260	0.224	0.192	0.166

(b) Divergent-flap internal static pressure ratios

Upper flap

	y/wt/2 = -0.50		y/wt/2 = 0.00				y/wt/2 = 0.50	
	x′/L		x′/L				x′/L	
NPR	0.333	0.667	0.200	0.400	0.600	0.800	0.333	0.667
2.003	0.266	0.486	0.238	0.295	0.460	0.513	0.272	0.520
4.009	0.263	0.155	0.229	0.249	0.168	0.218	0.269	0.159
6.008	0.261	0.155	0.228	0.249	0.167	0.217	0.268	0.159
7.313	0.260	0.155	0.231	0.249	0.167	0.217	0.266	0.159
8.002	0.260	0.155	0.233	0.250	0.166	0.217	0.266	0.159
9.996	0.260	0.155	0.233	0.250	0.166	0.216	0.267	0.159
11.500	0.261	0.154	0.228	0.249	0.167	0.216	0.267	0.159

Lower flap

	y/wt/2 = -0.50		y/wt/2 = 0.00				y/wt/2 = 0.50	
	x′/L		x′/L				x′/L	
NPR	0.333	0.667	0.200	0.400	0.600	0.800	0.333	0.667
2.003	0.258	0.469	0.309	0.335	0.430	0.499	0.257	0.518
4.009	0.255	0.169	0.305	0.238	0.162	0.228	0.256	0.170
6.008	0.254	0.169	0.304	0.237	0.161	0.228	0.255	0.169
7.313	0.254	0.168	0.303	0.237	0.161	0.229	0.255	0.168
8.002	0.254	0.167	0.303	0.237	0.161	0.230	0.255	0.167
9.996	0.254	0.167	0.303	0.237	0.161	0.230	0.255	0.166
11.500	0.254	0.167	0.301	0.237	0.161	0.228	0.255	0.167

Table 17. Nozzle Internal Static Pressure Ratios $p/p_{t,j}$ for SCF 2-D C-D Nozzle at AR = 2.508, $A_e/A_t = 1.63$, $\delta_{v,p} = 25°$, and $\delta_{v,y} = 0°$

(a) Sidewall internal static pressure ratios

x′/L, left side

NPR	-0.319	-0.207	-0.095	0.080	0.161	0.241	0.321	0.402	0.482	0.563
2.006	0.944	0.860	0.838	0.672	0.591	0.524	0.467	0.420	0.378	0.346
4.008	0.944	0.860	0.832	0.657	0.563	0.476	0.400	0.334	0.274	0.224
6.001	0.944	0.861	0.832	0.658	0.563	0.477	0.400	0.333	0.273	0.224
7.300	0.944	0.862	0.831	0.657	0.562	0.477	0.401	0.333	0.273	0.223
8.004	0.944	0.862	0.832	0.657	0.563	0.478	0.401	0.333	0.273	0.223
9.996	0.942	0.862	0.831	0.657	0.562	0.478	0.401	0.333	0.273	0.222
11.601	0.942	0.862	0.831	0.657	0.562	0.478	0.402	0.334	0.273	0.222

x′/L, right side

NPR	-0.319	-0.207	-0.095	0.080	0.161	0.241	0.321	0.402	0.482	0.563
2.006	0.938	0.859	0.792	0.682	0.602	0.526	0.472	0.416	0.379	0.352
4.008	0.934	0.849	0.776	0.663	0.566	0.467	0.400	0.331	0.277	0.229
6.001	0.934	0.849	0.775	0.663	0.566	0.466	0.400	0.330	0.276	0.228
7.300	0.935	0.848	0.773	0.663	0.565	0.465	0.401	0.330	0.275	0.228
8.004	0.934	0.847	0.773	0.663	0.565	0.465	0.401	0.329	0.275	0.227
9.996	0.934	0.847	0.772	0.663	0.565	0.464	0.401	0.330	0.275	0.227
11.601	0.933	0.848	0.773	0.663	0.564	0.465	0.402	0.330	0.275	0.227

(b) Divergent-flap internal static pressure ratios

Upper flap

	y/wt/2 = -0.50		y/wt/2 = 0.00				y/wt/2 = 0.50	
	x′/L		x′/L				x′/L	
NPR	0.320	0.639	0.192	0.383	0.575	0.767	0.320	0.639
2.006	0.510	0.318	0.642	0.459	0.341	0.395	0.515	0.322
4.008	0.448	0.183	0.598	0.368	0.216	0.138	0.452	0.186
6.001	0.449	0.183	0.596	0.368	0.214	0.137	0.452	0.186
7.300	0.449	0.183	0.595	0.368	0.214	0.137	0.453	0.186
8.004	0.450	0.183	0.594	0.368	0.214	0.137	0.453	0.186
9.996	0.450	0.182	0.595	0.369	0.214	0.136	0.453	0.186
11.601	0.450	0.182	0.595	0.370	0.214	0.136	0.453	0.186

Lower flap

	y/wt/2 = -0.50		y/wt/2 = 0.00				y/wt/2 = 0.50	
	x′/L		x′/L				x′/L	
NPR	0.285	0.570	0.171	0.342	0.513	0.684	0.285	0.570
2.006	0.362	0.422	0.381	0.363	0.375	0.416	0.367	0.407
4.008	0.228	0.208	0.092	0.227	0.250	0.201	0.235	0.210
6.001	0.226	0.208	0.088	0.230	0.250	0.200	0.234	0.210
7.300	0.224	0.208	0.088	0.230	0.249	0.200	0.233	0.210
8.004	0.224	0.208	0.087	0.229	0.249	0.200	0.233	0.210
9.996	0.224	0.207	0.086	0.228	0.248	0.200	0.233	0.210
11.601	0.223	0.208	0.086	0.229	0.248	0.199	0.233	0.211

Table 18. Nozzle Internal Static Pressure Ratios $p/p_{t,j}$ for SCF 2-D C-D Nozzle at AR = 2.508, $A_e/A_t = 1.63$, $\delta_{v,p} = 25°$, and $\delta_{v,y} = 7°$

(a) Sidewall internal static pressure ratios

x'/L, left side

NPR	-0.319	-0.207	-0.095	0.080	0.161	0.241	0.321	0.402	0.482	0.563
1.997	0.955	0.861	0.835	0.673	0.592	0.525	0.468	0.421	0.378	0.346
4.006	0.953	0.857	0.830	0.656	0.561	0.475	0.398	0.333	0.274	0.224
6.022	0.954	0.859	0.830	0.656	0.562	0.476	0.399	0.332	0.273	0.223
7.321	0.954	0.859	0.830	0.656	0.562	0.476	0.399	0.332	0.273	0.222
7.998	0.953	0.860	0.830	0.656	0.562	0.476	0.399	0.332	0.273	0.222
10.017	0.952	0.860	0.830	0.656	0.562	0.477	0.400	0.333	0.273	0.222
11.560	0.951	0.860	0.829	0.656	0.562	0.477	0.400	0.333	0.273	0.222

x'/L, right side

NPR	-0.431	-0.319	-0.207	-0.095	0.080	0.161	0.241	0.321	0.402	0.482	0.563
1.997	0.975	0.936	0.858	0.793	0.683	0.603	0.525	0.472	0.417	0.379	0.352
4.006	0.974	0.935	0.850	0.778	0.664	0.567	0.467	0.401	0.332	0.276	0.230
6.022	0.975	0.935	0.850	0.775	0.665	0.567	0.466	0.401	0.330	0.275	0.228
7.321	0.975	0.935	0.849	0.775	0.665	0.567	0.465	0.401	0.330	0.274	0.227
7.998	0.975	0.935	0.850	0.775	0.664	0.566	0.465	0.402	0.330	0.274	0.227
10.017	0.976	0.934	0.850	0.775	0.664	0.566	0.465	0.402	0.330	0.274	0.227
11.560	0.976	0.934	0.849	0.774	0.664	0.565	0.465	0.402	0.331	0.275	0.227

(b) Divergent-flap internal static pressure ratios

Upper flap

	y/wt/2 = -0.50		y/wt/2 = 0.00				y/wt/2 = 0.50	
	x'/L		x'/L				x'/L	
NPR	0.320	0.639	0.192	0.383	0.575	0.767	0.320	0.639
1.997	0.509	0.319	0.640	0.460	0.342	0.411	0.516	0.322
4.006	0.447	0.182	0.597	0.368	0.216	0.138	0.452	0.186
6.022	0.448	0.182	0.595	0.367	0.214	0.137	0.453	0.186
7.321	0.448	0.182	0.594	0.368	0.214	0.137	0.453	0.186
7.998	0.449	0.182	0.594	0.368	0.214	0.137	0.453	0.186
10.017	0.449	0.182	0.595	0.369	0.214	0.136	0.454	0.186
11.560	0.449	0.182	0.595	0.370	0.214	0.136	0.454	0.186

Lower flap

	y/wt/2 = -0.50		y/wt/2 = 0.00				y/wt/2 = 0.50	
	x'/L		x'/L				x'/L	
NPR	0.285	0.570	0.171	0.342	0.513	0.684	0.285	0.570
1.997	0.364	0.425	0.381	0.363	0.377	0.426	0.366	0.415
4.006	0.226	0.208	0.093	0.226	0.249	0.201	0.236	0.210
6.022	0.224	0.208	0.089	0.229	0.249	0.200	0.235	0.210
7.321	0.223	0.208	0.088	0.229	0.249	0.200	0.234	0.211
7.998	0.223	0.207	0.088	0.229	0.248	0.200	0.234	0.211
10.017	0.222	0.207	0.087	0.229	0.248	0.200	0.234	0.211
11.560	0.221	0.207	0.086	0.228	0.248	0.200	0.234	0.211

Table 19. Nozzle Internal Static Pressure Ratios $p/p_{t,j}$ for SCF 2-D C-D Nozzle at AR = 2.508, $A_e/A_t = 1.63$, $\delta_{v,p} = 25°$, and $\delta_{v,y} = 15°$

(a) Sidewall internal static pressure ratios

	x'/L, left side								
NPR	-0.207	-0.095	0.080	0.161	0.241	0.321	0.402	0.482	0.563
2.004	0.854	0.835	0.673	0.592	0.525	0.467	0.419	0.377	0.344
4.009	0.847	0.827	0.657	0.562	0.475	0.399	0.333	0.275	0.225
6.004	0.846	0.827	0.658	0.562	0.476	0.399	0.333	0.274	0.224
7.312	0.846	0.826	0.658	0.562	0.476	0.400	0.332	0.274	0.223
7.993	0.847	0.826	0.658	0.562	0.477	0.400	0.332	0.274	0.223
9.995	0.846	0.826	0.658	0.562	0.477	0.400	0.333	0.273	0.222
11.575	0.844	0.825	0.658	0.562	0.477	0.401	0.333	0.274	0.222

	x'/L, right side										
NPR	-0.431	-0.319	-0.207	-0.095	0.080	0.161	0.241	0.321	0.402	0.482	0.563
2.004	0.975	0.942	0.861	0.793	0.682	0.602	0.523	0.470	0.414	0.374	0.348
4.009	0.975	0.937	0.854	0.779	0.665	0.568	0.468	0.402	0.332	0.276	0.229
6.004	0.976	0.938	0.853	0.777	0.666	0.568	0.467	0.402	0.330	0.275	0.228
7.312	0.976	0.938	0.853	0.777	0.666	0.567	0.466	0.402	0.330	0.274	0.227
7.993	0.976	0.937	0.852	0.777	0.665	0.567	0.466	0.402	0.330	0.274	0.227
9.995	0.976	0.937	0.852	0.776	0.665	0.567	0.466	0.402	0.331	0.274	0.227
11.575	0.977	0.937	0.852	0.776	0.665	0.566	0.466	0.403	0.331	0.274	0.227

(b) Divergent-flap internal static pressure ratios

	Upper flap							
	y/wt/2 = -0.50		y/wt/2 = 0.00				y/wt/2 = 0.50	
	x'/L		x'/L				x'/L	
NPR	0.320	0.639	0.192	0.383	0.575	0.767	0.320	0.639
2.004	0.507	0.316	0.638	0.457	0.340	0.380	0.513	0.320
4.009	0.446	0.182	0.596	0.368	0.216	0.138	0.453	0.187
6.004	0.447	0.182	0.594	0.367	0.214	0.137	0.453	0.186
7.312	0.447	0.182	0.594	0.367	0.214	0.137	0.454	0.186
7.993	0.448	0.182	0.593	0.368	0.214	0.137	0.454	0.186
9.995	0.448	0.182	0.594	0.368	0.213	0.136	0.454	0.186
11.575	0.449	0.181	0.594	0.369	0.213	0.136	0.454	0.186

	Lower flap							
	y/wt/2 = -0.50		y/wt/2 = 0.00				y/wt/2 = 0.50	
	x'/L		x'/L				x'/L	
NPR	0.285	0.570	0.171	0.342	0.513	0.684	0.285	0.570
2.004	0.360	0.410	0.379	0.361	0.371	0.412	0.366	0.400
4.009	0.230	0.207	0.092	0.222	0.250	0.202	0.235	0.209
6.004	0.228	0.207	0.088	0.226	0.250	0.201	0.234	0.209
7.312	0.227	0.207	0.087	0.227	0.250	0.200	0.234	0.210
7.993	0.226	0.207	0.087	0.226	0.249	0.200	0.234	0.210
9.995	0.225	0.207	0.086	0.226	0.249	0.200	0.234	0.210
11.575	0.224	0.207	0.086	0.226	0.249	0.200	0.234	0.210

Table 20. Nozzle Internal Static Pressure Ratios $p/p_{t,j}$ for SCF 2-D C-D Nozzle at AR = 2.083, $A_e/A_t = 1.46$, $\delta_{v,p} = 0°$, and $\delta_{v,y} = 0°$

(a) Sidewall internal static pressure ratios

x′/L, left side

NPR	−0.281	−0.179	−0.078	0.080	0.161	0.241	0.321	0.401	0.481	0.562	0.642
1.987	0.955	0.665	0.701	0.503	0.400	0.354	0.305	0.288	0.440	0.458	0.473
4.027	0.960	0.658	0.701	0.502	0.392	0.353	0.299	0.257	0.226	0.198	0.182
5.017	0.960	0.654	0.700	0.502	0.391	0.353	0.299	0.256	0.224	0.196	0.179
5.025	0.961	0.654	0.700	0.502	0.391	0.353	0.299	0.256	0.224	0.196	0.178
5.894	0.961	0.650	0.700	0.503	0.391	0.353	0.299	0.255	0.222	0.195	0.177
7.012	0.961	0.646	0.699	0.503	0.391	0.353	0.299	0.254	0.221	0.194	0.175
9.013	0.960	0.643	0.698	0.505	0.390	0.353	0.301	0.254	0.220	0.193	0.174
11.303	0.959	0.641	0.698	0.504	0.390	0.350	0.302	0.255	0.221	0.193	0.174

x′/L, right side

NPR	−0.281	−0.179	−0.078	0.080	0.161	0.241	0.321	0.401	0.481	0.562	0.642
1.987	0.955	0.666	0.710	0.501	0.364	0.357	0.322	0.326	0.442	0.457	0.469
4.027	0.956	0.655	0.705	0.502	0.362	0.354	0.313	0.260	0.223	0.196	0.172
5.017	0.956	0.648	0.704	0.502	0.361	0.353	0.310	0.258	0.221	0.194	0.170
5.025	0.956	0.647	0.703	0.503	0.361	0.354	0.310	0.258	0.221	0.193	0.170
5.894	0.956	0.643	0.702	0.503	0.361	0.353	0.309	0.257	0.220	0.192	0.169
7.012	0.956	0.638	0.700	0.503	0.362	0.352	0.308	0.257	0.219	0.191	0.168
9.013	0.957	0.633	0.699	0.502	0.363	0.350	0.309	0.257	0.218	0.191	0.167
11.303	0.956	0.631	0.698	0.502	0.363	0.350	0.308	0.259	0.219	0.191	0.168

(b) Divergent-flap internal static pressure ratios

Upper flap

	y/wt/2 = −0.50		y/wt/2 = 0.00				y/wt/2 = 0.50	
	x′/L		x′/L				x′/L	
NPR	0.333	0.667	0.200	0.400	0.600	0.800	0.333	0.667
1.987	0.283	0.513	0.317	0.290	0.454	0.523	0.283	0.511
4.027	0.285	0.190	0.379	0.270	0.203	0.202	0.286	0.189
5.017	0.285	0.189	0.389	0.269	0.201	0.201	0.285	0.188
5.025	0.285	0.189	0.390	0.269	0.201	0.201	0.285	0.188
5.894	0.283	0.188	0.393	0.268	0.201	0.201	0.285	0.188
7.012	0.280	0.187	0.396	0.267	0.200	0.201	0.284	0.187
9.013	0.277	0.186	0.400	0.266	0.201	0.202	0.284	0.187
11.303	0.279	0.186	0.390	0.266	0.203	0.201	0.284	0.186

Lower flap

	y/wt/2 = −0.50		y/wt/2 = 0.00			y/wt/2 = 0.50	
	x′/L		x′/L			x′/L	
NPR	0.333	0.667	0.200	0.400	0.800	0.333	0.667
1.987	0.280	0.516	0.283	0.274	0.526	0.280	0.514
4.027	0.275	0.185	0.278	0.267	0.213	0.278	0.193
5.017	0.273	0.183	0.278	0.266	0.212	0.277	0.190
5.025	0.273	0.183	0.278	0.266	0.212	0.277	0.190
5.894	0.273	0.181	0.280	0.266	0.212	0.276	0.186
7.012	0.272	0.179	0.283	0.265	0.212	0.276	0.184
9.013	0.273	0.179	0.282	0.265	0.211	0.276	0.180
11.303	0.272	0.179	0.283	0.265	0.211	0.276	0.179

Table 21. Nozzle Internal Static Pressure Ratios $p/p_{t,j}$ for SCF 2-D C-D Nozzle at AR = 2.083, $A_e/A_t = 1.46$, $\delta_{v,p} = 0°$, and $\delta_{v,y} = 7°$

(a) Sidewall internal static pressure ratios

x′/L, left side

NPR	−0.179	−0.078	0.080	0.161	0.241	0.321	0.401	0.481	0.562	0.642
2.015	0.657	0.698	0.499	0.397	0.353	0.298	0.315	0.433	0.449	0.461
4.001	0.656	0.697	0.500	0.391	0.352	0.298	0.255	0.223	0.196	0.178
4.995	0.651	0.697	0.501	0.390	0.352	0.298	0.254	0.222	0.195	0.176
5.894	0.648	0.697	0.501	0.391	0.352	0.299	0.253	0.221	0.194	0.176
6.996	0.645	0.696	0.501	0.390	0.352	0.299	0.253	0.220	0.194	0.174
9.001	0.643	0.695	0.501	0.390	0.351	0.300	0.252	0.220	0.193	0.174
11.257	0.643	0.695	0.502	0.390	0.348	0.302	0.253	0.220	0.193	0.174

x′/L, right side

NPR	−0.281	−0.179	−0.078	0.080	0.161	0.241	0.321	0.401	0.481	0.562	0.642
2.015	0.955	0.662	0.712	0.505	0.364	0.361	0.316	0.320	0.434	0.448	0.461
4.001	0.956	0.655	0.707	0.505	0.361	0.357	0.311	0.259	0.223	0.195	0.172
4.995	0.956	0.647	0.704	0.505	0.362	0.357	0.310	0.258	0.222	0.194	0.171
5.894	0.956	0.642	0.704	0.505	0.362	0.357	0.308	0.258	0.221	0.193	0.170
6.996	0.955	0.637	0.702	0.505	0.362	0.357	0.308	0.258	0.220	0.192	0.169
9.001	0.955	0.635	0.701	0.505	0.363	0.353	0.309	0.258	0.219	0.191	0.168
11.257	0.955	0.633	0.701	0.505	0.363	0.353	0.308	0.260	0.220	0.192	0.168

(b) Divergent-flap internal static pressure ratios

Upper flap

	y/wt/2 = −0.50		y/wt/2 = 0.00				y/wt/2 = 0.50	
	x′/L		x′/L				x′/L	
NPR	0.333	0.667	0.200	0.400	0.600	0.800	0.333	0.667
2.015	0.292	0.507	0.393	0.273	0.440	0.518	0.290	0.499
4.001	0.286	0.189	0.391	0.270	0.199	0.202	0.287	0.189
4.995	0.284	0.188	0.391	0.269	0.200	0.201	0.286	0.188
5.894	0.281	0.187	0.393	0.268	0.199	0.201	0.286	0.188
6.996	0.279	0.187	0.396	0.267	0.199	0.201	0.285	0.187
9.001	0.275	0.186	0.401	0.266	0.200	0.202	0.285	0.186
11.252	0.302	0.197	0.413	0.263	0.205	0.214	0.280	0.247
11.257	0.278	0.186	0.390	0.266	0.203	0.202	0.284	0.185

Lower flap

	y/wt/2 = −0.50		y/wt/2 = 0.00			y/wt/2 = 0.50	
	x′/L		x′/L			x′/L	
NPR	0.333	0.667	0.200	0.400	0.800	0.333	0.667
2.015	0.280	0.510	0.281	0.271	0.520	0.279	0.506
4.001	0.277	0.187	0.276	0.268	0.214	0.277	0.198
4.995	0.276	0.184	0.276	0.267	0.213	0.276	0.193
5.894	0.276	0.182	0.277	0.267	0.212	0.276	0.190
6.996	0.275	0.181	0.279	0.266	0.212	0.276	0.187
9.001	0.275	0.180	0.282	0.266	0.211	0.275	0.183
11.252	0.295	0.178	0.279	0.229	0.224	0.274	0.242
11.257	0.274	0.180	0.284	0.267	0.211	0.276	0.180

Table 22. Nozzle Internal Static Pressure Ratios $p/p_{t,j}$ for SCF 2-D C-D Nozzle at AR = 2.083, $A_e/A_t = 1.46$, $\delta_{v,p} = 0°$, and $\delta_{v,y} = 15°$

(a) Sidewall internal static pressure ratios

	x′/L, left side									
NPR	−0.179	−0.078	0.080	0.161	0.241	0.321	0.401	0.481	0.562	0.642
2.020	0.720	0.693	0.500	0.402	0.351	0.297	0.411	0.455	0.460	0.466
4.008	0.713	0.694	0.501	0.398	0.350	0.297	0.254	0.222	0.196	0.179
4.998	0.713	0.694	0.501	0.398	0.350	0.297	0.253	0.221	0.195	0.177
5.902	0.714	0.694	0.501	0.397	0.350	0.297	0.252	0.220	0.195	0.176
7.001	0.716	0.693	0.502	0.397	0.350	0.298	0.252	0.219	0.194	0.175
9.030	0.717	0.693	0.502	0.396	0.350	0.299	0.252	0.219	0.193	0.174
11.259	0.721	0.693	0.503	0.396	0.349	0.300	0.252	0.219	0.193	0.174

	x′/L, right side											
NPR	−0.382	−0.281	−0.179	−0.078	0.080	0.161	0.241	0.321	0.401	0.481	0.562	0.642
2.020	0.973	0.956	0.665	0.713	0.507	0.364	0.364	0.319	0.284	0.432	0.445	0.457
4.008	0.973	0.957	0.659	0.709	0.508	0.363	0.360	0.313	0.260	0.224	0.195	0.172
4.998	0.973	0.956	0.651	0.707	0.508	0.363	0.360	0.311	0.259	0.222	0.194	0.170
5.902	0.974	0.956	0.648	0.706	0.508	0.363	0.360	0.310	0.259	0.222	0.193	0.170
7.001	0.975	0.957	0.643	0.706	0.508	0.363	0.360	0.310	0.258	0.221	0.192	0.169
9.030	0.975	0.956	0.640	0.704	0.508	0.364	0.357	0.310	0.259	0.220	0.192	0.168
11.259	0.976	0.956	0.639	0.704	0.508	0.365	0.356	0.309	0.260	0.221	0.192	0.168

(b) Divergent-flap internal static pressure ratios

Upper flap

	y/wt/2 = −0.50		y/wt/2 = 0.00				y/wt/2 = 0.50	
	x′/L		x′/L				x′/L	
NPR	0.333	0.667	0.200	0.400	0.600	0.800	0.333	0.667
2.020	0.293	0.513	0.390	0.274	0.448	0.519	0.288	0.499
4.008	0.286	0.188	0.390	0.270	0.199	0.202	0.286	0.190
4.998	0.284	0.187	0.390	0.269	0.199	0.201	0.284	0.189
5.902	0.282	0.186	0.391	0.268	0.198	0.201	0.284	0.188
7.001	0.280	0.186	0.393	0.268	0.198	0.201	0.283	0.187
9.030	0.275	0.185	0.400	0.267	0.198	0.202	0.283	0.186
11.259	0.278	0.185	0.389	0.266	0.201	0.202	0.283	0.186

Lower flap

	y/wt/2 = −0.50		y/wt/2 = 0.00			y/wt/2 = 0.50	
	x′/L		x′/L			x′/L	
NPR	0.333	0.667	0.200	0.400	0.800	0.333	0.667
2.020	0.283	0.524	0.284	0.272	0.520	0.278	0.501
4.008	0.278	0.185	0.277	0.268	0.213	0.275	0.191
4.998	0.277	0.183	0.276	0.267	0.212	0.275	0.189
5.902	0.276	0.182	0.276	0.267	0.212	0.274	0.187
7.001	0.276	0.181	0.278	0.267	0.211	0.275	0.185
9.030	0.276	0.179	0.280	0.267	0.211	0.274	0.181
11.259	0.275	0.179	0.282	0.267	0.211	0.275	0.179

Table 23. Nozzle Internal Static Pressure Ratios $p/p_{t,j}$ for SCF 2-D C-D Nozzle at AR = 2.083, $A_e/A_t = 1.46$, $\delta_{v,p} = 0°$, and $\delta_{v,y} = 20°$

(a) Sidewall internal static pressure ratios

x′/L, left side

NPR	-0.179	-0.078	0.080	0.161	0.241	0.321	0.401	0.481	0.562	0.642
2.014	0.532	0.580	0.538	0.422	0.354	0.296	0.257	0.413	0.430	0.449
2.027	0.533	0.580	0.539	0.421	0.351	0.295	0.255	0.411	0.428	0.446
4.015	0.536	0.573	0.538	0.419	0.348	0.292	0.250	0.217	0.192	0.175
5.002	0.538	0.571	0.538	0.419	0.347	0.292	0.249	0.217	0.192	0.174
5.903	0.540	0.572	0.537	0.419	0.350	0.292	0.249	0.216	0.192	0.173
7.013	0.539	0.572	0.538	0.418	0.347	0.291	0.248	0.215	0.191	0.172
8.743	0.539	0.571	0.538	0.419	0.356	0.295	0.251	0.217	0.192	0.174

x′/L, right side

NPR	-0.382	-0.281	-0.179	-0.078	0.080	0.161	0.241	0.321	0.401	0.481	0.562	0.642
2.014	0.972	0.958	0.670	0.718	0.508	0.363	0.362	0.310	0.393	0.448	0.457	0.466
2.027	0.972	0.958	0.669	0.717	0.508	0.363	0.362	0.309	0.384	0.445	0.455	0.464
4.015	0.975	0.958	0.662	0.711	0.508	0.363	0.358	0.301	0.254	0.216	0.189	0.163
5.002	0.977	0.958	0.657	0.710	0.509	0.363	0.357	0.300	0.254	0.216	0.188	0.162
5.903	0.978	0.958	0.653	0.709	0.509	0.363	0.357	0.300	0.254	0.216	0.188	0.162
7.013	0.978	0.958	0.648	0.707	0.509	0.364	0.357	0.298	0.253	0.214	0.186	0.161
8.743	0.978	0.958	0.645	0.707	0.509	0.365	0.356	0.302	0.256	0.216	0.188	0.162

(b) Divergent-flap internal static pressure ratios

Upper flap

	y/wt/2 = -0.50		y/wt/2 = 0.00				y/wt/2 = 0.50	
	x′/L		x′/L				x′/L	
NPR	0.333	0.667	0.200	0.400	0.600	0.800	0.333	0.667
2.014	0.298	0.481	0.326	0.266	0.447	0.507	0.272	0.516
2.027	0.297	0.476	0.326	0.265	0.442	0.503	0.272	0.514
4.015	0.290	0.177	0.325	0.262	0.180	0.205	0.269	0.170
5.002	0.288	0.177	0.325	0.262	0.179	0.205	0.268	0.169
5.903	0.287	0.178	0.325	0.262	0.182	0.205	0.267	0.171
7.013	0.285	0.177	0.326	0.261	0.179	0.205	0.266	0.168
8.743	0.282	0.180	0.331	0.263	0.189	0.205	0.266	0.175

Lower flap

	y/wt/2 = -0.50		y/wt/2 = 0.00				y/wt/2 = 0.50	
	x′/L		x′/L				x′/L	
NPR	0.333	0.667	0.200	0.400	0.600	0.800	0.333	0.667
2.014	0.297	0.489	0.318	0.267	0.454	0.517	0.267	0.515
2.027	0.297	0.483	0.328	0.266	0.446	0.513	0.266	0.514
4.015	0.295	0.177	0.334	0.262	0.185	0.212	0.263	0.173
5.002	0.294	0.176	0.332	0.262	0.183	0.212	0.262	0.173
5.903	0.291	0.176	0.316	0.263	0.189	0.212	0.263	0.172
7.013	0.292	0.176	0.329	0.262	0.181	0.212	0.262	0.172
8.743	0.285	0.176	0.277	0.264	0.202	0.213	0.265	0.170

Table 24. Nozzle Internal Static Pressure Ratios $p/p_{t,j}$ for SCF 2-D C-D Nozzle at AR = 2.083, $A_e/A_t = 1.46$, $\delta_{v,p} = 25°$, and $\delta_{v,y} = 0°$

(a) Sidewall internal static pressure ratios

x′/L, left side

NPR	-0.281	-0.179	-0.078	0.080	0.161	0.241	0.321	0.401	0.481
2.011	0.966	0.733	0.795	0.676	0.579	0.498	0.430	0.384	0.356
4.016	0.969	0.734	0.789	0.667	0.566	0.483	0.405	0.336	0.278
4.992	0.968	0.733	0.789	0.667	0.565	0.482	0.405	0.336	0.277
5.000	0.969	0.733	0.789	0.667	0.566	0.482	0.405	0.336	0.277
5.892	0.968	0.731	0.789	0.667	0.565	0.482	0.405	0.336	0.276
7.007	0.969	0.728	0.788	0.668	0.565	0.483	0.405	0.336	0.276
9.027	0.967	0.730	0.787	0.667	0.564	0.483	0.405	0.336	0.277
11.827	0.966	0.731	0.787	0.667	0.563	0.484	0.406	0.337	0.277

x′/L, right side

NPR	-0.281	-0.179	-0.078	0.080	0.161	0.241	0.321	0.401	0.481
2.011	0.964	0.740	0.797	0.676	0.589	0.511	0.439	0.398	0.363
4.016	0.964	0.727	0.787	0.670	0.578	0.489	0.405	0.340	0.279
4.992	0.964	0.724	0.785	0.669	0.579	0.489	0.405	0.340	0.279
5.000	0.965	0.724	0.786	0.669	0.579	0.489	0.405	0.339	0.279
5.892	0.964	0.722	0.784	0.669	0.578	0.489	0.404	0.339	0.278
7.007	0.964	0.719	0.783	0.669	0.579	0.489	0.405	0.339	0.278
9.027	0.964	0.719	0.783	0.668	0.579	0.489	0.405	0.340	0.278
11.827	0.964	0.721	0.783	0.668	0.579	0.490	0.406	0.341	0.278

(b) Divergent-flap internal static pressure ratios

Upper flap

	y/wt/2 = -0.50		y/wt/2 = 0.00				y/wt/2 = 0.50	
	x′/L		x′/L				x′/L	
NPR	0.315	0.629	0.189	0.378	0.566	0.755	0.315	0.629
2.011	0.490	0.282	0.637	0.425	0.286	0.424	0.490	0.275
4.016	0.461	0.191	0.612	0.378	0.224	0.142	0.458	0.192
4.992	0.461	0.191	0.610	0.377	0.224	0.141	0.458	0.191
5.000	0.461	0.190	0.610	0.377	0.224	0.141	0.457	0.191
5.892	0.461	0.190	0.609	0.377	0.223	0.141	0.457	0.191
7.007	0.462	0.190	0.609	0.376	0.223	0.140	0.457	0.191
9.027	0.463	0.190	0.609	0.376	0.223	0.140	0.457	0.190
11.827	0.463	0.189	0.609	0.377	0.223	0.140	0.458	0.191

Lower flap

	y/wt/2 = -0.50		y/wt/2 = 0.00				y/wt/2 = 0.50	
	x′/L		x′/L				x′/L	
NPR	0.290	0.579	0.174	0.347	0.521	0.695	0.290	0.579
2.011	0.329	0.404	0.314	0.328	0.371	0.421	0.327	0.398
4.016	0.280	0.238	0.139	0.283	0.281	0.217	0.273	0.241
4.992	0.279	0.238	0.138	0.284	0.280	0.216	0.273	0.240
5.000	0.279	0.238	0.138	0.283	0.280	0.216	0.273	0.240
5.892	0.279	0.237	0.137	0.283	0.280	0.216	0.273	0.240
7.007	0.278	0.237	0.136	0.282	0.279	0.216	0.273	0.239
9.027	0.279	0.237	0.136	0.282	0.279	0.215	0.273	0.239
11.827	0.278	0.237	0.136	0.281	0.278	0.215	0.273	0.240

Table 25. Nozzle Internal Static Pressure Ratios $p/p_{t,j}$ for SCF 2-D C-D Nozzle at AR = 2.083, $A_e/A_t = 1.46$, $\delta_{v,p} = 25^\circ$, and $\delta_{v,y} = 7^\circ$

(a) Sidewall internal static pressure ratios

x′/L, left side

NPR	-0.179	-0.078	0.080	0.161	0.241	0.321	0.401	0.481
2.018	0.740	0.793	0.673	0.579	0.497	0.428	0.383	0.357
4.015	0.734	0.787	0.666	0.566	0.481	0.403	0.336	0.278
5.007	0.734	0.788	0.666	0.565	0.481	0.403	0.335	0.277
5.894	0.733	0.787	0.666	0.565	0.482	0.403	0.335	0.277
7.009	0.731	0.787	0.666	0.564	0.482	0.404	0.335	0.277
9.016	0.732	0.786	0.666	0.564	0.483	0.404	0.336	0.277
11.823	0.735	0.785	0.666	0.563	0.483	0.405	0.336	0.277

x′/L, right side

NPR	-0.281	-0.179	-0.078	0.080	0.161	0.241	0.321	0.401	0.481
2.018	0.964	0.743	0.799	0.679	0.590	0.511	0.438	0.394	0.359
4.015	0.964	0.731	0.789	0.671	0.579	0.490	0.406	0.340	0.279
5.007	0.964	0.726	0.786	0.671	0.579	0.490	0.405	0.340	0.278
5.894	0.964	0.723	0.787	0.671	0.580	0.490	0.405	0.340	0.278
7.009	0.964	0.721	0.785	0.670	0.580	0.490	0.405	0.340	0.277
9.016	0.963	0.721	0.785	0.670	0.580	0.490	0.406	0.340	0.278
11.823	0.963	0.723	0.784	0.669	0.580	0.491	0.406	0.341	0.278

(b) Divergent-flap internal static pressure ratios

Upper flap

	y/wt/2 = -0.50		y/wt/2 = 0.00				y/wt/2 = 0.50	
	x′/L		x′/L				x′/L	
NPR	0.315	0.629	0.189	0.378	0.566	0.755	0.315	0.629
2.018	0.490	0.282	0.636	0.425	0.285	0.422	0.489	0.277
4.015	0.461	0.191	0.611	0.378	0.224	0.141	0.458	0.192
5.007	0.461	0.190	0.609	0.377	0.224	0.141	0.457	0.191
5.894	0.461	0.190	0.609	0.377	0.223	0.141	0.457	0.191
7.009	0.462	0.190	0.608	0.376	0.223	0.140	0.458	0.191
9.016	0.462	0.189	0.608	0.377	0.223	0.140	0.458	0.191
11.823	0.463	0.189	0.609	0.377	0.223	0.140	0.458	0.191

Lower flap

	y/wt/2 = -0.50		y/wt/2 = 0.00				y/wt/2 = 0.50	
	x′/L		x′/L				x′/L	
NPR	0.290	0.579	0.174	0.347	0.521	0.695	0.290	0.579
2.018	0.328	0.402	0.314	0.328	0.371	0.419	0.328	0.398
4.015	0.280	0.238	0.140	0.283	0.281	0.217	0.273	0.241
5.007	0.280	0.238	0.138	0.283	0.280	0.216	0.273	0.240
5.894	0.279	0.238	0.138	0.283	0.280	0.216	0.273	0.240
7.009	0.279	0.237	0.137	0.282	0.279	0.216	0.272	0.240
9.016	0.279	0.237	0.136	0.282	0.279	0.215	0.272	0.240
11.823	0.279	0.237	0.136	0.281	0.278	0.215	0.273	0.239

Table 26. Nozzle Internal Static Pressure Ratios $p/p_{t,j}$ for SCF 2-D C-D Nozzle at AR = 2.083, $A_e/A_t = 1.46$, $\delta_{v,p} = 25°$, and $\delta_{v,y} = 15°$

(a) Sidewall internal static pressure ratios

x′/L, left side

NPR	-0.179	-0.078	0.080	0.161	0.241	0.321	0.401	0.481
2.011	0.799	0.792	0.673	0.578	0.496	0.430	0.388	0.360
4.002	0.796	0.786	0.665	0.565	0.479	0.402	0.336	0.278
5.016	0.793	0.786	0.666	0.566	0.480	0.403	0.336	0.278
5.906	0.795	0.786	0.666	0.565	0.480	0.402	0.336	0.277
7.018	0.795	0.786	0.666	0.565	0.480	0.403	0.336	0.277
9.016	0.797	0.785	0.666	0.564	0.481	0.404	0.337	0.277
11.816	0.798	0.785	0.667	0.564	0.481	0.405	0.337	0.278

x′/L, right side

NPR	-0.382	-0.281	-0.179	-0.078	0.080	0.161	0.241	0.321	0.401	0.481
2.011	0.978	0.967	0.746	0.798	0.679	0.591	0.512	0.437	0.391	0.355
4.002	0.979	0.966	0.733	0.790	0.672	0.579	0.490	0.405	0.340	0.278
5.016	0.978	0.965	0.729	0.789	0.672	0.581	0.490	0.406	0.340	0.278
5.906	0.979	0.965	0.726	0.787	0.672	0.581	0.490	0.405	0.340	0.277
7.018	0.980	0.965	0.724	0.787	0.672	0.581	0.490	0.405	0.339	0.277
9.016	0.980	0.964	0.725	0.786	0.671	0.581	0.491	0.406	0.340	0.277
11.816	0.981	0.964	0.726	0.785	0.671	0.581	0.492	0.406	0.341	0.278

(b) Divergent-flap internal static pressure ratios

Upper flap

	y/wt/2 = -0.50		y/wt/2 = 0.00				y/wt/2 = 0.50	
	x′/L		x′/L				x′/L	
NPR	0.315	0.629	0.189	0.378	0.566	0.755	0.315	0.629
2.011	0.490	0.287	0.636	0.426	0.286	0.425	0.490	0.279
4.002	0.460	0.191	0.611	0.378	0.224	0.142	0.459	0.192
5.016	0.460	0.191	0.609	0.378	0.224	0.141	0.458	0.192
5.906	0.461	0.190	0.608	0.377	0.223	0.141	0.458	0.192
7.018	0.461	0.190	0.608	0.377	0.223	0.140	0.458	0.191
9.016	0.462	0.190	0.607	0.377	0.223	0.140	0.458	0.191
11.816	0.462	0.189	0.608	0.377	0.223	0.140	0.459	0.191

Lower flap

	y/wt/2 = -0.50		y/wt/2 = 0.00				y/wt/2 = 0.50	
	x′/L		x′/L				x′/L	
NPR	0.290	0.579	0.174	0.347	0.521	0.695	0.290	0.579
2.011	0.333	0.404	0.316	0.331	0.374	0.420	0.332	0.402
4.002	0.281	0.238	0.140	0.282	0.280	0.217	0.273	0.241
5.016	0.280	0.238	0.139	0.282	0.280	0.217	0.273	0.240
5.906	0.280	0.237	0.138	0.282	0.280	0.216	0.272	0.240
7.018	0.280	0.237	0.137	0.281	0.279	0.216	0.272	0.240
9.016	0.280	0.237	0.136	0.281	0.278	0.216	0.272	0.240
11.816	0.280	0.237	0.136	0.279	0.278	0.215	0.272	0.240

Table 27. Nozzle Internal Static Pressure Ratios $p/p_{t,j}$ for SCF 2-D C-D Nozzle at AR = 2.083, $A_e/A_t = 1.46$, $\delta_{v,p} = 25°$, and $\delta_{v,y} = 20°$

(a) Sidewall internal static pressure ratios

x'/L, left side

NPR	-0.179	-0.078	0.080	0.161	0.241	0.321	0.401	0.481
2.007	0.678	0.753	0.694	0.596	0.524	0.464	0.413	0.368
3.997	0.665	0.747	0.684	0.577	0.489	0.410	0.342	0.283
5.006	0.667	0.746	0.684	0.577	0.490	0.411	0.341	0.282
5.906	0.665	0.746	0.685	0.577	0.490	0.411	0.341	0.282
7.012	0.666	0.746	0.685	0.577	0.490	0.412	0.342	0.282
9.016	0.668	0.740	0.686	0.577	0.492	0.412	0.342	0.282
10.864	0.669	0.738	0.686	0.577	0.492	0.412	0.342	0.282

x'/L, right side

NPR	-0.382	-0.281	-0.179	-0.078	0.080	0.161	0.241	0.321	0.401	0.481
2.007	0.979	0.964	0.748	0.798	0.678	0.590	0.511	0.438	0.394	0.358
3.997	0.980	0.966	0.735	0.790	0.671	0.578	0.488	0.404	0.338	0.275
5.006	0.980	0.965	0.730	0.788	0.671	0.579	0.487	0.403	0.337	0.274
5.906	0.981	0.966	0.728	0.788	0.671	0.579	0.487	0.403	0.337	0.274
7.012	0.981	0.966	0.727	0.787	0.670	0.579	0.488	0.403	0.337	0.273
9.016	0.982	0.965	0.726	0.785	0.670	0.579	0.489	0.404	0.337	0.273
10.864	0.982	0.965	0.726	0.786	0.670	0.579	0.489	0.404	0.338	0.274

(b) Divergent-flap internal static pressure ratios

Upper flap

	y/wt/2 = -0.50		y/wt/2 = 0.00				y/wt/2 = 0.50	
	x'/L		x'/L				x'/L	
NPR	0.315	0.629	0.189	0.378	0.566	0.755	0.315	0.629
2.007	0.503	0.282	0.633	0.429	0.295	0.430	0.491	0.280
3.997	0.461	0.193	0.605	0.376	0.224	0.142	0.457	0.190
5.006	0.460	0.192	0.601	0.375	0.223	0.141	0.454	0.190
5.906	0.461	0.192	0.599	0.375	0.223	0.141	0.455	0.190
7.012	0.462	0.192	0.599	0.375	0.223	0.141	0.454	0.190
9.016	0.462	0.192	0.602	0.375	0.223	0.140	0.455	0.189
10.864	0.462	0.192	0.602	0.375	0.223	0.140	0.455	0.189

Lower flap

	y/wt/2 = -0.50		y/wt/2 = 0.00				y/wt/2 = 0.50	
	x'/L		x'/L				x'/L	
NPR	0.290	0.579	0.174	0.347	0.521	0.695	0.290	0.579
2.007	0.337	0.408	0.317	0.333	0.374	0.421	0.333	0.402
3.997	0.284	0.235	0.138	0.271	0.283	0.218	0.263	0.240
5.006	0.283	0.234	0.137	0.271	0.282	0.218	0.263	0.239
5.906	0.284	0.234	0.136	0.271	0.282	0.217	0.262	0.239
7.012	0.283	0.234	0.135	0.270	0.281	0.217	0.262	0.238
9.016	0.282	0.233	0.135	0.269	0.281	0.217	0.261	0.237
10.864	0.282	0.234	0.134	0.267	0.281	0.217	0.261	0.237

Table 28. Nozzle Internal Static Pressure Ratios $p/p_{t,j}$ for SCF 2-D C-D Nozzle at AR = 2.083, $A_e/A_t = 1.63$, $\delta_{v,p} = 0°$, and $\delta_{v,y} = 0°$

(a) Sidewall internal static pressure ratios

x′/L, left side

NPR	−0.282	−0.180	−0.078	0.081	0.161	0.242	0.322	0.403	0.483	0.564	0.644
2.009	0.958	0.654	0.696	0.499	0.361	0.319	0.275	0.434	0.453	0.459	0.470
4.006	0.962	0.654	0.697	0.501	0.358	0.314	0.272	0.235	0.201	0.176	0.157
6.006	0.961	0.648	0.697	0.501	0.358	0.313	0.272	0.235	0.200	0.174	0.155
7.304	0.961	0.644	0.696	0.501	0.358	0.313	0.272	0.234	0.199	0.174	0.154
7.999	0.961	0.643	0.696	0.501	0.358	0.312	0.271	0.235	0.199	0.174	0.154
10.003	0.960	0.641	0.695	0.502	0.358	0.313	0.271	0.235	0.198	0.173	0.153
11.556	0.959	0.639	0.695	0.502	0.358	0.313	0.271	0.235	0.199	0.173	0.153

x′/L, right side

NPR	−0.282	−0.180	−0.078	0.081	0.161	0.242	0.322	0.403	0.483	0.564	0.644
2.009	0.957	0.653	0.698	0.499	0.366	0.334	0.272	0.435	0.451	0.459	0.467
4.006	0.956	0.645	0.694	0.499	0.365	0.328	0.267	0.238	0.202	0.174	0.153
6.006	0.956	0.636	0.693	0.500	0.365	0.326	0.266	0.236	0.201	0.173	0.151
7.304	0.956	0.631	0.692	0.500	0.366	0.325	0.267	0.236	0.200	0.172	0.150
7.999	0.956	0.630	0.692	0.500	0.366	0.325	0.267	0.236	0.200	0.171	0.150
10.003	0.956	0.627	0.691	0.500	0.366	0.324	0.266	0.236	0.201	0.171	0.150
11.556	0.956	0.627	0.690	0.500	0.367	0.325	0.265	0.236	0.201	0.171	0.149

(b) Divergent-flap internal static pressure ratios

Upper flap

	y/wt/2 = −0.50		y/wt/2 = 0.00				y/wt/2 = 0.50	
	x′/L		x′/L				x′/L	
NPR	0.333	0.667	0.200	0.400	0.600	0.800	0.333	0.667
2.009	0.258	0.523	0.372	0.350	0.483	0.521	0.261	0.520
4.006	0.254	0.166	0.369	0.258	0.164	0.198	0.258	0.163
6.006	0.252	0.165	0.366	0.258	0.164	0.198	0.256	0.163
7.304	0.251	0.163	0.365	0.257	0.163	0.197	0.255	0.163
7.999	0.251	0.162	0.364	0.257	0.162	0.197	0.255	0.163
10.003	0.251	0.162	0.362	0.256	0.162	0.197	0.255	0.163
11.556	0.251	0.162	0.360	0.257	0.162	0.197	0.256	0.164

Lower flap

	y/wt/2 = −0.50		y/wt/2 = 0.00				y/wt/2 = 0.50	
	x′/L		x′/L				x′/L	
NPR	0.333	0.667	0.200	0.400	0.600	0.800	0.333	0.667
2.009	0.262	0.526	0.257	0.335	0.490	0.521	0.257	0.521
4.006	0.260	0.153	0.257	0.251	0.165	0.197	0.256	0.153
6.006	0.259	0.152	0.259	0.249	0.164	0.196	0.255	0.152
7.304	0.259	0.151	0.262	0.249	0.164	0.195	0.255	0.152
7.999	0.259	0.151	0.263	0.249	0.164	0.195	0.255	0.151
10.003	0.258	0.151	0.264	0.249	0.164	0.196	0.254	0.152
11.556	0.258	0.151	0.265	0.249	0.164	0.196	0.255	0.151

Table 29. Nozzle Internal Static Pressure Ratios $p/p_{t,j}$ for SCF 2-D C-D Nozzle at AR = 2.083, $A_e/A_t = 1.63$, $\delta_{v,p} = 0°$, and $\delta_{v,y} = 7°$

(a) Sidewall internal static pressure ratios

x′/L, left side

NPR	-0.180	-0.078	0.081	0.161	0.242	0.322	0.403	0.483	0.564	0.644
1.999	0.658	0.695	0.497	0.361	0.318	0.273	0.437	0.451	0.457	0.468
3.999	0.654	0.695	0.498	0.358	0.312	0.271	0.234	0.200	0.175	0.155
5.995	0.648	0.694	0.500	0.357	0.311	0.270	0.234	0.199	0.174	0.154
7.297	0.644	0.694	0.500	0.357	0.310	0.269	0.234	0.198	0.173	0.153
8.023	0.642	0.693	0.500	0.358	0.310	0.269	0.234	0.198	0.173	0.153
9.990	0.642	0.693	0.501	0.357	0.310	0.269	0.234	0.197	0.172	0.153
11.436	0.641	0.693	0.501	0.357	0.310	0.269	0.234	0.197	0.172	0.152

x′/L, right side

NPR	-0.282	-0.180	-0.078	0.081	0.161	0.242	0.322	0.403	0.483	0.564	0.644
1.999	0.954	0.654	0.700	0.501	0.368	0.335	0.274	0.438	0.453	0.460	0.470
3.999	0.955	0.648	0.697	0.501	0.366	0.329	0.269	0.238	0.202	0.175	0.153
5.995	0.955	0.639	0.694	0.501	0.366	0.328	0.269	0.236	0.201	0.173	0.151
7.297	0.955	0.633	0.693	0.502	0.366	0.327	0.269	0.236	0.201	0.172	0.150
8.023	0.955	0.632	0.693	0.502	0.367	0.327	0.269	0.236	0.201	0.172	0.150
9.990	0.955	0.629	0.693	0.502	0.367	0.326	0.268	0.237	0.201	0.172	0.150
11.436	0.955	0.630	0.693	0.502	0.368	0.326	0.267	0.236	0.202	0.172	0.150

(b) Divergent-flap internal static pressure ratios

Upper flap

	y/wt/2 = -0.50		y/wt/2 = 0.00				y/wt/2 = 0.50	
	x′/L		x′/L				x′/L	
NPR	0.333	0.667	0.200	0.400	0.600	0.800	0.333	0.667
1.999	0.257	0.523	0.370	0.352	0.485	0.521	0.262	0.521
3.999	0.253	0.165	0.368	0.259	0.164	0.197	0.259	0.163
5.995	0.251	0.164	0.365	0.257	0.163	0.197	0.257	0.163
7.297	0.250	0.162	0.364	0.257	0.163	0.196	0.256	0.163
8.023	0.250	0.162	0.363	0.257	0.162	0.196	0.255	0.163
9.990	0.250	0.161	0.363	0.256	0.162	0.196	0.255	0.164
11.436	0.250	0.161	0.361	0.257	0.162	0.196	0.256	0.164

Lower flap

	y/wt/2 = -0.50		y/wt/2 = 0.00				y/wt/2 = 0.50	
	x′/L		x′/L				x′/L	
NPR	0.333	0.667	0.200	0.400	0.600	0.800	0.333	0.667
1.999	0.262	0.527	0.257	0.341	0.489	0.522	0.258	0.521
3.999	0.259	0.153	0.257	0.251	0.165	0.196	0.257	0.154
5.995	0.258	0.152	0.258	0.250	0.165	0.196	0.256	0.153
7.297	0.258	0.151	0.263	0.249	0.164	0.196	0.256	0.152
8.023	0.258	0.151	0.264	0.249	0.164	0.196	0.255	0.152
9.990	0.258	0.151	0.264	0.249	0.164	0.196	0.255	0.152
11.436	0.258	0.151	0.265	0.249	0.164	0.196	0.256	0.152

Table 30. Nozzle Internal Static Pressure Ratios $p/p_{t,j}$ for SCF 2-D C-D Nozzle at AR = 2.083, $A_e/A_t = 1.63$, $\delta_{v,p} = 0°$, and $\delta_{v,y} = 15°$

(a) Sidewall internal static pressure ratios

x'/L, left side

NPR	-0.180	-0.078	0.081	0.161	0.242	0.322	0.403	0.483	0.564	0.644
2.007	0.719	0.692	0.496	0.364	0.318	0.281	0.450	0.458	0.462	0.469
3.998	0.716	0.691	0.498	0.360	0.315	0.271	0.232	0.199	0.175	0.155
6.014	0.717	0.690	0.499	0.360	0.315	0.270	0.232	0.198	0.173	0.153
7.301	0.717	0.690	0.500	0.359	0.314	0.269	0.232	0.197	0.173	0.153
8.003	0.718	0.690	0.499	0.360	0.315	0.269	0.232	0.197	0.172	0.152
10.013	0.720	0.689	0.500	0.361	0.312	0.268	0.233	0.196	0.172	0.152
11.321	0.722	0.689	0.501	0.360	0.312	0.268	0.234	0.197	0.172	0.151

x'/L, right side

NPR	-0.383	-0.282	-0.180	-0.078	0.081	0.161	0.242	0.322	0.403	0.483	0.564	0.644
2.007	0.973	0.958	0.656	0.704	0.503	0.369	0.336	0.273	0.431	0.449	0.456	0.465
3.998	0.974	0.957	0.652	0.699	0.503	0.367	0.330	0.270	0.239	0.204	0.176	0.153
6.014	0.975	0.957	0.642	0.698	0.504	0.368	0.328	0.270	0.238	0.202	0.174	0.151
7.301	0.975	0.956	0.638	0.697	0.504	0.368	0.328	0.270	0.238	0.202	0.173	0.151
8.003	0.975	0.956	0.637	0.696	0.504	0.369	0.327	0.270	0.238	0.202	0.173	0.150
10.013	0.976	0.956	0.635	0.696	0.504	0.369	0.327	0.270	0.237	0.202	0.172	0.150
11.321	0.976	0.956	0.635	0.696	0.504	0.370	0.327	0.269	0.237	0.202	0.172	0.150

(b) Divergent-flap internal static pressure ratios

Upper flap

	y/wt/2 = -0.50		y/wt/2 = 0.00				y/wt/2 = 0.50	
	x'/L		x'/L				x'/L	
NPR	0.333	0.667	0.200	0.400	0.600	0.800	0.333	0.667
2.007	0.257	0.520	0.369	0.353	0.487	0.520	0.261	0.521
3.998	0.252	0.164	0.366	0.258	0.165	0.198	0.258	0.164
6.014	0.250	0.163	0.363	0.258	0.164	0.198	0.256	0.164
7.301	0.250	0.162	0.362	0.257	0.163	0.198	0.255	0.164
8.003	0.250	0.161	0.362	0.257	0.163	0.198	0.255	0.164
10.013	0.249	0.160	0.362	0.257	0.163	0.198	0.255	0.164
11.321	0.250	0.160	0.360	0.257	0.163	0.198	0.256	0.164

Lower flap

	y/wt/2 = -0.50		y/wt/2 = 0.00				y/wt/2 = 0.50	
	x'/L		x'/L				x'/L	
NPR	0.333	0.667	0.200	0.400	0.600	0.800	0.333	0.667
2.007	0.261	0.526	0.259	0.341	0.493	0.521	0.257	0.520
3.998	0.259	0.153	0.256	0.252	0.165	0.197	0.256	0.154
6.014	0.258	0.151	0.257	0.251	0.165	0.197	0.255	0.153
7.301	0.258	0.151	0.259	0.250	0.165	0.197	0.255	0.152
8.003	0.258	0.151	0.261	0.249	0.165	0.197	0.255	0.152
10.013	0.258	0.151	0.263	0.250	0.165	0.196	0.255	0.152
11.321	0.258	0.150	0.263	0.250	0.165	0.197	0.256	0.152

Table 31. Nozzle Internal Static Pressure Ratios $p/p_{t,j}$ for SCF 2-D C-D Nozzle at AR = 2.083, $A_e/A_t = 1.63$, $\delta_{v,p} = 0°$, and $\delta_{v,y} = 20°$

(a) Sidewall internal static pressure ratios

x′/L, left side

NPR	−0.180	−0.078	0.081	0.161	0.242	0.322	0.403	0.483	0.564	0.644
2.001	0.529	0.579	0.527	0.402	0.325	0.271	0.400	0.429	0.438	0.456
3.997	0.534	0.571	0.527	0.399	0.323	0.269	0.227	0.195	0.169	0.151
6.012	0.538	0.568	0.527	0.398	0.323	0.268	0.227	0.194	0.168	0.150
7.312	0.536	0.569	0.527	0.398	0.323	0.268	0.226	0.193	0.168	0.149
8.006	0.536	0.569	0.527	0.398	0.323	0.268	0.226	0.193	0.168	0.149
8.726	0.536	0.570	0.527	0.398	0.323	0.268	0.226	0.193	0.168	0.148

x′/L, right side

NPR	−0.383	−0.282	−0.180	−0.078	0.081	0.161	0.242	0.322	0.403	0.483	0.564	0.644
2.001	0.975	0.957	0.664	0.706	0.503	0.372	0.335	0.277	0.446	0.458	0.464	0.471
3.997	0.977	0.957	0.657	0.702	0.503	0.368	0.329	0.267	0.231	0.197	0.170	0.148
6.012	0.977	0.957	0.648	0.700	0.504	0.369	0.328	0.267	0.229	0.196	0.169	0.147
7.312	0.978	0.957	0.643	0.698	0.504	0.369	0.327	0.268	0.228	0.195	0.168	0.146
8.006	0.977	0.958	0.642	0.698	0.505	0.370	0.327	0.268	0.228	0.195	0.168	0.146
8.726	0.978	0.957	0.641	0.698	0.505	0.370	0.327	0.268	0.228	0.195	0.167	0.146

(b) Divergent-flap internal static pressure ratios

Upper flap

	y/wt/2 = −0.50		y/wt/2 = 0.00				y/wt/2 = 0.50	
	x′/L		x′/L				x′/L	
NPR	0.333	0.667	0.200	0.400	0.600	0.800	0.333	0.667
2.001	0.261	0.500	0.297	0.291	0.474	0.523	0.256	0.527
3.997	0.256	0.155	0.296	0.254	0.165	0.205	0.253	0.150
6.012	0.254	0.155	0.293	0.254	0.164	0.206	0.251	0.150
7.312	0.254	0.154	0.293	0.254	0.164	0.206	0.250	0.150
8.006	0.254	0.154	0.292	0.254	0.164	0.207	0.250	0.150
8.726	0.254	0.154	0.292	0.254	0.164	0.207	0.250	0.150

Lower flap

	y/wt/2 = −0.50		y/wt/2 = 0.00				y/wt/2 = 0.50	
	x′/L		x′/L				x′/L	
NPR	0.333	0.667	0.200	0.400	0.600	0.800	0.333	0.667
2.001	0.267	0.501	0.284	0.383	0.451	0.524	0.247	0.519
3.997	0.263	0.152	0.279	0.249	0.163	0.203	0.246	0.150
6.012	0.261	0.152	0.274	0.249	0.163	0.204	0.246	0.149
7.312	0.259	0.151	0.273	0.249	0.163	0.205	0.246	0.149
8.006	0.259	0.151	0.272	0.249	0.163	0.205	0.246	0.149
8.726	0.260	0.151	0.271	0.249	0.163	0.205	0.246	0.149

Table 32. Nozzle Internal Static Pressure Ratios $p/p_{t,j}$ for SCF 2-D C-D Nozzle at AR = 2.083, $A_e/A_t = 1.63$, $\delta_{v,p} = 20°$, and $\delta_{v,y} = 0°$

(a) Sidewall internal static pressure ratios

x′/L, left side

NPR	−0.282	−0.180	−0.078	0.081	0.161	0.242	0.322	0.403	0.483	0.564	0.644
2.003	0.963	0.705	0.763	0.630	0.533	0.475	0.460	0.422	0.389	0.357	0.334
4.005	0.964	0.696	0.751	0.614	0.507	0.429	0.358	0.299	0.251	0.211	0.178
6.014	0.964	0.693	0.750	0.614	0.507	0.430	0.358	0.299	0.250	0.210	0.176
7.306	0.964	0.690	0.750	0.614	0.507	0.430	0.358	0.299	0.250	0.209	0.175
8.009	0.964	0.689	0.749	0.614	0.506	0.430	0.358	0.299	0.250	0.209	0.174
10.004	0.963	0.689	0.749	0.614	0.506	0.430	0.359	0.299	0.250	0.208	0.174
11.675	0.963	0.689	0.748	0.614	0.505	0.430	0.360	0.299	0.250	0.208	0.173

x′/L, right side

NPR	−0.282	−0.180	−0.078	0.081	0.161	0.242	0.322	0.403	0.483	0.564	0.644
2.003	0.961	0.711	0.763	0.632	0.543	0.493	0.446	0.424	0.389	0.357	0.343
4.005	0.960	0.697	0.751	0.618	0.522	0.433	0.350	0.303	0.251	0.207	0.176
6.014	0.961	0.687	0.750	0.619	0.522	0.431	0.348	0.303	0.249	0.206	0.174
7.306	0.961	0.683	0.749	0.619	0.522	0.431	0.348	0.302	0.249	0.206	0.173
8.009	0.960	0.683	0.749	0.619	0.522	0.431	0.348	0.302	0.249	0.206	0.173
10.004	0.960	0.681	0.748	0.618	0.522	0.431	0.347	0.303	0.249	0.205	0.173
11.675	0.960	0.680	0.748	0.618	0.522	0.432	0.347	0.304	0.249	0.205	0.173

(b) Divergent-flap internal static pressure ratios

Upper flap

	y/wt/2 = −0.50		y/wt/2 = 0.00				y/wt/2 = 0.50	
	x′/L		x′/L				x′/L	
NPR	0.327	0.654	0.197	0.392	0.589	0.785	0.327	0.654
2.003	0.470	0.334	0.597	0.431	0.358	0.425	0.474	0.338
4.005	0.412	0.178	0.557	0.345	0.208	0.135	0.413	0.177
6.014	0.413	0.178	0.555	0.344	0.207	0.134	0.411	0.176
7.306	0.413	0.178	0.555	0.344	0.206	0.134	0.411	0.176
8.009	0.414	0.178	0.555	0.344	0.206	0.134	0.410	0.176
10.004	0.414	0.177	0.554	0.345	0.206	0.133	0.411	0.176
11.675	0.414	0.177	0.553	0.346	0.206	0.133	0.411	0.176

Lower flap

	y/wt/2 = −0.50		y/wt/2 = 0.00				y/wt/2 = 0.50	
	x′/L		x′/L				x′/L	
NPR	0.299	0.599	0.180	0.359	0.539	0.718	0.299	0.599
2.003	0.372	0.397	0.382	0.370	0.379	0.403	0.372	0.391
4.005	0.224	0.213	0.113	0.230	0.252	0.199	0.219	0.210
6.014	0.222	0.213	0.110	0.232	0.252	0.198	0.218	0.210
7.306	0.222	0.212	0.109	0.233	0.251	0.198	0.218	0.209
8.009	0.222	0.213	0.109	0.233	0.250	0.198	0.217	0.209
10.004	0.221	0.212	0.109	0.234	0.250	0.198	0.216	0.209
11.675	0.221	0.212	0.108	0.232	0.250	0.198	0.216	0.209

Table 33. Nozzle Internal Static Pressure Ratios $p/p_{t,j}$ for SCF 2-D C-D Nozzle at AR = 2.083, $A_e/A_t = 1.63$, $\delta_{v,p} = 20^\circ$, and $\delta_{v,y} = 7^\circ$

(a) Sidewall internal static pressure ratios

x′/L, left side

NPR	−0.180	−0.078	0.081	0.161	0.242	0.322	0.403	0.483	0.564	0.644
2.004	0.710	0.758	0.629	0.532	0.476	0.459	0.420	0.387	0.357	0.335
4.001	0.697	0.749	0.612	0.507	0.428	0.358	0.298	0.250	0.211	0.178
6.013	0.693	0.748	0.613	0.506	0.428	0.358	0.298	0.249	0.209	0.176
7.315	0.692	0.748	0.612	0.505	0.428	0.358	0.298	0.249	0.209	0.175
8.001	0.690	0.747	0.612	0.505	0.429	0.358	0.298	0.249	0.208	0.174
10.003	0.691	0.747	0.612	0.505	0.429	0.359	0.298	0.249	0.208	0.174
11.555	0.692	0.746	0.612	0.504	0.429	0.359	0.299	0.249	0.208	0.174

x′/L, right side

NPR	−0.282	−0.180	−0.078	0.081	0.161	0.242	0.322	0.403	0.483	0.564	0.644
2.004	0.959	0.712	0.767	0.633	0.544	0.489	0.445	0.425	0.391	0.358	0.341
4.001	0.959	0.698	0.754	0.620	0.522	0.433	0.350	0.306	0.251	0.210	0.175
6.013	0.960	0.689	0.752	0.621	0.524	0.432	0.348	0.305	0.250	0.208	0.174
7.315	0.959	0.686	0.750	0.620	0.524	0.432	0.348	0.305	0.249	0.207	0.173
8.001	0.959	0.684	0.751	0.621	0.524	0.432	0.348	0.305	0.249	0.206	0.173
10.003	0.959	0.683	0.750	0.620	0.524	0.433	0.348	0.305	0.249	0.206	0.173
11.555	0.959	0.683	0.750	0.620	0.524	0.433	0.348	0.305	0.249	0.206	0.173

(b) Divergent-flap internal static pressure ratios

Upper flap

	y/wt/2 = −0.50		y/wt/2 = 0.00				y/wt/2 = 0.50	
	x′/L		x′/L				x′/L	
NPR	0.327	0.654	0.197	0.392	0.589	0.785	0.327	0.654
2.004	0.468	0.335	0.597	0.430	0.357	0.425	0.471	0.339
4.001	0.411	0.178	0.556	0.345	0.208	0.135	0.412	0.178
6.013	0.412	0.178	0.554	0.344	0.207	0.134	0.411	0.177
7.315	0.412	0.177	0.554	0.344	0.207	0.134	0.410	0.177
8.001	0.412	0.177	0.554	0.344	0.206	0.134	0.411	0.177
10.003	0.413	0.176	0.553	0.345	0.206	0.134	0.411	0.176
11.555	0.413	0.176	0.552	0.345	0.206	0.133	0.411	0.176

Lower flap

	y/wt/2 = −0.50		y/wt/2 = 0.00				y/wt/2 = 0.50	
	x′/L		x′/L				x′/L	
NPR	0.299	0.599	0.180	0.359	0.539	0.718	0.299	0.599
2.004	0.371	0.396	0.381	0.370	0.379	0.403	0.371	0.392
4.001	0.223	0.213	0.111	0.232	0.252	0.199	0.218	0.210
6.013	0.222	0.213	0.109	0.233	0.251	0.199	0.218	0.209
7.315	0.221	0.213	0.109	0.234	0.250	0.198	0.218	0.209
8.001	0.222	0.213	0.109	0.234	0.250	0.198	0.217	0.209
10.003	0.221	0.213	0.109	0.233	0.249	0.198	0.217	0.209
11.555	0.220	0.212	0.108	0.233	0.249	0.198	0.217	0.209

Table 34. Nozzle Internal Static Pressure Ratios $p/p_{t,j}$ for SCF 2-D C-D Nozzle at AR = 2.083, $A_e/A_t = 1.63$, $\delta_{v,p} = 20°$, and $\delta_{v,y} = 15°$

(a) Sidewall internal static pressure ratios

x′/L, left side

NPR	−0.180	−0.078	0.081	0.161	0.242	0.322	0.403	0.483	0.564	0.644
2.003	0.769	0.756	0.628	0.531	0.476	0.458	0.419	0.384	0.353	0.329
3.999	0.757	0.746	0.611	0.506	0.427	0.356	0.297	0.250	0.210	0.178
6.005	0.757	0.746	0.611	0.506	0.428	0.356	0.297	0.249	0.210	0.176
7.299	0.759	0.746	0.612	0.505	0.429	0.357	0.297	0.249	0.209	0.176
8.001	0.759	0.745	0.612	0.505	0.429	0.357	0.297	0.249	0.209	0.175
10.012	0.762	0.745	0.612	0.505	0.429	0.357	0.297	0.249	0.209	0.175
11.777	0.763	0.745	0.612	0.504	0.430	0.358	0.298	0.249	0.209	0.175

x′/L, right side

NPR	−0.383	−0.282	−0.180	−0.078	0.081	0.161	0.242	0.322	0.403	0.483	0.564	0.644
2.003	0.972	0.961	0.716	0.767	0.635	0.544	0.480	0.441	0.423	0.390	0.358	0.342
3.999	0.976	0.960	0.700	0.756	0.622	0.524	0.434	0.350	0.306	0.250	0.209	0.174
6.005	0.976	0.960	0.691	0.753	0.622	0.525	0.433	0.349	0.305	0.249	0.207	0.173
7.299	0.977	0.961	0.688	0.753	0.622	0.525	0.433	0.348	0.305	0.249	0.206	0.173
8.001	0.977	0.960	0.688	0.752	0.622	0.525	0.433	0.349	0.305	0.249	0.206	0.173
10.012	0.978	0.960	0.686	0.752	0.622	0.525	0.433	0.349	0.305	0.249	0.206	0.173
11.777	0.978	0.960	0.684	0.752	0.621	0.525	0.434	0.349	0.306	0.249	0.206	0.172

(b) Divergent-flap internal static pressure ratios

Upper flap

	y/wt/2 = −0.50		y/wt/2 = 0.00				y/wt/2 = 0.50	
	x′/L		x′/L				x′/L	
NPR	0.327	0.654	0.197	0.392	0.589	0.785	0.327	0.654
2.003	0.469	0.331	0.596	0.427	0.356	0.431	0.467	0.340
3.999	0.411	0.178	0.555	0.344	0.208	0.135	0.412	0.178
6.005	0.411	0.177	0.552	0.343	0.207	0.134	0.411	0.177
7.299	0.412	0.177	0.552	0.343	0.206	0.134	0.412	0.177
8.001	0.412	0.177	0.552	0.344	0.206	0.134	0.412	0.177
10.012	0.413	0.177	0.551	0.344	0.206	0.134	0.412	0.177
11.777	0.413	0.176	0.551	0.345	0.206	0.134	0.412	0.177

Lower flap

	y/wt/2 = −0.50		y/wt/2 = 0.00				y/wt/2 = 0.50	
	x′/L		x′/L				x′/L	
NPR	0.299	0.599	0.180	0.359	0.539	0.718	0.299	0.599
2.003	0.371	0.395	0.379	0.369	0.378	0.403	0.371	0.394
3.999	0.224	0.213	0.112	0.231	0.251	0.199	0.217	0.210
6.005	0.223	0.212	0.110	0.232	0.250	0.198	0.217	0.210
7.299	0.223	0.212	0.109	0.233	0.250	0.198	0.217	0.210
8.001	0.223	0.212	0.109	0.233	0.250	0.198	0.216	0.210
10.012	0.222	0.212	0.109	0.233	0.250	0.198	0.216	0.210
11.777	0.222	0.212	0.109	0.232	0.249	0.198	0.216	0.210

Table 35. Nozzle Internal Static Pressure Ratios $p/p_{t,j}$ for SCF 2-D C-D Nozzle at AR = 2.083, $A_e/A_t = 1.63$, $\delta_{v,p} = 20°$, and $\delta_{v,y} = 20°$

(a) Sidewall internal static pressure ratios

x′/L, left side

NPR	−0.180	−0.078	0.081	0.161	0.242	0.322	0.403	0.483	0.564	0.644
2.006	0.634	0.699	0.664	0.577	0.514	0.460	0.419	0.382	0.352	0.331
4.000	0.612	0.676	0.636	0.521	0.433	0.363	0.304	0.255	0.215	0.182
6.011	0.613	0.670	0.637	0.521	0.434	0.364	0.305	0.255	0.213	0.180
7.312	0.612	0.668	0.637	0.521	0.434	0.365	0.304	0.255	0.213	0.179
8.010	0.612	0.668	0.637	0.520	0.434	0.365	0.304	0.254	0.213	0.179
10.005	0.612	0.668	0.637	0.520	0.434	0.365	0.305	0.255	0.212	0.178

x′/L, right side

NPR	−0.383	−0.282	−0.180	−0.078	0.081	0.161	0.242	0.322	0.403	0.483	0.564	0.644
2.006	0.980	0.963	0.715	0.768	0.634	0.542	0.477	0.438	0.424	0.394	0.363	0.344
4.000	0.979	0.962	0.701	0.755	0.620	0.522	0.431	0.347	0.301	0.246	0.204	0.170
6.011	0.979	0.961	0.694	0.753	0.621	0.523	0.430	0.346	0.300	0.245	0.203	0.169
7.312	0.979	0.961	0.690	0.753	0.620	0.523	0.430	0.345	0.300	0.244	0.202	0.169
8.010	0.979	0.962	0.689	0.752	0.621	0.523	0.430	0.345	0.300	0.244	0.202	0.169
10.005	0.980	0.961	0.686	0.752	0.620	0.523	0.430	0.345	0.300	0.245	0.201	0.168

(b) Divergent-flap internal static pressure ratios

Upper flap

	y/wt/2 = −0.50		y/wt/2 = 0.00				y/wt/2 = 0.50	
	x′/L		x′/L				x′/L	
NPR	0.327	0.654	0.197	0.392	0.589	0.785	0.327	0.654
2.006	0.489	0.330	0.594	0.436	0.354	0.436	0.468	0.339
4.000	0.413	0.181	0.546	0.341	0.207	0.135	0.407	0.175
6.011	0.414	0.181	0.544	0.340	0.206	0.135	0.407	0.174
7.312	0.414	0.180	0.544	0.341	0.205	0.134	0.406	0.174
8.010	0.414	0.180	0.544	0.341	0.205	0.134	0.406	0.174
10.005	0.415	0.179	0.544	0.341	0.205	0.134	0.406	0.174

Lower flap

	y/wt/2 = −0.50		y/wt/2 = 0.00				y/wt/2 = 0.50	
	x′/L		x′/L				x′/L	
NPR	0.299	0.599	0.180	0.359	0.539	0.718	0.299	0.599
2.006	0.371	0.395	0.379	0.369	0.378	0.404	0.370	0.395
4.000	0.236	0.211	0.107	0.219	0.254	0.199	0.208	0.208
6.011	0.236	0.211	0.105	0.218	0.253	0.199	0.207	0.207
7.312	0.236	0.211	0.104	0.219	0.253	0.198	0.207	0.207
8.010	0.236	0.210	0.104	0.219	0.252	0.198	0.206	0.207
10.005	0.235	0.210	0.102	0.220	0.252	0.198	0.205	0.207

Table 36. Nozzle Internal Static Pressure Ratios $p/p_{t,j}$ for SCF 2-D C-D Nozzle at AR = 1.265, $A_e/A_t = 1.46$, $\delta_{v,p} = 0°$, and $\delta_{v,y} = 0°$

(a) Sidewall internal static pressure ratios

x′/L, left side

NPR	−0.194	−0.106	−0.018	0.080	0.160	0.241	0.321	0.401	0.482	0.562	0.642
1.991	0.964	0.941	0.426	0.439	0.367	0.284	0.233	0.210	0.272	0.377	0.462
4.003	0.967	0.945	0.416	0.445	0.363	0.281	0.230	0.208	0.262	0.254	0.238
5.014	0.966	0.946	0.413	0.447	0.362	0.280	0.229	0.207	0.262	0.254	0.237
5.903	0.967	0.946	0.412	0.447	0.362	0.280	0.229	0.207	0.262	0.253	0.236
7.008	0.967	0.947	0.410	0.447	0.361	0.280	0.228	0.206	0.261	0.253	0.236
8.995	0.966	0.947	0.409	0.447	0.361	0.280	0.228	0.206	0.260	0.252	0.235
11.429	0.965	0.947	0.409	0.446	0.361	0.281	0.228	0.206	0.260	0.251	0.235

x′/L, right side

NPR	−0.194	−0.106	−0.018	0.080	0.160	0.241	0.321	0.401	0.482	0.562	0.642
1.991	0.956	0.947	0.431	0.443	0.366	0.290	0.237	0.217	0.306	0.391	0.456
4.003	0.958	0.943	0.422	0.444	0.362	0.282	0.234	0.209	0.271	0.259	0.232
5.014	0.958	0.943	0.419	0.445	0.362	0.280	0.233	0.208	0.270	0.258	0.231
5.903	0.959	0.943	0.418	0.446	0.363	0.279	0.232	0.207	0.269	0.258	0.231
7.008	0.959	0.943	0.416	0.446	0.363	0.279	0.232	0.206	0.269	0.257	0.231
8.995	0.960	0.943	0.416	0.446	0.363	0.278	0.231	0.205	0.269	0.257	0.231
11.429	0.960	0.944	0.416	0.446	0.363	0.278	0.231	0.204	0.268	0.256	0.231

(b) Divergent-flap internal static pressure ratios

Upper flap

	y/wt/2 = −0.50		y/wt/2 = 0.00				y/wt/2 = 0.50	
	x′/L		x′/L				x′/L	
NPR	0.333	0.667	0.200	0.400	0.600	0.800	0.333	0.667
1.991	0.292	0.429	0.388	0.249	0.411	0.471	0.291	0.435
4.003	0.287	0.216	0.386	0.248	0.197	0.182	0.287	0.217
5.014	0.286	0.215	0.386	0.248	0.188	0.181	0.285	0.216
5.903	0.285	0.215	0.386	0.247	0.183	0.181	0.285	0.216
7.008	0.285	0.214	0.386	0.247	0.179	0.181	0.284	0.216
8.995	0.285	0.215	0.386	0.247	0.173	0.180	0.285	0.216
11.429	0.285	0.215	0.386	0.247	0.170	0.180	0.286	0.215

Lower flap

	y/wt/2 = −0.50		y/wt/2 = 0.00				y/wt/2 = 0.50	
	x′/L		x′/L				x′/L	
NPR	0.333	0.667	0.200	0.400	0.600	0.800	0.333	0.667
1.991	0.290	0.418	0.397	0.250	0.396	0.469	0.289	0.428
4.003	0.287	0.222	0.393	0.248	0.185	0.186	0.288	0.216
5.014	0.286	0.222	0.393	0.248	0.179	0.185	0.288	0.215
5.903	0.286	0.222	0.393	0.247	0.175	0.185	0.287	0.215
7.008	0.286	0.221	0.394	0.247	0.174	0.184	0.287	0.215
8.995	0.286	0.221	0.395	0.247	0.171	0.184	0.287	0.215
11.429	0.287	0.221	0.395	0.247	0.168	0.183	0.288	0.216

Table 37. Nozzle Internal Static Pressure Ratios $p/p_{t,j}$ for SCF 2-D C-D Nozzle at AR = 1.265, $A_e/A_t = 1.46$, $\delta_{v,p} = 0°$, and $\delta_{v,y} = 15°$

(a) Sidewall internal static pressure ratios

x′/L, left side

NPR	-0.018	0.080	0.160	0.241	0.321	0.401	0.482	0.562	0.642
2.011	0.423	0.441	0.365	0.278	0.228	0.208	0.276	0.400	0.466
4.006	0.417	0.447	0.360	0.277	0.227	0.205	0.269	0.254	0.237
4.997	0.414	0.450	0.359	0.276	0.226	0.204	0.268	0.253	0.236
5.902	0.411	0.451	0.359	0.276	0.226	0.204	0.268	0.252	0.236
6.999	0.411	0.451	0.359	0.276	0.225	0.204	0.267	0.251	0.235
8.996	0.411	0.451	0.358	0.277	0.225	0.204	0.267	0.250	0.235
11.552	0.411	0.450	0.357	0.277	0.225	0.203	0.265	0.250	0.236

x′/L, right side

NPR	-0.282	-0.194	-0.106	-0.018	0.080	0.160	0.241	0.321	0.401	0.482	0.562	0.642
2.011	0.957	0.969	0.948	0.443	0.452	0.366	0.289	0.240	0.224	0.342	0.419	0.454
4.006	0.962	0.972	0.944	0.429	0.453	0.363	0.282	0.236	0.214	0.269	0.257	0.230
4.997	0.963	0.971	0.944	0.425	0.455	0.363	0.280	0.235	0.212	0.269	0.258	0.230
5.902	0.964	0.972	0.944	0.423	0.455	0.363	0.279	0.234	0.210	0.268	0.258	0.229
6.999	0.966	0.972	0.944	0.422	0.455	0.363	0.278	0.234	0.209	0.268	0.257	0.230
8.996	0.967	0.973	0.944	0.420	0.454	0.363	0.278	0.233	0.207	0.267	0.257	0.230
11.552	0.967	0.972	0.945	0.420	0.454	0.363	0.278	0.233	0.206	0.267	0.257	0.230

(b) Divergent-flap internal static pressure ratios

Upper flap

	y/wt/2 = -0.50		y/wt/2 = 0.00				y/wt/2 = 0.50	
	x′/L		x′/L				x′/L	
NPR	0.333	0.667	0.200	0.400	0.600	0.800	0.333	0.667
2.011	0.291	0.435	0.389	0.250	0.404	0.485	0.292	0.458
4.006	0.287	0.215	0.388	0.248	0.204	0.183	0.288	0.215
4.997	0.286	0.215	0.387	0.248	0.197	0.182	0.287	0.215
5.902	0.285	0.214	0.387	0.248	0.191	0.182	0.287	0.215
6.999	0.285	0.214	0.388	0.247	0.184	0.181	0.286	0.215
8.996	0.285	0.215	0.388	0.247	0.177	0.181	0.287	0.214
11.552	0.286	0.216	0.388	0.248	0.173	0.180	0.288	0.214

Lower flap

	y/wt/2 = -0.50		y/wt/2 = 0.00				y/wt/2 = 0.50	
	x′/L		x′/L				x′/L	
NPR	0.333	0.667	0.200	0.400	0.600	0.800	0.333	0.667
2.011	0.290	0.431	0.399	0.249	0.398	0.490	0.290	0.468
4.006	0.287	0.222	0.397	0.248	0.206	0.186	0.289	0.217
4.997	0.287	0.222	0.398	0.247	0.197	0.186	0.289	0.216
5.902	0.286	0.222	0.399	0.247	0.191	0.185	0.289	0.216
6.999	0.286	0.222	0.399	0.247	0.190	0.184	0.289	0.216
8.996	0.287	0.222	0.399	0.247	0.186	0.184	0.289	0.217
11.552	0.287	0.223	0.399	0.247	0.179	0.184	0.289	0.217

Table 38. Nozzle Internal Static Pressure Ratios $p/p_{t,j}$ for SCF 2-D C-D Nozzle at AR = 1.265, $A_e/A_t = 1.46$, $\delta_{v,p} = 0°$, and $\delta_{v,y} = 25°$

(a) Sidewall internal static pressure ratios

x′/L, left side

NPR	-0.018	0.080	0.160	0.241	0.321	0.401	0.482	0.562	0.642
1.999	0.354	0.453	0.360	0.274	0.227	0.219	0.365	0.452	0.496
4.000	0.341	0.459	0.358	0.273	0.226	0.212	0.273	0.257	0.240
5.005	0.339	0.459	0.357	0.273	0.226	0.210	0.273	0.256	0.240
5.902	0.337	0.459	0.357	0.273	0.225	0.209	0.272	0.256	0.239
7.012	0.337	0.458	0.356	0.273	0.225	0.209	0.272	0.255	0.239
7.704	0.338	0.458	0.355	0.272	0.225	0.208	0.272	0.255	0.239

x′/L, right side

NPR	-0.282	-0.194	-0.106	-0.018	0.080	0.160	0.241	0.321	0.401	0.482	0.562	0.642
1.999	0.971	0.974	0.950	0.449	0.458	0.365	0.286	0.281	0.395	0.415	0.430	0.453
4.000	0.976	0.975	0.947	0.436	0.459	0.363	0.279	0.230	0.199	0.182	0.169	0.251
5.005	0.976	0.975	0.947	0.432	0.460	0.363	0.277	0.229	0.198	0.181	0.168	0.250
5.902	0.977	0.975	0.947	0.430	0.461	0.363	0.276	0.228	0.197	0.180	0.167	0.250
7.012	0.977	0.975	0.946	0.428	0.460	0.363	0.276	0.228	0.196	0.180	0.166	0.250
7.704	0.978	0.976	0.947	0.428	0.460	0.362	0.275	0.228	0.196	0.179	0.166	0.250

(b) Divergent-flap internal static pressure ratios

Upper flap

	y/wt/2 = -0.50		y/wt/2 = 0.00				y/wt/2 = 0.50	
	x′/L		x′/L				x′/L	
NPR	0.333	0.667	0.200	0.400	0.600	0.800	0.333	0.667
1.999	0.295	0.475	0.328	0.253	0.476	0.515	0.262	0.495
4.000	0.291	0.220	0.325	0.252	0.163	0.174	0.258	0.148
5.005	0.290	0.219	0.325	0.251	0.163	0.173	0.256	0.147
5.902	0.289	0.219	0.325	0.251	0.162	0.173	0.256	0.147
7.012	0.289	0.218	0.324	0.251	0.162	0.172	0.255	0.146
7.704	0.289	0.218	0.324	0.251	0.162	0.172	0.255	0.146

Lower flap

	y/wt/2 = -0.50		y/wt/2 = 0.00				y/wt/2 = 0.50	
	x′/L		x′/L				x′/L	
NPR	0.333	0.667	0.200	0.400	0.600	0.800	0.333	0.667
1.999	0.293	0.482	0.329	0.252	0.488	0.516	0.253	0.488
4.000	0.291	0.228	0.328	0.250	0.165	0.177	0.252	0.154
5.005	0.291	0.228	0.327	0.250	0.164	0.176	0.251	0.152
5.902	0.291	0.229	0.328	0.250	0.164	0.175	0.251	0.150
7.012	0.291	0.228	0.328	0.249	0.164	0.175	0.251	0.149
7.704	0.291	0.228	0.328	0.249	0.164	0.175	0.250	0.148

Table 39. Nozzle Internal Static Pressure Ratios $p/p_{t,j}$ for SCF 2-D C-D Nozzle at AR = 1.265, $A_e/A_t = 1.46$, $\delta_{v,p} = 25°$, and $\delta_{v,y} = 0°$

(a) Sidewall internal static pressure ratios

NPR	x′/L, left side								
	-0.194	-0.106	-0.018	0.080	0.160	0.241	0.321	0.401	0.482
1.998	0.968	0.948	0.511	0.657	0.563	0.486	0.409	0.348	0.287
3.998	0.973	0.956	0.508	0.656	0.558	0.480	0.400	0.336	0.270
5.006	0.973	0.954	0.512	0.656	0.558	0.481	0.400	0.336	0.269
5.902	0.973	0.955	0.507	0.655	0.557	0.482	0.401	0.336	0.269
7.005	0.972	0.954	0.505	0.654	0.557	0.482	0.401	0.336	0.269
9.006	0.971	0.955	0.507	0.654	0.555	0.483	0.401	0.336	0.268
11.840	0.970	0.954	0.507	0.655	0.555	0.483	0.401	0.337	0.267

NPR	x′/L, right side								
	-0.194	-0.106	-0.018	0.080	0.160	0.241	0.321	0.401	0.482
1.998	0.963	0.955	0.523	0.664	0.568	0.486	0.411	0.344	0.293
3.998	0.964	0.951	0.512	0.658	0.565	0.476	0.402	0.331	0.278
5.006	0.964	0.951	0.508	0.656	0.565	0.475	0.401	0.331	0.277
5.902	0.965	0.950	0.522	0.658	0.565	0.475	0.401	0.330	0.277
7.005	0.965	0.951	0.529	0.659	0.565	0.475	0.401	0.330	0.276
9.006	0.965	0.951	0.532	0.659	0.564	0.475	0.402	0.331	0.276
11.840	0.966	0.952	0.523	0.660	0.563	0.476	0.402	0.331	0.276

(b) Divergent-flap internal static pressure ratios

Upper flap

NPR	y/wt/2 = -0.50		y/wt/2 = 0.00				y/wt/2 = 0.50	
	x′/L		x′/L				x′/L	
	0.315	0.630	0.189	0.378	0.567	0.756	0.315	0.630
1.998	0.463	0.427	0.620	0.392	0.418	0.469	0.466	0.430
3.998	0.454	0.187	0.613	0.381	0.225	0.141	0.459	0.191
5.006	0.453	0.187	0.612	0.380	0.224	0.140	0.458	0.191
5.902	0.453	0.186	0.612	0.380	0.224	0.140	0.459	0.191
7.005	0.453	0.186	0.612	0.380	0.224	0.139	0.458	0.190
9.006	0.453	0.185	0.611	0.381	0.224	0.139	0.458	0.190
11.840	0.453	0.185	0.611	0.381	0.224	0.139	0.459	0.190

Lower flap

NPR	y/wt/2 = -0.50		y/wt/2 = 0.00				y/wt/2 = 0.50	
	x′/L		x′/L				x′/L	
	0.289	0.579	0.174	0.347	0.521	0.695	0.289	0.579
1.998	0.297	0.481	0.193	0.337	0.456	0.505	0.296	0.480
3.998	0.281	0.240	0.156	0.309	0.252	0.204	0.281	0.243
5.006	0.280	0.239	0.156	0.309	0.251	0.204	0.281	0.242
5.902	0.280	0.239	0.156	0.308	0.251	0.203	0.281	0.243
7.005	0.279	0.239	0.156	0.307	0.250	0.203	0.281	0.243
9.006	0.279	0.239	0.156	0.306	0.250	0.203	0.280	0.243
11.840	0.278	0.239	0.156	0.306	0.250	0.203	0.280	0.242

Table 40. Nozzle Internal Static Pressure Ratios $p/p_{t,j}$ for SCF 2-D C-D Nozzle at AR = 1.265, $A_e/A_t = 1.46$, $\delta_{v,p} = 25°$, and $\delta_{v,y} = 15°$

(a) Sidewall internal static pressure ratios

	x'/L, left side						
NPR	-0.018	0.080	0.160	0.241	0.321	0.401	0.482
2.001	0.514	0.653	0.556	0.479	0.404	0.337	0.277
4.008	0.511	0.650	0.553	0.480	0.403	0.334	0.273
5.014	0.513	0.650	0.553	0.481	0.402	0.334	0.272
5.907	0.511	0.649	0.553	0.481	0.402	0.335	0.271
7.007	0.513	0.648	0.552	0.481	0.402	0.335	0.271
9.006	0.513	0.650	0.552	0.483	0.403	0.336	0.270
11.905	0.515	0.654	0.551	0.483	0.403	0.337	0.269
11.910	0.512	0.653	0.551	0.483	0.403	0.337	0.269

	x'/L, right side									
NPR	-0.282	-0.194	-0.106	-0.018	0.080	0.160	0.241	0.321	0.401	0.482
2.001	0.966	0.973	0.957	0.528	0.663	0.566	0.482	0.406	0.340	0.283
4.008	0.969	0.976	0.953	0.531	0.663	0.566	0.475	0.404	0.335	0.278
5.014	0.969	0.976	0.952	0.532	0.662	0.566	0.474	0.403	0.335	0.277
5.907	0.970	0.976	0.953	0.536	0.661	0.566	0.474	0.403	0.334	0.276
7.007	0.971	0.976	0.952	0.537	0.661	0.566	0.473	0.402	0.334	0.276
9.006	0.972	0.976	0.953	0.541	0.661	0.566	0.474	0.403	0.334	0.276
11.905	0.973	0.976	0.954	0.540	0.661	0.565	0.474	0.403	0.335	0.276
11.910	0.973	0.976	0.954	0.538	0.661	0.565	0.474	0.403	0.335	0.276

(b) Divergent-flap internal static pressure ratios

Upper flap

	y/wt/2 = -0.50		y/wt/2 = 0.00				y/wt/2 = 0.50	
	x'/L		x'/L				x'/L	
NPR	0.315	0.630	0.189	0.378	0.567	0.756	0.315	0.630
2.001	0.458	0.443	0.616	0.385	0.451	0.473	0.459	0.443
4.008	0.456	0.190	0.614	0.383	0.225	0.141	0.459	0.191
5.014	0.456	0.190	0.613	0.383	0.224	0.140	0.458	0.191
5.907	0.456	0.190	0.613	0.383	0.224	0.140	0.458	0.190
7.007	0.457	0.189	0.613	0.383	0.223	0.139	0.458	0.190
9.006	0.457	0.189	0.613	0.384	0.224	0.139	0.459	0.190
11.905	0.458	0.189	0.613	0.385	0.224	0.139	0.459	0.190
11.910	0.458	0.189	0.613	0.385	0.224	0.139	0.459	0.190

Lower flap

	y/wt/2 = -0.50		y/wt/2 = 0.00				y/wt/2 = 0.50	
	x'/L		x'/L				x'/L	
NPR	0.289	0.579	0.174	0.347	0.521	0.695	0.289	0.579
2.001	0.291	0.506	0.164	0.352	0.499	0.513	0.281	0.508
4.008	0.286	0.241	0.159	0.308	0.254	0.206	0.279	0.240
5.014	0.285	0.240	0.159	0.307	0.254	0.206	0.279	0.239
5.907	0.285	0.240	0.160	0.306	0.253	0.206	0.278	0.239
7.007	0.284	0.240	0.159	0.306	0.253	0.206	0.278	0.239
9.006	0.284	0.240	0.159	0.305	0.253	0.205	0.278	0.239
11.905	0.283	0.240	0.159	0.305	0.253	0.205	0.278	0.239
11.910	0.283	0.240	0.159	0.304	0.253	0.205	0.277	0.238

Table 41. Nozzle Internal Static Pressure Ratios $p/p_{t,j}$ for SCF 2-D C-D Nozzle at AR = 1.265, $A_e/A_t = 1.46$, $\delta_{v,p} = 25°$, and $\delta_{v,y} = 25°$

(a) Sidewall internal static pressure ratios

	x′/L, left side						
NPR	−0.018	0.080	0.160	0.241	0.321	0.401	0.482
1.999	0.630	0.618	0.550	0.508	0.434	0.373	0.311
4.005	0.632	0.613	0.539	0.491	0.408	0.342	0.278
4.998	0.634	0.611	0.540	0.491	0.408	0.342	0.277
5.985	0.635	0.610	0.540	0.492	0.408	0.342	0.277
6.996	0.634	0.609	0.540	0.492	0.408	0.342	0.276
8.844	0.635	0.611	0.539	0.493	0.408	0.342	0.276
8.844	0.635	0.610	0.540	0.493	0.407	0.342	0.276

	x′/L, right side									
NPR	−0.282	−0.194	−0.106	−0.018	0.080	0.160	0.241	0.321	0.401	0.482
1.999	0.976	0.979	0.957	0.530	0.662	0.566	0.496	0.414	0.352	0.300
4.005	0.979	0.979	0.954	0.525	0.658	0.559	0.473	0.397	0.329	0.274
4.998	0.979	0.978	0.953	0.528	0.657	0.559	0.467	0.396	0.329	0.273
5.985	0.979	0.978	0.953	0.530	0.657	0.560	0.446	0.396	0.328	0.272
6.996	0.980	0.978	0.953	0.533	0.656	0.559	0.372	0.396	0.328	0.272
8.844	0.982	0.979	0.953	0.537	0.655	0.560	0.355	0.397	0.329	0.272
8.844	0.981	0.979	0.953	0.537	0.655	0.560	0.373	0.396	0.328	0.272

(b) Divergent-flap internal static pressure ratios

Upper flap

	y/wt/2 = −0.50, x′/L		y/wt/2 = 0.00, x′/L				y/wt/2 = 0.50, x′/L	
NPR	0.315	0.630	0.189	0.378	0.567	0.756	0.315	0.630
1.999	0.474	0.384	0.617	0.402	0.254	0.437	0.464	0.350
4.005	0.457	0.195	0.608	0.381	0.227	0.143	0.453	0.191
4.998	0.456	0.195	0.606	0.380	0.226	0.143	0.452	0.190
5.985	0.457	0.194	0.606	0.380	0.226	0.142	0.452	0.190
6.996	0.457	0.194	0.606	0.381	0.226	0.142	0.452	0.190
8.844	0.457	0.194	0.606	0.382	0.226	0.142	0.452	0.190
8.844	0.457	0.194	0.606	0.382	0.226	0.142	0.452	0.190

Lower flap

	y/wt/2 = −0.50, x′/L		y/wt/2 = 0.00, x′/L				y/wt/2 = 0.50, x′/L	
NPR	0.289	0.579	0.174	0.347	0.521	0.695	0.289	0.579
1.999	0.324	0.449	0.234	0.328	0.409	0.483	0.309	0.447
4.005	0.293	0.235	0.156	0.288	0.254	0.203	0.266	0.238
4.998	0.292	0.234	0.156	0.287	0.253	0.203	0.266	0.238
5.985	0.292	0.234	0.158	0.286	0.253	0.202	0.265	0.237
6.996	0.292	0.234	0.159	0.285	0.253	0.202	0.265	0.237
8.844	0.291	0.233	0.159	0.284	0.253	0.202	0.265	0.237
8.844	0.293	0.234	0.159	0.284	0.253	0.202	0.264	0.237

Table 42. Nozzle Internal Static Pressure Ratios $p/p_{t,j}$ for SCF 2-D C-D Nozzle at AR = 1.265, $A_e/A_t = 1.63$, $\delta_{v,p} = 0°$, and $\delta_{v,y} = 0°$

(a) Sidewall internal static pressure ratios

x′/L, left side

NPR	−0.195	−0.106	−0.018	0.081	0.161	0.242	0.322	0.403	0.483	0.564	0.644
1.995	0.957	0.940	0.420	0.440	0.359	0.269	0.238	0.346	0.372	0.403	0.445
4.011	0.962	0.945	0.412	0.446	0.353	0.267	0.211	0.179	0.172	0.219	0.216
6.024	0.963	0.947	0.408	0.448	0.352	0.266	0.210	0.178	0.169	0.218	0.215
7.299	0.963	0.947	0.408	0.448	0.352	0.266	0.210	0.178	0.167	0.217	0.215
7.996	0.964	0.946	0.409	0.448	0.351	0.265	0.210	0.178	0.166	0.217	0.215
10.007	0.963	0.947	0.408	0.447	0.352	0.265	0.209	0.178	0.165	0.216	0.215
11.453	0.963	0.947	0.409	0.447	0.352	0.266	0.209	0.178	0.164	0.216	0.215

x′/L, right side

NPR	−0.195	−0.106	−0.018	0.081	0.161	0.242	0.322	0.403	0.483	0.564	0.644
1.995	0.954	0.951	0.436	0.442	0.359	0.270	0.304	0.372	0.393	0.415	0.445
4.011	0.957	0.944	0.430	0.445	0.356	0.264	0.211	0.182	0.178	0.224	0.215
6.024	0.958	0.944	0.423	0.446	0.356	0.261	0.209	0.180	0.175	0.223	0.215
7.299	0.959	0.945	0.420	0.446	0.356	0.260	0.208	0.179	0.174	0.223	0.215
7.996	0.959	0.945	0.420	0.446	0.356	0.260	0.207	0.179	0.173	0.223	0.215
10.007	0.959	0.945	0.419	0.446	0.356	0.260	0.207	0.178	0.172	0.223	0.215
11.453	0.960	0.946	0.418	0.446	0.356	0.259	0.207	0.178	0.170	0.223	0.215

(b) Divergent-flap internal static pressure ratios

Upper flap

	y/wt/2 = −0.50		y/wt/2 = 0.00				y/wt/2 = 0.50	
	x′/L		x′/L				x′/L	
NPR	0.333	0.667	0.200	0.400	0.600	0.800	0.333	0.667
1.995	0.277	0.478	0.369	0.241	0.457	0.519	0.276	0.491
4.011	0.273	0.142	0.366	0.239	0.150	0.165	0.273	0.140
6.024	0.271	0.141	0.365	0.239	0.149	0.165	0.272	0.140
7.299	0.271	0.141	0.364	0.239	0.149	0.164	0.271	0.140
7.996	0.270	0.141	0.365	0.239	0.149	0.164	0.271	0.140
10.007	0.270	0.141	0.365	0.239	0.148	0.164	0.272	0.140
11.453	0.271	0.141	0.366	0.239	0.148	0.164	0.272	0.140

Lower flap

	y/wt/2 = −0.50		y/wt/2 = 0.00				y/wt/2 = 0.50	
	x′/L		x′/L				x′/L	
NPR	0.333	0.667	0.200	0.400	0.600	0.800	0.333	0.667
1.995	0.271	0.480	0.365	0.239	0.467	0.517	0.270	0.487
4.011	0.269	0.142	0.360	0.236	0.149	0.164	0.269	0.140
6.024	0.268	0.141	0.360	0.235	0.148	0.163	0.268	0.140
7.299	0.268	0.141	0.361	0.235	0.148	0.163	0.268	0.140
7.996	0.268	0.141	0.360	0.235	0.148	0.163	0.268	0.140
10.007	0.269	0.140	0.361	0.235	0.148	0.163	0.268	0.139
11.453	0.269	0.141	0.361	0.235	0.148	0.163	0.269	0.139

Table 43. Nozzle Internal Static Pressure Ratios $p/p_{t,j}$ for SCF 2-D C-D Nozzle at AR = 1.265, $A_e/A_t = 1.63$, $\delta_{v,p} = 0°$, and $\delta_{v,y} = 15°$

(a) Sidewall internal static pressure ratios

x'/L, left side

NPR	-0.018	0.081	0.161	0.242	0.322	0.403	0.483	0.564	0.644
2.005	0.420	0.441	0.356	0.268	0.271	0.361	0.383	0.406	0.440
4.018	0.414	0.447	0.353	0.265	0.208	0.177	0.179	0.224	0.217
5.999	0.410	0.450	0.351	0.264	0.207	0.176	0.173	0.222	0.216
7.302	0.410	0.450	0.350	0.264	0.207	0.175	0.170	0.221	0.216
8.004	0.410	0.450	0.350	0.264	0.207	0.175	0.169	0.220	0.216
10.014	0.410	0.450	0.350	0.264	0.206	0.175	0.167	0.220	0.216
11.479	0.410	0.450	0.350	0.263	0.206	0.175	0.166	0.219	0.216

x'/L, right side

NPR	-0.283	-0.195	-0.106	-0.018	0.081	0.161	0.242	0.322	0.403	0.483	0.564	0.644
2.005	0.957	0.969	0.949	0.449	0.452	0.360	0.269	0.265	0.357	0.380	0.406	0.441
4.018	0.963	0.971	0.944	0.435	0.454	0.357	0.262	0.212	0.184	0.185	0.223	0.217
5.999	0.965	0.972	0.945	0.428	0.455	0.357	0.259	0.211	0.182	0.182	0.223	0.217
7.302	0.965	0.972	0.945	0.427	0.454	0.356	0.259	0.209	0.181	0.180	0.223	0.217
8.004	0.966	0.972	0.945	0.426	0.454	0.356	0.259	0.209	0.181	0.179	0.223	0.217
10.014	0.967	0.972	0.946	0.425	0.454	0.357	0.258	0.209	0.180	0.177	0.223	0.217
11.479	0.967	0.972	0.946	0.425	0.454	0.357	0.258	0.209	0.180	0.176	0.223	0.217

(b) Divergent-flap internal static pressure ratios

Upper flap

	y/wt/2 = -0.50		y/wt/2 = 0.00				y/wt/2 = 0.50	
	x'/L		x'/L				x'/L	
NPR	0.333	0.667	0.200	0.400	0.600	0.800	0.333	0.667
2.005	0.280	0.483	0.369	0.242	0.453	0.514	0.278	0.483
4.018	0.275	0.141	0.365	0.240	0.149	0.165	0.274	0.141
5.999	0.273	0.141	0.364	0.240	0.149	0.165	0.273	0.141
7.302	0.272	0.141	0.364	0.239	0.148	0.165	0.272	0.141
8.004	0.272	0.141	0.365	0.239	0.148	0.164	0.272	0.140
10.014	0.273	0.141	0.366	0.239	0.148	0.164	0.272	0.140
11.479	0.273	0.141	0.366	0.239	0.148	0.164	0.273	0.140

Lower flap

	y/wt/2 = -0.50		y/wt/2 = 0.00				y/wt/2 = 0.50	
	x'/L		x'/L				x'/L	
NPR	0.333	0.667	0.200	0.400	0.600	0.800	0.333	0.667
2.005	0.274	0.482	0.362	0.239	0.462	0.514	0.271	0.481
4.018	0.271	0.142	0.359	0.236	0.149	0.163	0.270	0.141
5.999	0.270	0.141	0.360	0.236	0.148	0.163	0.270	0.140
7.302	0.270	0.141	0.360	0.235	0.148	0.163	0.269	0.140
8.004	0.270	0.141	0.360	0.235	0.148	0.163	0.269	0.140
10.014	0.270	0.141	0.361	0.235	0.148	0.163	0.270	0.140
11.479	0.270	0.141	0.361	0.236	0.148	0.163	0.270	0.139

Table 44. Nozzle Internal Static Pressure Ratios $p/p_{t,j}$ for SCF 2-D C-D Nozzle at AR = 1.265, $A_e/A_t = 1.63$, $\delta_{v,p} = 0°$, and $\delta_{v,y} = 25°$

(a) Sidewall internal static pressure ratios

x′/L, left side

NPR	-0.018	0.081	0.161	0.242	0.322	0.403	0.483	0.564	0.644
2.023	0.352	0.450	0.352	0.265	0.226	0.353	0.361	0.385	0.435
4.022	0.338	0.453	0.349	0.264	0.204	0.179	0.192	0.226	0.220
6.021	0.335	0.452	0.349	0.264	0.204	0.178	0.185	0.225	0.219
7.316	0.335	0.452	0.348	0.264	0.204	0.177	0.182	0.224	0.219
7.673	0.335	0.452	0.349	0.264	0.204	0.177	0.182	0.223	0.219

x′/L, right side

NPR	-0.283	-0.195	-0.106	-0.018	0.081	0.161	0.242	0.322	0.403	0.483	0.564	0.644
2.023	0.972	0.975	0.951	0.452	0.459	0.360	0.267	0.370	0.408	0.417	0.428	0.449
4.022	0.976	0.976	0.947	0.439	0.459	0.356	0.260	0.208	0.177	0.155	0.143	0.179
6.021	0.977	0.976	0.947	0.434	0.460	0.356	0.257	0.206	0.175	0.153	0.141	0.175
7.316	0.978	0.975	0.947	0.433	0.460	0.355	0.257	0.206	0.174	0.153	0.140	0.173
7.673	0.978	0.975	0.947	0.432	0.460	0.356	0.257	0.205	0.174	0.153	0.140	0.172

(b) Divergent-flap internal static pressure ratios

Upper flap

	y/wt/2 = -0.50		y/wt/2 = 0.00				y/wt/2 = 0.50	
	x′/L		x′/L				x′/L	
NPR	0.333	0.667	0.200	0.400	0.600	0.800	0.333	0.667
2.023	0.284	0.485	0.303	0.253	0.487	0.505	0.243	0.486
4.022	0.280	0.140	0.300	0.245	0.150	0.162	0.240	0.130
6.021	0.278	0.140	0.299	0.244	0.149	0.160	0.238	0.130
7.316	0.278	0.140	0.298	0.244	0.148	0.160	0.237	0.129
7.673	0.278	0.140	0.298	0.244	0.148	0.160	0.237	0.129

Lower flap

	y/wt/2 = -0.50		y/wt/2 = 0.00				y/wt/2 = 0.50	
	x′/L		x′/L				x′/L	
NPR	0.333	0.667	0.200	0.400	0.600	0.800	0.333	0.667
2.023	0.277	0.487	0.296	0.263	0.485	0.506	0.240	0.479
4.022	0.274	0.141	0.295	0.240	0.148	0.159	0.234	0.129
6.021	0.274	0.140	0.295	0.239	0.148	0.158	0.233	0.129
7.316	0.273	0.140	0.295	0.238	0.148	0.158	0.233	0.128
7.673	0.273	0.140	0.295	0.238	0.148	0.158	0.233	0.128

Table 45. Nozzle Internal Static Pressure Ratios $p/p_{t,j}$ for SCF 2-D C-D Nozzle at AR = 1.265, $A_e/A_t = 1.63$, $\delta_{v,p} = 25°$, and $\delta_{v,y} = 0°$

(a) Sidewall internal static pressure ratios

x′/L, left side

NPR	-0.195	-0.106	-0.018	0.081	0.161	0.242	0.322	0.403	0.483	0.564
2.031	0.970	0.948	0.513	0.663	0.573	0.512	0.454	0.397	0.340	0.302
3.998	0.972	0.951	0.494	0.647	0.546	0.468	0.394	0.327	0.265	0.222
5.995	0.973	0.953	0.492	0.648	0.545	0.469	0.394	0.327	0.264	0.220
7.305	0.972	0.953	0.492	0.646	0.546	0.469	0.394	0.327	0.263	0.219
8.005	0.972	0.954	0.491	0.645	0.545	0.470	0.393	0.327	0.263	0.218
9.996	0.970	0.954	0.493	0.646	0.544	0.471	0.393	0.328	0.262	0.218
12.009	0.970	0.954	0.488	0.648	0.544	0.471	0.394	0.327	0.262	0.217

x′/L, right side

NPR	-0.195	-0.106	-0.018	0.081	0.161	0.242	0.322	0.403	0.483	0.564
2.031	0.963	0.956	0.518	0.650	0.571	0.505	0.448	0.395	0.350	0.309
3.998	0.963	0.950	0.507	0.639	0.551	0.463	0.390	0.325	0.271	0.225
5.995	0.964	0.950	0.530	0.641	0.551	0.462	0.391	0.324	0.270	0.224
7.305	0.965	0.950	0.533	0.640	0.551	0.462	0.391	0.323	0.270	0.223
8.005	0.965	0.950	0.532	0.640	0.550	0.461	0.391	0.323	0.269	0.222
9.996	0.965	0.950	0.532	0.642	0.550	0.462	0.392	0.323	0.269	0.222
12.009	0.965	0.951	0.541	0.640	0.550	0.462	0.392	0.323	0.270	0.222

(b) Divergent-flap internal static pressure ratios

Upper flap

	y/wt/2 = -0.50		y/wt/2 = 0.00				y/wt/2 = 0.50	
	x′/L		x′/L				x′/L	
NPR	0.319	0.639	0.191	0.383	0.575	0.767	0.319	0.639
2.031	0.486	0.276	0.621	0.426	0.303	0.466	0.486	0.274
3.998	0.446	0.188	0.602	0.372	0.220	0.138	0.448	0.188
5.995	0.446	0.189	0.599	0.372	0.219	0.137	0.447	0.188
7.305	0.447	0.189	0.599	0.371	0.219	0.136	0.447	0.187
8.005	0.447	0.189	0.599	0.371	0.218	0.136	0.446	0.188
9.996	0.447	0.189	0.599	0.371	0.218	0.136	0.446	0.188
12.009	0.447	0.189	0.599	0.372	0.218	0.136	0.446	0.188

Lower flap

	y/wt/2 = -0.50		y/wt/2 = 0.00				y/wt/2 = 0.50	
	x′/L		x′/L				x′/L	
NPR	0.285	0.570	0.171	0.342	0.512	0.683	0.285	0.570
2.031	0.340	0.438	0.303	0.348	0.419	0.468	0.336	0.438
3.998	0.245	0.215	0.187	0.276	0.215	0.183	0.232	0.215
5.995	0.245	0.215	0.193	0.277	0.215	0.183	0.230	0.214
7.305	0.244	0.214	0.193	0.276	0.215	0.182	0.231	0.214
8.005	0.243	0.214	0.181	0.274	0.216	0.182	0.230	0.213
9.996	0.244	0.214	0.190	0.276	0.215	0.181	0.232	0.214
12.009	0.243	0.214	0.186	0.276	0.215	0.180	0.229	0.213

Table 46. Nozzle Internal Static Pressure Ratios $p/p_{t,j}$ for SCF 2-D C-D Nozzle at AR = 1.265, $A_e/A_t = 1.63$, $\delta_{v,p} = 25°$, and $\delta_{v,y} = 15°$

(a) Sidewall internal static pressure ratios

x′/L, left side

NPR	-0.018	0.081	0.161	0.242	0.322	0.403	0.483	0.564
2.010	0.516	0.661	0.567	0.509	0.450	0.390	0.337	0.297
4.002	0.500	0.644	0.541	0.468	0.393	0.323	0.265	0.222
6.002	0.501	0.642	0.541	0.469	0.392	0.323	0.264	0.220
7.304	0.497	0.643	0.540	0.469	0.392	0.323	0.263	0.220
8.006	0.500	0.643	0.540	0.470	0.392	0.323	0.263	0.219
10.000	0.499	0.645	0.539	0.470	0.392	0.323	0.262	0.219

x′/L, right side

NPR	-0.283	-0.195	-0.106	-0.018	0.081	0.161	0.242	0.322	0.403	0.483	0.564
2.010	0.964	0.975	0.960	0.538	0.658	0.570	0.495	0.442	0.391	0.346	0.306
4.002	0.968	0.976	0.952	0.518	0.645	0.553	0.461	0.392	0.326	0.271	0.223
6.002	0.970	0.975	0.951	0.520	0.646	0.553	0.459	0.391	0.324	0.269	0.222
7.304	0.971	0.976	0.952	0.521	0.646	0.553	0.459	0.391	0.324	0.269	0.221
8.006	0.971	0.976	0.951	0.523	0.645	0.552	0.459	0.391	0.324	0.268	0.221
10.000	0.972	0.976	0.953	0.526	0.645	0.552	0.460	0.391	0.325	0.268	0.220

(b) Divergent-flap internal static pressure ratios

Upper flap

	y/wt/2 = -0.50		y/wt/2 = 0.00				y/wt/2 = 0.50	
	x′/L		x′/L				x′/L	
NPR	0.319	0.639	0.191	0.383	0.575	0.767	0.319	0.639
2.010	0.482	0.272	0.621	0.423	0.300	0.461	0.481	0.273
4.002	0.446	0.188	0.602	0.374	0.220	0.139	0.450	0.188
6.002	0.446	0.188	0.601	0.374	0.219	0.138	0.449	0.188
7.304	0.446	0.187	0.600	0.374	0.219	0.137	0.449	0.188
8.006	0.447	0.187	0.601	0.374	0.219	0.138	0.449	0.188
10.000	0.447	0.187	0.601	0.374	0.219	0.137	0.450	0.188

Lower flap

	y/wt/2 = -0.50		y/wt/2 = 0.00				y/wt/2 = 0.50	
	x′/L		x′/L				x′/L	
NPR	0.285	0.570	0.171	0.342	0.512	0.683	0.285	0.570
2.010	0.327	0.440	0.293	0.338	0.414	0.473	0.329	0.441
4.002	0.239	0.213	0.128	0.267	0.222	0.182	0.228	0.212
6.002	0.247	0.217	0.189	0.274	0.216	0.184	0.229	0.213
7.304	0.246	0.217	0.188	0.274	0.216	0.183	0.228	0.213
8.006	0.237	0.212	0.127	0.266	0.221	0.181	0.226	0.211
10.000	0.245	0.216	0.185	0.274	0.216	0.182	0.228	0.213

Table 47. Nozzle Internal Static Pressure Ratios $p/p_{t,j}$ for SCF 2-D C-D Nozzle at AR = 1.265, $A_e/A_t = 1.63$, $\delta_{v,p} = 25°$, and $\delta_{v,y} = 25°$

(a) Sidewall internal static pressure ratios

	x′/L, left side							
NPR	−0.018	0.081	0.161	0.242	0.322	0.403	0.483	0.564
2.002	0.623	0.618	0.563	0.525	0.455	0.392	0.338	0.299
4.004	0.608	0.596	0.525	0.480	0.399	0.329	0.269	0.225
6.009	0.611	0.595	0.526	0.480	0.399	0.329	0.268	0.222
8.001	0.611	0.598	0.525	0.481	0.399	0.329	0.266	0.221
9.245	0.612	0.599	0.525	0.481	0.399	0.328	0.266	0.220
9.303	0.611	0.600	0.526	0.481	0.399	0.328	0.266	0.220
7.312	0.612	0.599	0.525	0.480	0.399	0.328	0.267	0.221

	x′/L, right side										
NPR	−0.283	−0.195	−0.106	−0.018	0.081	0.161	0.242	0.322	0.403	0.483	0.564
2.002	0.977	0.977	0.959	0.543	0.653	0.572	0.503	0.449	0.396	0.348	0.303
4.004	0.978	0.978	0.954	0.521	0.638	0.546	0.454	0.385	0.320	0.265	0.219
6.009	0.979	0.978	0.954	0.523	0.639	0.546	0.453	0.384	0.319	0.263	0.217
8.001	0.981	0.978	0.953	0.523	0.639	0.546	0.452	0.384	0.318	0.263	0.216
9.245	0.981	0.978	0.953	0.526	0.639	0.546	0.453	0.384	0.318	0.263	0.216
9.303	0.981	0.978	0.953	0.526	0.639	0.546	0.452	0.384	0.318	0.263	0.216
7.312	0.980	0.978	0.953	0.521	0.640	0.546	0.452	0.384	0.318	0.263	0.216

(b) Divergent-flap internal static pressure ratios

Upper flap

	y/wt/2 = −0.50		y/wt/2 = 0.00				y/wt/2 = 0.50	
	x′/L		x′/L				x′/L	
NPR	0.319	0.639	0.191	0.383	0.575	0.767	0.319	0.639
2.002	0.492	0.277	0.618	0.430	0.296	0.468	0.487	0.269
4.004	0.447	0.190	0.595	0.371	0.220	0.140	0.443	0.186
6.009	0.446	0.190	0.594	0.370	0.219	0.139	0.442	0.185
8.001	0.447	0.189	0.593	0.371	0.219	0.139	0.442	0.185
9.245	0.447	0.189	0.594	0.371	0.219	0.139	0.442	0.185
9.303	0.447	0.189	0.594	0.371	0.219	0.139	0.442	0.185
7.312	0.447	0.189	0.594	0.371	0.219	0.139	0.442	0.185

Lower flap

	y/wt/2 = −0.50		y/wt/2 = 0.00				y/wt/2 = 0.50	
	x′/L		x′/L				x′/L	
NPR	0.285	0.570	0.171	0.342	0.512	0.683	0.285	0.570
2.002	0.349	0.436	0.297	0.355	0.411	0.461	0.344	0.434
4.004	0.249	0.207	0.122	0.242	0.226	0.181	0.210	0.211
6.009	0.248	0.206	0.126	0.241	0.225	0.180	0.209	0.209
8.001	0.247	0.206	0.127	0.239	0.225	0.180	0.208	0.209
9.245	0.247	0.206	0.128	0.239	0.224	0.180	0.208	0.208
9.303	0.247	0.206	0.127	0.238	0.224	0.179	0.207	0.208
7.312	0.247	0.206	0.127	0.240	0.225	0.180	0.208	0.209

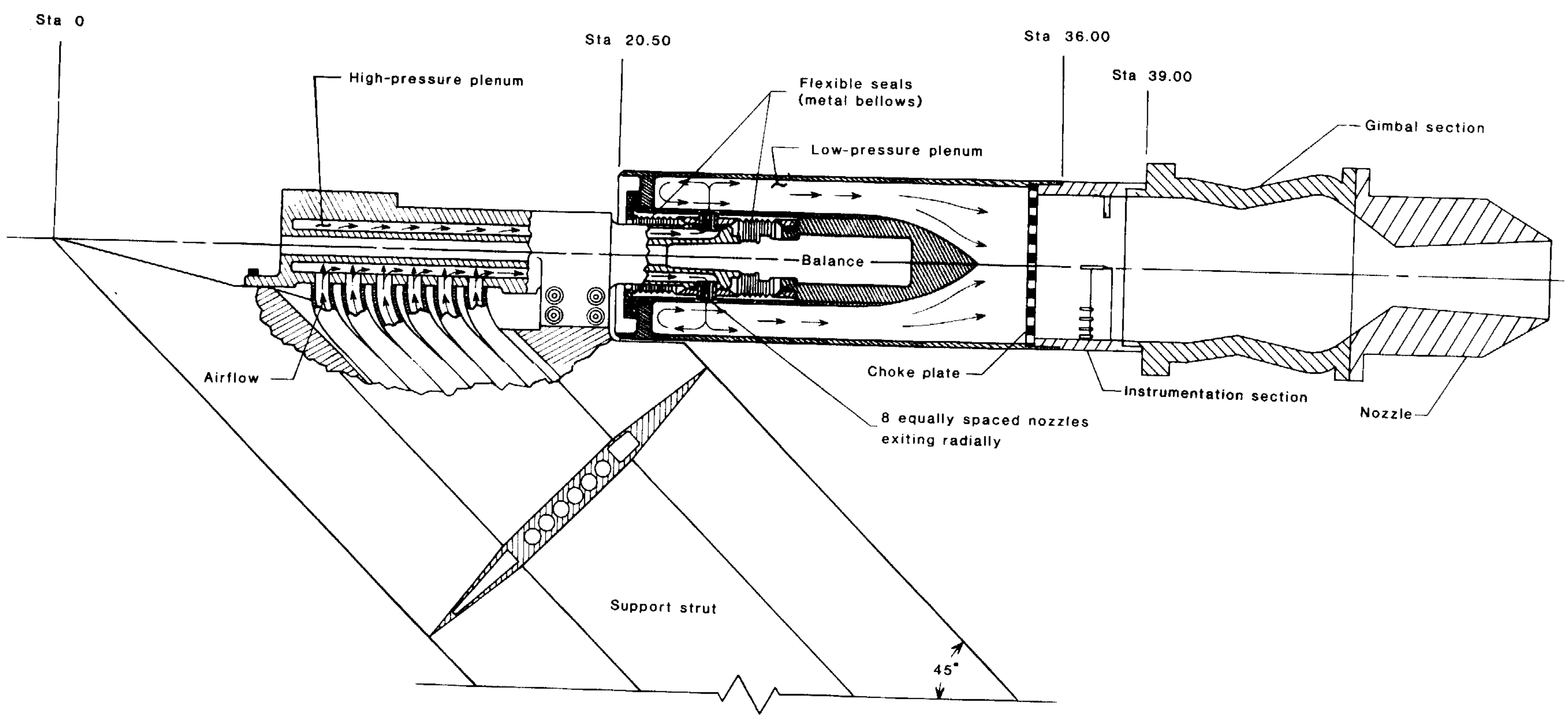

Figure 1. Sketch showing side view of gimbal nozzle concept installed on high-pressure air-propulsion simulation hardware. All linear dimensions are given in inches.

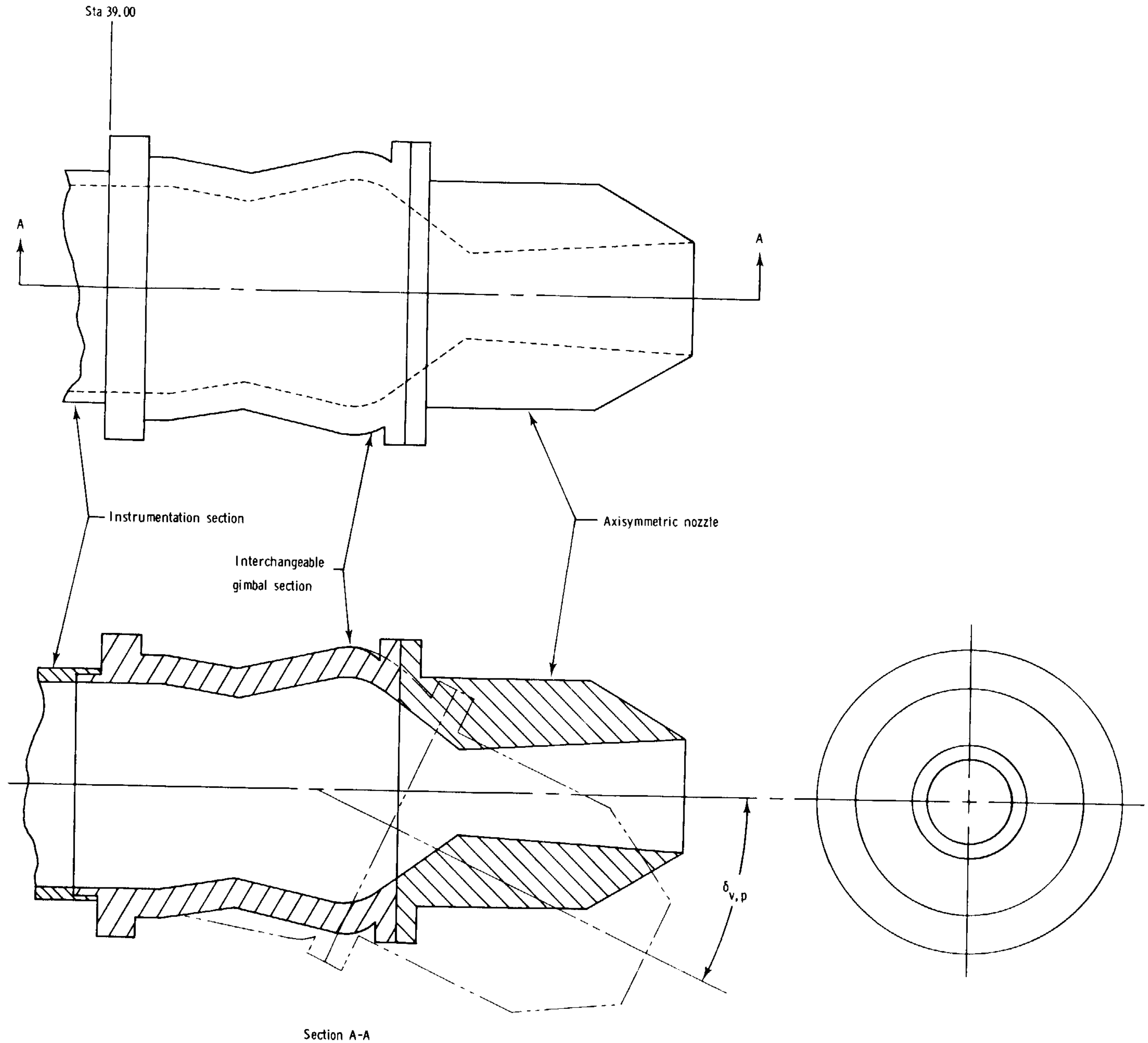

Figure 2. Three-view sketch of typical gimballed axisymmetric C-D nozzle.

ORIGINAL PAGE IS
OF POOR QUALITY

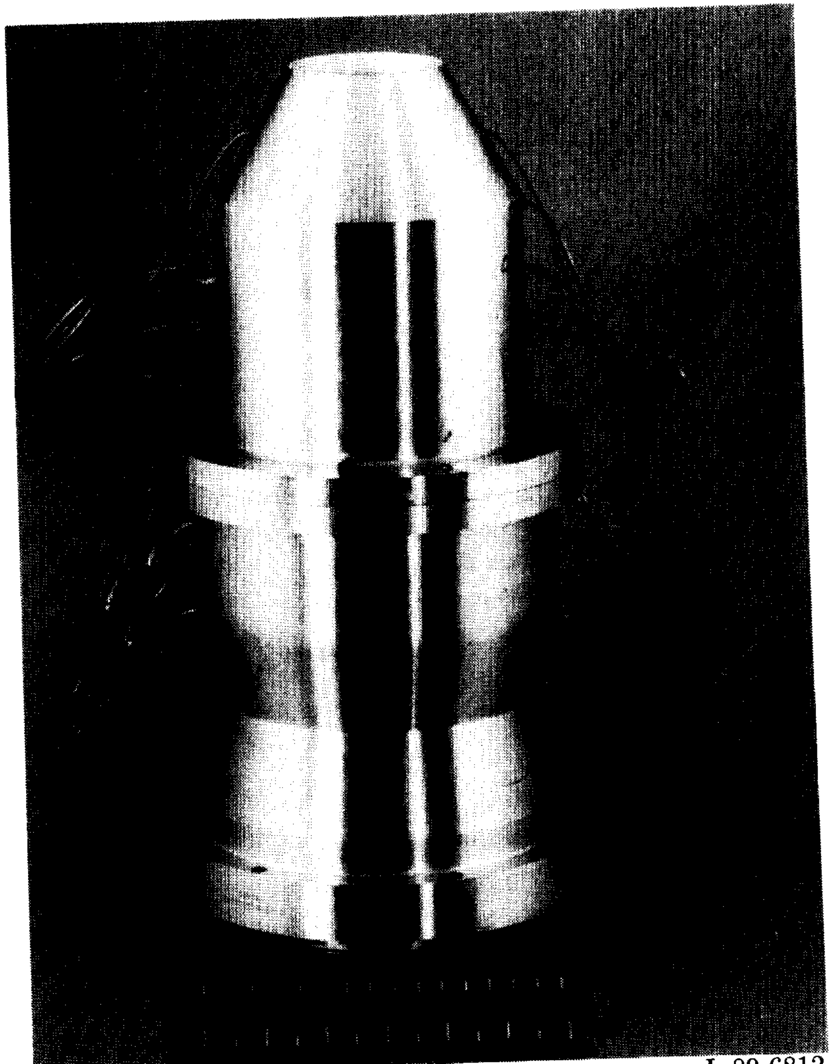

L-89-6812

(a) $\delta_{v,p} = 0°$.

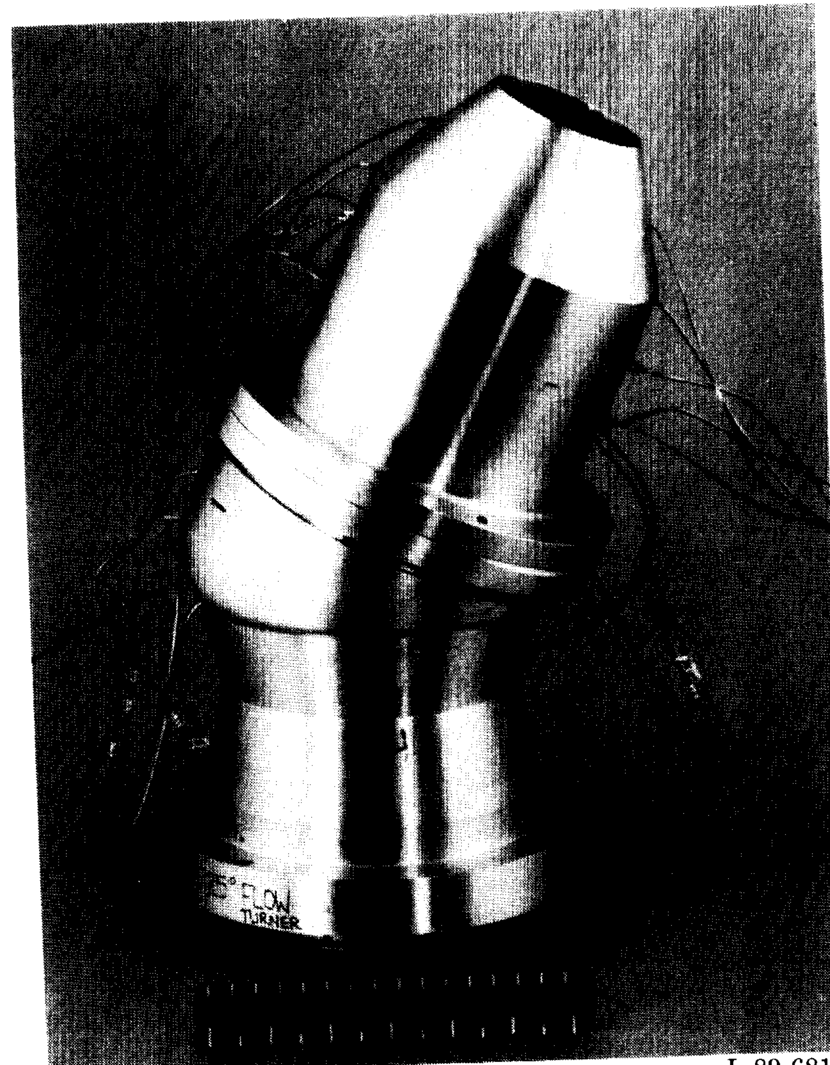

L-89-6813

(b) $\delta_{v,p} = 25°$.

Figure 3. Photographs showing gimballed axisymmetric C-D nozzle.

Static pressure orifice locations								
	Stations for bottom row, in.				Stations for top row, in.			
$\delta_{v,p}$ =	0°	10°	20°	25°	0°	10°	20°	25°
	43.199	43.199	43.199	43.199	-	-	-	-
	43.899	43.824	43.899	43.866	43.899	43.919	43.899	43.899
	44.599	44.449	44.599	44.532	44.599	44.646	44.599	44.599
	45.299	45.074	45.299	45.199	45.299	45.372	45.299	45.299
	45.999	45.699	-	-	45.999	46.099	45.999	45.999
	-	-	-	-	46.299	46.499	46.699	46.699
	-	-	-	-	-	-	47.119	47.119

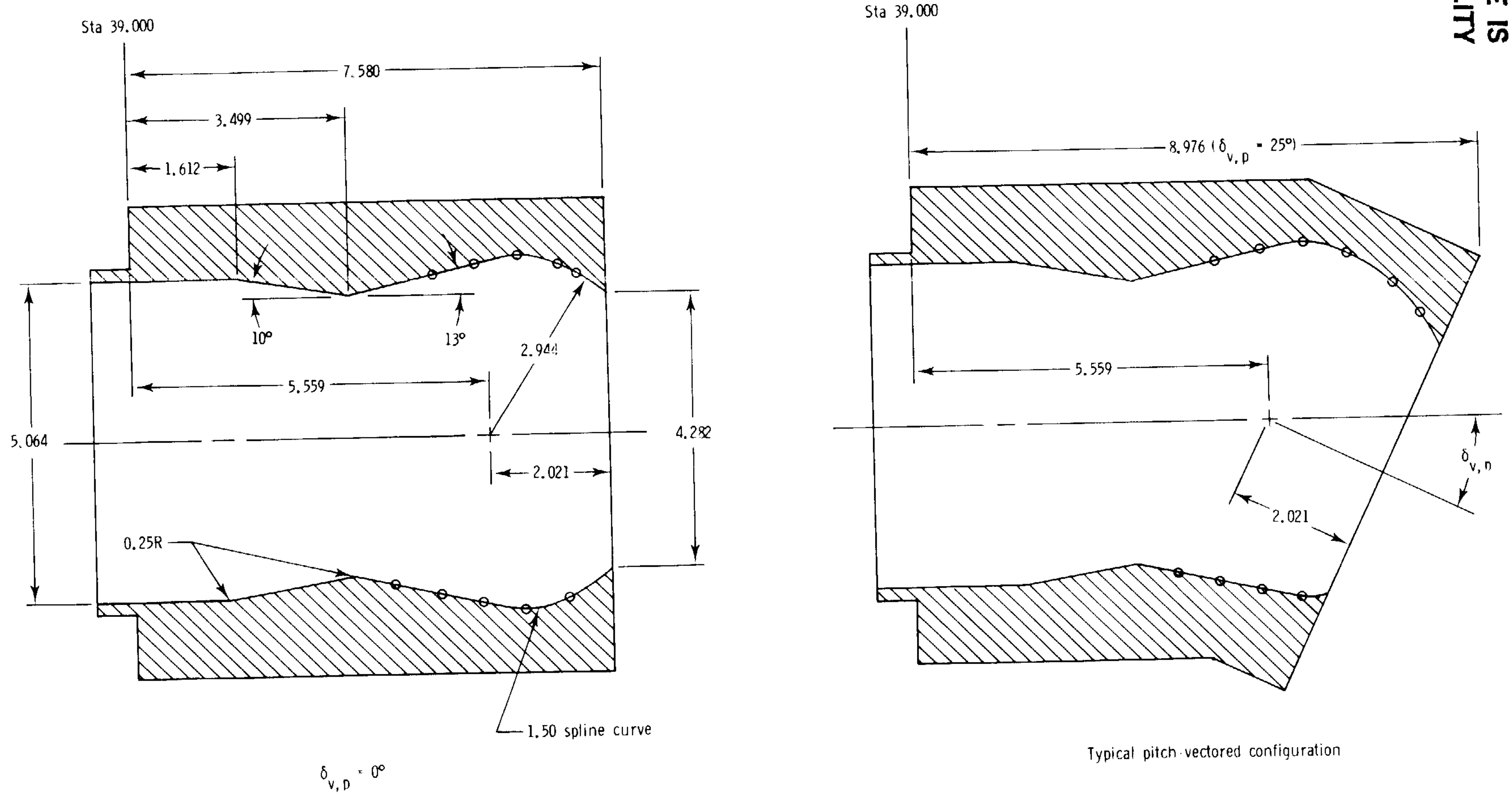

(a) Gimbal section.

Figure 4. Sketches showing important internal flow path dimensions and static pressure orifice locations for gimballed axisymmetric nozzle configurations. All linear dimensions are given in inches.

Static pressure orifice locations		
x, in.	Sta, in. ($\delta_{v,p}$ = 0°)	Φ, deg
-0.313	47.770	0 and 180
0.379	48.962	↓
2.070	50.153	
3.262	51.345	
4.453	52.536	

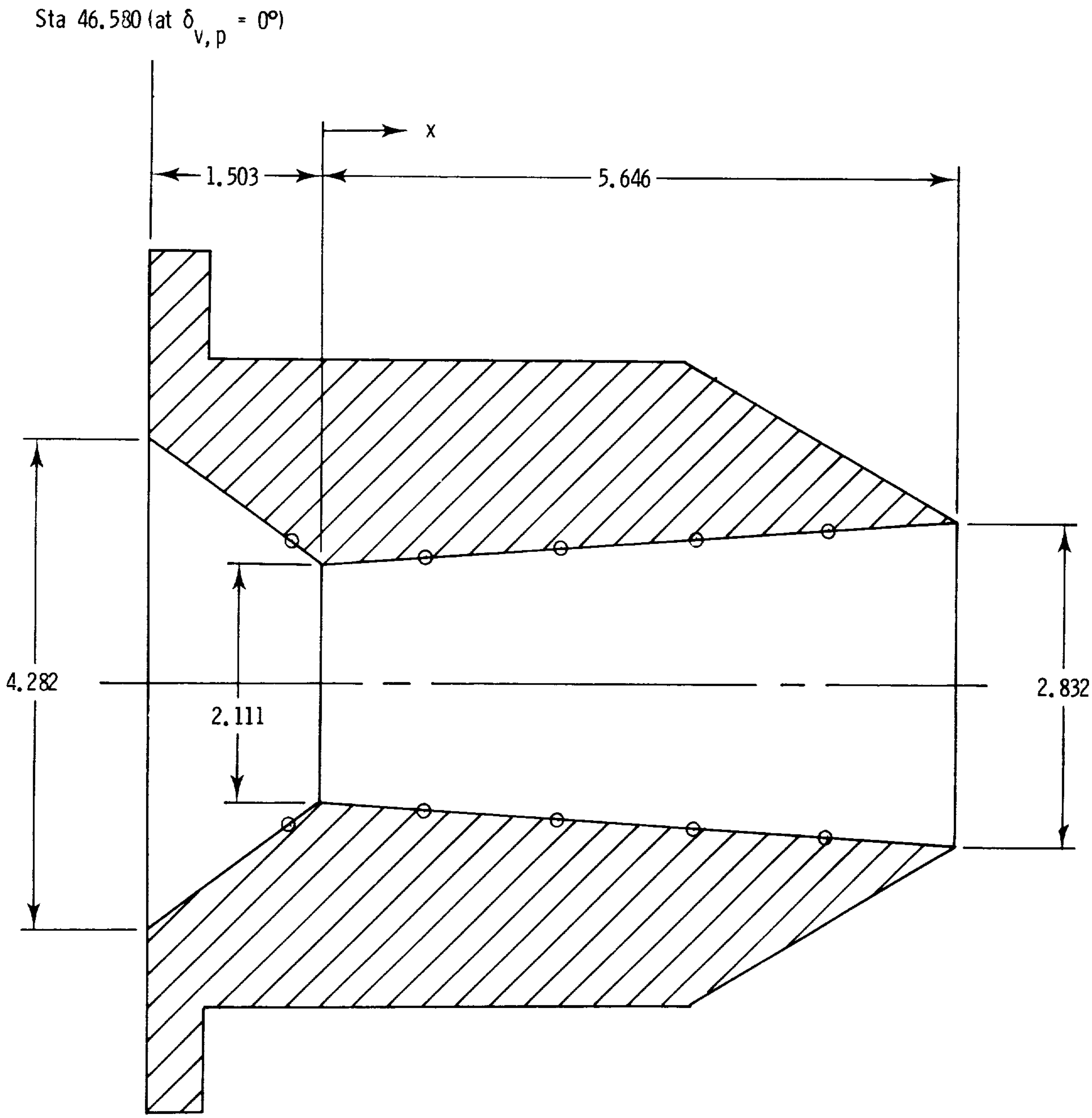

(b) Axisymmetric convergent-divergent nozzle.

Figure 4. Concluded.

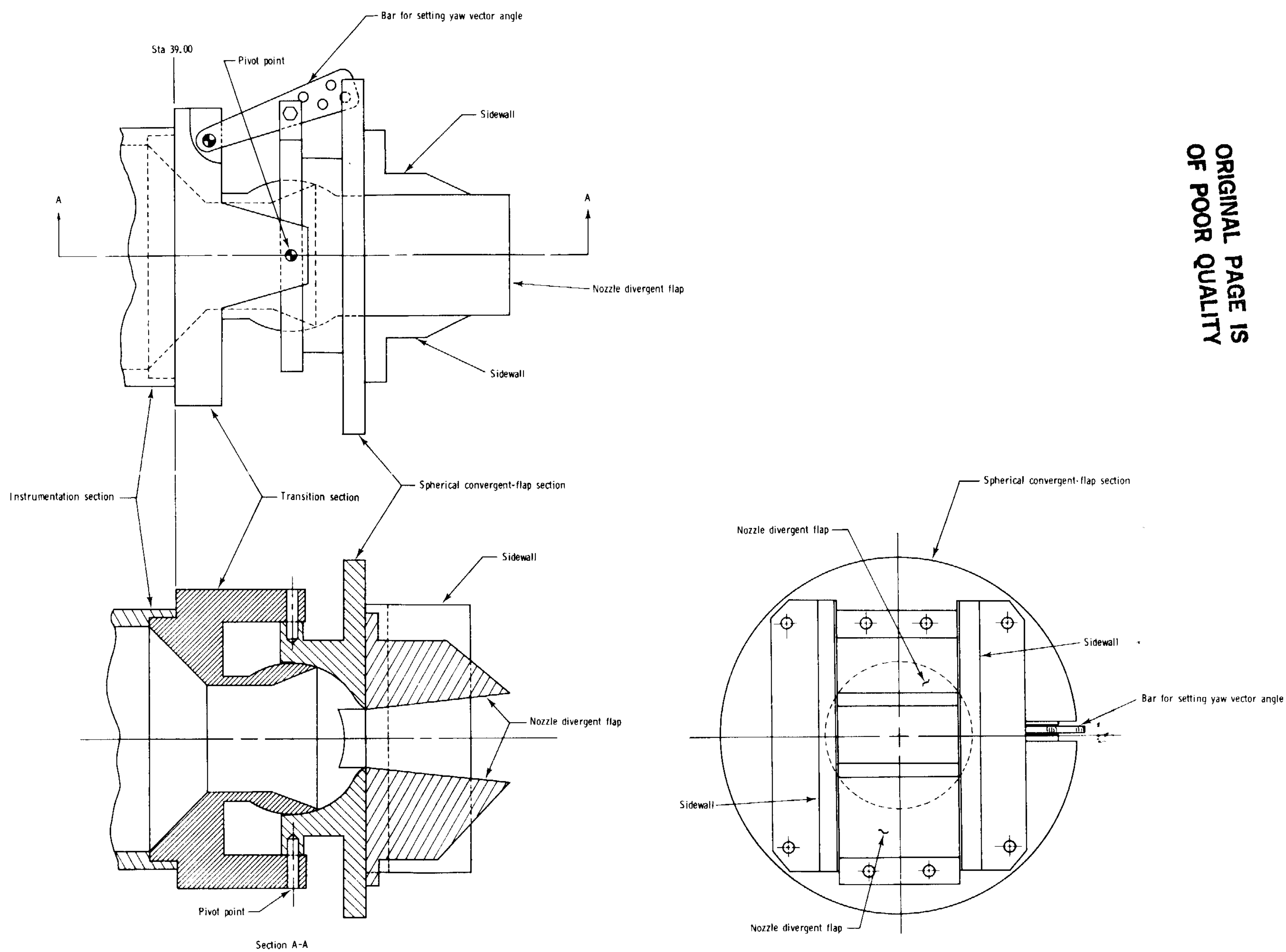

Figure 5. Three-view sketch of typical unvectored, SCF nonaxisymmetric nozzle configuration.

ORIGINAL PAGE
BLACK AND WHITE PHOTOGRAPH

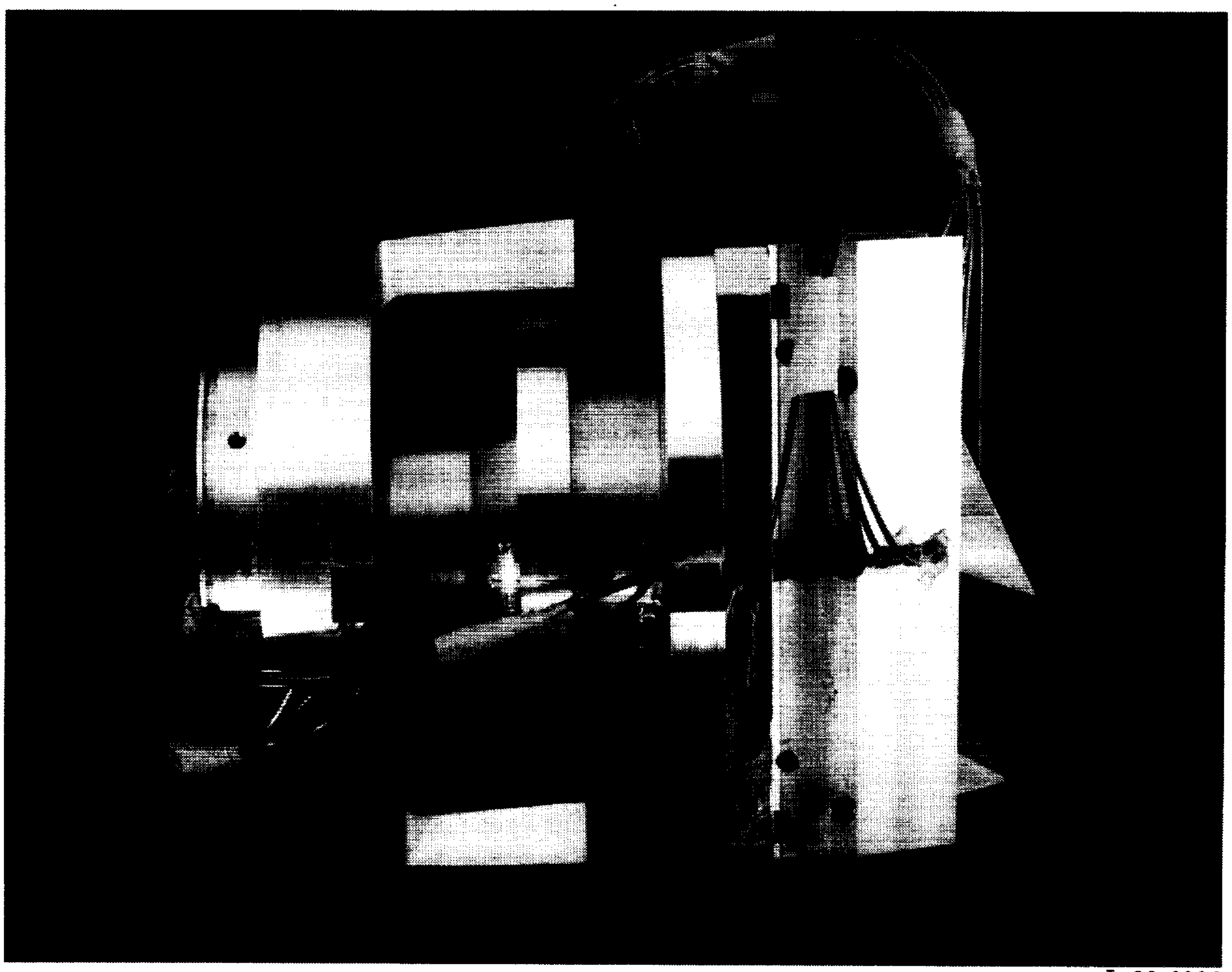

L-88-6836

Figure 6. Photograph of spherical-convergent-flap nonaxisymmetric nozzle. $\delta_{v,p} = 25°$; $\delta_{v,y} = 0°$.

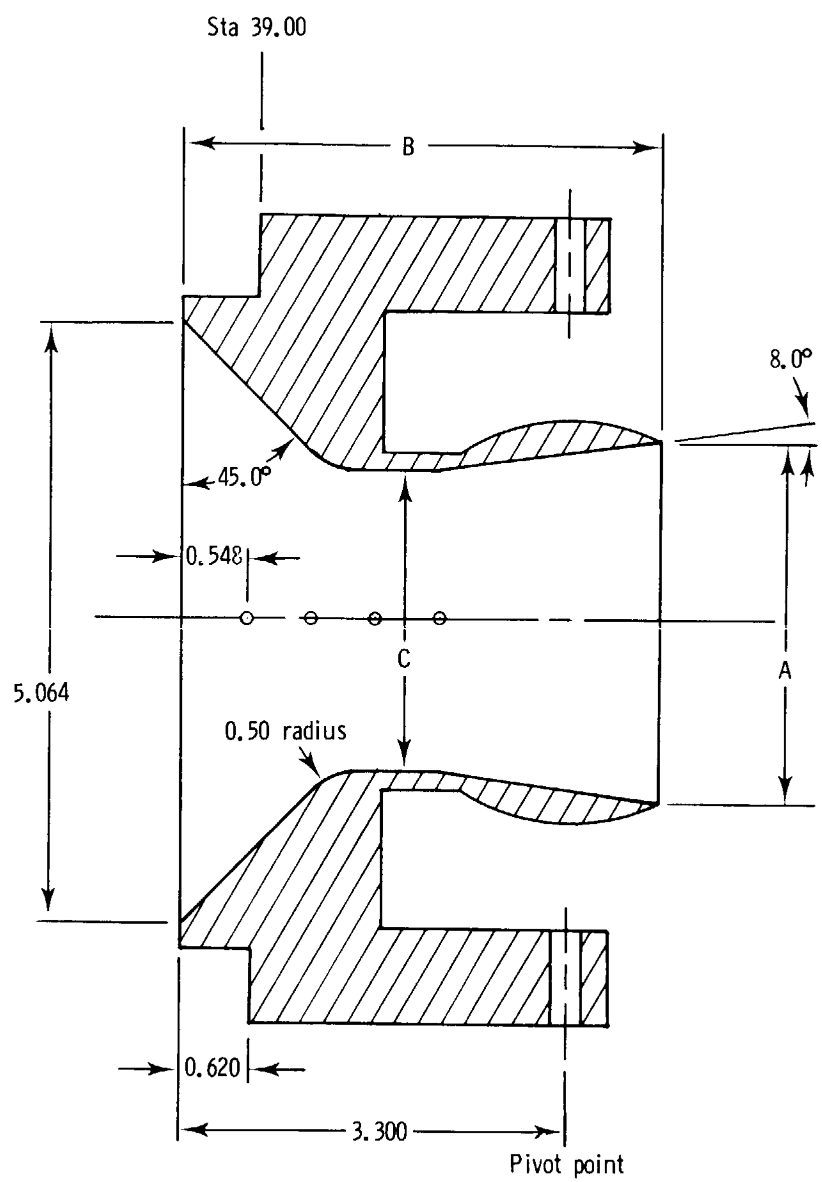

AR	A, in.	B, in.	C, in.
2.508	3.284	3.732	2.800
2.083	3.195	3.875	2.640
1.265	3.081	4.014	2.540

Static pressure orifice locations		
AR	Sta, in.	Φ, deg
2.508 and 2.083	39.928	90 and 270
	40.379	
	40.829	
	41.280	
1.265	39.928	
	40.476	
	41.024	
	41.572	

Note: Transition section is axisymmetric

(a) Transition section.

Figure 7. Sketches showing important internal flow path dimensions and static pressure orifice locations for spherical-convergent-flap nozzle configurations. All linear dimensions are given in inches.

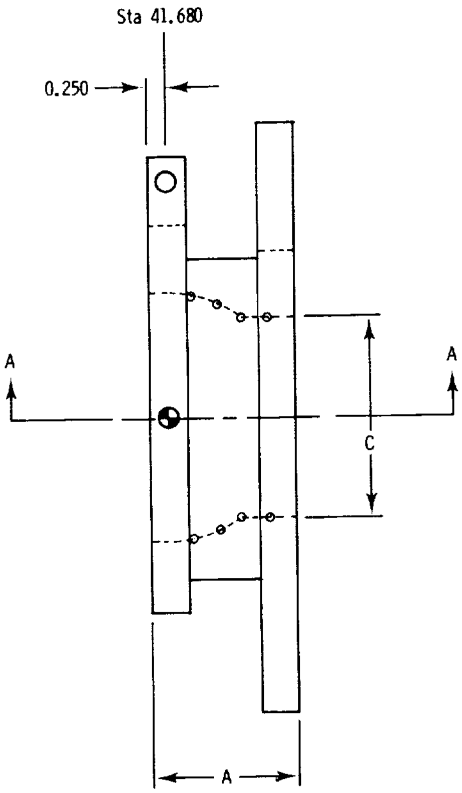

AR	A, in.	B, in.	C, in.
2.508	1.900	1.180	2.960
2.083	1.870	1.296	2.700
1.265	1.788	1.660	2.100

Static pressure orifice locations at $\delta_{v,y} = 0°$		
AR	Sta, in.	Φ, deg
2.508 and 2.083	42.020	90 and 270
	42.360	
	42.700	
	43.040	
1.265	42.020	
	42.393	
	42.767	
	43.140	

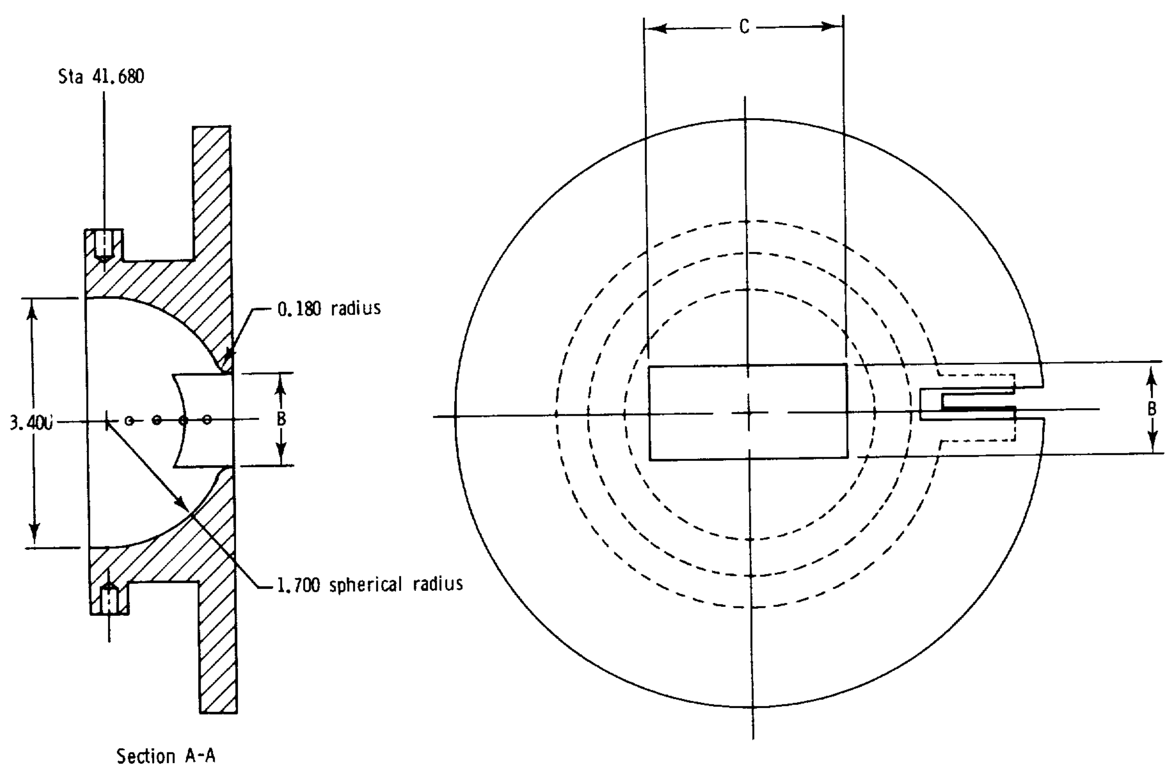

(b) Spherical-convergent-flap section.

Figure 7. Continued.

AR	A_e/A_t	$\delta_{v,p}$, deg.	Throat Sta, in.	Sidewall T.E. Sta, in.	w_t, in.	h_t, in.	Upper divergent flap α, deg.	Upper divergent flap T.E. Sta, in.	Upper divergent flap T.E. WL, in.	Lower divergent flap α, deg.	Lower divergent flap T.E. Sta, in.	Lower divergent flap T.E. WL, in.
2.508	1.46	0.0	43.330	45.530	2.960	1.180	5.085	46.380	0.861	5.085	46.380	-0.861
	1.46	25.0					-19.915	46.209	-0.453	30.085	45.980	-2.125
	1.63	0.0					6.972	46.369	0.962	6.972	46.369	-0.962
	1.63	25.0					-18.028	46.242	-0.358	31.972	45.928	-2.211
2.083	1.46	0.0	43.300	45.720	2.700	1.296	5.085	46.650	0.946	5.085	46.650	-0.946
	1.46	25.0					-19.915	46.462	-0.498	30.085	46.210	-2.334
	1.63	0.0					6.972	46.638	1.056	6.972	46.638	-1.056
	1.63	20.0					-13.028	46.576	-0.110	26.972	46.297	-2.173
1.265	1.46	0.0	43.218	46.288	2.100	1.660	5.133	47.468	1.212	5.133	47.468	-1.212
	1.46	25.0					-19.867	47.231	-0.620	30.133	46.908	-2.972
	1.63	0.0					7.039	47.453	1.353	7.039	47.453	-1.353
	1.63	25.0					-17.961	47.277	-0.486	32.039	46.835	-3.094

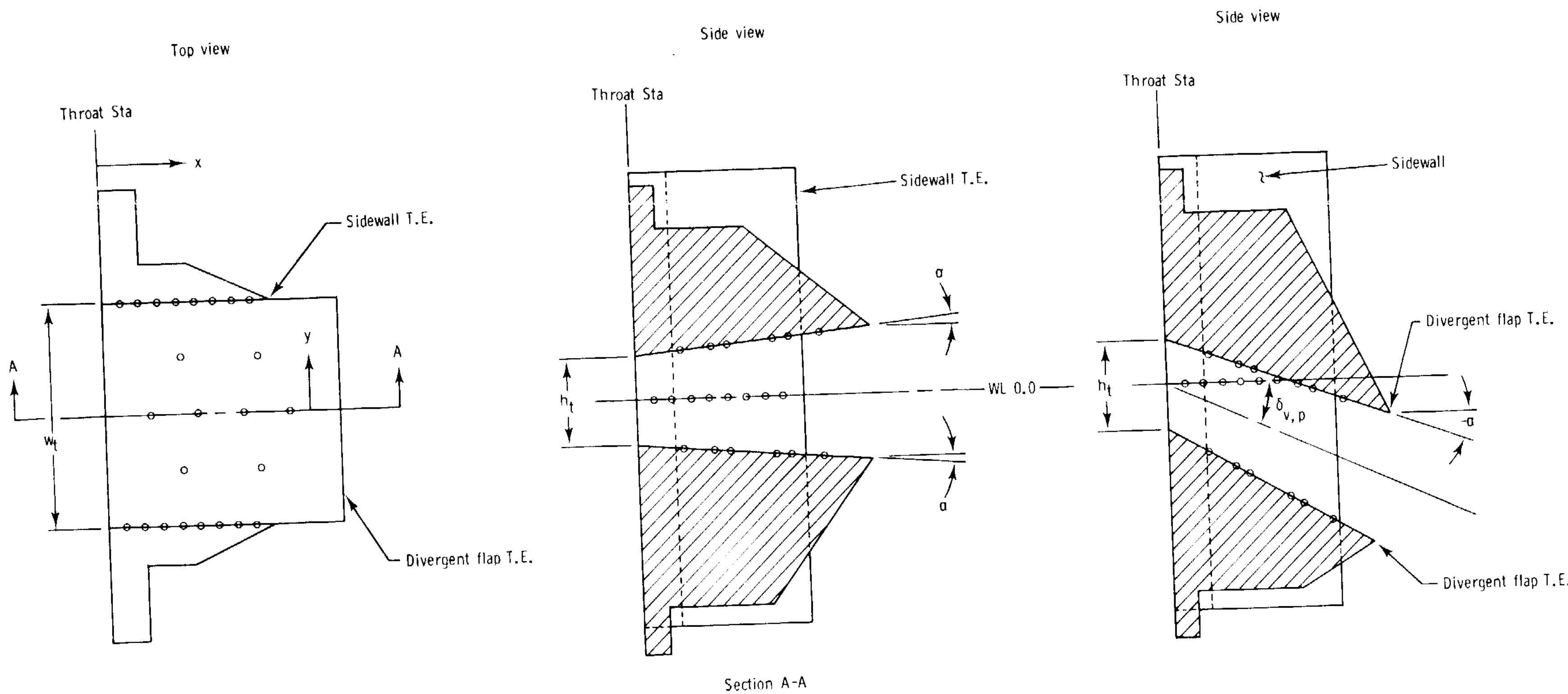

(c) Sidewalls and divergent flaps.

Figure 7. Concluded.

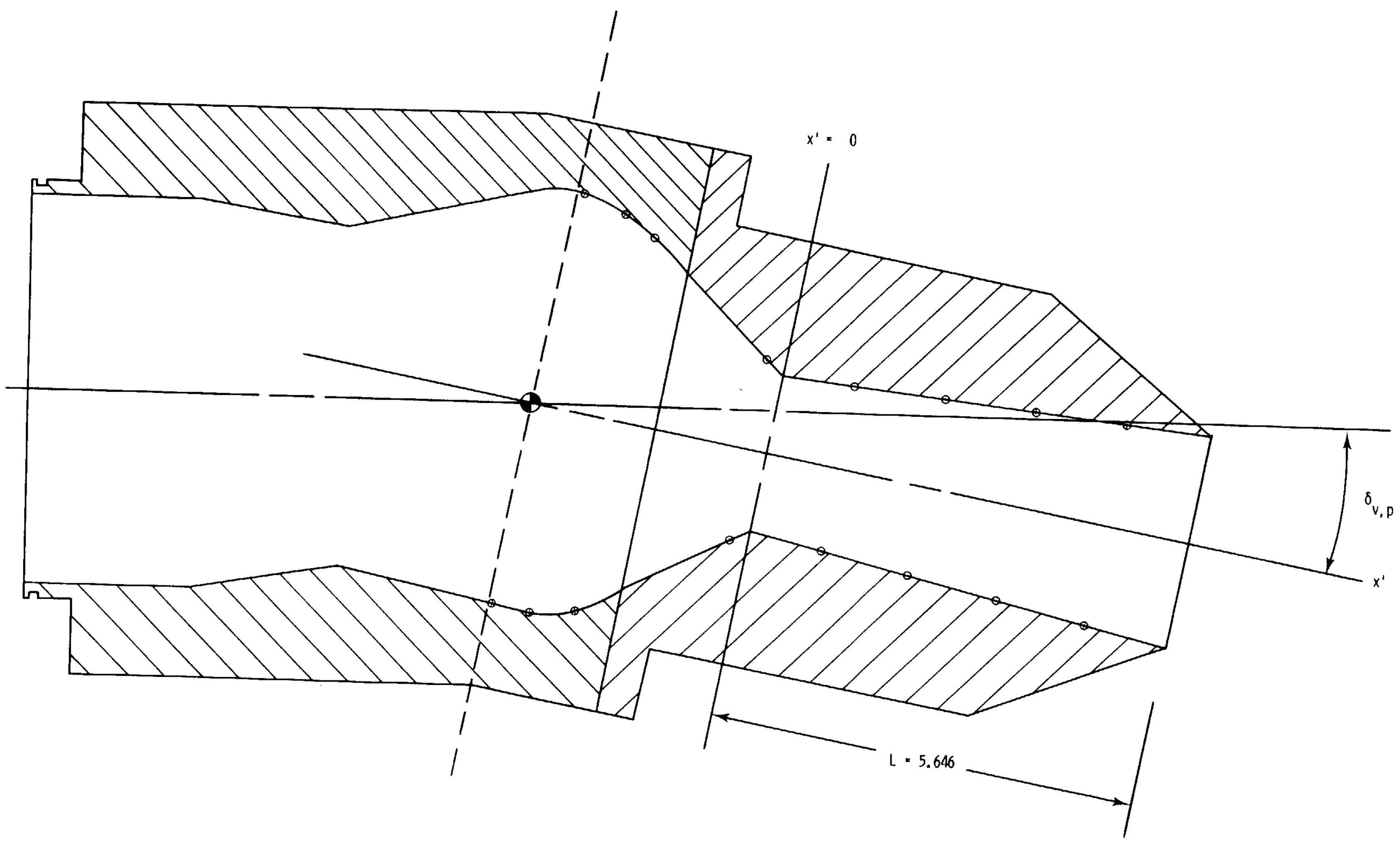

Figure 8. Alternate axis system for static pressure orifices on gimballed axisymmetric nozzle. Linear dimensions are given in inches.

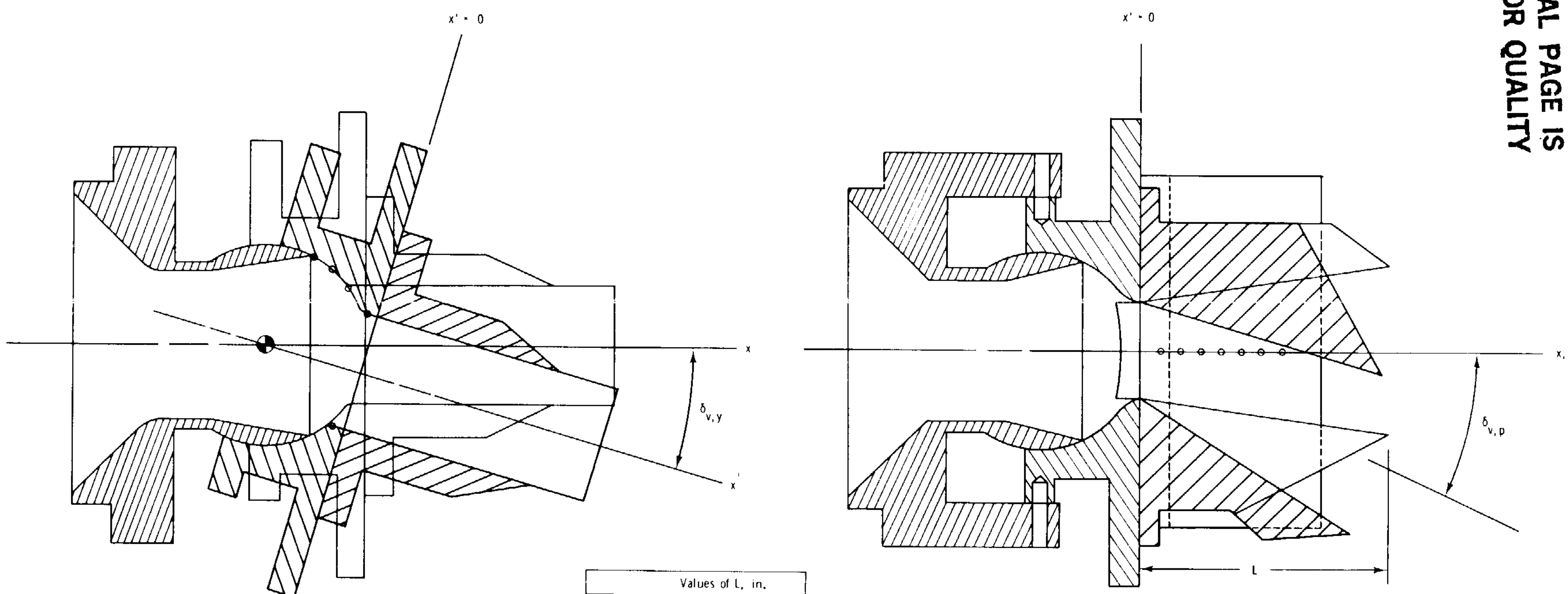

Values of L, in.			
	AR		
A_e/A_t	2.508	2.083	1.265
1.46	3.050	3.350	4.250
1.63	3.039	3.338	4.239

Figure 9. Alternate axis system for static pressure orifices on SCF 2-D C-D nozzle.

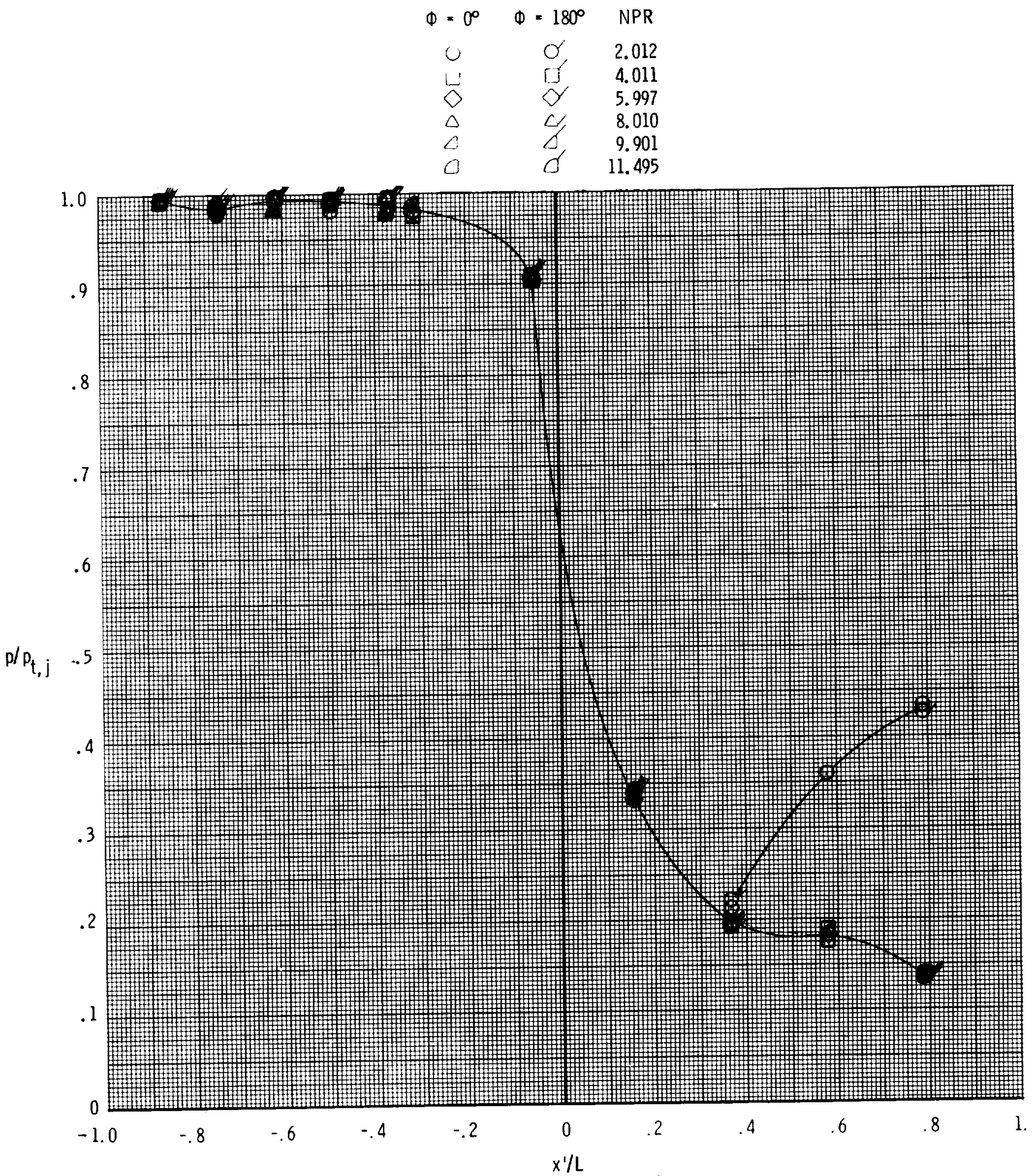

Figure 10. Effect of nozzle pressure ratio on internal static pressure distributions of gimballed axisymmetric nozzle. $\delta_{v,p} = 0°$.

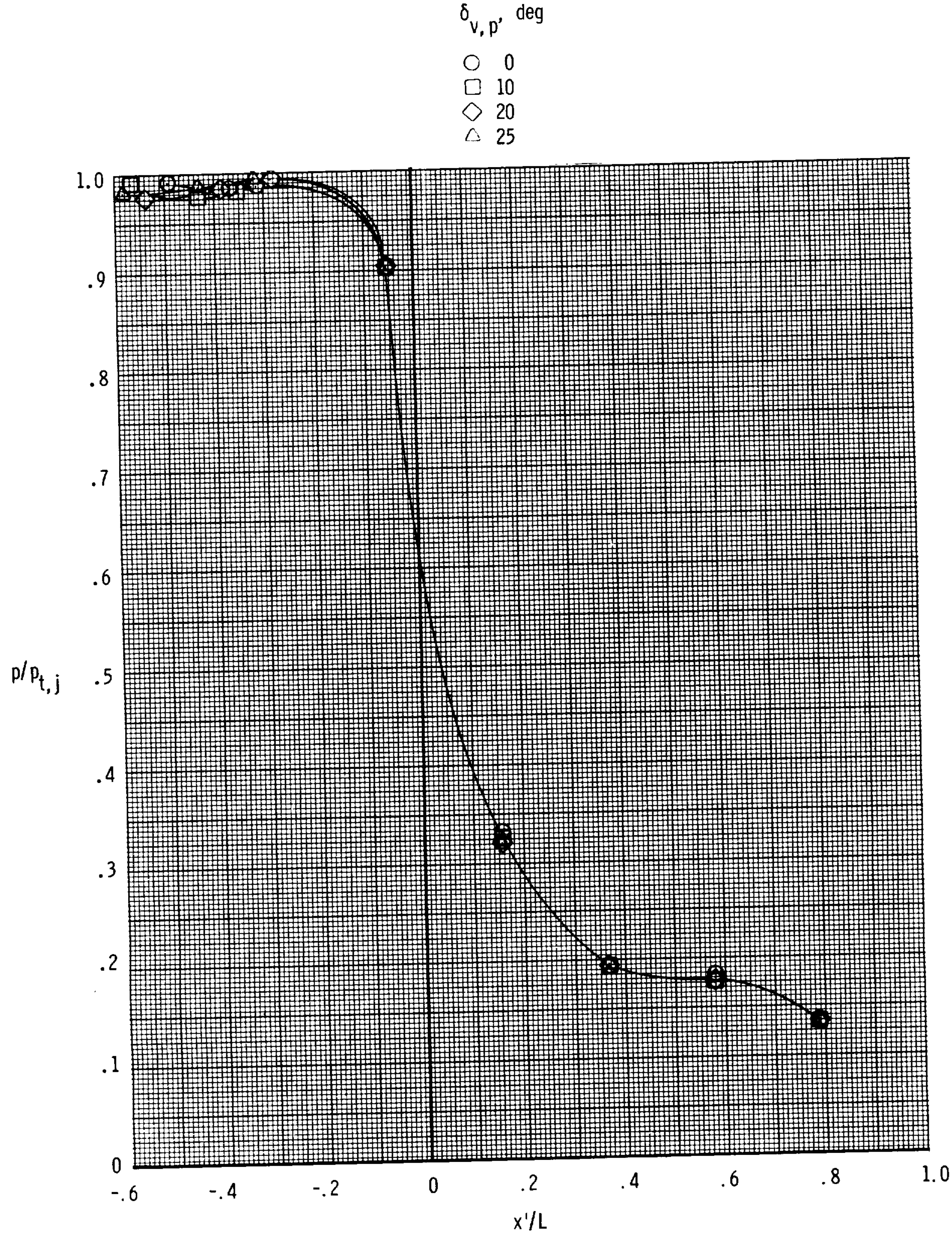

(a) Top orifice row ($\phi = 0°$).

Figure 11. Effect of geometric pitch thrust vector angle on internal static pressure distributions of gimballed axisymmetric nozzle. NPR = 9.0.

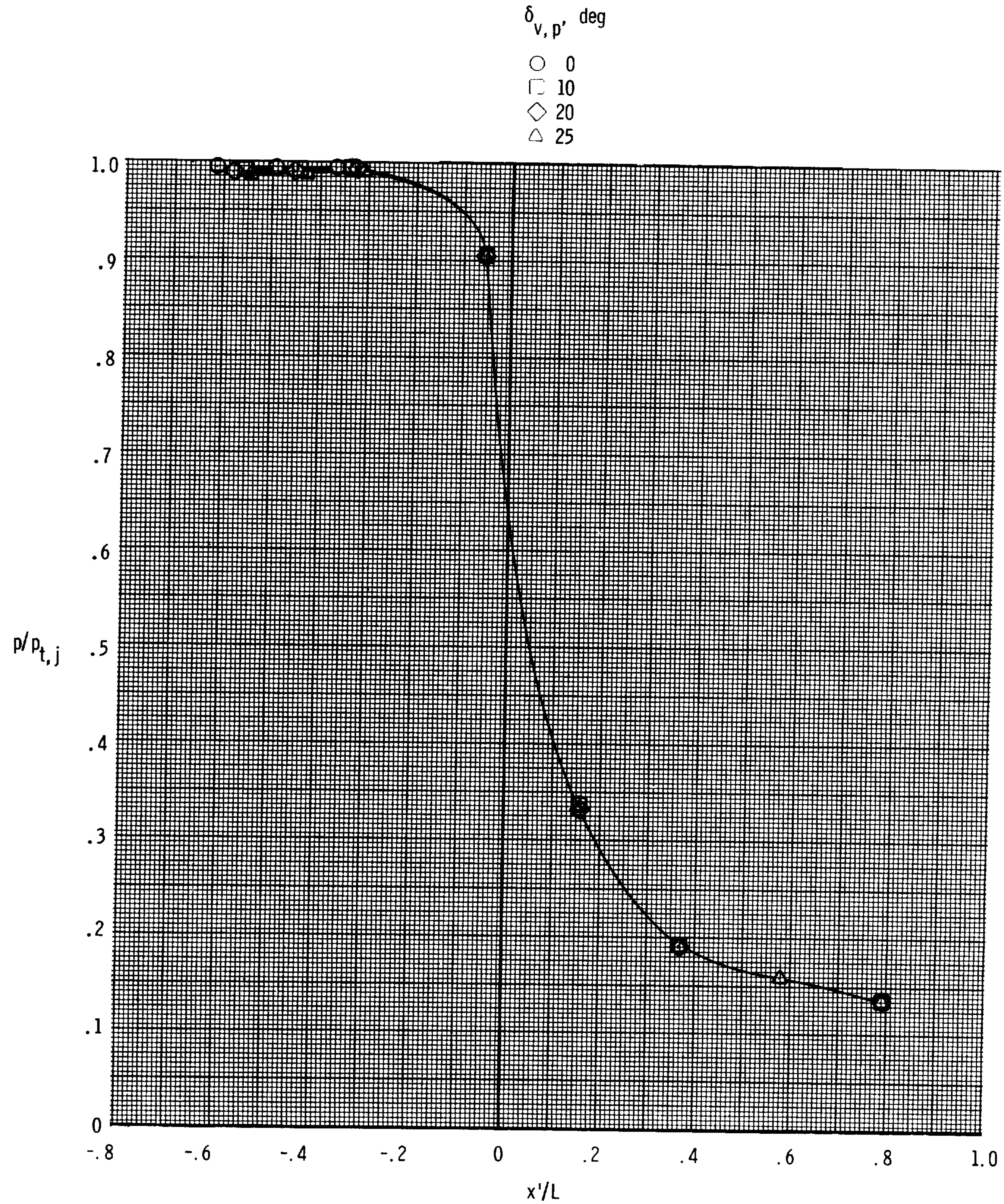

(b) Bottom orifice row ($\phi = 180°$).

Figure 11. Concluded.

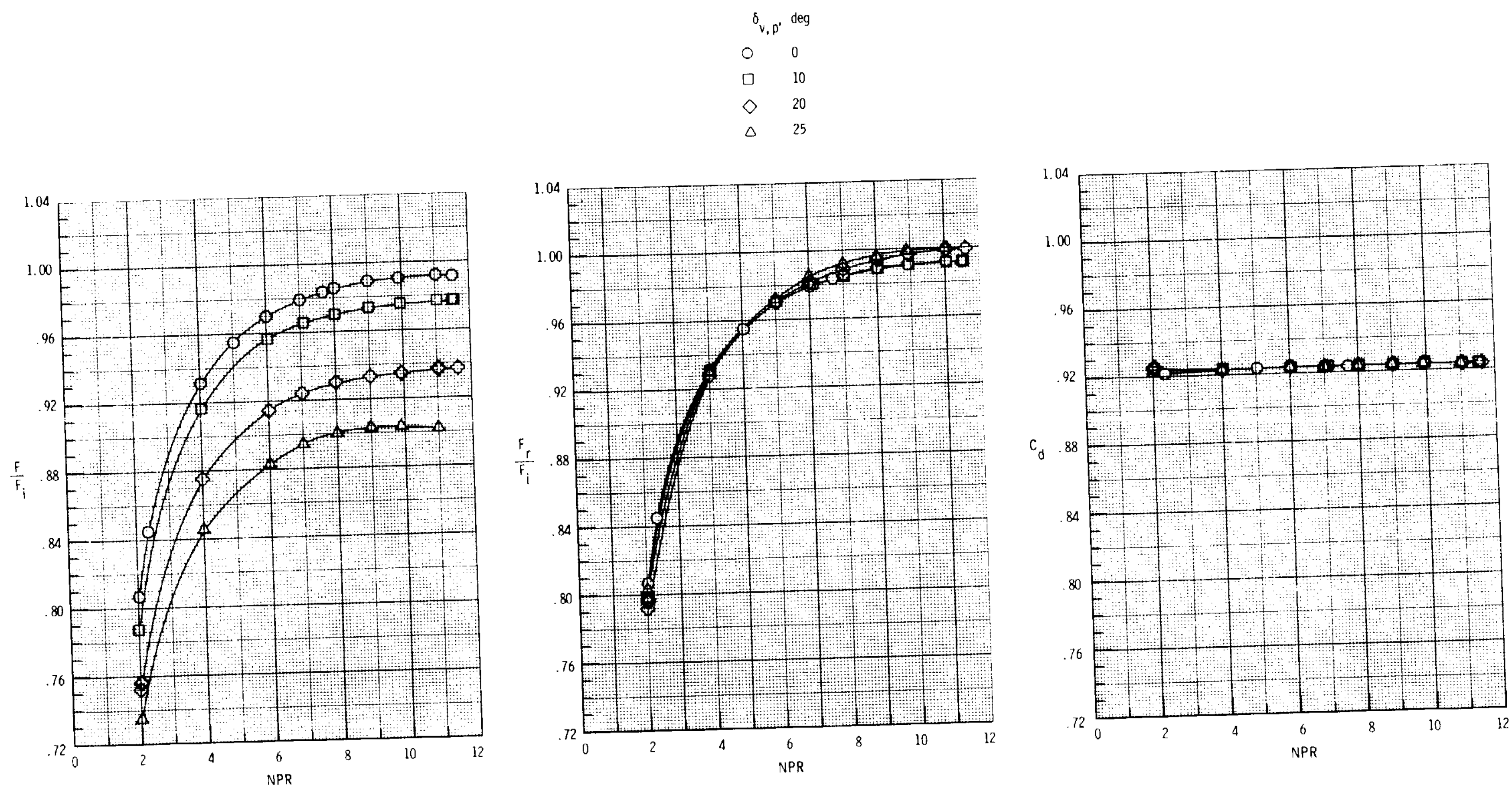

(a) Thrust ratios and discharge coefficient.

Figure 12. Effect of geometric pitch vector angle on internal performance of a gimballed axisymmetric C-D nozzle.

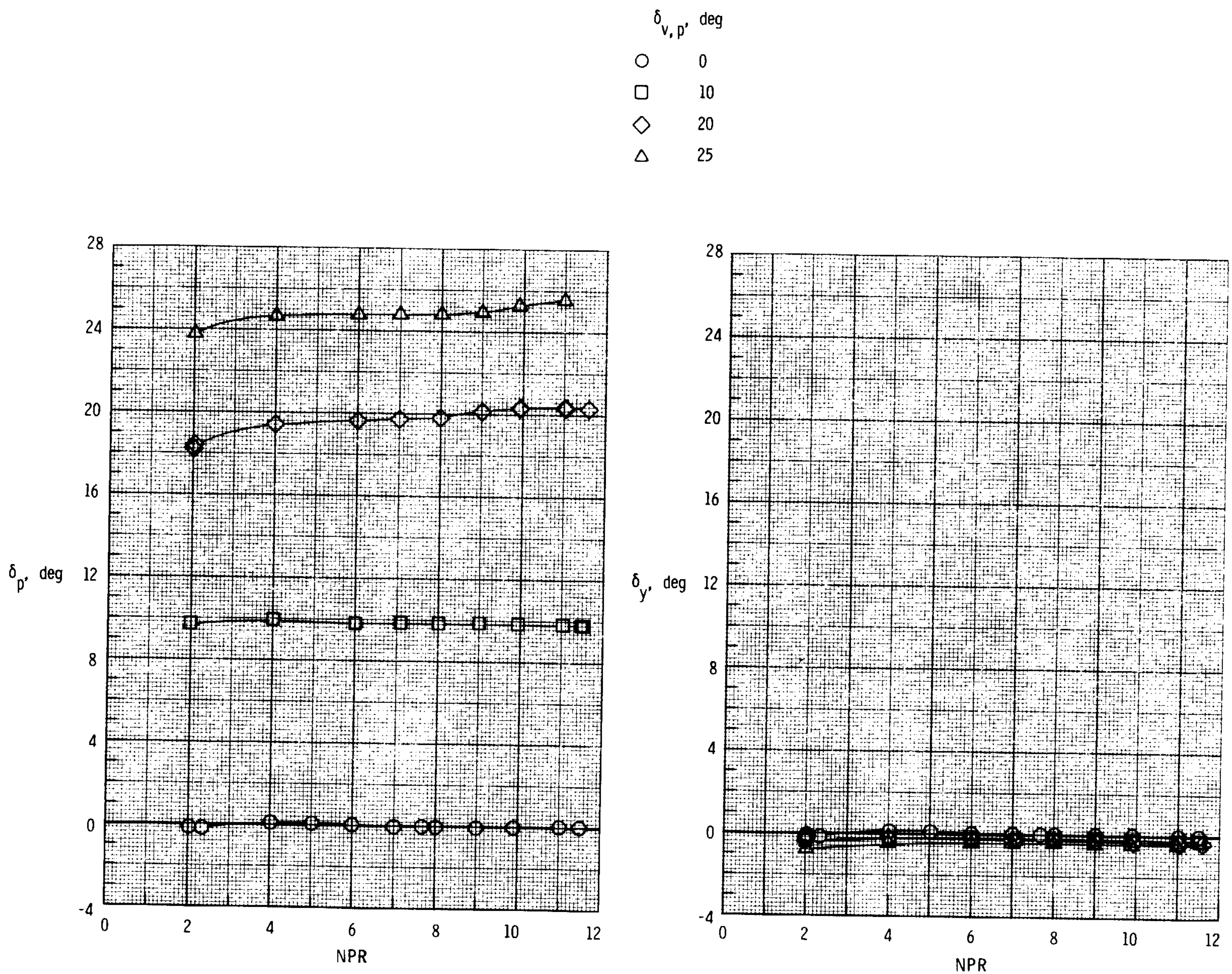

(b) Resultant thrust vector angles.

Figure 12. Concluded.

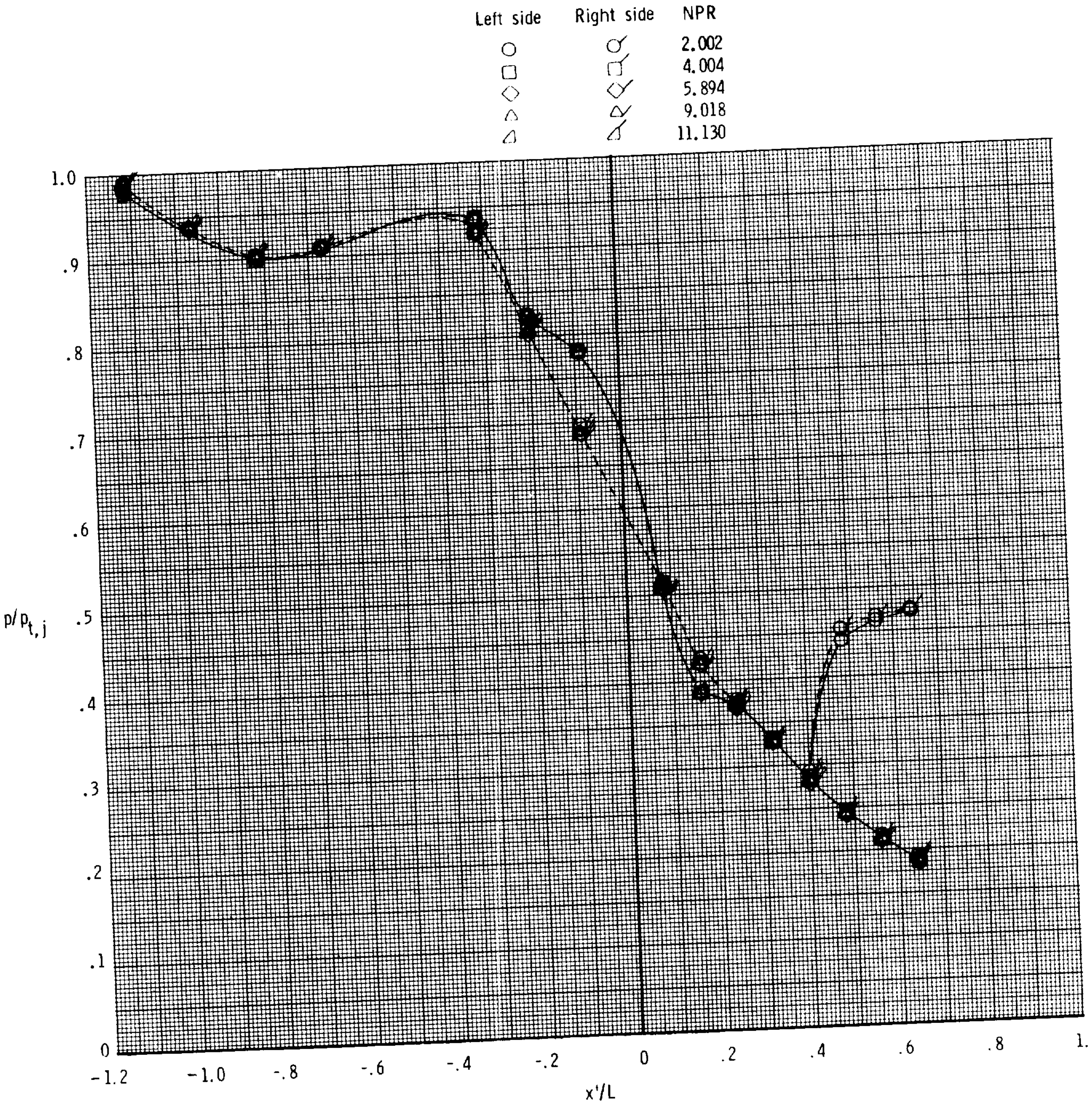

(a) $A_e/A_t = 1.46$; sidewalls.

Figure 13. Effect of nozzle pressure ratio on internal static pressure distributions of SCF 2-D C-D nozzle at AR = 2.508. $\delta_{v,p} = \delta_{v,y} = 0°$; solid line indicates left sidewall or upper flap; dashed line indicates right sidewall or lower flap.

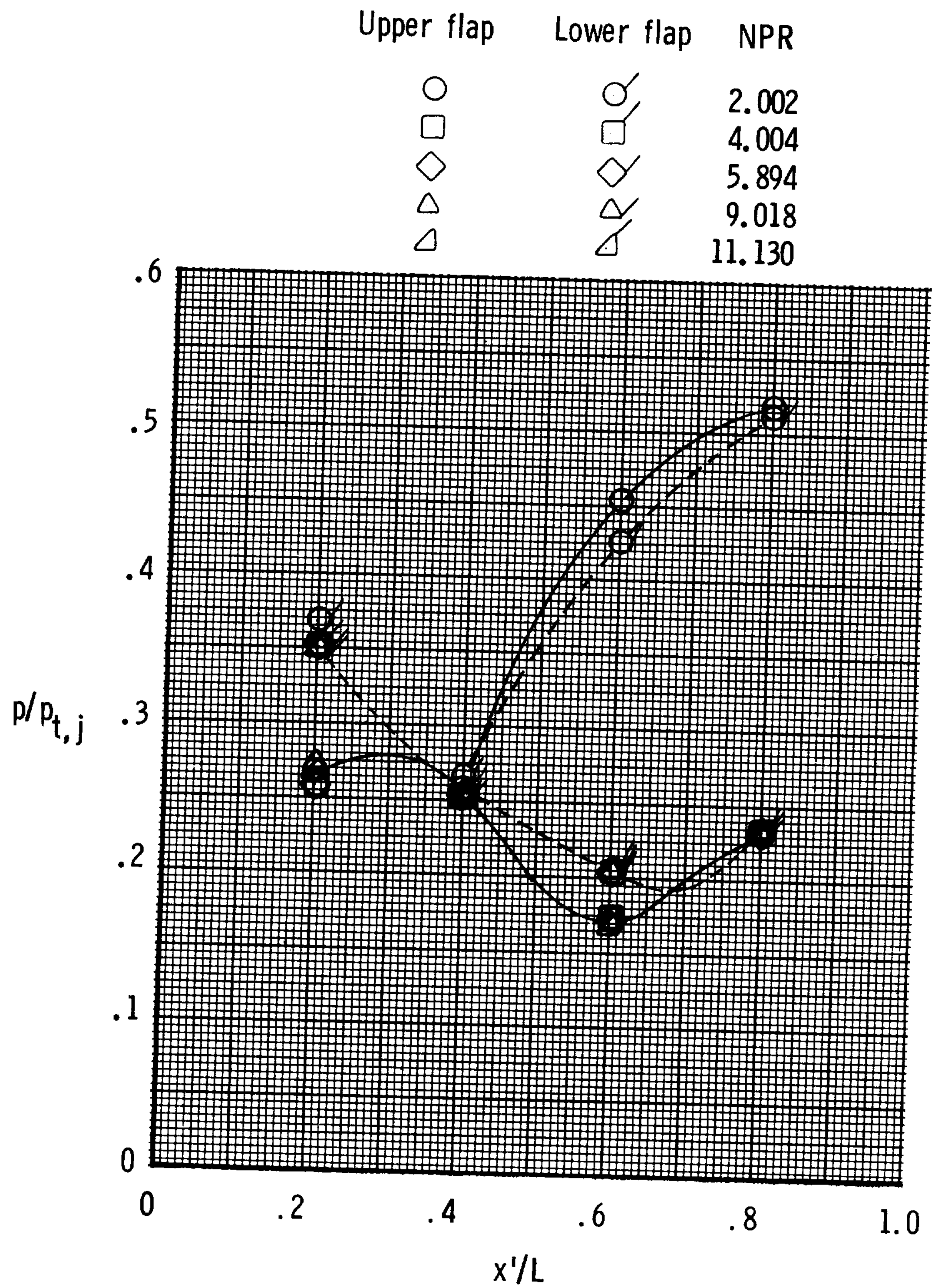

(b) $A_e/A_t = 1.46$; divergent flaps.

Figure 13. Continued.

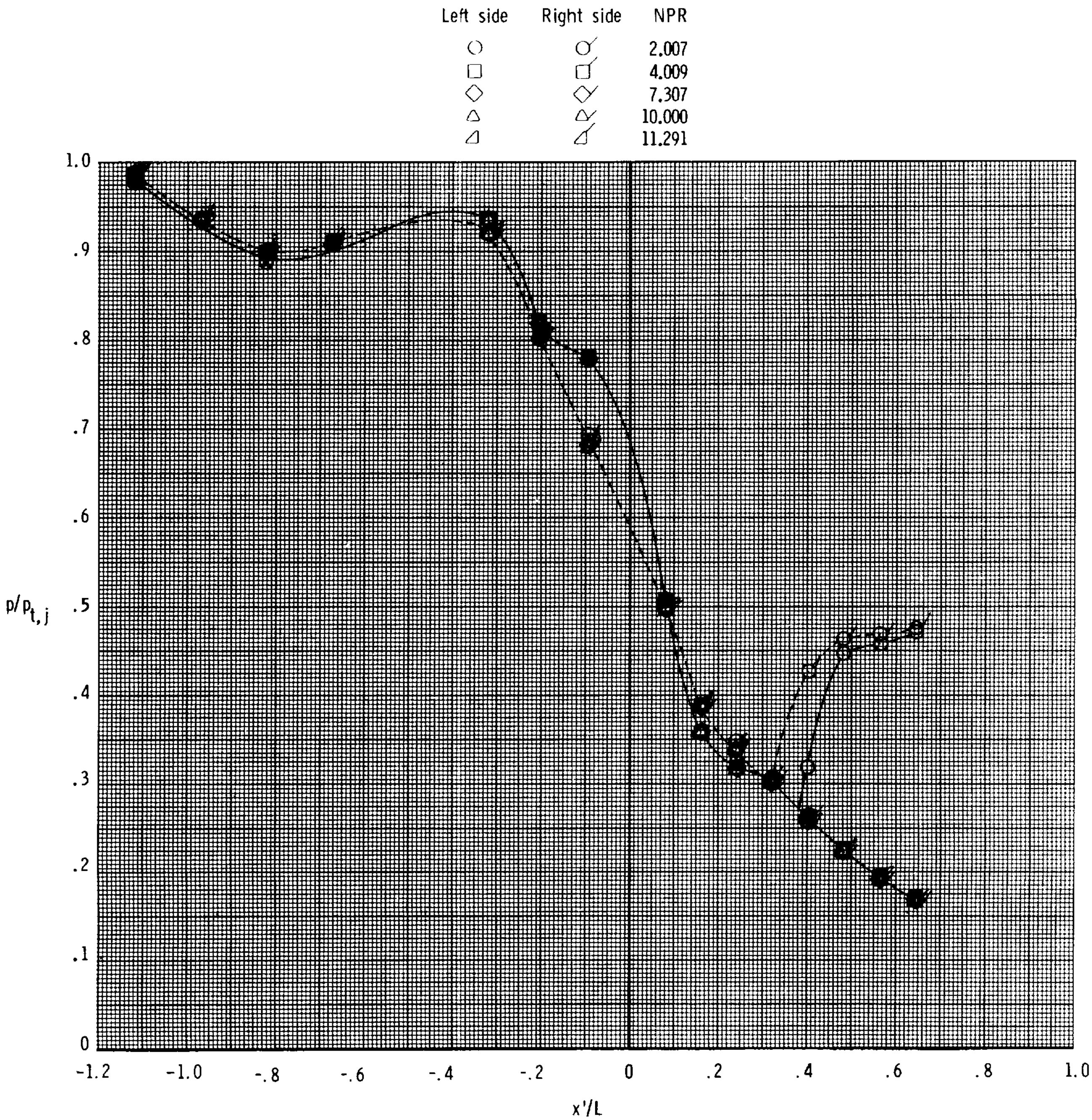

(c) $A_e/A_t = 1.63$; sidewalls.

Figure 13. Continued.

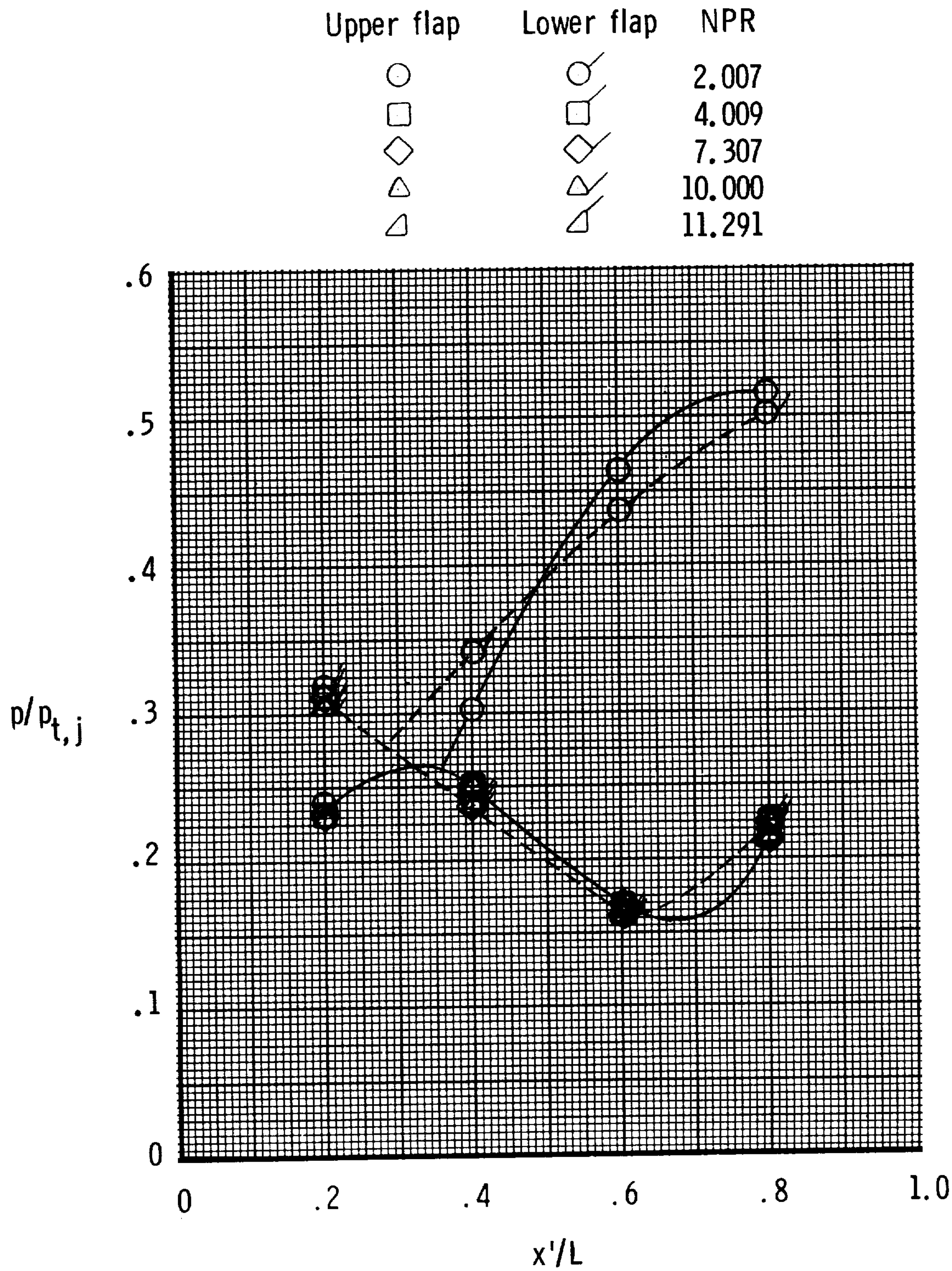

(d) $A_e/A_t = 1.63$; divergent flaps.

Figure 13. Concluded.

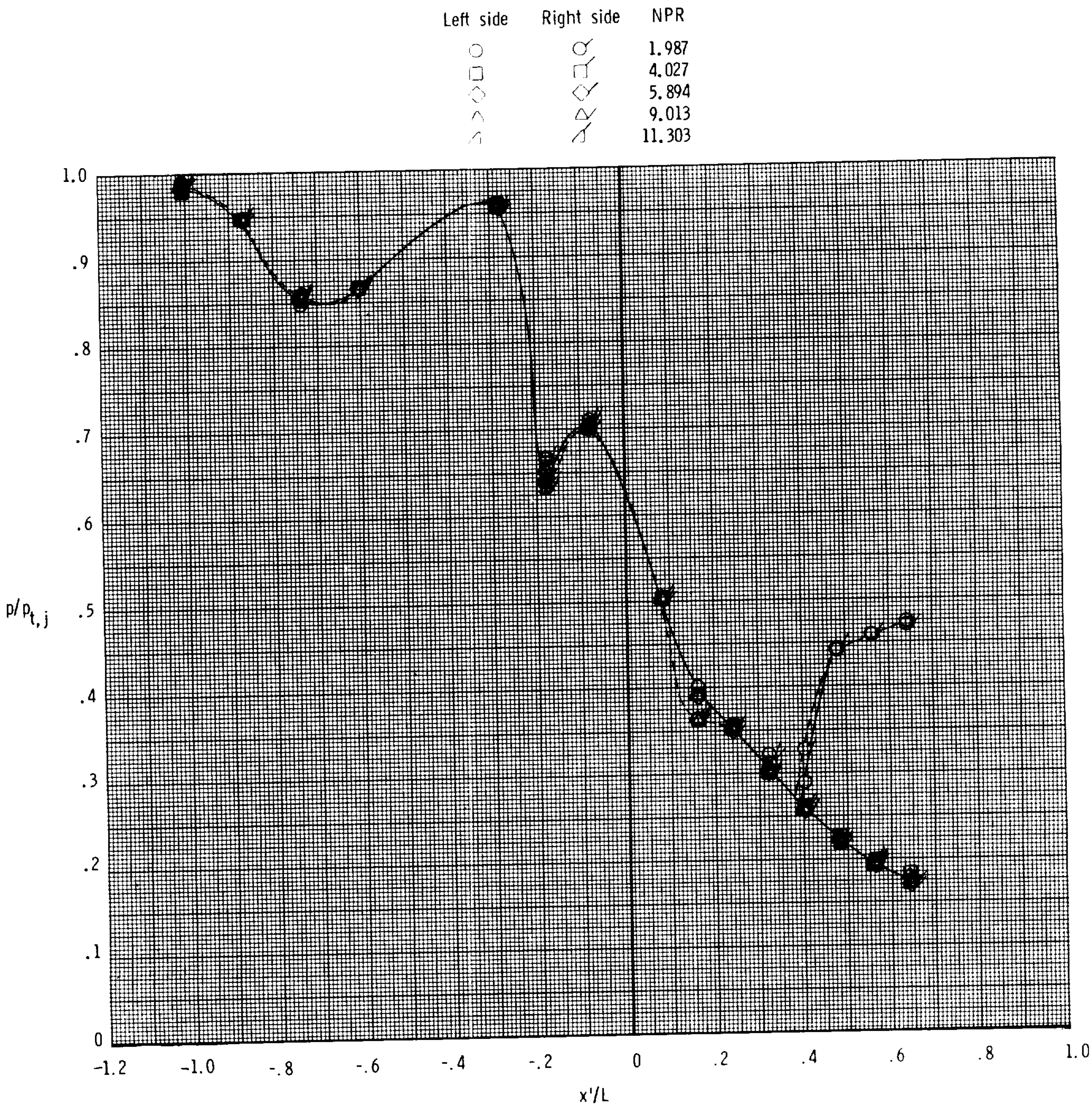

(a) $A_e/A_t = 1.46$; sidewalls.

Figure 14. Effect of nozzle pressure ratio on internal static pressure distributions of SCF 2-D C-D nozzle at AR = 2.083. $\delta_{v,p} = \delta_{v,y} = 0°$; solid line indicates left sidewall or upper flap; dashed line indicates right sidewall or lower flap.

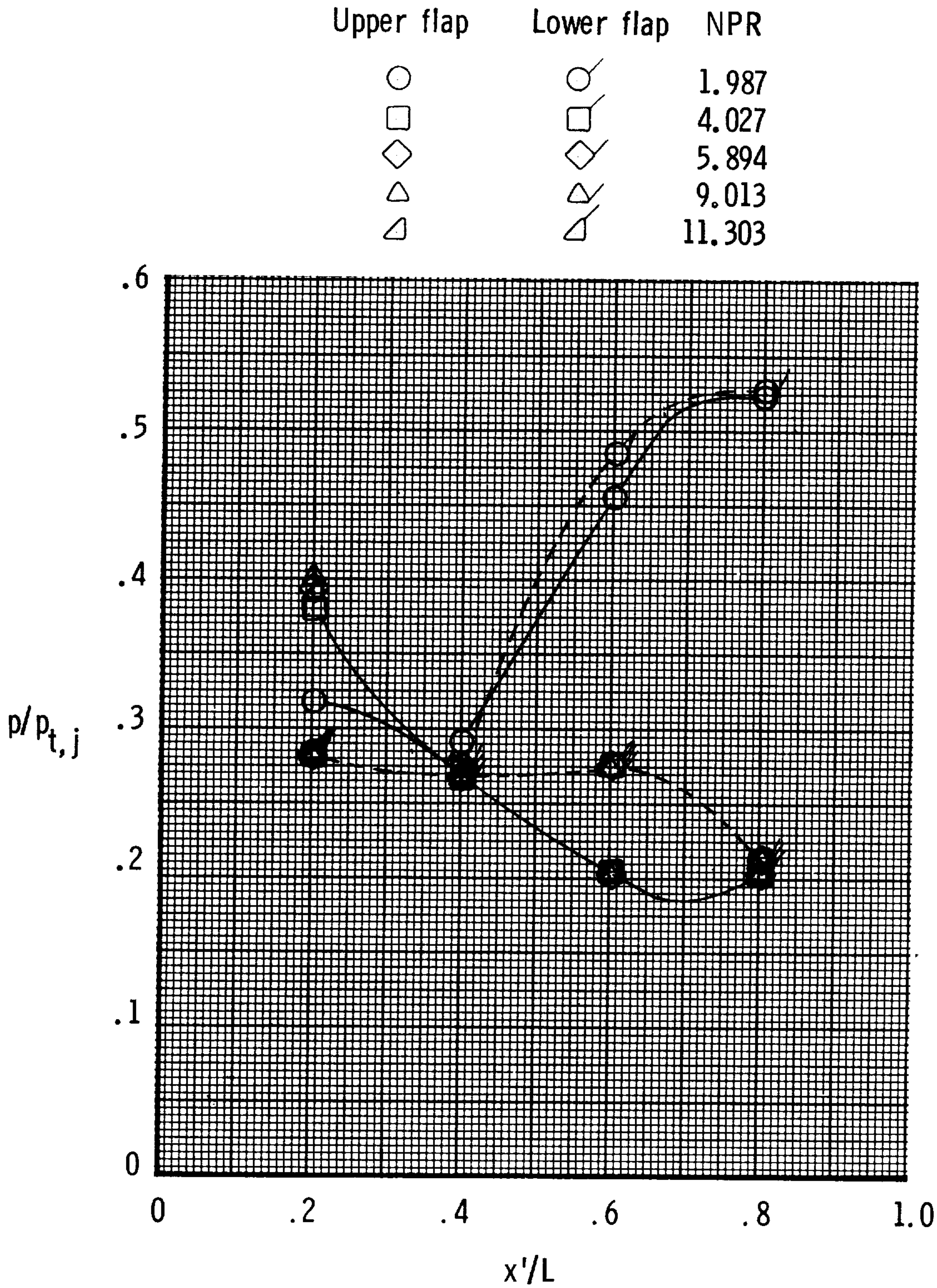

(b) $A_e/A_t = 1.46$; divergent flaps.

Figure 14. Continued.

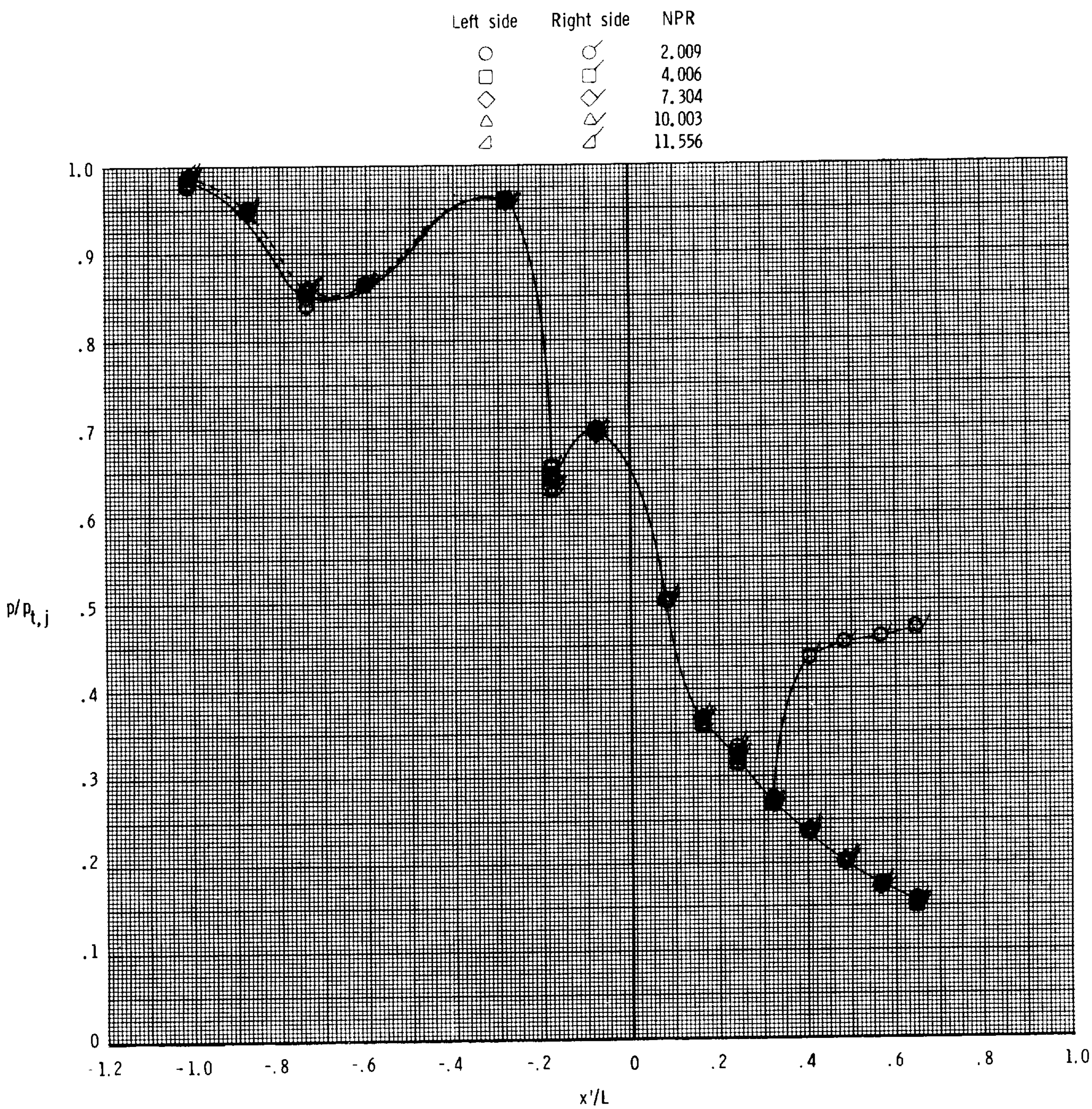

(c) $A_e/A_t = 1.63$; sidewalls.

Figure 14. Continued.

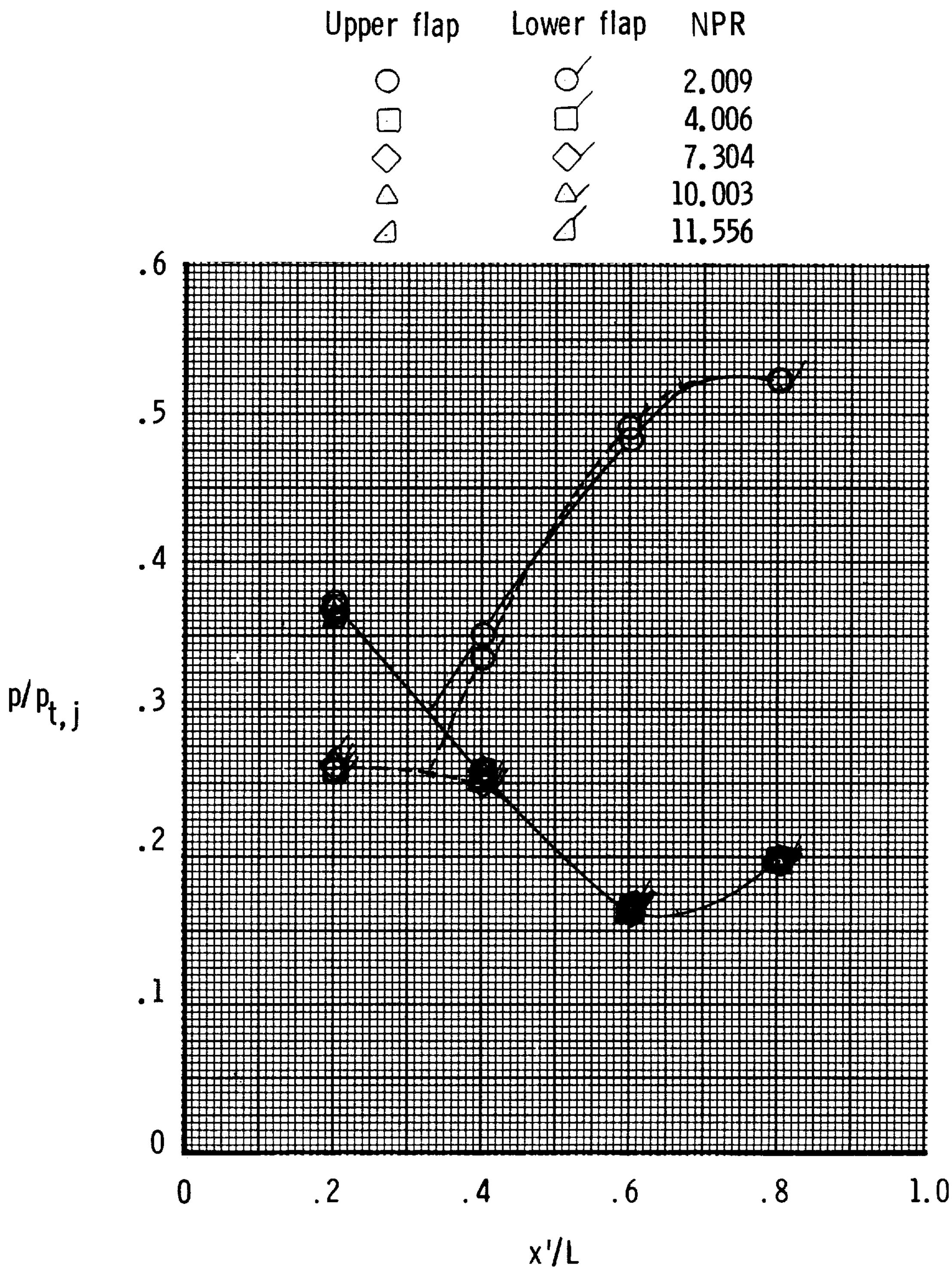

(d) $A_e/A_t = 1.63$; divergent flaps.

Figure 14. Concluded.

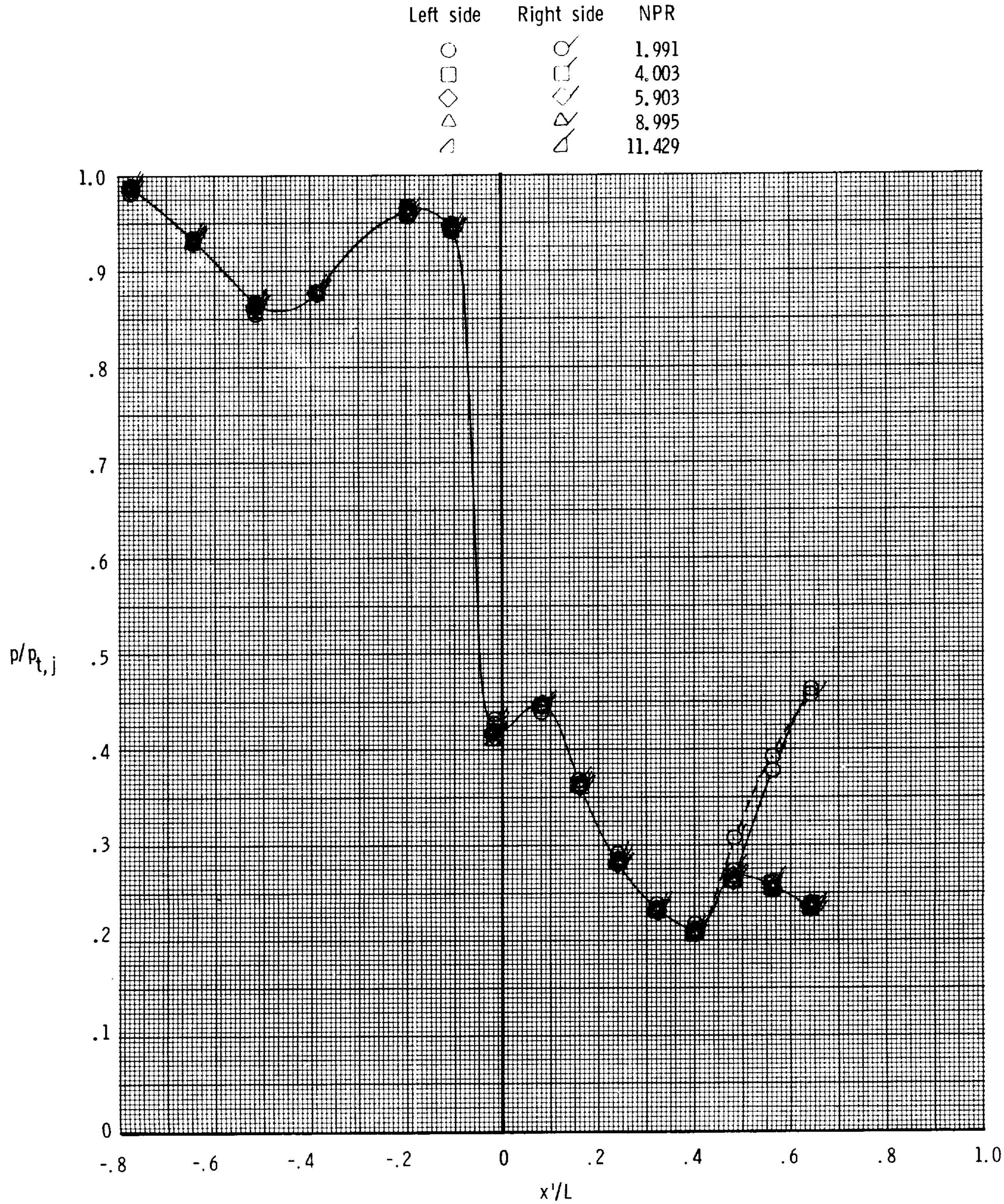

(a) $A_e/A_t = 1.46$; sidewalls.

Figure 15. Effect of nozzle pressure ratio on internal static pressure distributions of SCF 2-D C-D nozzle at AR = 1.265. $\delta_{v,p} = \delta_{v,y} = 0°$; solid line indicates left sidewall or upper flap; dashed line indicates right sidewall or lower flap.

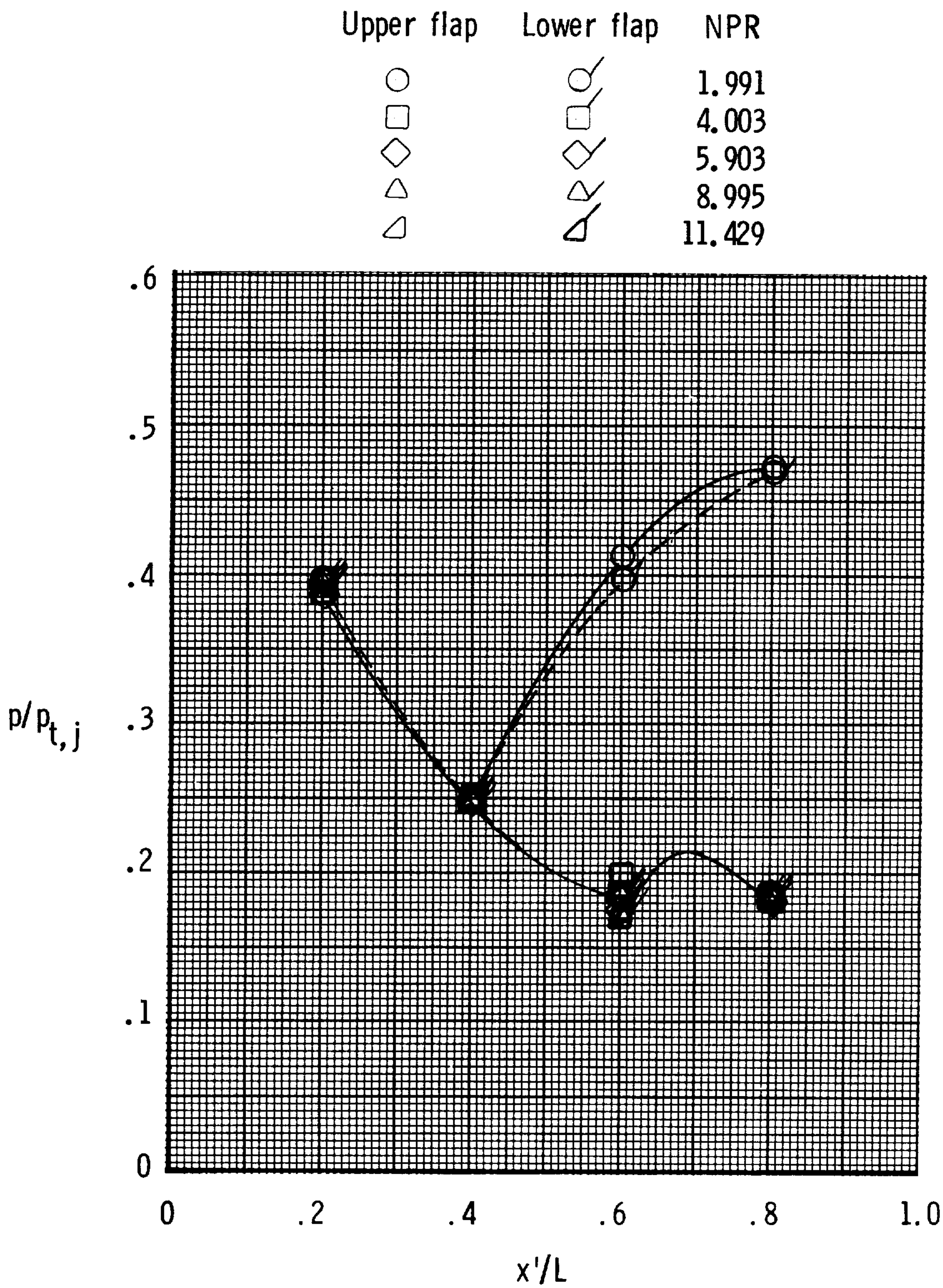

(b) $A_e/A_t = 1.46$; divergent flaps.

Figure 15. Continued.

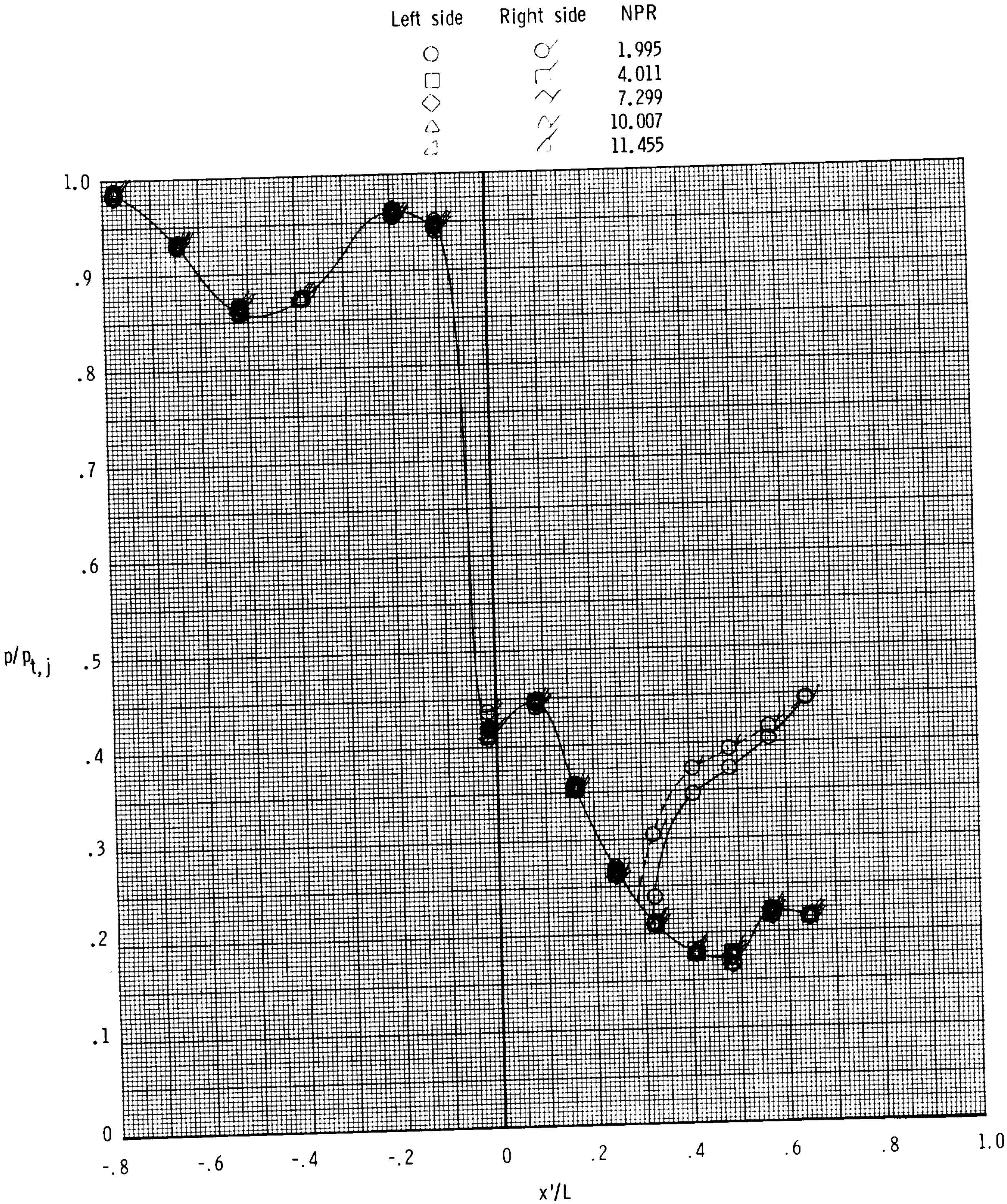

(c) $A_e/A_t = 1.63$; sidewalls.

Figure 15. Continued.

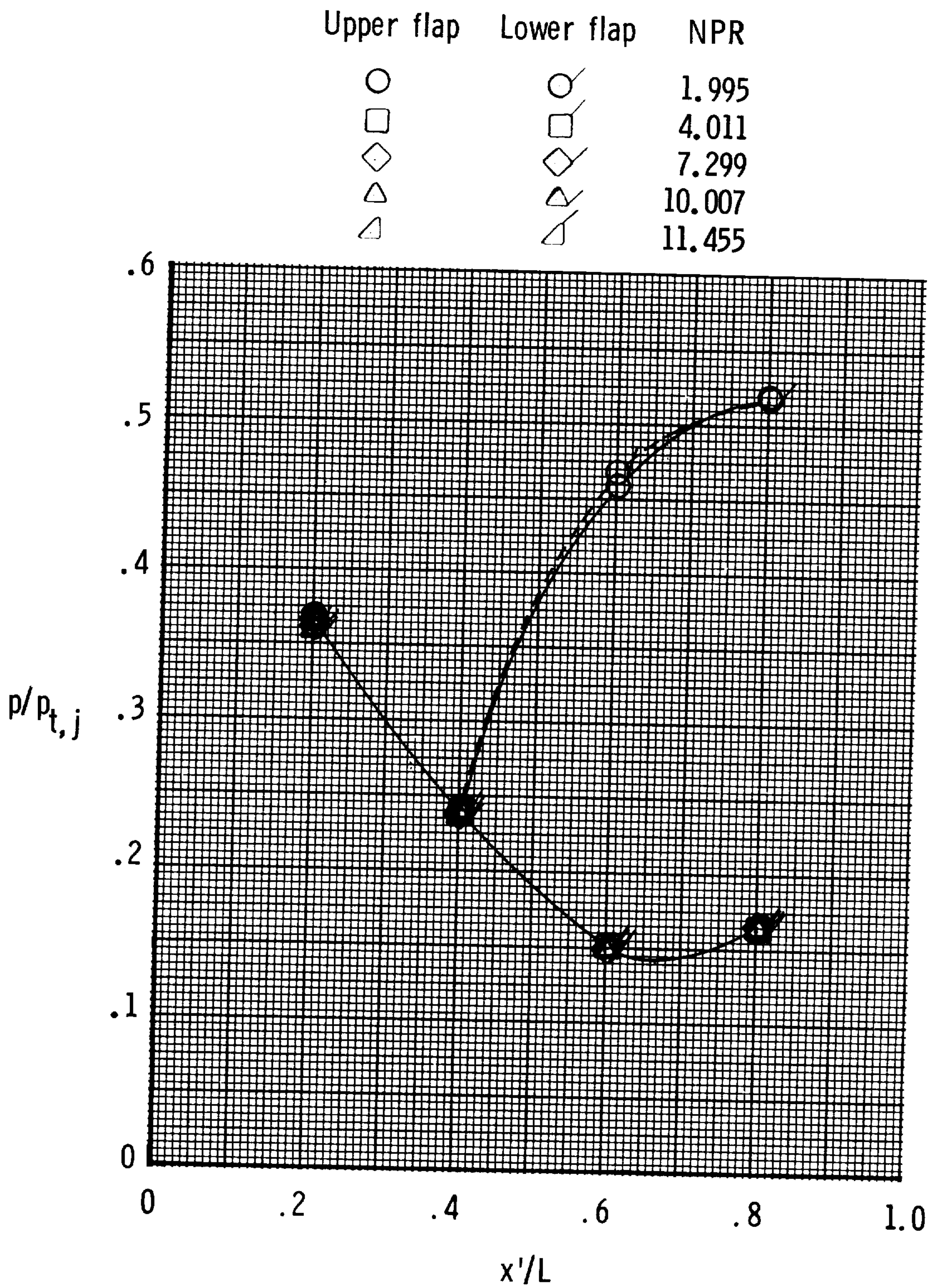

(d) $A_e/A_t = 1.63$; divergent flaps.

Figure 15. Concluded.

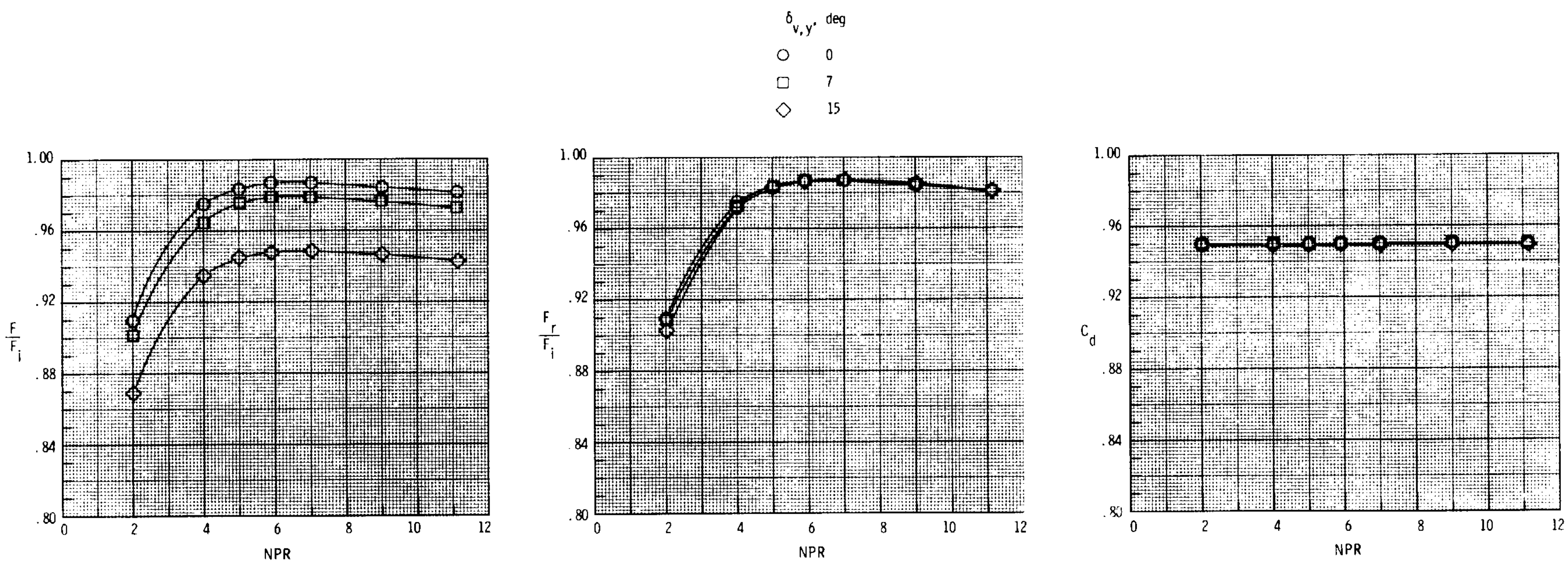

(a) Thrust performance with $\delta_{v,p} = 0°$.

Figure 16. Effect of NPR on internal performance of SCF 2-D C-D nozzle with AR = 2.508 and $A_e/A_t = 1.46$.

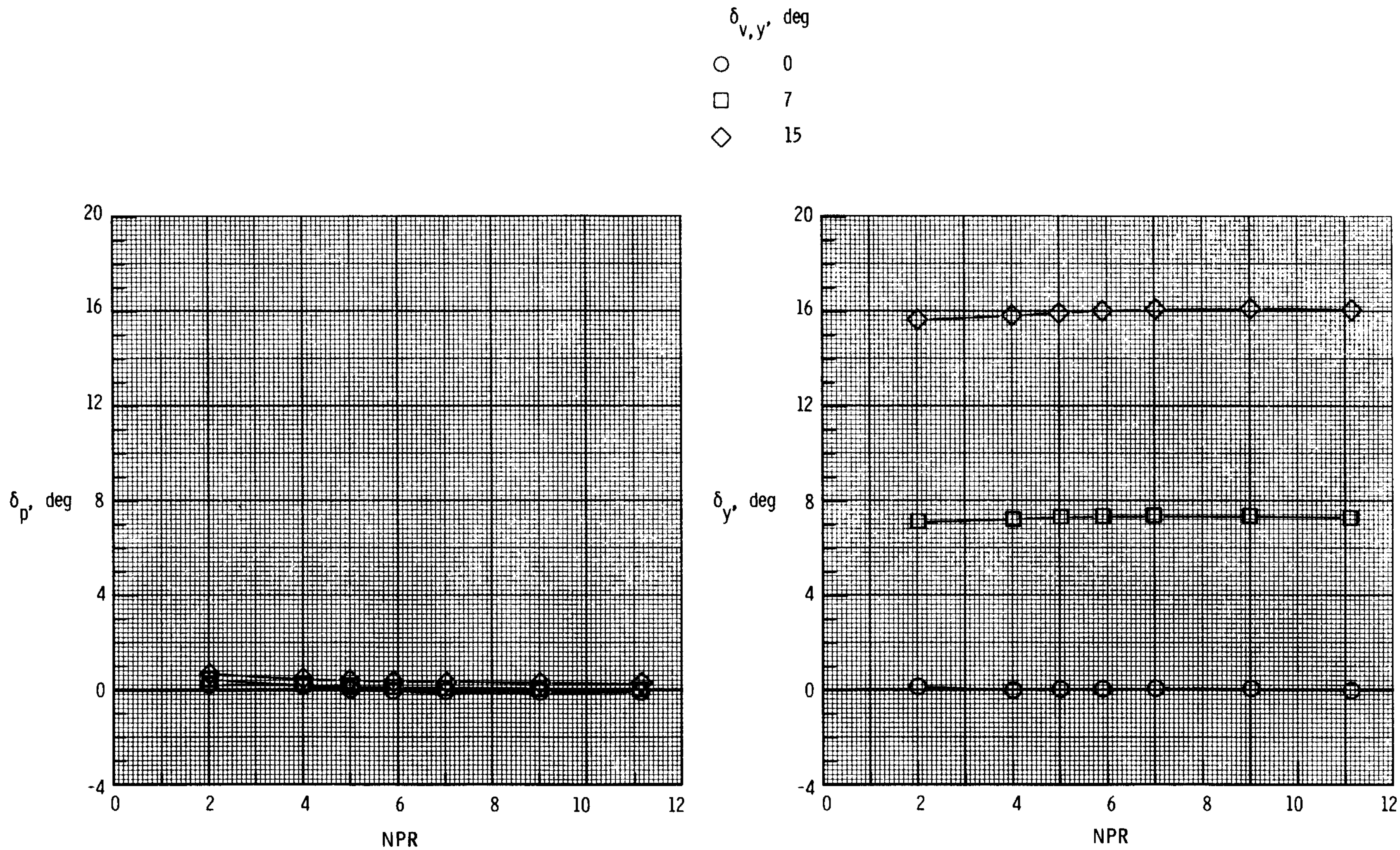

(b) Resultant thrust vector angles with $\delta_{v,p} = 0°$.

Figure 16. Continued.

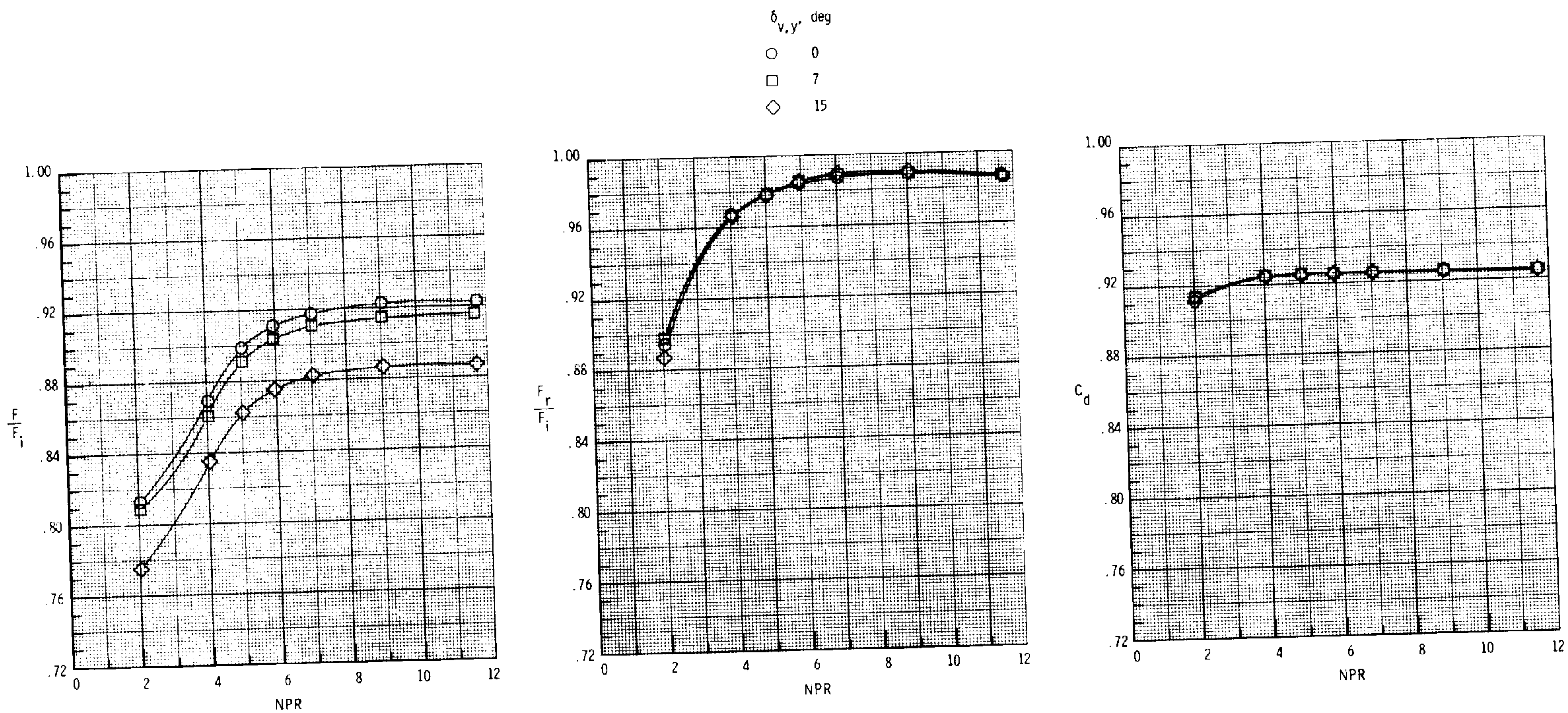

(c) Thrust performance with $\delta_{v,p} = 25°$.

Figure 16. Continued.

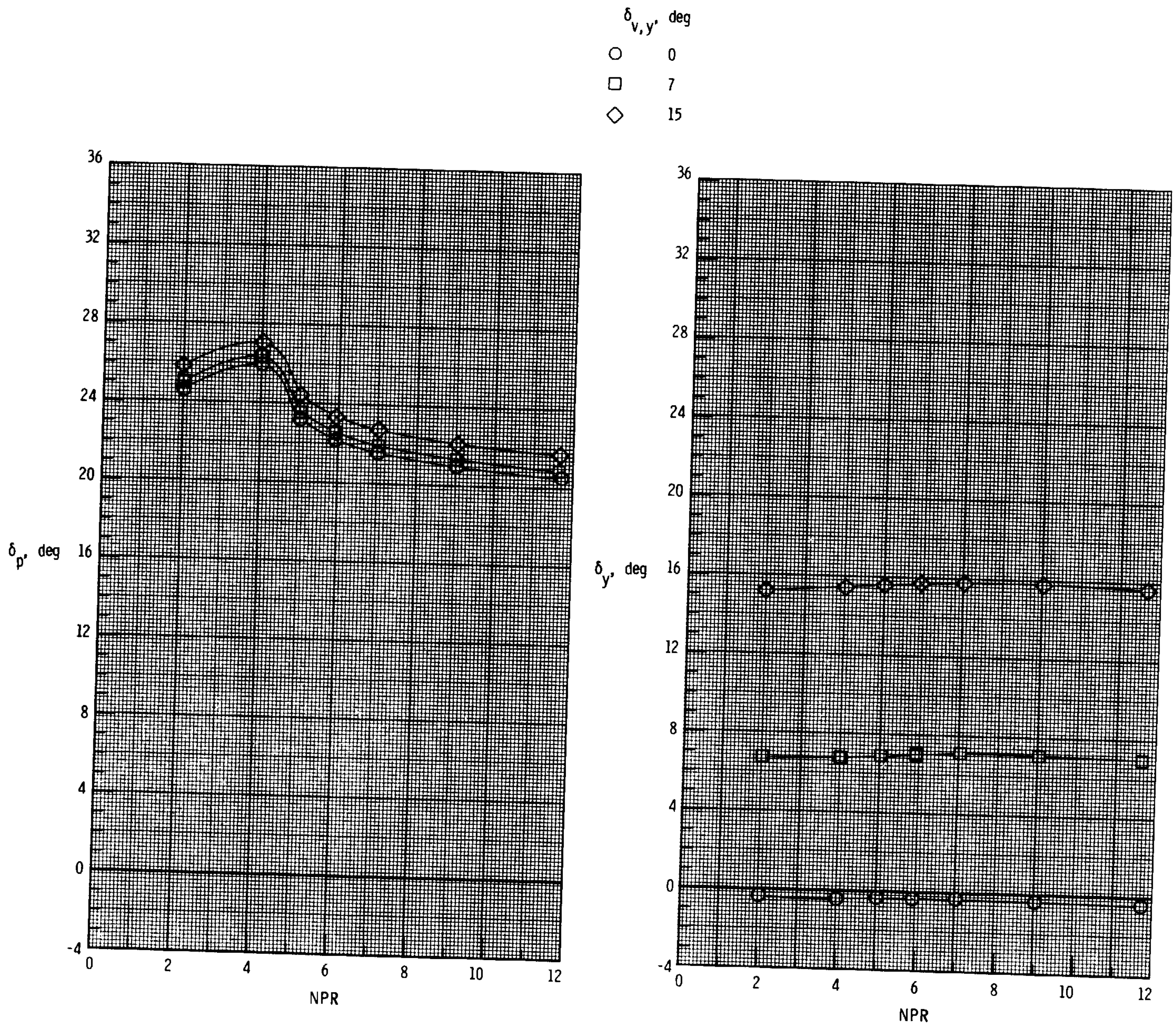

(d) Resultant thrust vector angles with $\delta_{v,p} = 25°$.

Figure 16. Concluded.

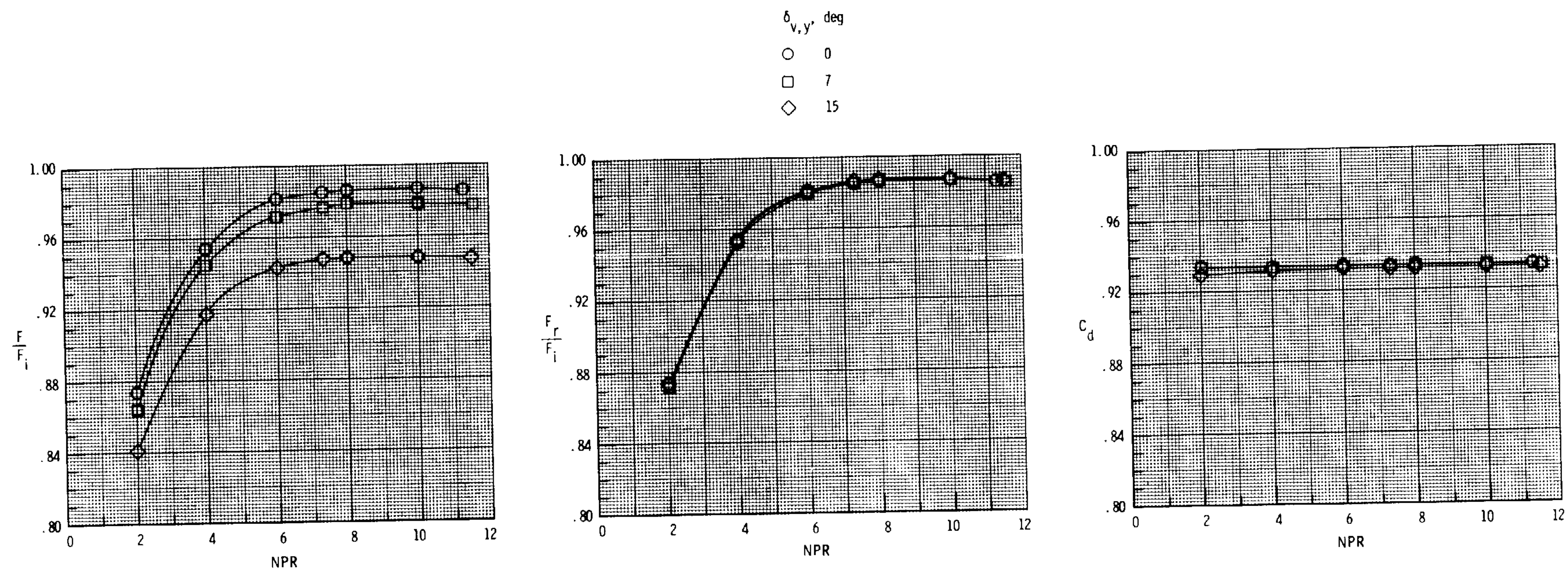

(a) Thrust performance with $\delta_{v,p} = 0°$.

Figure 17. Effect of NPR on internal performance of SCF 2-D C-D nozzle with AR = 2.508 and $A_e/A_t = 1.63$.

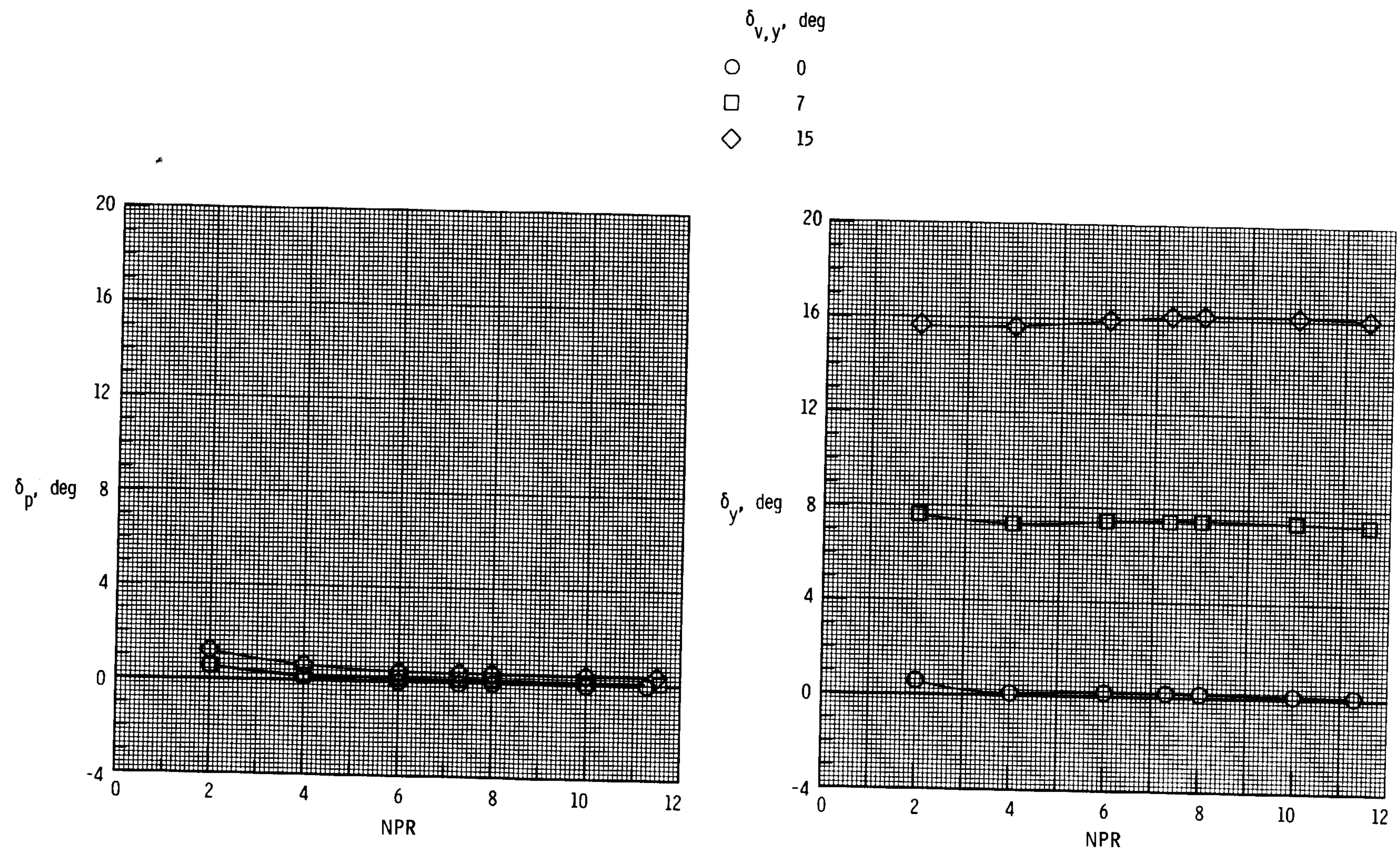

(b) Resultant thrust vector angles with $\delta_{v,p} = 0°$.

Figure 17. Continued.

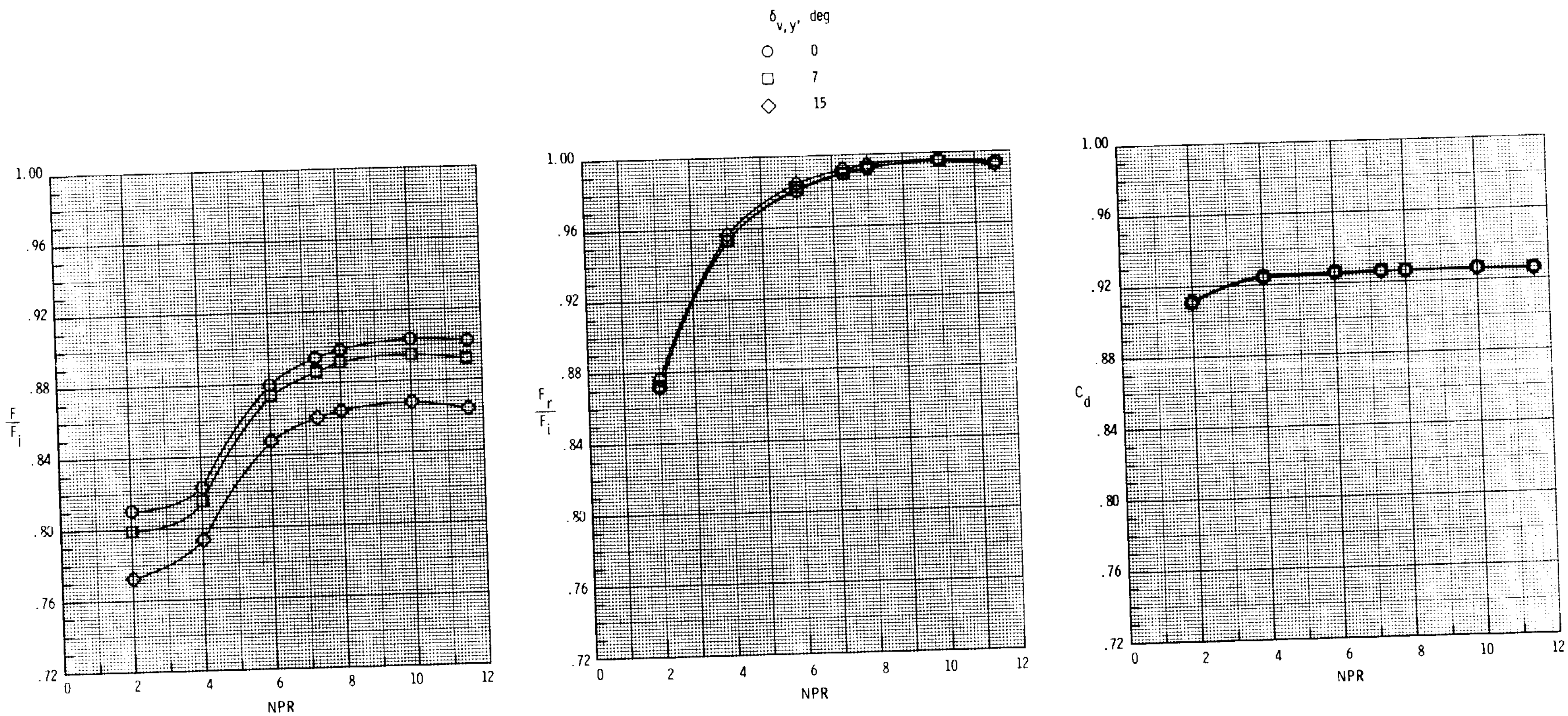

(c) Thrust performance with $\delta_{v,p} = 25°$.

Figure 17. Continued.

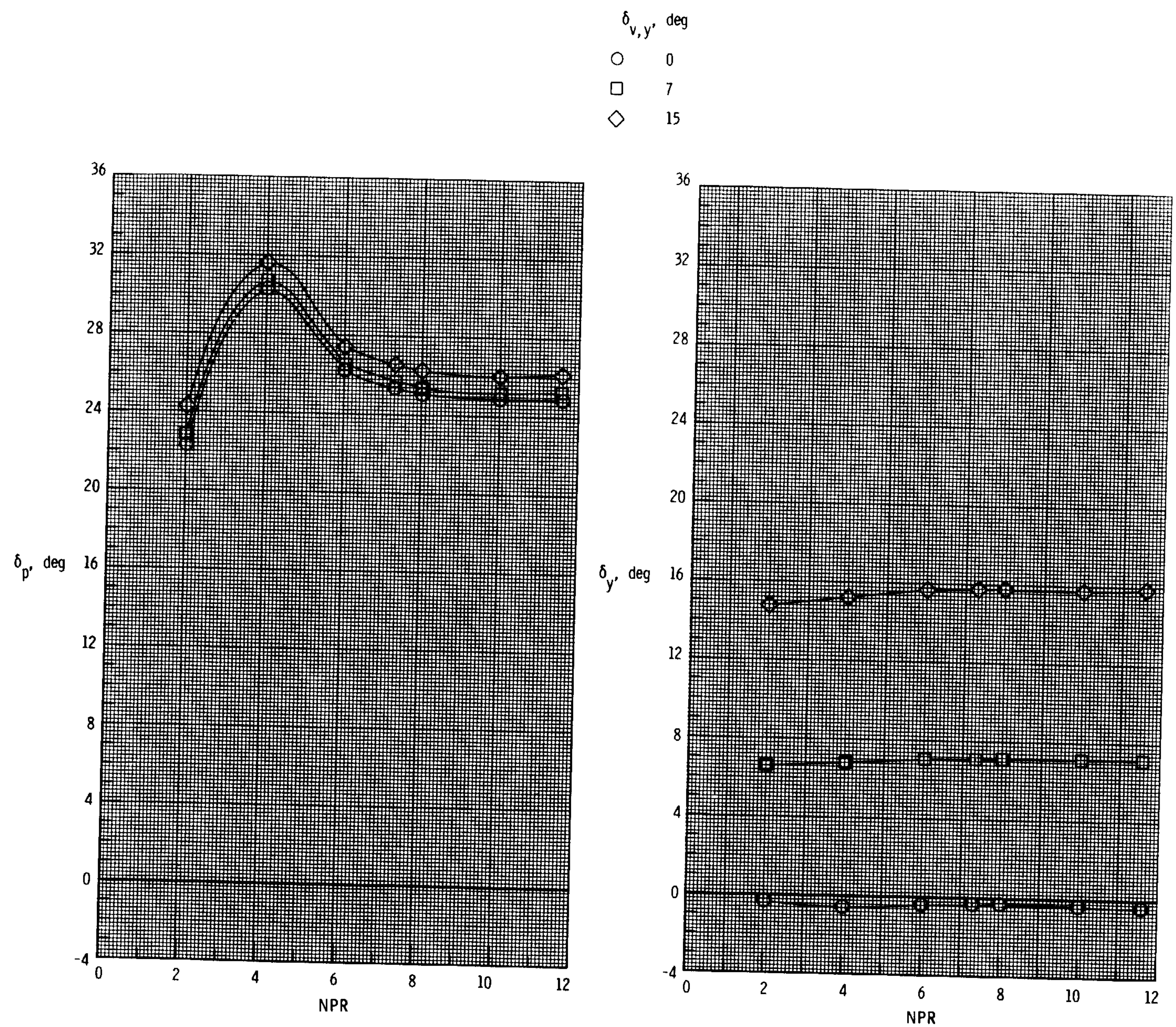

(d) Resultant thrust vector angles with $\delta_{v,p} = 25°$.

Figure 17. Concluded.

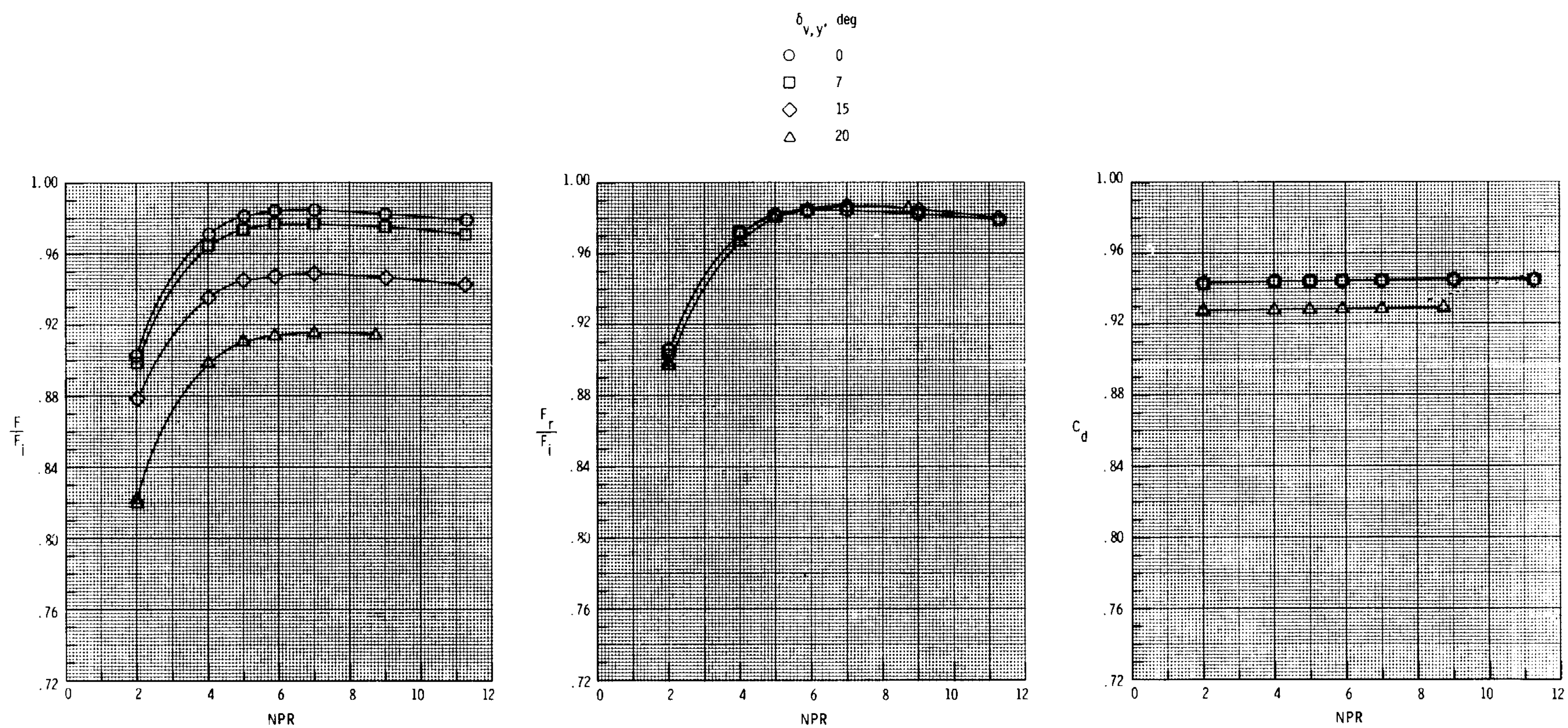

(a) Thrust performance with $\delta_{v,p} = 0°$.

Figure 18. Effect of NPR on internal performance of SCF 2-D C-D nozzle with AR = 2.083 and $A_e/A_t = 1.46$.

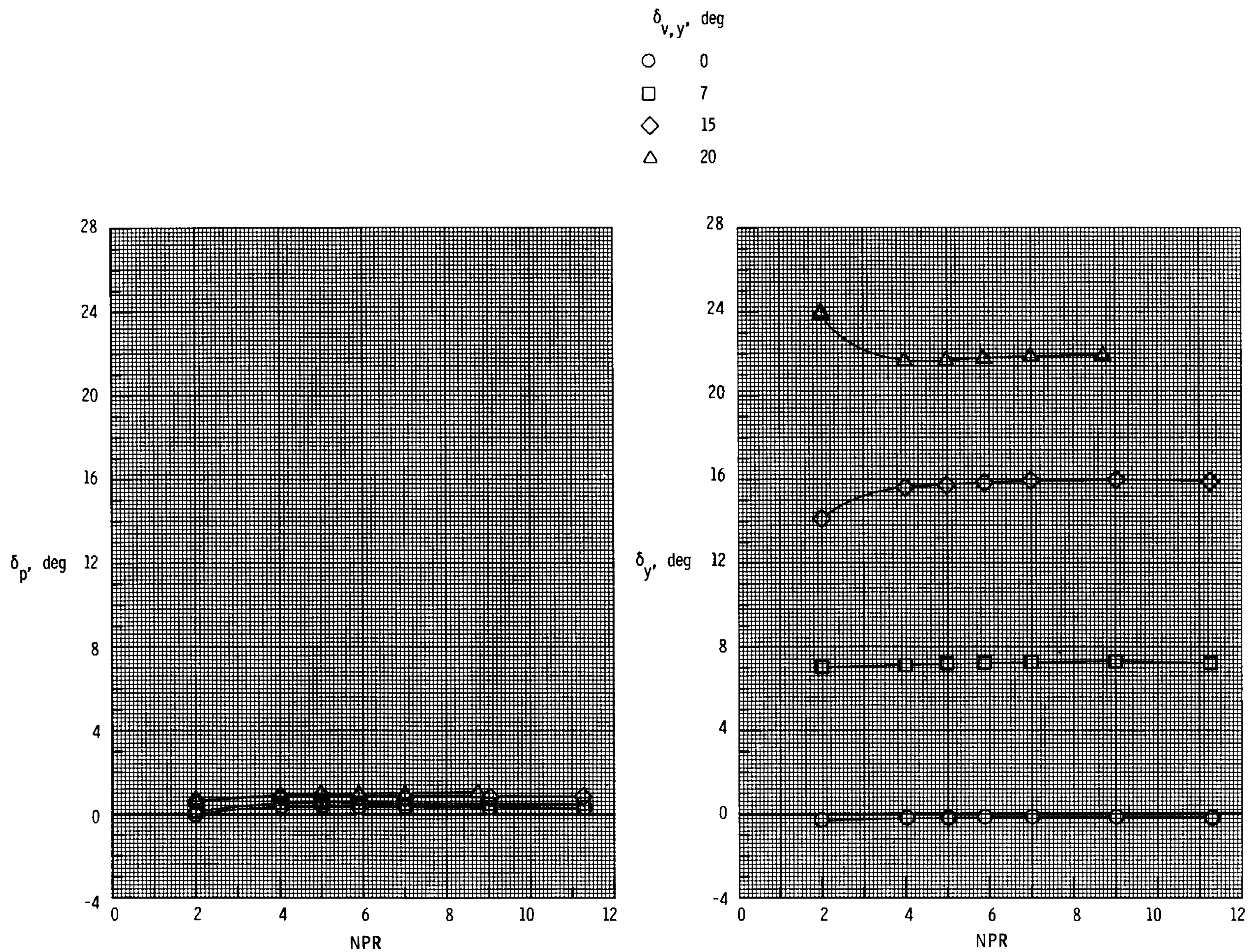

(b) Resultant thrust vector angle with $\delta_{v,p} = 0°$.

Figure 18. Continued.

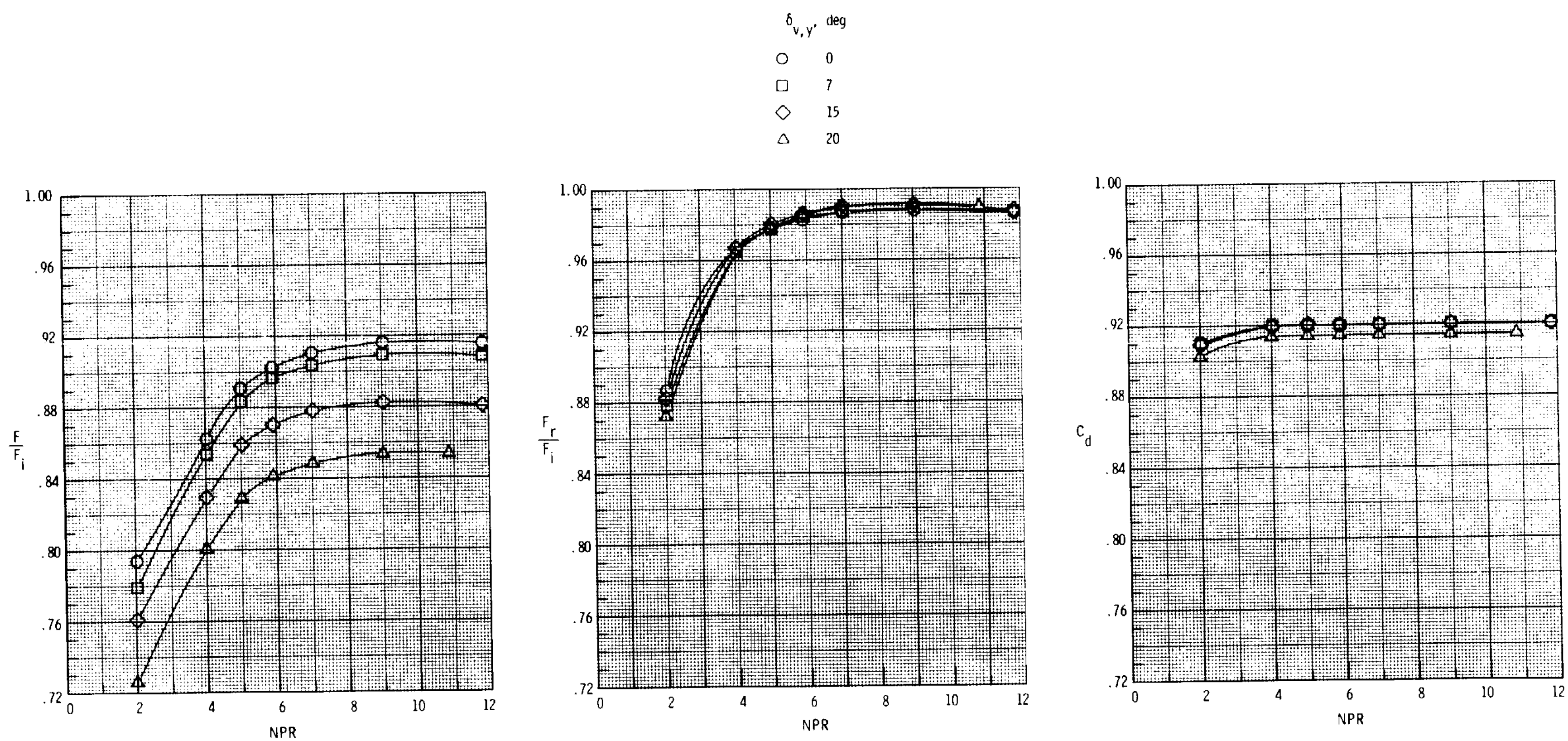

(c) Thrust performance with $\delta_{v,p} = 25°$.

Figure 18. Continued.

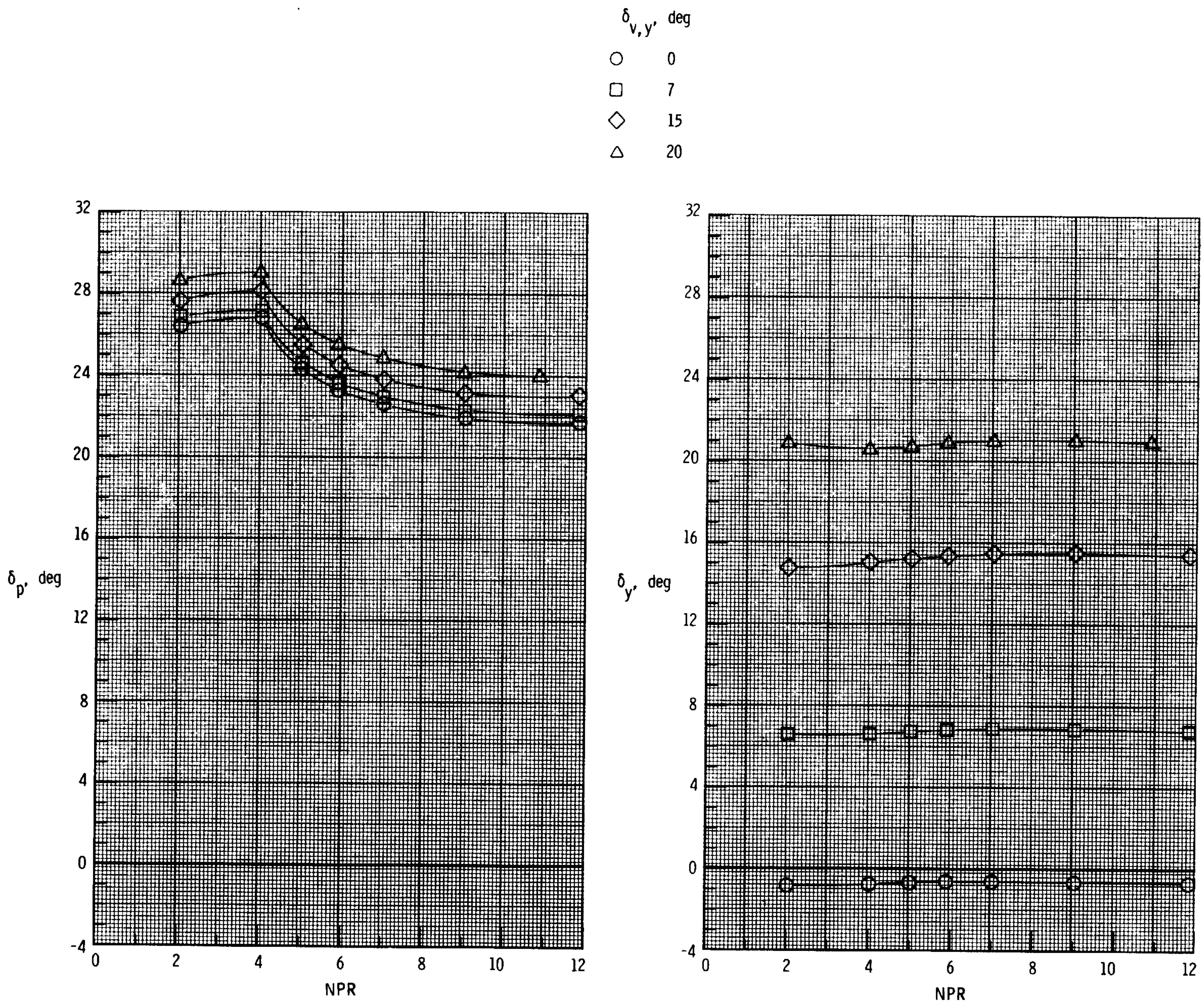

(d) Resultant thrust vector angles with $\delta_{v,p} = 25°$.

Figure 18. Concluded.

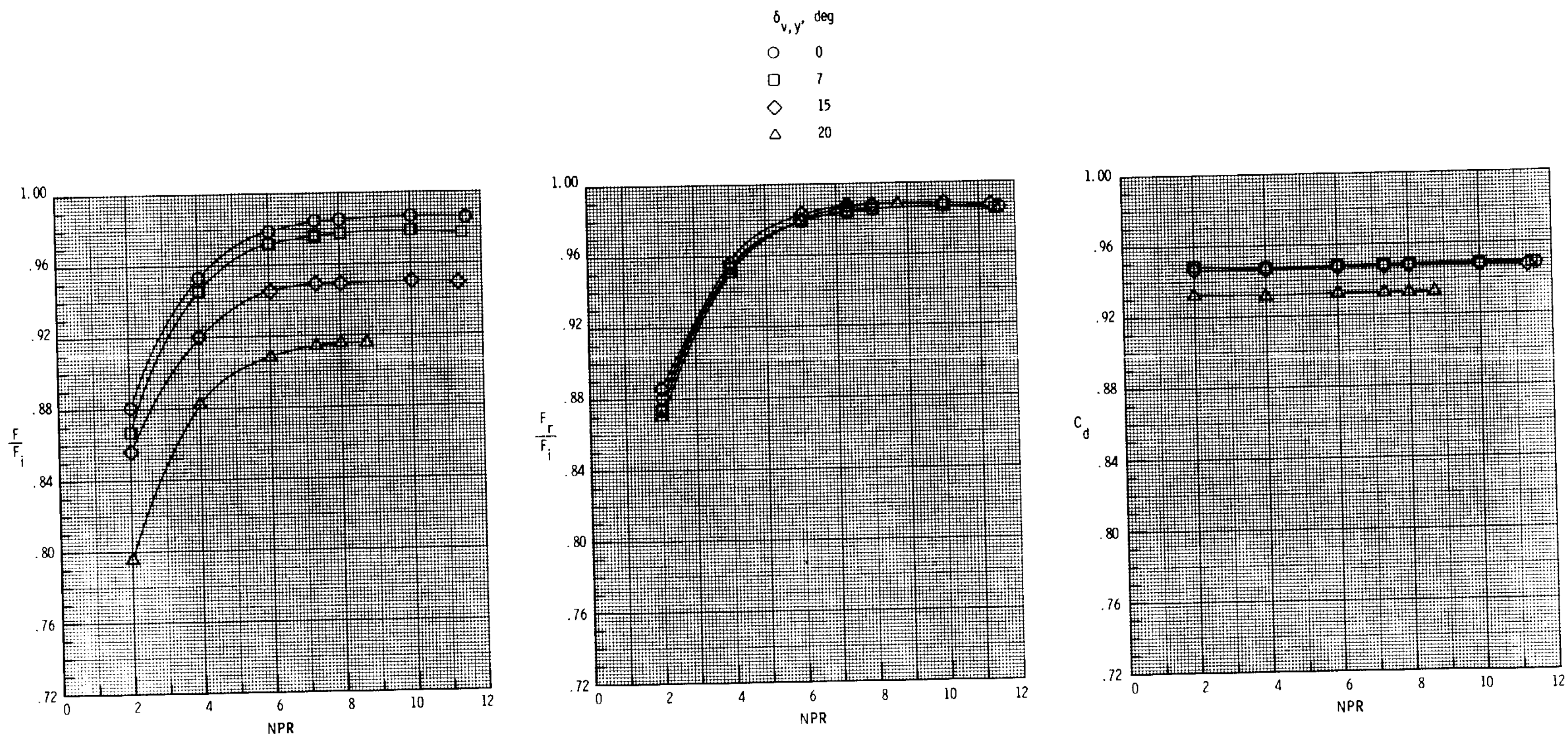

(a) Thrust performance with $\delta_{v,p} = 0°$.

Figure 19. Effect of NPR on performance of SCF 2-D C-D nozzle with AR = 2.083 and $A_e/A_t = 1.63$.

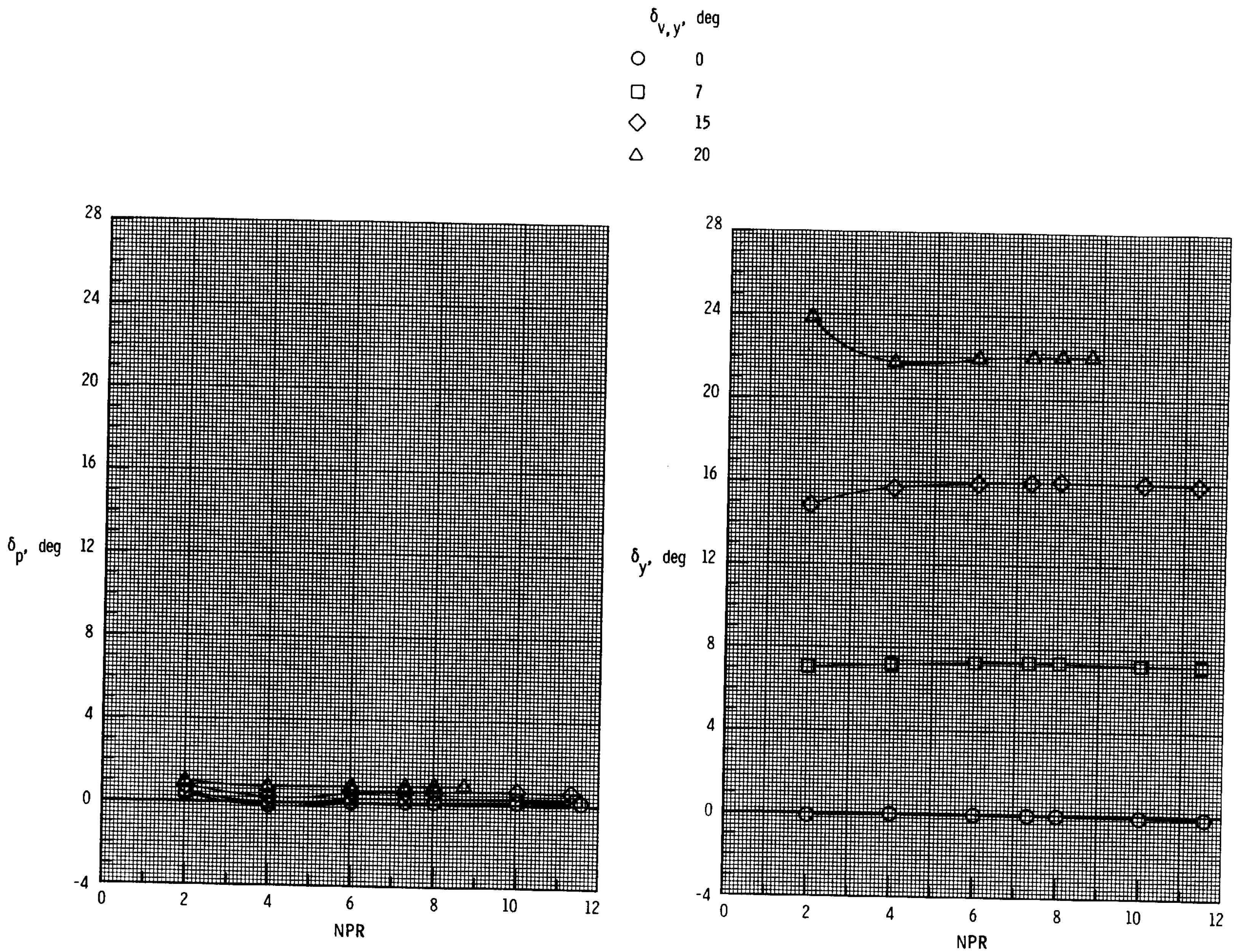

(b) Resultant thrust vector angles with $\delta_{v,p} = 0°$.

Figure 19. Continued.

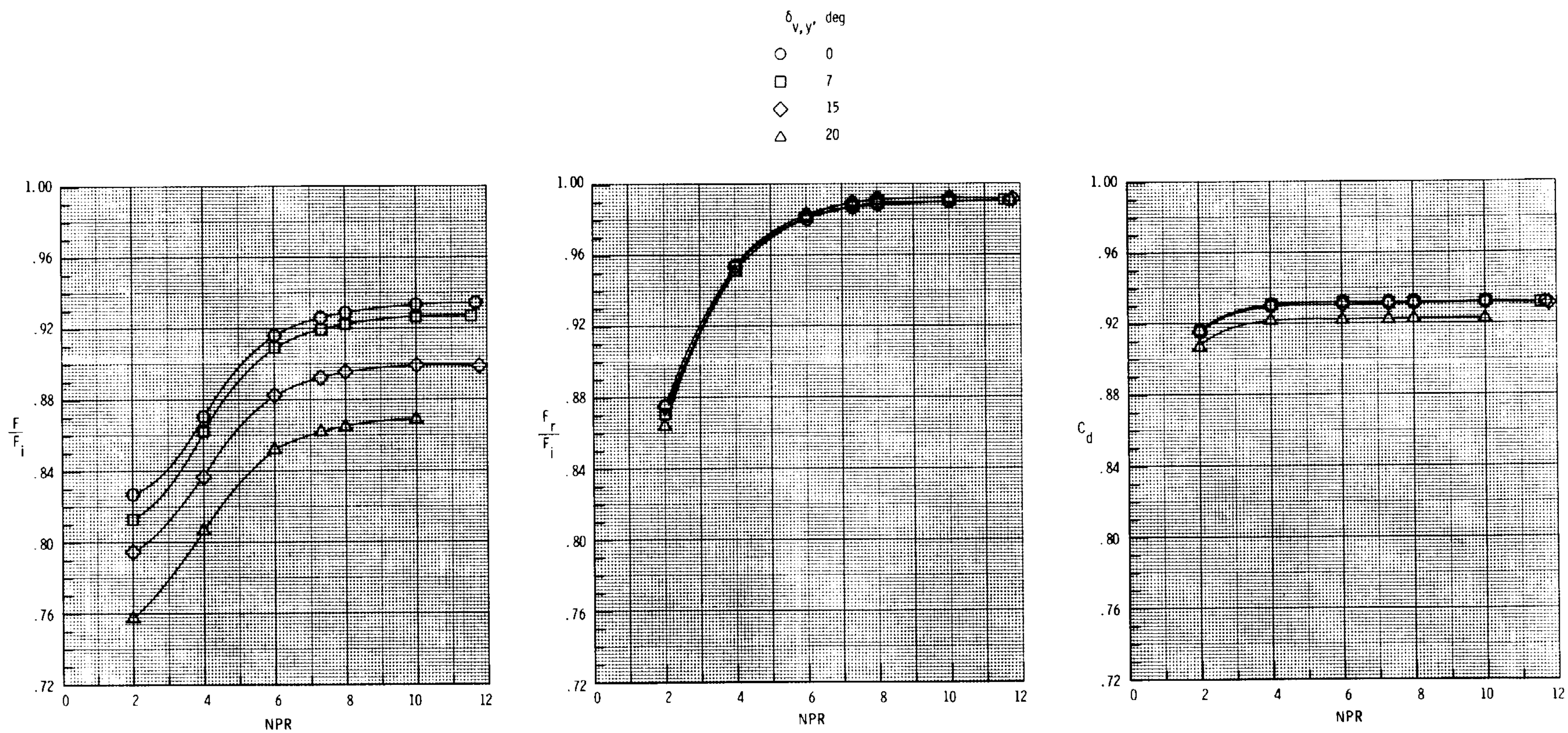

(c) Thrust performance with $\delta_{v,p} = 20°$.

Figure 19. Continued.

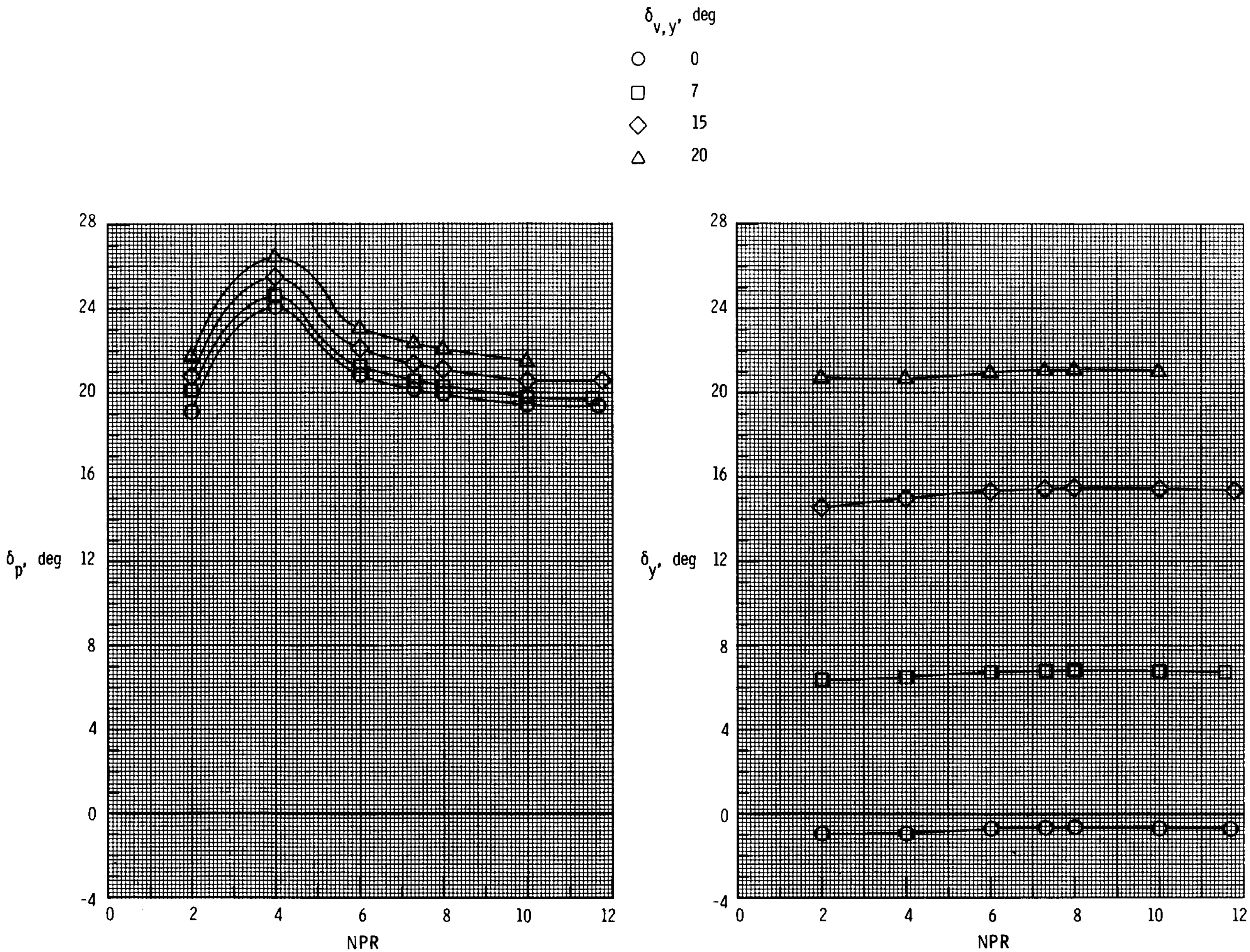

(d) Resultant thrust vector angles with $\delta_{v,p} = 20°$.

Figure 19. Concluded.

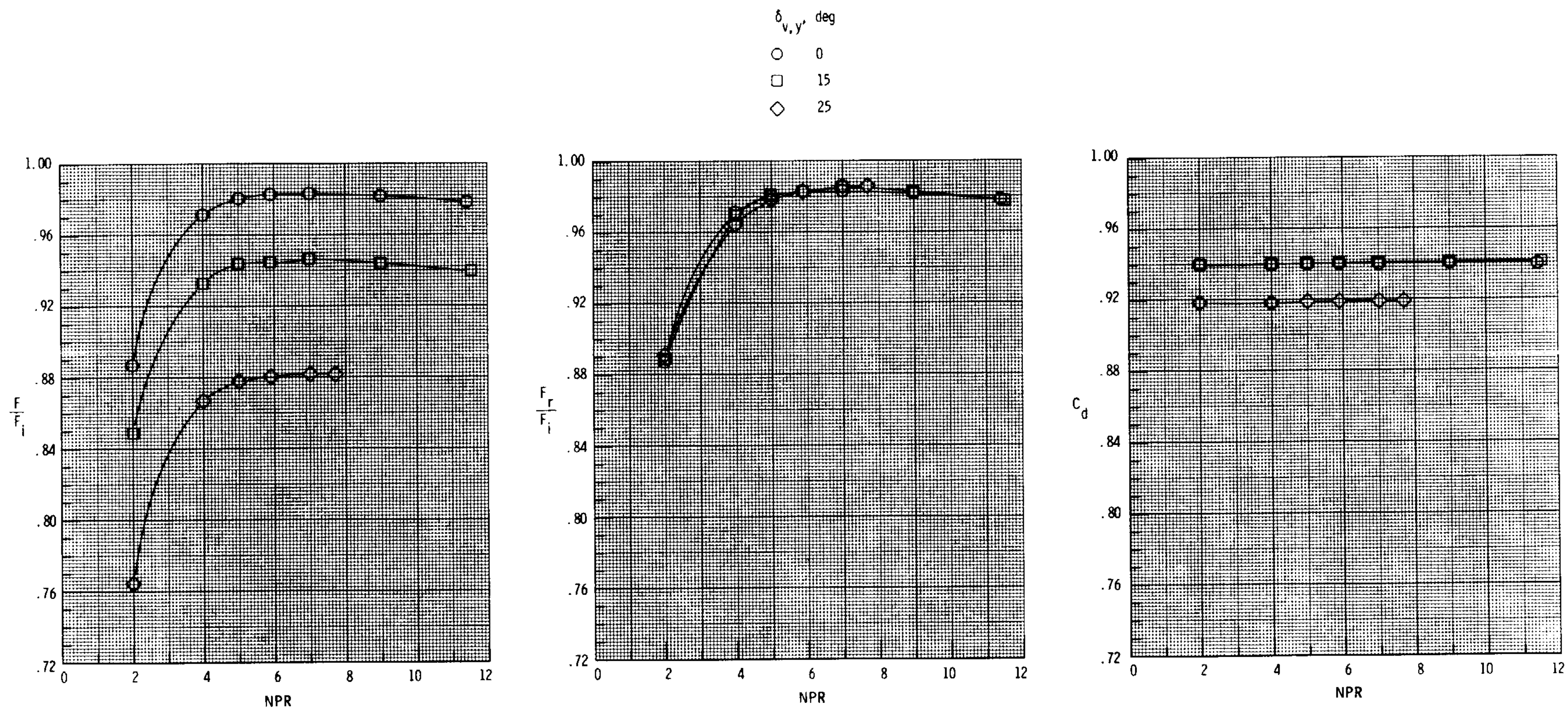

(a) Thrust performance with $\delta_{v,p} = 0°$.

Figure 20. Effect of NPR on performance of SCF 2-D C-D nozzle with AR = 1.265 and $A_e/A_t = 1.46$.

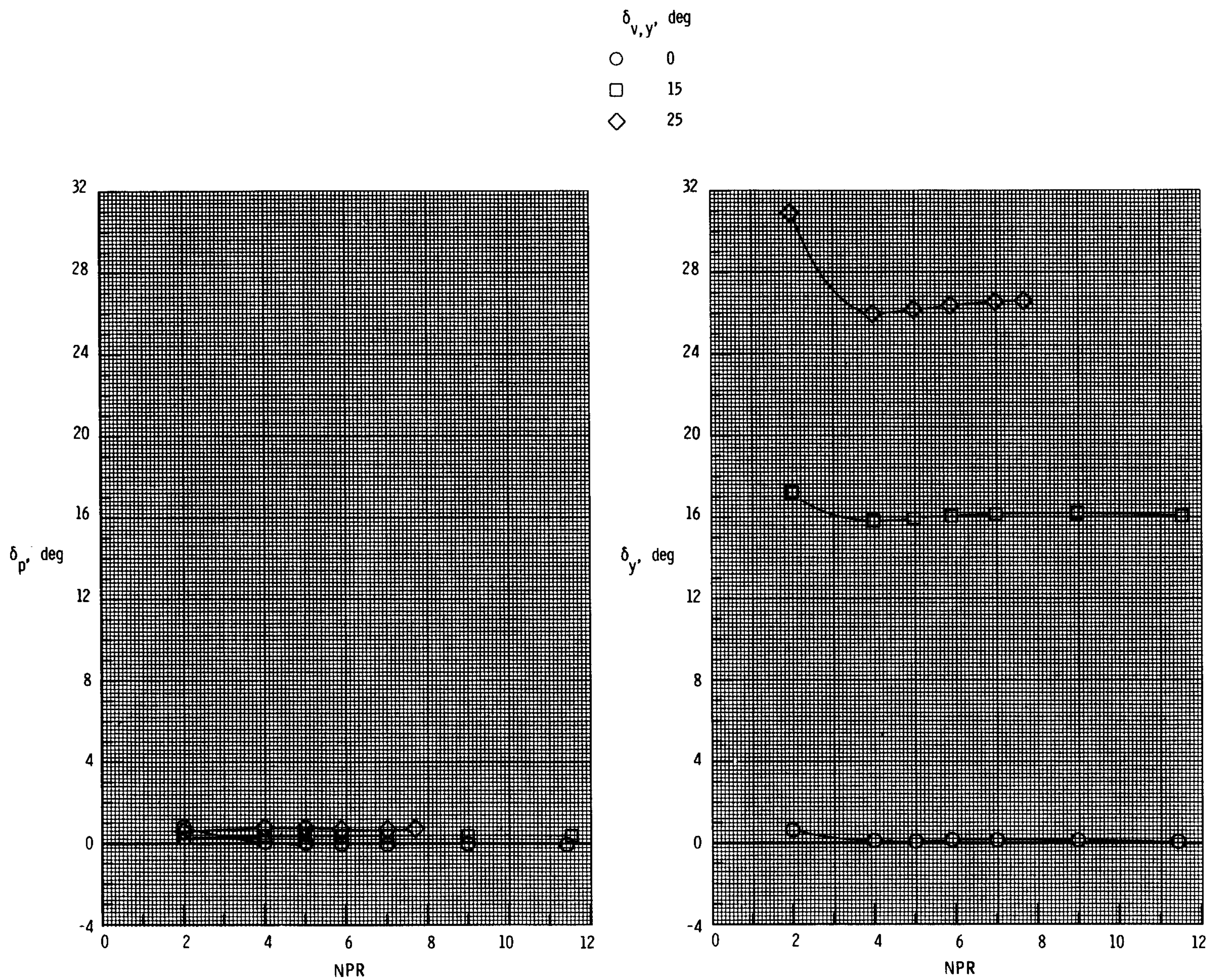

(b) Resultant thrust vector angles with $\delta_{v,p} = 0°$.

Figure 20. Continued.

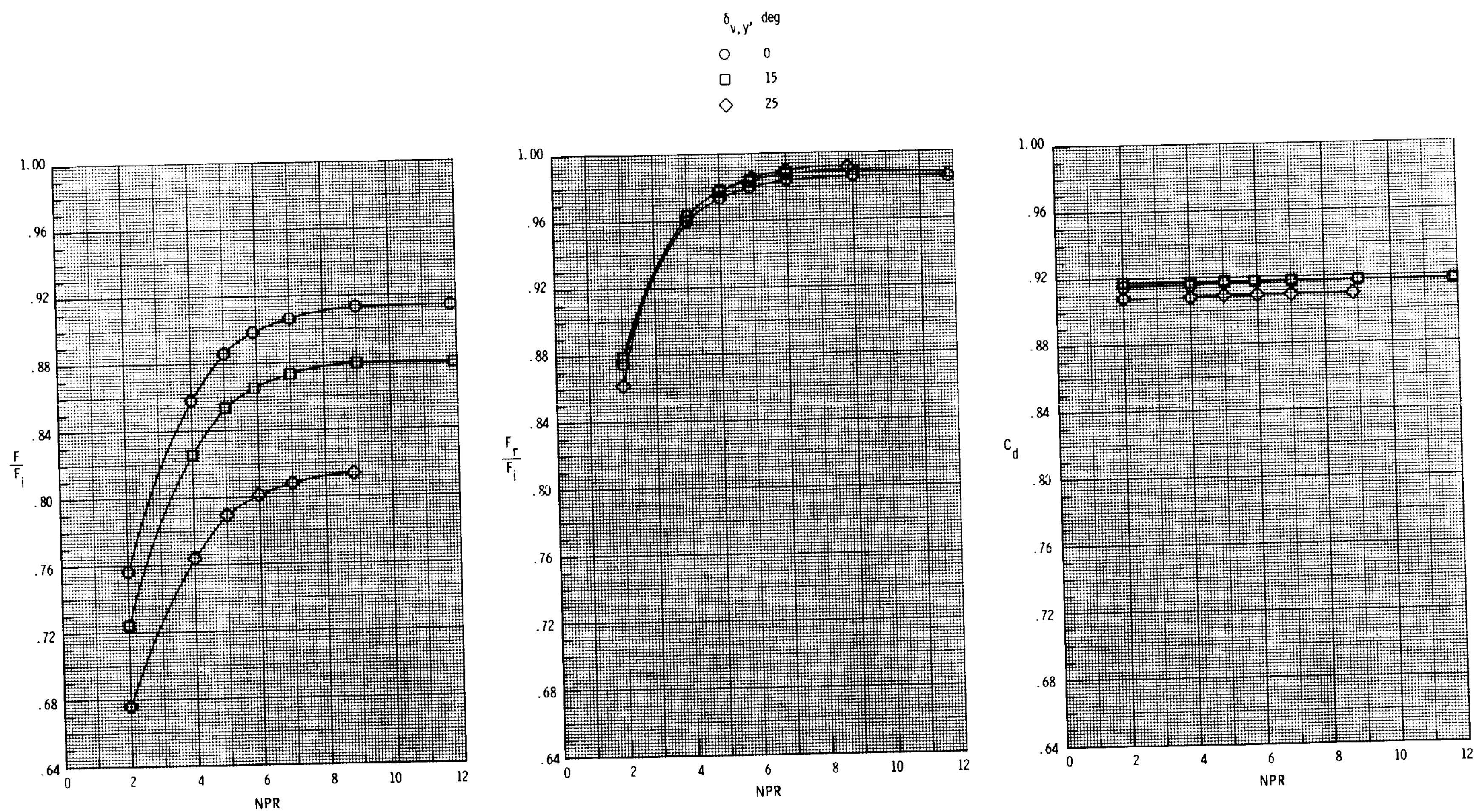

(c) Thrust performance with $\delta_{v,p} = 25°$.

Figure 20. Continued.

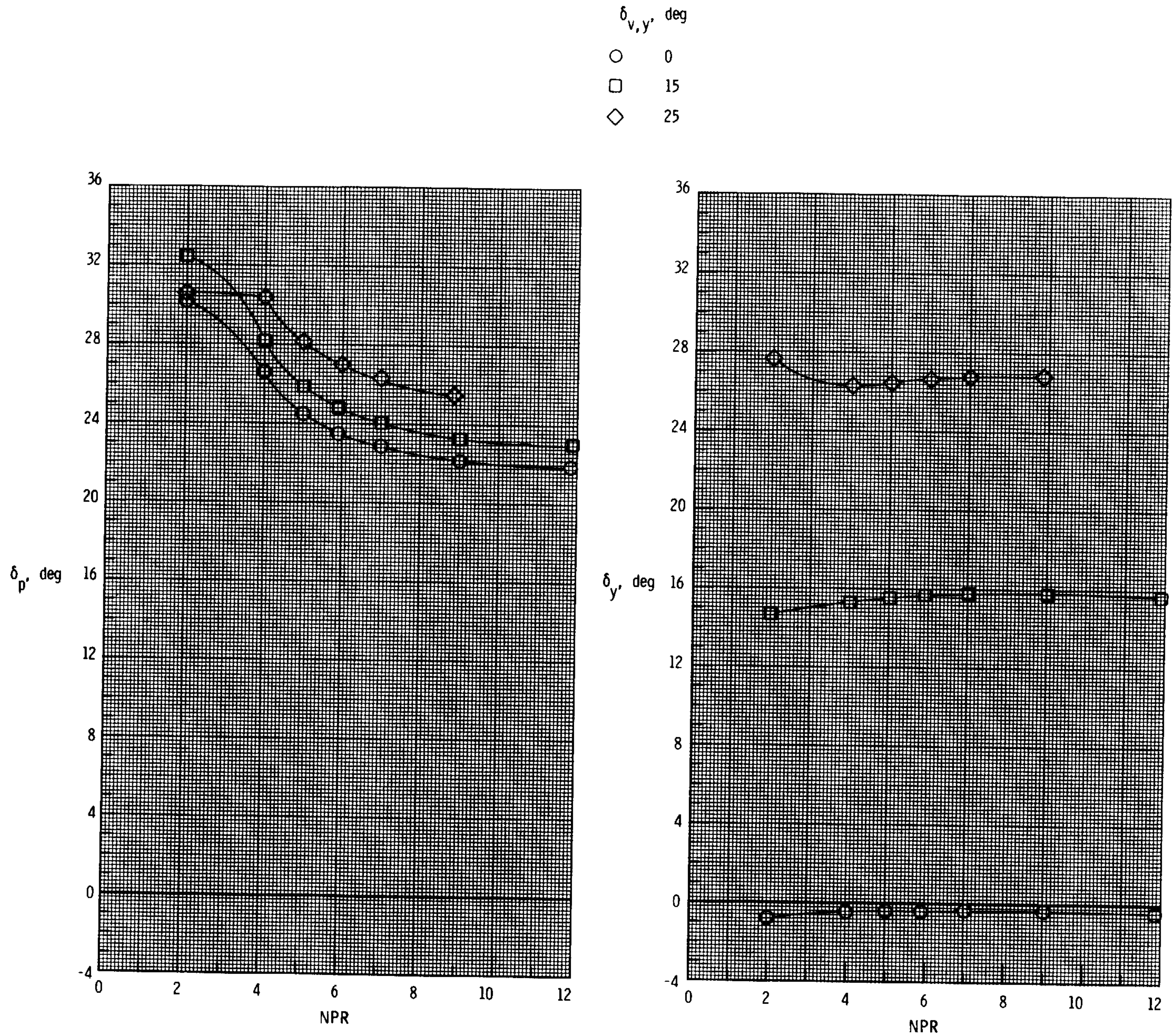

(d) Resultant thrust vector angles with $\delta_{v,p} = 25°$.

Figure 20. Concluded.

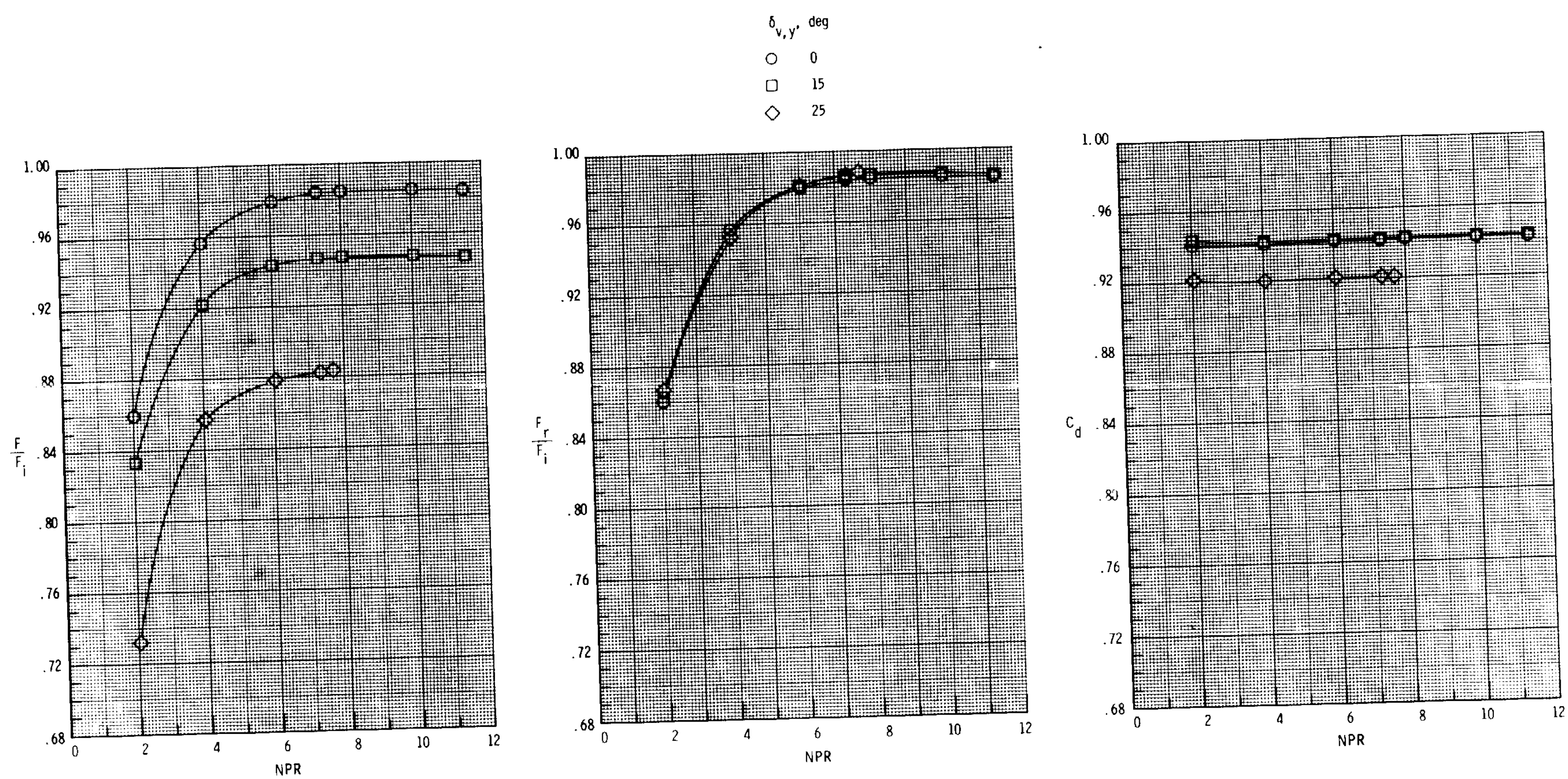

(a) Thrust performance with $\delta_{v,p} = 0°$.

Figure 21. Effect of NPR on performance of SCF 2-D C-D nozzle with AR = 1.265 and $A_e/A_t = 1.63$.

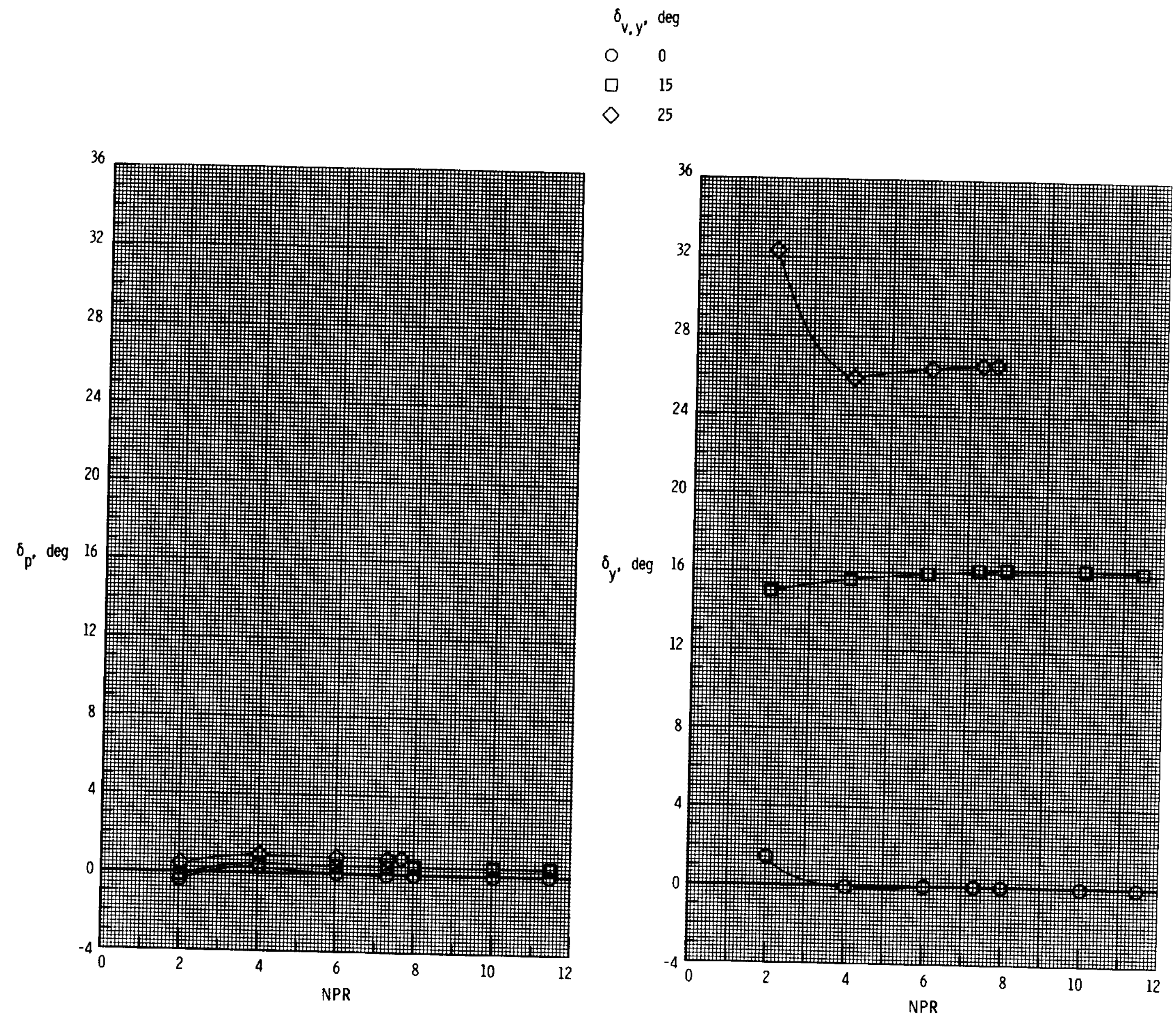

(b) Resultant thrust vector angles with $\delta_{v,p} = 0°$.

Figure 21. Continued.

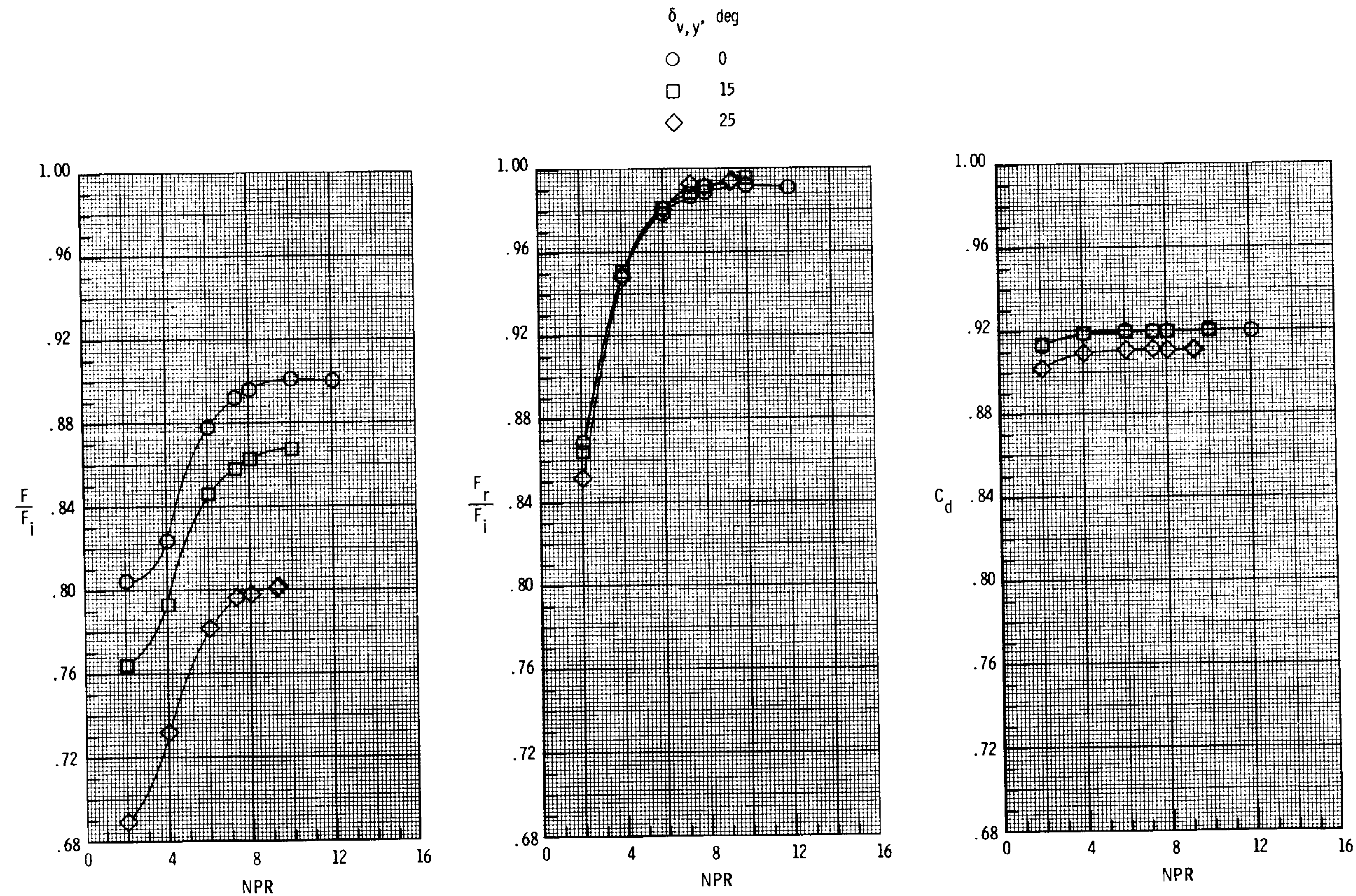

(c) Thrust performance with $\delta_{v,p} = 25°$.

Figure 21. Continued.

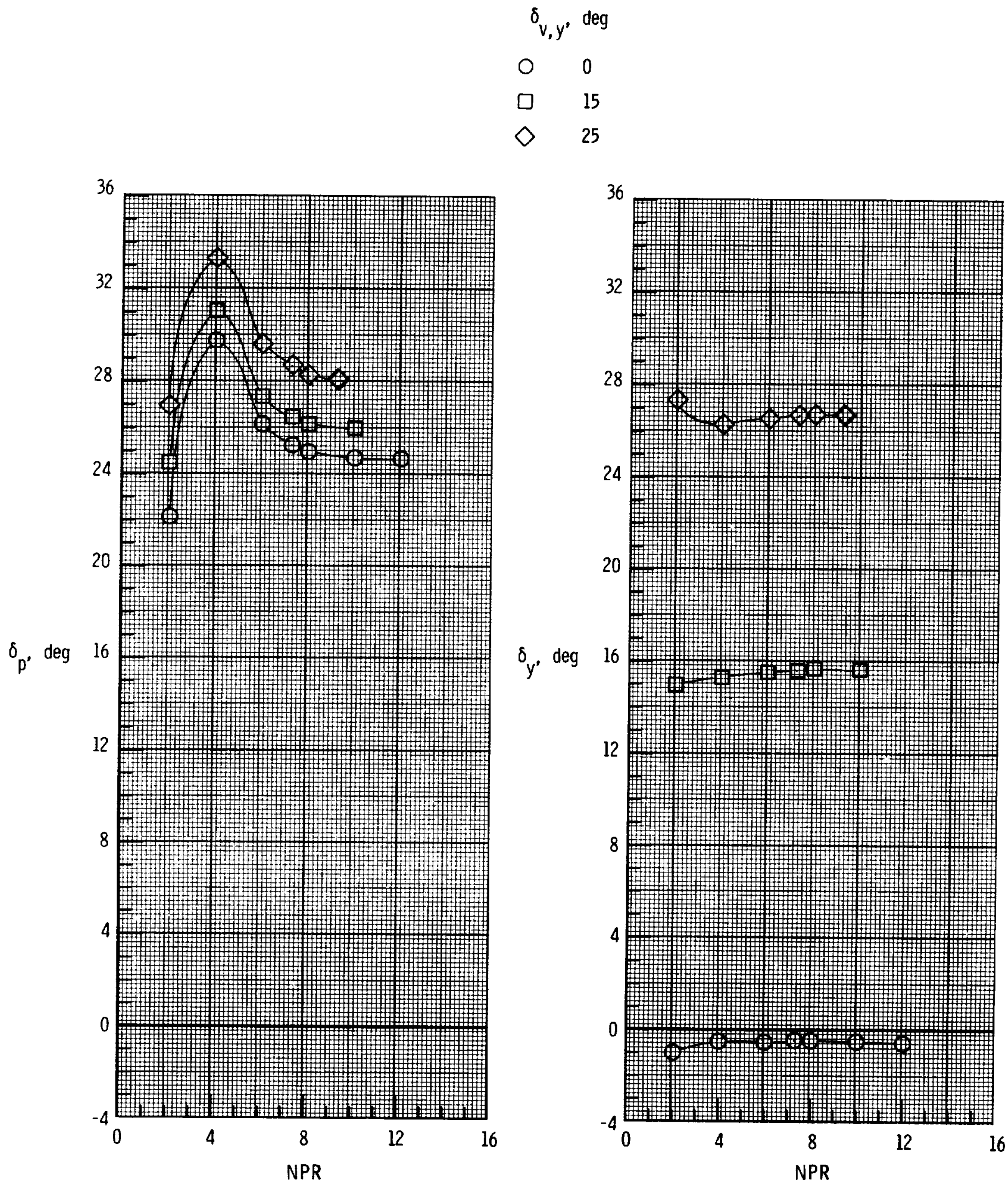

(d) Resultant thrust vector angles with $\delta_{v,p} = 25°$.

Figure 21. Concluded.

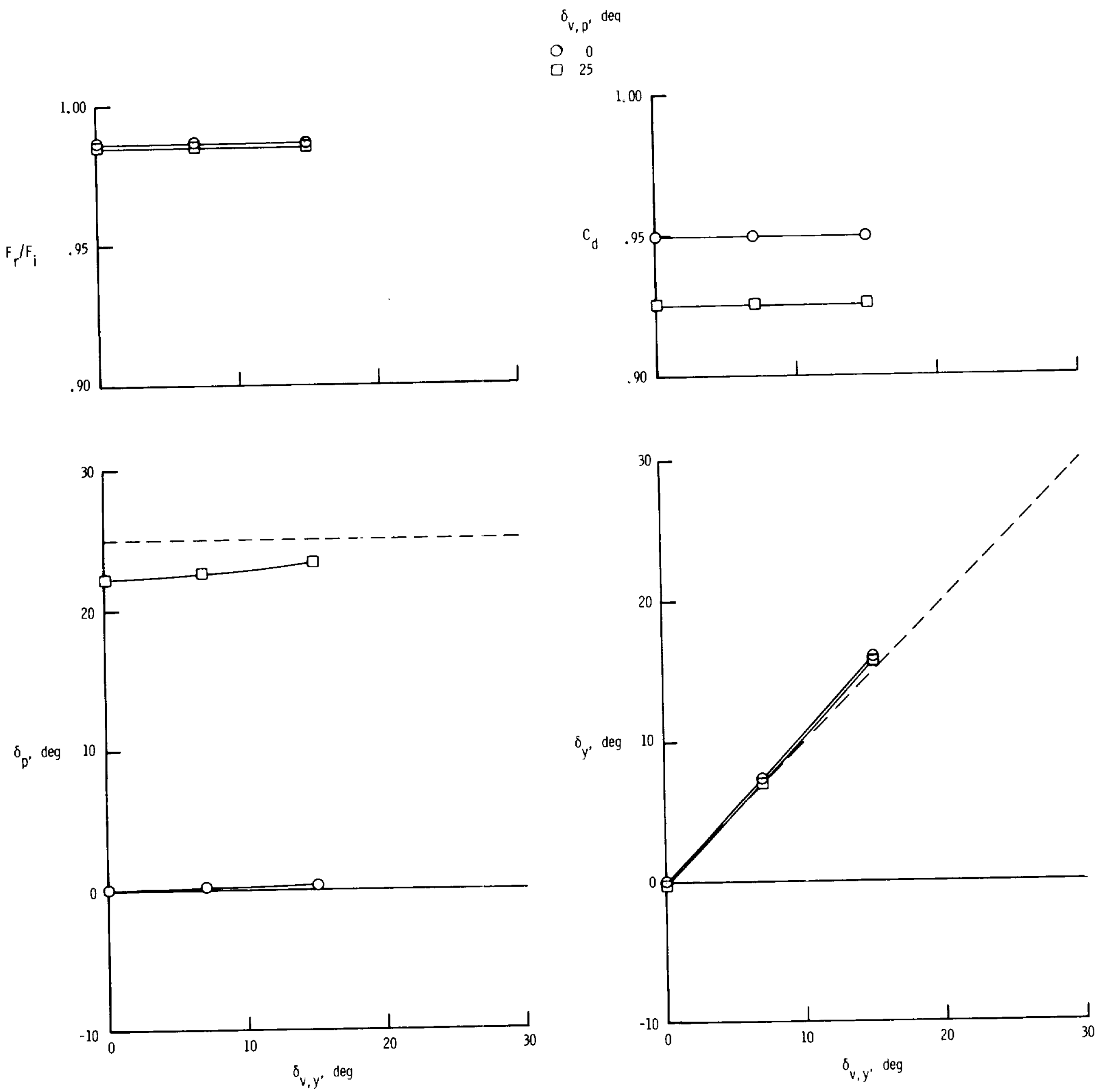

(a) AR = 2.508; $A_e/A_t = 1.46$; NPR = $(\mathrm{NPR})_d = 5.92$.

Figure 22. Effect of geometric thrust vector angle on SCF 2-D C-D nozzle performance. Dashed line indicates design value of resultant thrust vector angles.

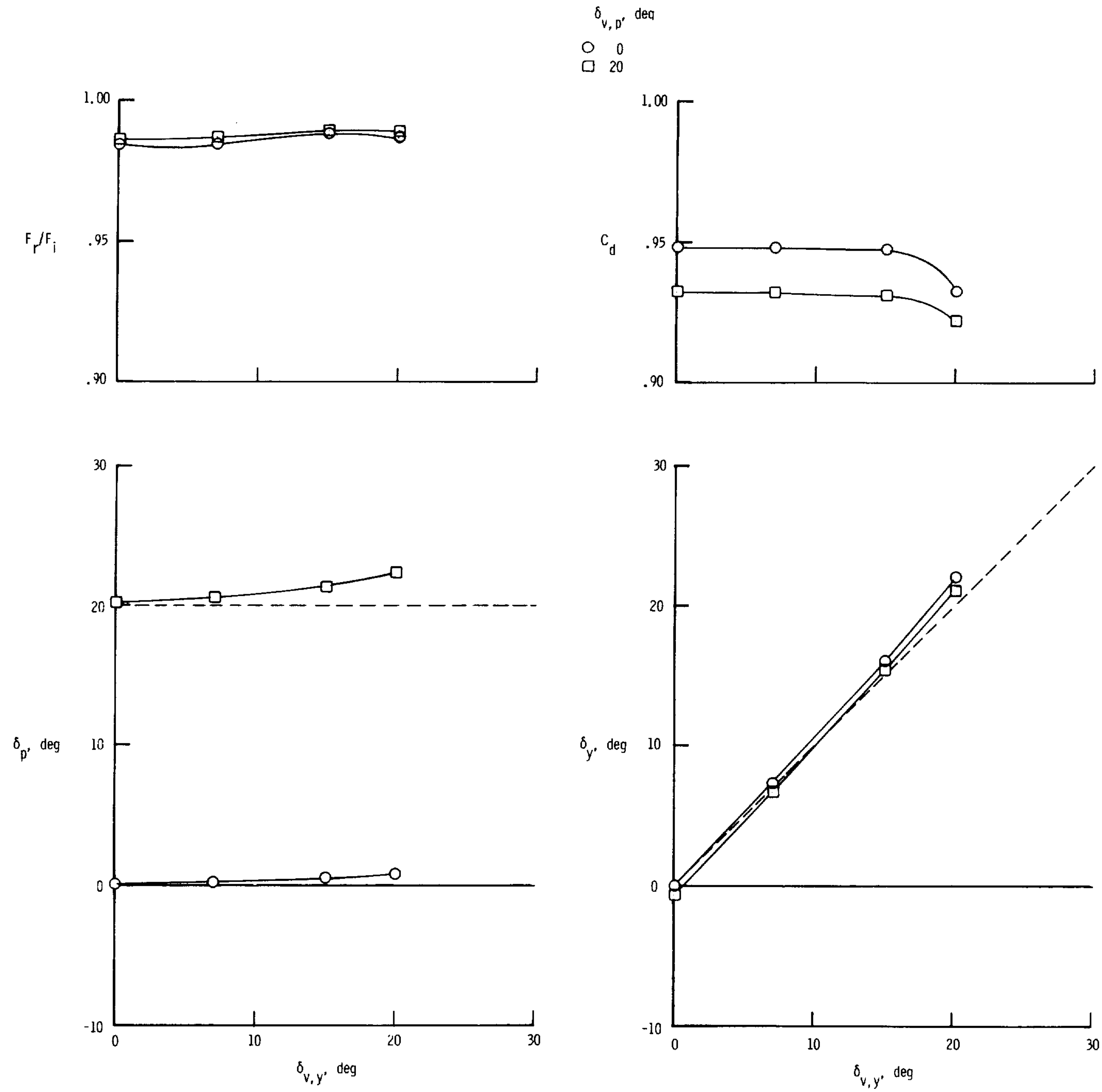

(b) AR = 2.083; $A_e/A_t = 1.63$; $(\mathrm{NPR})_d = 7.33$.

Figure 22. Continued.

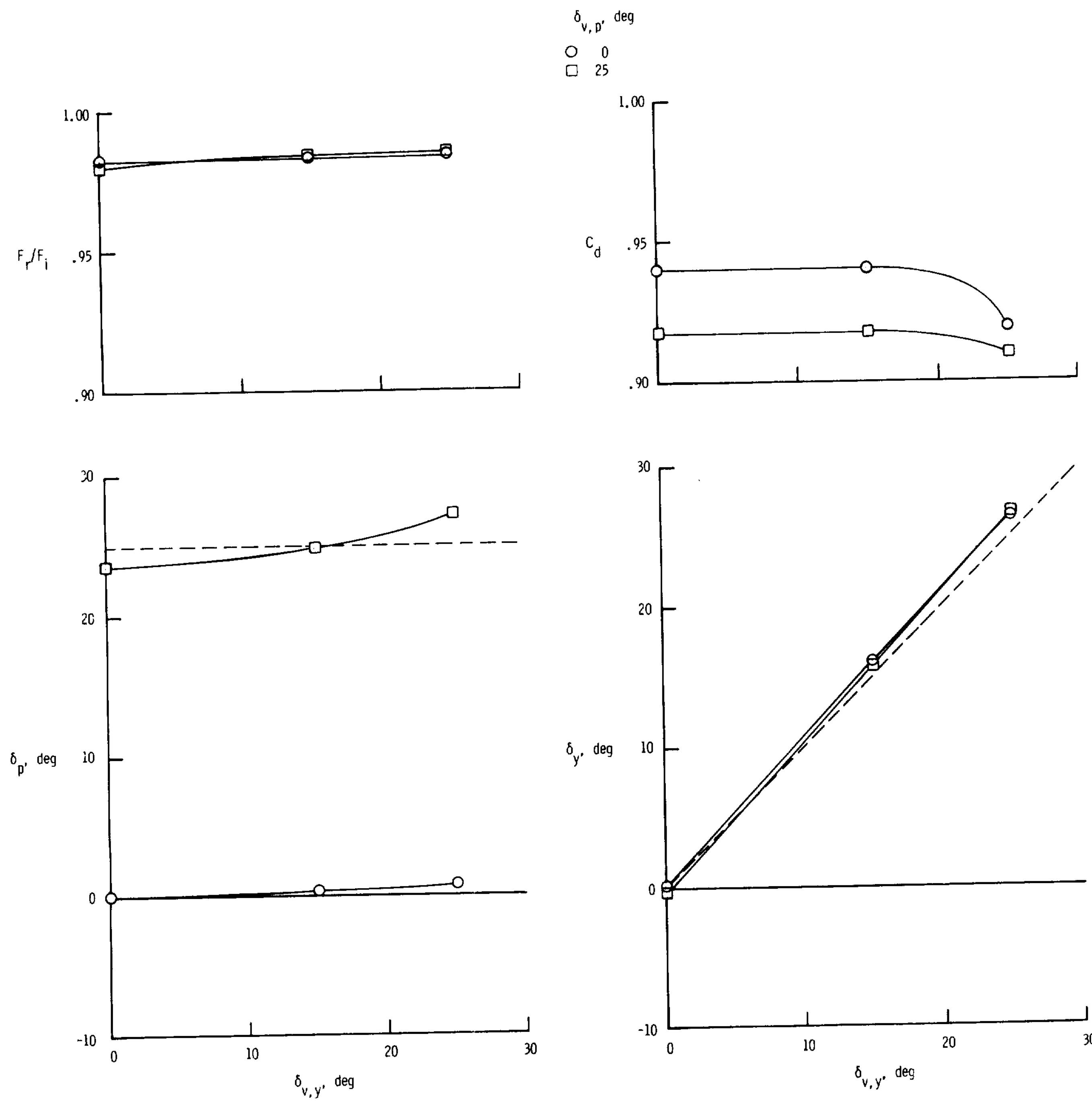

(c) AR = 1.265; $A_e/A_t = 1.46$; NPR = $(\text{NPR})_d = 5.92$.

Figure 22. Concluded.

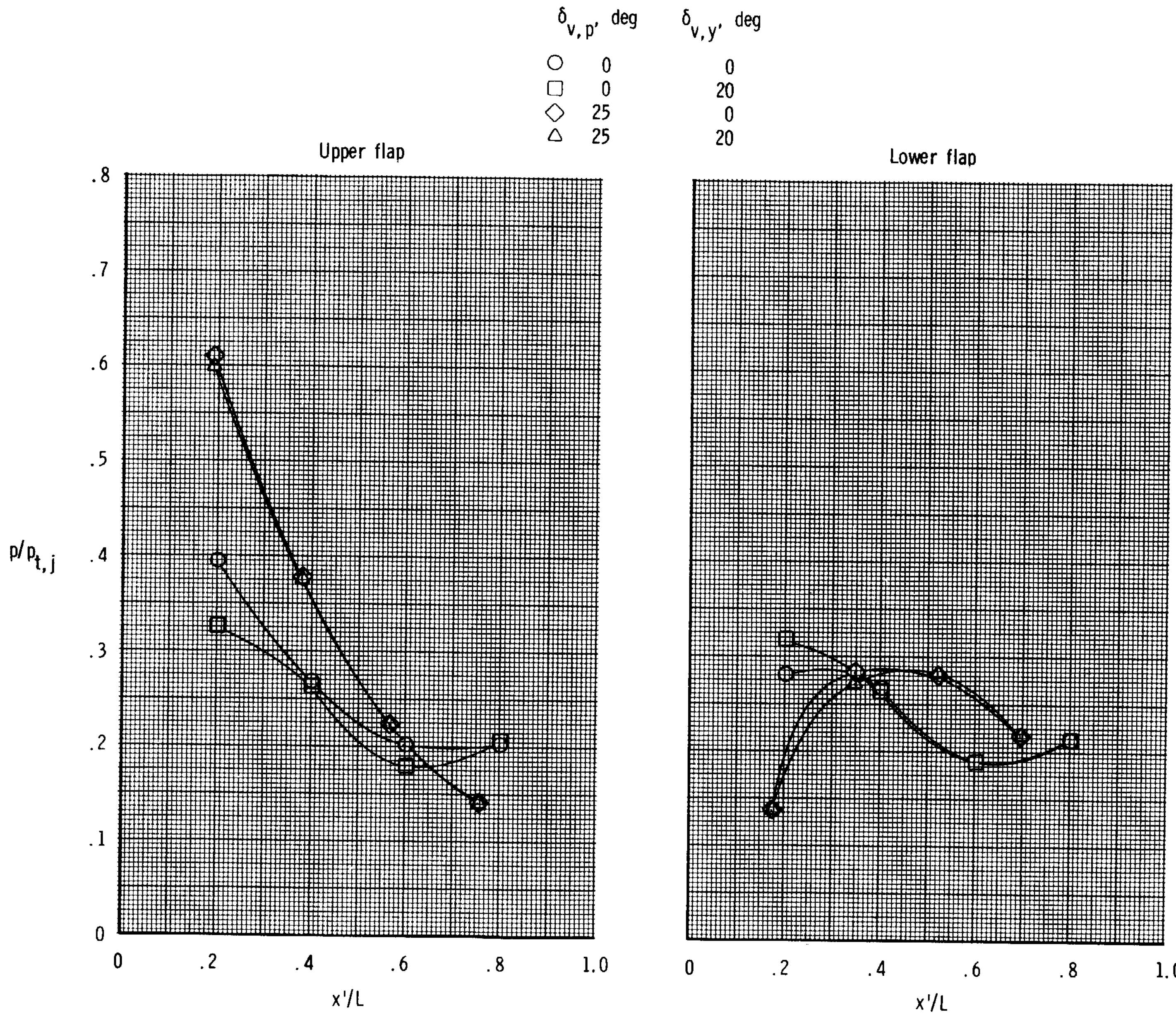

(a) Divergent flaps.

Figure 23. Effect of geometric thrust vector angle on internal static pressure distributions of SCF 2-D C-D nozzle. AR = 2.083; $A_e/A_t = 1.46$; nominal NPR = 5.9.

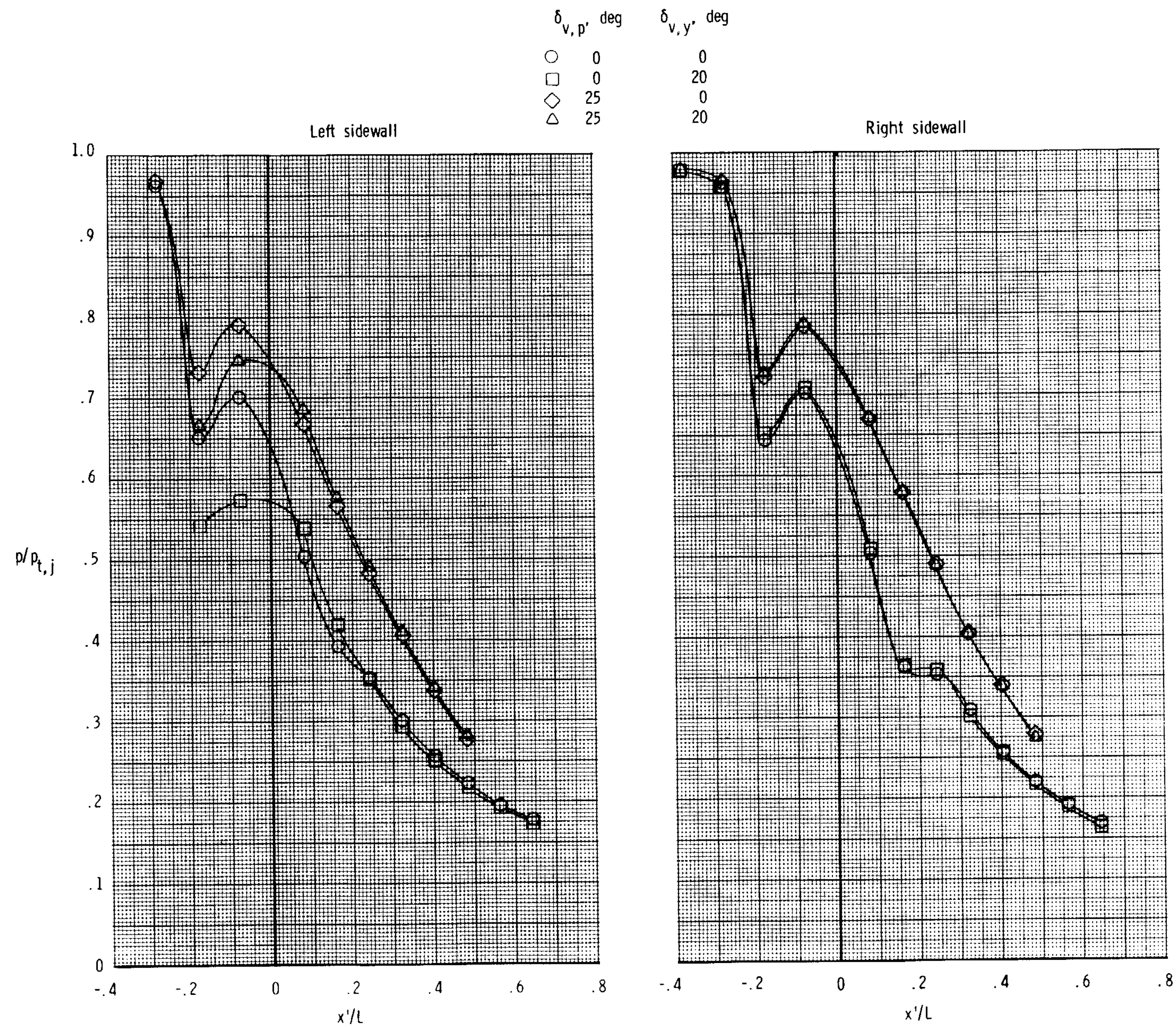

(b) Sidewalls.

Figure 23. Concluded.

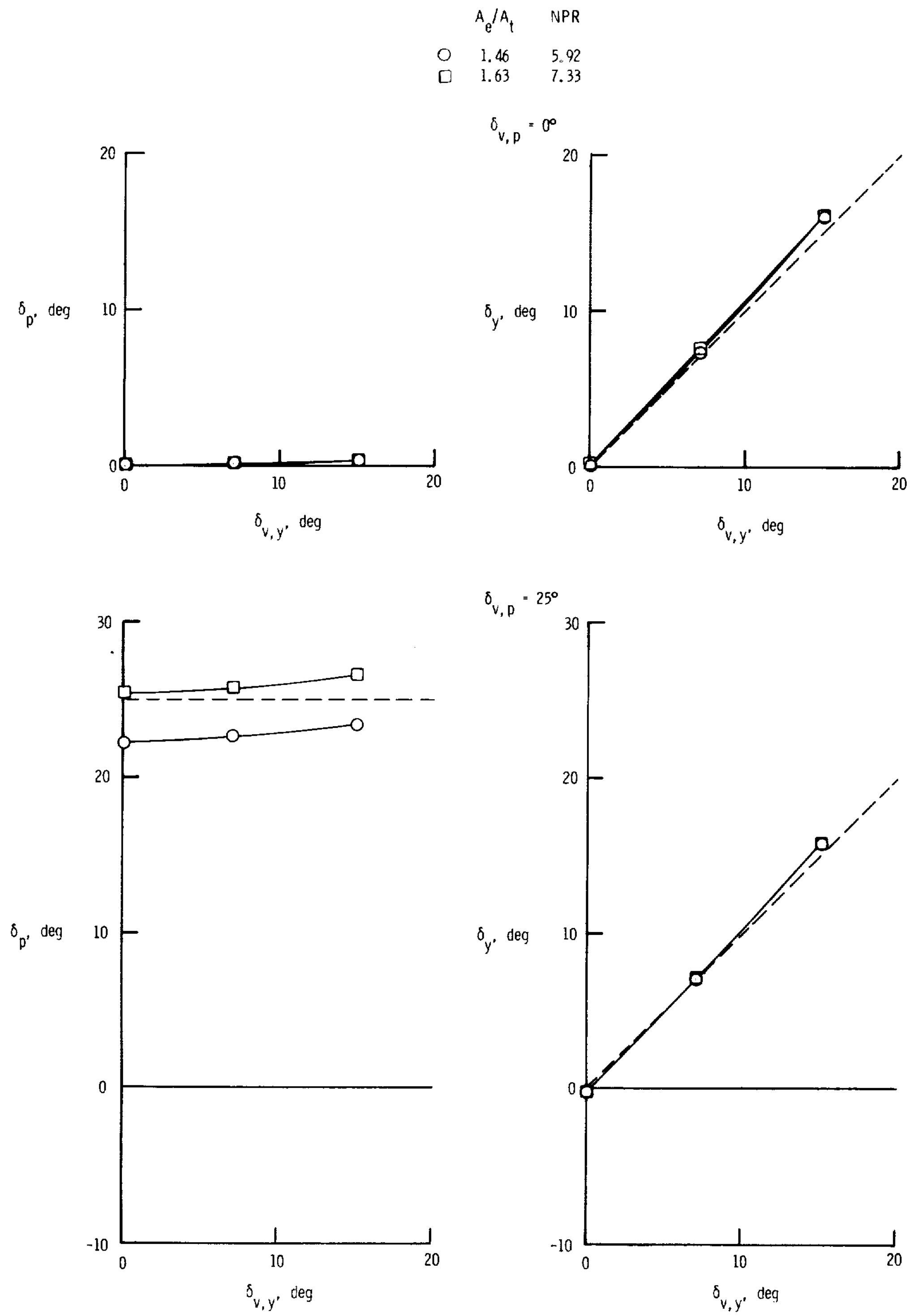

(a) AR = 2.508.

Figure 24. Effect of nozzle expansion ratio A_e/A_t on resultant thrust vector angles. Dashed lines indicate design value of resultant thrust vector angles.

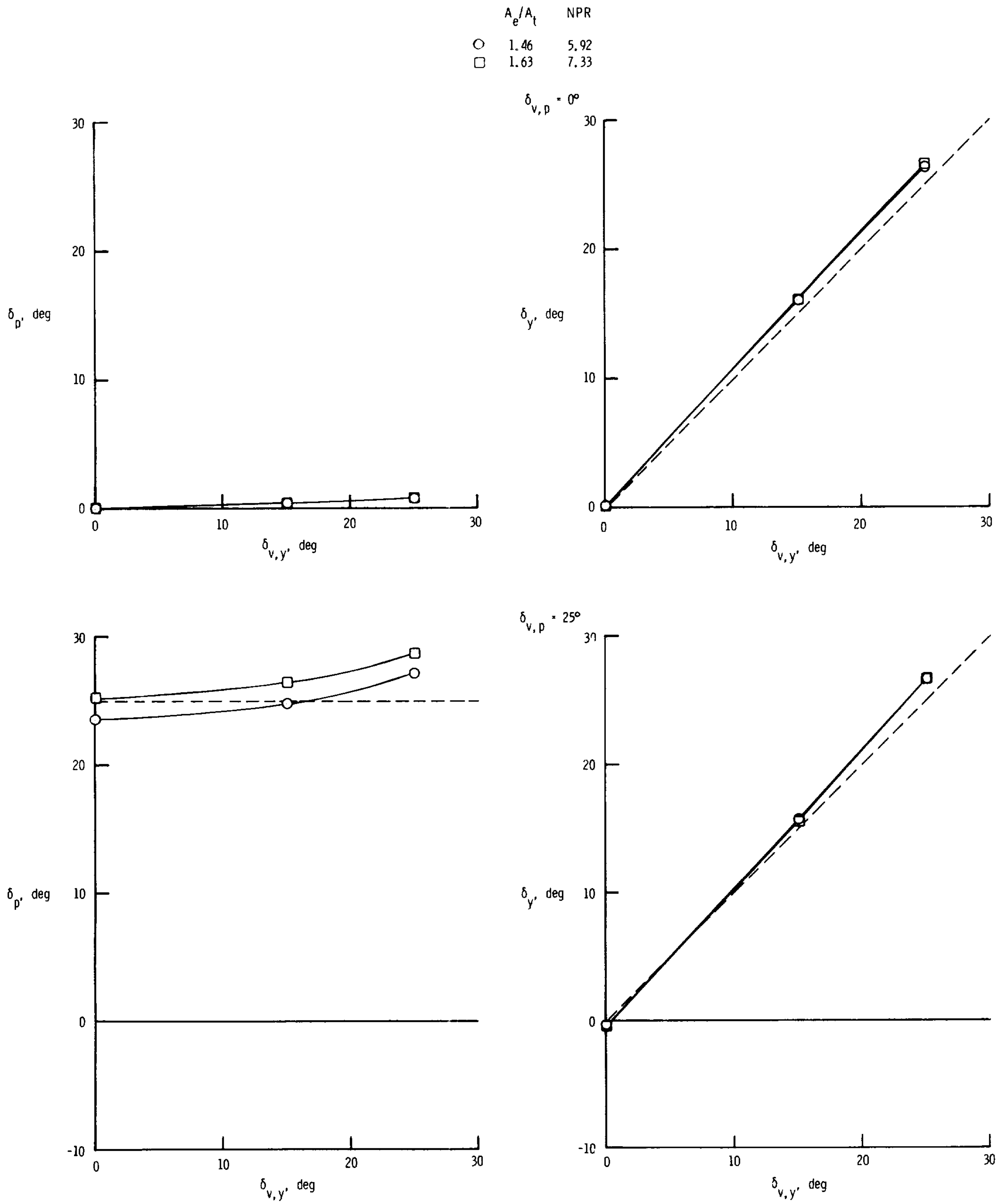

(b) AR = 1.265.

Figure 24. Concluded.

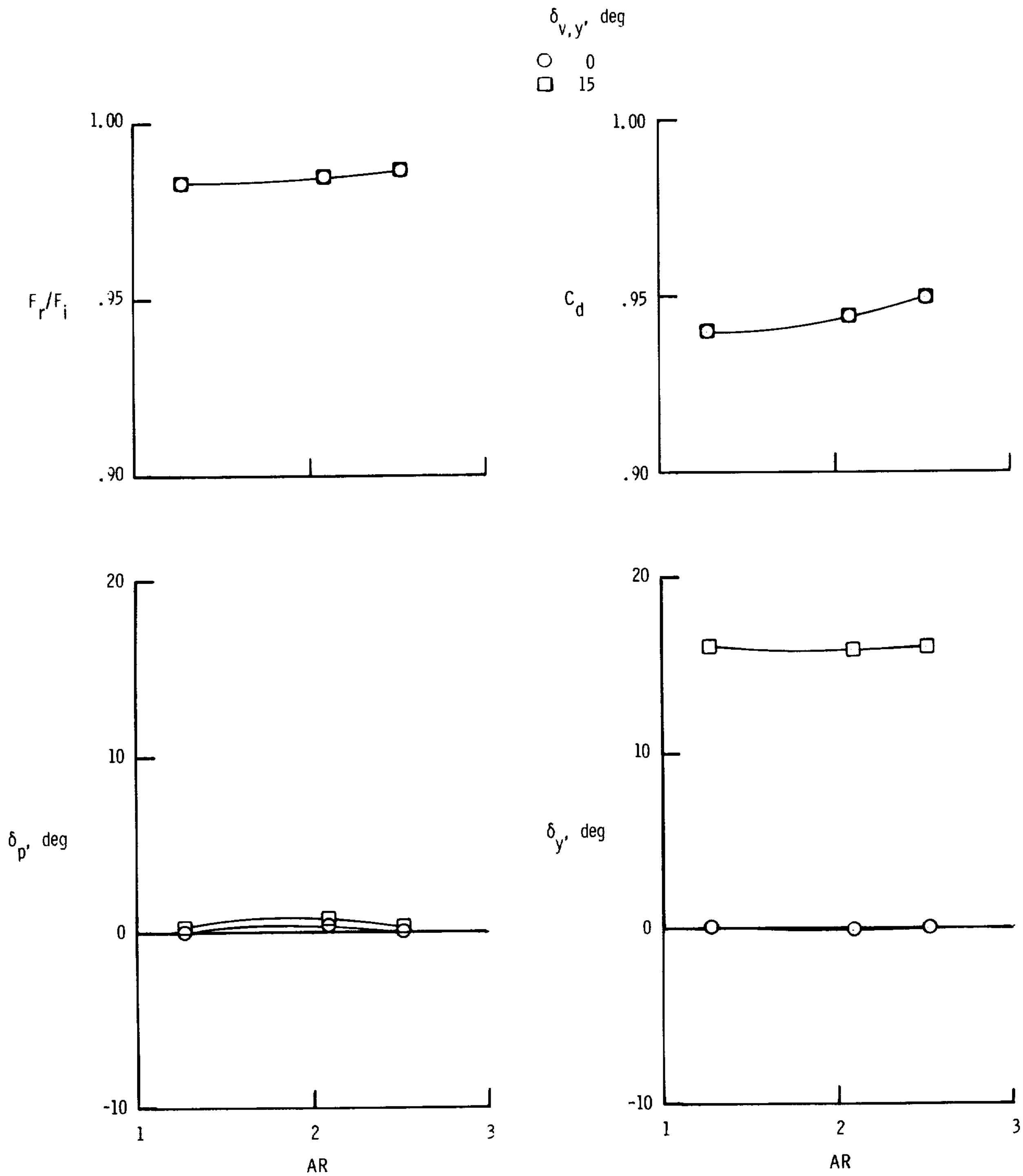

(a) $A_e/A_t = 1.46$; NPR = 5.92; $\delta_{v,p} = 0°$.

Figure 25. Effect of nozzle aspect ratio on SCF 2-D C-D nozzle performance.

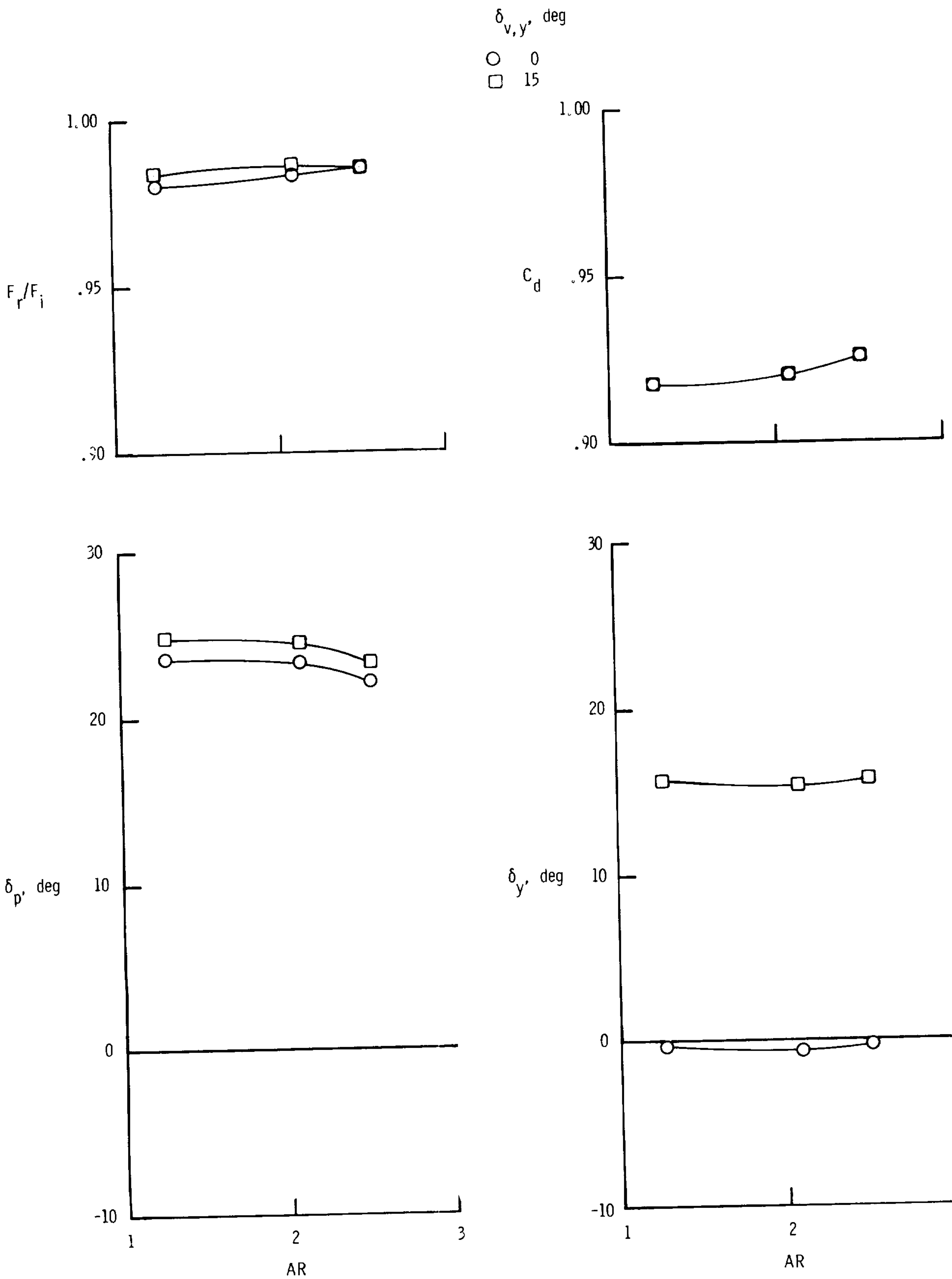

(b) $A_e/A_t = 1.46$; NPR = 5.92; $\delta_{v,p} = 25°$.

Figure 25. Continued.

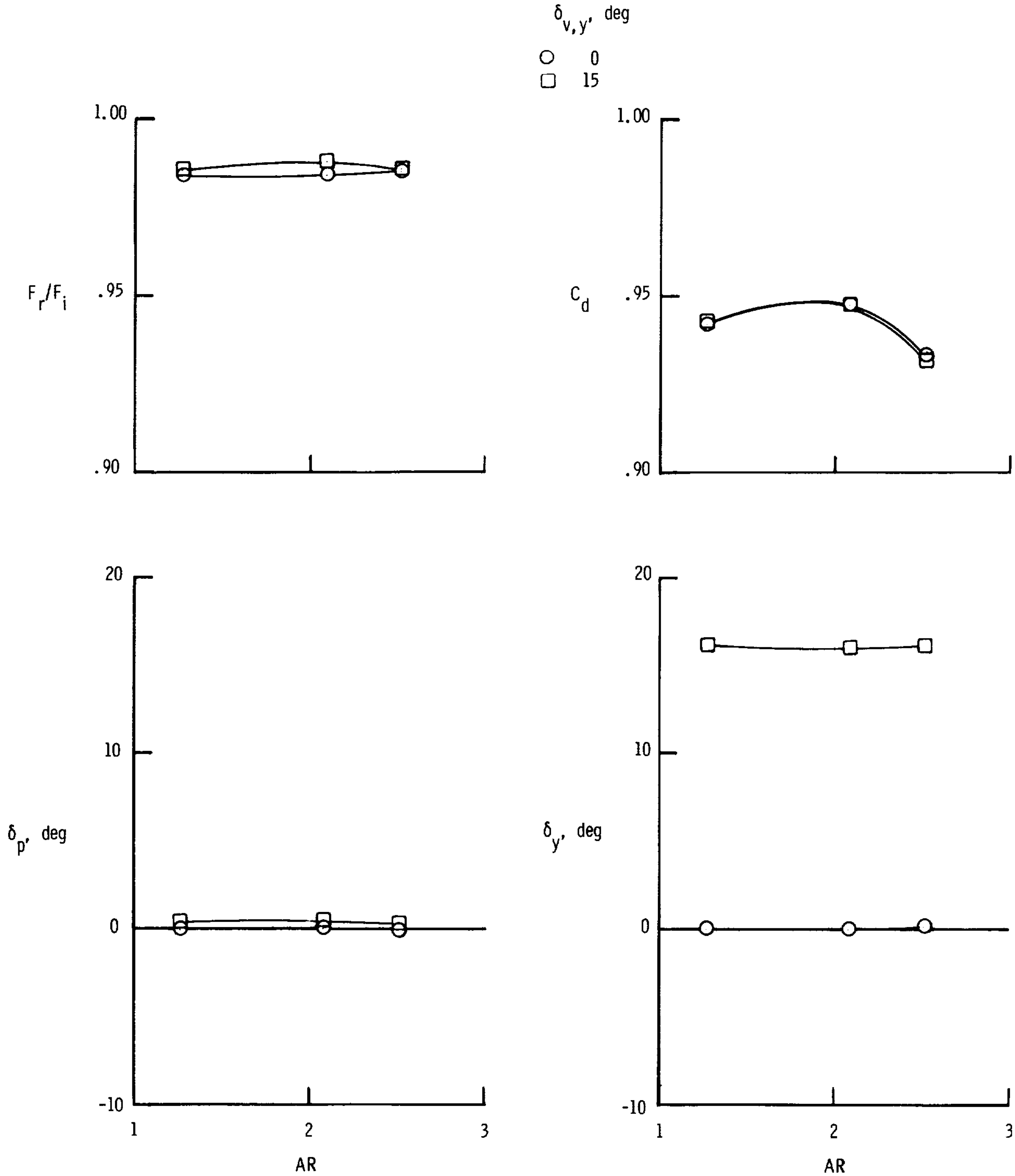

(c) $A_e/A_t = 1.63$; NPR = 7.33; $\delta_{v,p} = 0°$.

Figure 25. Concluded.

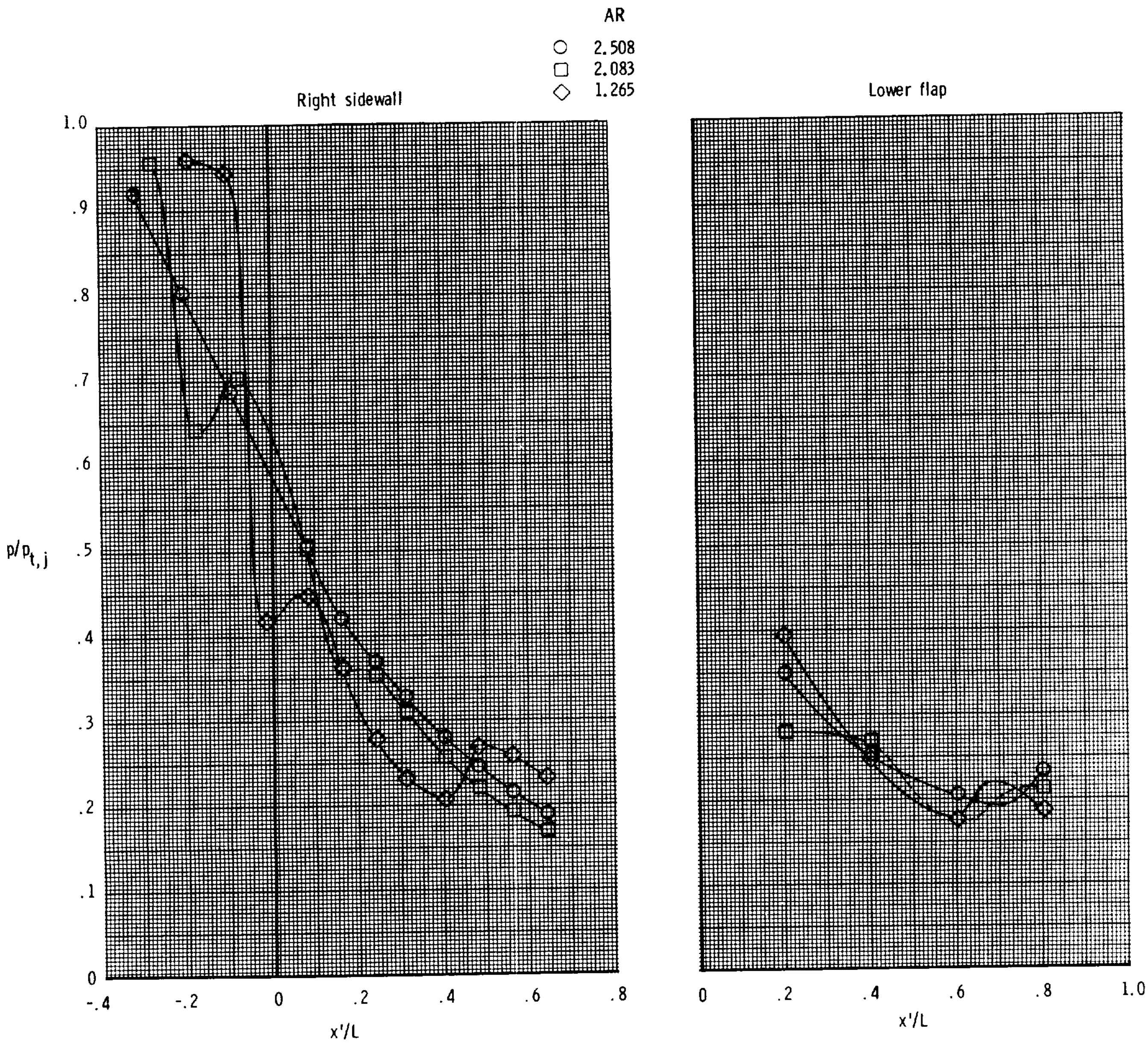

(a) $A_e/A_t = 1.46$; nominal NPR = 5.9.

Figure 26. Effect of throat aspect ratio on internal static pressure distributions of SCF 2-D C-D nozzle. $\delta_{v,p} = \delta_{v,y} = 0°$.

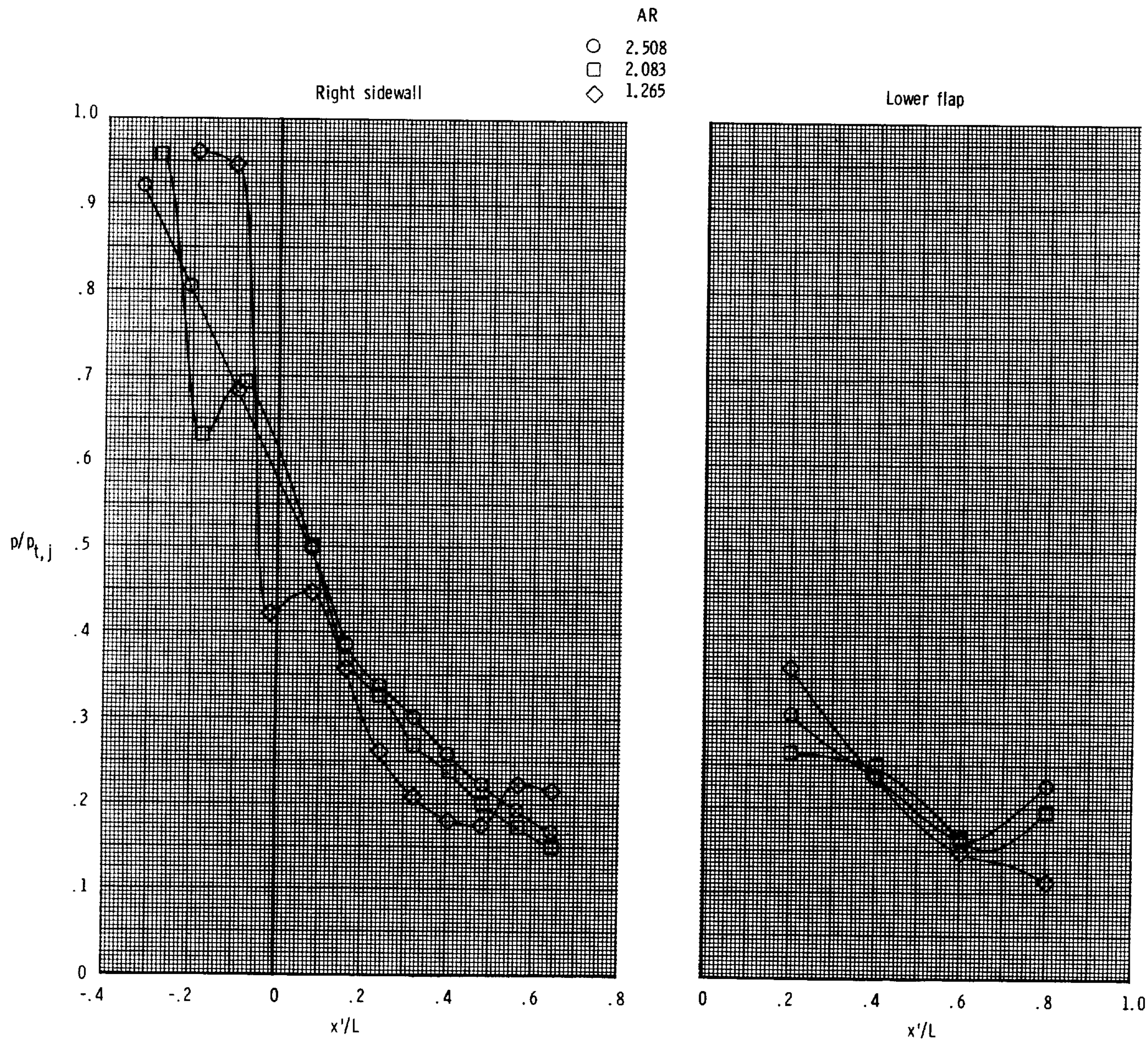

(b) $A_e/A_t = 1.63$; nominal NPR = 7.3.

Figure 26. Concluded.

National Aeronautics and Space Administration

Report Documentation Page

1. Report No. NASA TP-2991	2. Government Accession No.	3. Recipient's Catalog No.
4. Title and Subtitle Internal Performance of Two Nozzles Utilizing Gimbal Concepts for Thrust Vectoring		5. Report Date April 1990
		6. Performing Organization Code
7. Author(s) Bobby L. Berrier and John G. Taylor		8. Performing Organization Report No. L-16722
9. Performing Organization Name and Address NASA Langley Research Center Hampton, VA 23665-5225		10. Work Unit No. 505-68-91-06
		11. Contract or Grant No.
12. Sponsoring Agency Name and Address National Aeronautics and Space Administration Washington, DC 20546-0001		13. Type of Report and Period Covered Technical Paper
		14. Sponsoring Agency Code

15. Supplementary Notes

16. Abstract
An investigation was conducted in the static test facility of the Langley 16-Foot Transonic Tunnel to evaluate the internal performance of an axisymmetric convergent-divergent nozzle and a nonaxisymmetric convergent-divergent nozzle, both of which utilized a gimbal-type mechanism for thrust vectoring in at least one plane. The nonaxisymmetric nozzle used the gimbal concept for yaw thrust vectoring only, and pitch thrust vectoring was accomplished by simultaneous deflection of the upper and lower divergent flaps. The model geometric parameters investigated were pitch vector angle for the axisymmetric nozzle and pitch vector angle, yaw vector angle, nozzle throat aspect ratio, and nozzle expansion ratio for the nonaxisymmetric nozzle. All tests were conducted with no external flow, and nozzle pressure ratio was varied from 2.0 to approximately 12.0.

17. Key Words (Suggested by Authors(s)) Internal performance, Thrust, Nozzle, Thrust vectoring, Gimbal	18. Distribution Statement Unclassified—Unlimited. Subject Category 02

19. Security Classif. (of this report) Unclassified	20. Security Classif. (of this page) Unclassified	21. No. of Pages 127	22. Price A07

NASA FORM 1626 OCT 86

NASA-Langley, 1990

For sale by the National Technical Information Service, Springfield, Virginia 22161-2171